Identification and Characterization of *Chlamydia*-containing sphere formation, a unique and novel egress mechanism

Inaugural-Dissertation

to obtain the academic degree
Doctor rerum naturalium (Dr. rer. nat.)

submitted to the Department of Biology, Chemistry, Pharmacy
of Freie Universität Berlin

by
Jana Scholz

Berlin, 2024

This work was realized from July 2021 until December 2024 in the Unit ‘Sexually transmitted bacterial Pathogens (STI) and HIV’ at the Robert Koch Institute, Berlin and was supervised by Dr. Dagmar Heuer.

1st reviewer:	Dr. Dagmar Heuer
2nd reviewer:	Prof. Dr. Oliver Daumke
Date of defense:	February 25, 2025

Acknowledgements

This space I want to fill with thanks to those who supported me during my doctoral thesis:

First of all, I want to thank my supervisor Dr. Dagmar Heuer for the exciting and challenging project, for her continuous input and for the scientific and personal guidance throughout my work. Thanks for having the confidence in me to realize this project and for having the confidence in my results to be presentable and worth to publish. I also would like to thank Prof. Dr. Oliver Daumke for taking his time to serve as my second supervisor and reviewer.

Next, I want to thank all the experienced scientists at the RKI who supported me scientifically and personally during my doctoral thesis. Special thanks go to Dr. Sebastian Banhart, Dr. Kathleen Klaper and Dr. Stephan Fuchs for numerous discussions, (mostly) good advice, and an open ear when it was needed.

Many thanks go as well to my colleagues, especially to Dr. Christian Blumenscheit, Jascha Eggert, Dr. Alyssa Ingmundson, Henning Krüger, Andrea Martini, Dr. Hana Tlapák, and Madita Winkler. To say it with Albus Dumbledore: “It is not our abilities that show who we truly are, it is our choices.” I´m want to thank you for all the times that you made the choice to help me, whether it be with splitting my cells or with a piece of cake.

I want to give special thanks to our collaborators: Silvio Bürge, Gudrun Holland and Dr. Michael Laue from the Advanced Light and Electron Microscopy Unit at the RKI and Dr. Laura Bindila and Julia Maria Post from the Lipidomics Core Facility at the University of Mainz. I am very grateful for learning about your techniques and the discussions we had.

My thanks also go to the DFG for funding this project within the SPP2225, especially for enabling the method workshop about “OMICS Analyses of Infection and Pathogen Egress” in Mainz.

Last but not least I would like to thank my family and friends who supported me at every step.

Declaration of authorship

I hereby declare that I alone am responsible for the content of my doctoral dissertation and that I have only used the sources or references cited in the dissertation.

Parts of this thesis have already been published in the following articles:

1 *Chlamydia*-containing spheres are a novel and predominant form of egress by the pathogen *Chlamydia psittaci*

Jana Scholz, Gudrun Holland, Michael Laue, Sebastian Banhart, Dagmar Heuer

mBio 15, 2024, https://doi.org/10.1128/mbio.01288-24

preprint available at https://doi.org/10.1101/2023.08.28.555065

2 Entschlüsselung eines neuen Austrittswegs von Chlamydien

Jana Scholz and Dagmar Heuer

BIOspektrum 30, 2024, https://doi.org/10.1007/s12268-024-2334-3

3 Recruitment of the cellular lipid transport protein CERT to *C. psittaci* inclusions regulates the timing of bacterial egress

Jana Scholz, Gudrun Holland, Michael Laue, Sebastian Banhart, Dagmar Heuer

Submitted to *Scientific Reports*

Preprint available at https://doi.org/10.1101/2024.11.26.625409

Berlin, December 6, 2024

Place, Date Jana Scholz

Table of content

Acknowledgements iii
Declaration of authorship iv
Table of content v
Zusammenfassung ix
Abstract xi
1 Introduction 1
1.1 The family of *Chlamydiacea* within the order of *Chlamydiales* 1
1.1.1 Taxonomy of *Chlamydiacea* 1
1.1.2 Relevance of *Chlamydia psittaci* 2
1.1.3 Relevance of *Chlamydia trachomatis* 3
1.1.4 The developmental cycle of *Chlamydia* 4
1.2 Egress of intracellular pathogens 7
1.2.1 Overview 7
1.2.2 Non-lytic egress 9
1.2.3 Egress by apoptotic host cell death 10
1.3 Lipids during chlamydial infections 11
1.3.1 Sphingolipid metabolism of eukaryotic cells 11
1.3.2 Sphingolipid acquisition of *Chlamydia* 12
1.3.3 The role of CERT for chlamydial sphingolipid acquisition 13
1.3.4 CERT-stabilized ER-inclusion-membrane contact sides 14
1.3.5 The role of other lipids during chlamydial infections 16
1.4 Aim of this study 17
2 Material and Methods 18
2.1 Material 18
2.1.1 Organisms 18
2.1.2 Nucleic Acids 18
2.1.3 Media, Buffers, and Solutions 20
2.1.4 Antibodies 22
2.1.5 Chemicals 23
2.1.6 Kits and Enzymes 25
2.1.7 Consumables 26
2.1.8 Equipment 28
2.1.9 Software 28
2.2 Methods 30
2.2.1 Cell culture methods 30
2.2.2 Microscopy analysis 32
2.2.3 Nucleic acid techniques 36

2.2.4 Protein techniques 39
2.2.5 Lipid techniques 40
2.2.6 Computational methods 42
2.2.7 Statistical Analysis 42
3 Results 43
3.1 Analysis of intracellular development of *C. psittaci* indicates that massive infectious EB release can initiate at 40 h pi 43
3.1.1 Infectious progeny formation during the intracellular development of *C. psittaci* starts at 26 h pi and reaches its maximum between 40 h pi and 48 h pi 43
3.1.2 RB-to-EB redifferentiation of *C. psittaci* starts at 24 h pi and EBs accumulate within the inclusion at 42 h pi 44
3.1.3 Localization of chlamydial HSP60 and IncA during the intracellular development of *C. psittaci* confirms that at 42 h pi egress could initiate 46
3.2 *Chlamydia*-containing spheres (CCS) are a novel and predominant form of egress by the pathogen *C. psittaci* 49
3.2.1 *C. psittaci* egresses from the cellular monolayer through formation of *Chlamydia*-containing spheres (CCS) 49
3.2.2 *C. psittaci* CCS formation is fundamentally different to *C. trachomatis* extrusion formation 51
3.2.3 Ultrastructural characterization of *C. psittaci* egress by TEM 53
3.2.4 CCS formation as egress form of *C. psittaci* occurs in lung cell infections 55
3.2.5 CCS formation is the predominant egress pathway of *C. psittaci* and is also present, but less frequent for *C. trachomatis* 56
3.2.6 The occurrence and the frequency of CCS formation and extrusion formation as non-lytic egress pathways *C. trachomatis* are time-dependent 60
3.2.7 The exposure of sphingolipids in the *C. psittaci* inclusion membrane to the cytosol precedes its destabilization and subsequent CCS formation 60
3.2.8 Similar to apoptotic cells, CCS expose PS to the outer membrane leaflet 62
3.2.9 CCS differ from late apoptotic cells by retaining their membrane barrier function for different non-permeable dyes 64
3.2.10 CCS differ from apoptotic cells by lacking fragmentation of the nucleus 65
3.2.11 CCS formation correlates in time with a proteolytic activity specific for a DEVD-containing substrate, but not with caspase-3 activation 66
3.2.12 Caspase inhibitors do not block CCS formation and the proteolytic cleavage of the DEVD-containing substrate 68
3.2.13 CCS formation depends on extracellular calcium concentration 70
3.2.14 Varying extracellular calcium concentrations affect intracellular calcium increase and proteolytic DEVD-cleavage in late infections 72
3.2.15 A peak in the cytosolic calcium concentration is followed by a rapid increase in DEVD-cleaving activity and CCS formation 74
3.3 Recruitment of the cellular lipid transport protein CERT to *C. psittaci* inclusions regulates the timing of bacterial egress 77

3.3.1 CCS formation of *C. psittaci* temporally correlates with a reduction in CERT recruitment 77
3.3.2 Localization of CERT regulates CCS formation 79
3.3.3 CERT-KO induces early CCS formation by a sequence of events analogous to mature CCS 81
3.3.4 Similar to mature CCS formation, CERT-KO-induced early CCS formation is calcium-dependent 83
3.3.5 CERT-KO induces the formation of RB-containing, non-infectious CCS 85
3.4 Lipid composition of *C. psittaci* infections 87
3.4.1 Middle and late *C. psittaci* infections have distinct lipidomes 88
3.4.2 Specific phospholipid species are increased in *C. psittaci*-infected cells 89
3.4.3 Direct comparison of the lipidome of *C. psittaci*-infected HeLa cells during RB replication and prior to egress showed an increase of C14-containing phospholipid species late in infection 91
3.4.4 Phospholipids increased in infection likely originate from both the bacteria and host 93
4 Discussion 96
4.1 CCS formation is a unique and novel chlamydial egress mechanism that can be linked with the specific biology of *C. psittaci* 97
4.1.1 CCS formation differs fundamentally from extrusion formation of *C. trachomatis* 98
4.1.2 Common features and differences of lytic egress, CCS formation, and extrusion formation 99
4.1.3 The role of the different chlamydial egress mechanisms for host-pathogen interaction 101
4.1.4 The potential role of the different chlamydial egress mechanisms for chlamydial pathogenicity 102
4.2 CCS formation differs substantially from known host cell death pathways and egress pathways of other intracellular pathogens 104
4.2.1 Comparison of CCS formation with host cell death 104
4.2.2 Comparison of CCS formation with egress pathways of other intracellular pathogens 105
4.3 The stabilization of the inclusion membrane is critical for regulation of chlamydial egress 106
4.3.1 The role of CERT-stabilized MCS for the stability of the inclusion membrane 106
4.3.2 The role of sphingolipids for the stability of the inclusion membrane 108
4.3.3 The role of phospholipids for the stability of the inclusion membrane 109
4.4 Conclusion 111
5 References 112
6 Appendix 125
6.1 Supplementary Figures 125
6.2 Supplementary Tables 130

6.3 List of abbreviations 137
6.4 List of Figures 139
6.5 List of Tables 141
Publications xiii
Articles xiii
Talks xiv
Curriculum Vitae xv

Zusammenfassung

Zur Gattung *Chlamydia* werden elf pathogene Arten gezählt, darunter der humanspezifische, sexuell übertragbare Erreger *C. trachomatis* und der zoonotische Erreger *C. psittaci*, der im Menschen atypische Lungenentzündungen hervorrufen kann. Während ihres intrazellulären Entwicklungszyklus liegen Chlamydien in zwei verschiedenen Zustandsformen vor: als infektiöse Elementarkörperchen (EK) oder als stoffwechselaktive, sich teilende Retikularkörperchen (RK). Zu Beginn der intrazellulären Entwicklung treten EK in die Wirtszelle ein, dort differenzieren sie in einem membranumschlossenen Kompartiment, der bakteriellen Inklusion, zu RK. Die RK entziehen dem Wirt Nährstoffe, um sich zu vermehren. Nachdem sie zu EK redifferenziert sind, treten sie aus der Wirtszelle aus und können im Anschluss weitere Zellen infizieren. Für den Wirtszellaustritt von Chlamydien waren in der Vergangenheit zwei Wege beschrieben: Der lytische Austritt und die Chlamydien-spezifische, nicht-lytische Bildung von Extrusionen.

In dieser Arbeit wurde zunächst die intrazelluläre Entwicklung von *C. psittaci* in HeLa-Zellen untersucht. Dabei wurde gezeigt, dass *C. psittaci* ca. 12 Stunden nach Beginn der Infektion zu RK differenziert ist und beginnt, sich zu teilen. Nach ca. 24 Stunden begannen die ersten RK, zu EK zu redifferenzieren. Nach ca. 34 Stunden lagen EK, RK und intermediäre Formen von *C. psittaci* in ähnlicher Anzahl vor, während ab ca. 42 Stunden nach Beginn der Infektion vor allem EK vorlagen und die Infektiosität ihr Maximum erreichte, sodass dieser Zeitpunkt für weitere Untersuchungen des Wirtszellaustritts gewählt wurde.

In dieser Arbeit durchgeführte Untersuchungen des Wirtszellaustritts zeigen, dass *C. psittaci* vor allem einen zuvor unbeschriebenen Mechanismus zum Wirtszellaustritt nutzt: die Bildung von *Chlamydia-containing spheres* (CCS). CCS-Bildung beginnt mit der proteolytischen Spaltung eines Tetrapeptids der Sequenz Aspartat-Glutamat-Valin-Aspartat (DEVD) innerhalb der chlamydialen Inklusion. Danach steigt die Calciumkonzentration im Zytosol der infizierten Epithelzellen an und die Plasmamembran der Wirtszelle bildet Membranbläschen aus. Auch die Inklusionsmembran wird destabilisiert und in der ganzen Zelle ist sodann die Spaltung des Tetrapeptids zu beobachten. Indem sich die komplette Wirtszelle aus dem Zellverband herauslöst, wird die CCS-Bildung vollendet. Die mit infektiösen Chlamydien und zellulären Bestandteilen wie z.B. dem degenerierten Zellkern gefüllte CCS ist also nur von einer Membran umhüllt, die Phosphatidylserin präsentiert, aber dabei undurchlässig für Farbstoffe wir Trypanrot oder SYTOX Green bleibt. Interessanterweise konnte bei *C. psittaci*-Infektionen keine Extrusionsbildung beobachten werden, während CCS-Bildung prädominant war, und es konnte feststellt werden, dass auch *C. trachomatis* in der Lage ist, CCS zu bilden.

Des Weiteren wurden in dieser Arbeit Untersuchungen zur Stabilisierung der Inklusionsmembran von *C. psittaci* mittels Rekrutierung des humanen *ceramide transport*

protein (CERT) während der intrazellulären Entwicklung von *C. psittaci* und zu ihrer Destabilisierung während der CCS-Bildung durchgeführt. Dabei wurde gezeigt, dass CERT während der intrazellulären Entwicklung rekrutiert wird, diese Rekrutierung aber zu späten Infektionszeitpunkten vor der CCS-Bildung verloren geht. Ein früherer Verlust von CERT an der Inklusionsmembran führte zu einer verfrühten Bildung von unreifen CCS, die nicht-infektiöse Bakterien enthalten.

Abschließend wurde die Lipidzusammensetzung von *C. psittaci*-infizierten HeLa-Zellen während der intrazellulären Entwicklung und vor dem Wirtszellaustritt untersucht. Dabei konnte gezeigt werden, dass sowohl während der intrazellulären Entwicklung als auch vor dem Wirtszellaustritt vermehrt Phospholipidspezies mit gesättigten, ungradezahligen Fettsäureketten zu finden sind, die also ein allgemeines Merkmal für die Infektion darstellen. Vor dem Wirtzellaustritt ist die Konzentration einzelner Phospholipidspezies mit kürzeren Fettsäuren stark erhöht, die als ein spezifisches Merkmal für späte Infektionen dienen können.

Insgesamt zeigt diese Studie, dass der chlamydiale Wirtszellaustritt mittels CCS-Bildung ein bedeutender Teil des chlamydialen Entwicklungszyklus ist. Dieser ist sowohl von vermutlich bakteriellen Faktoren wie einer DEVD-spaltenden Protease oder von einem CERT-rekrutierenden Faktor als auch von Wirtszellfaktoren wie dem Ceramidtransporter CERT, dem zellulären Calcium-Haushalt oder dem Lipidstoffwechsel abhängig. Der zoonotische Erreger *C. psittaci* und der humanspezifische Erreger *C. trachomatis* nutzen unterschiedliche Strategien zum Wirtszellaustritt, wobei CCS-Bildung bei *C. psittaci* prädominant ist. Dies lässt vermuten, dass auch die unterschiedliche Biologie der verschiedenen Chlamydien-Spezies inklusive Wirtsspektrum, Strategien zum Schutz vor zellulären Abwehrmechanismen und die bakterielle Pathogenität von der Wirtszellaustrittsstrategie beeinflusst werden.

Abstract

The genus *Chlamydia* comprises eleven pathogenic species, including the human specific, sexually transmitted pathogen *C. trachomatis* and the zoonotic pathogen *C. psittaci*, that causes lung infections. During their intracellular development, *Chlamydia* exist in two distinct forms, the infectious elementary bodies (EBs) and the metabolizing and replicating reticulate bodies (RBs). Intracellular development initiates with the invasion of EBs, which differentiate to RBs inside of a membrane-bound compartment, the chlamydial inclusion. RBs abuse host cellular metabolites to replicate. After redifferentiation to EBs, they egress from the host to start a new round of infection. Two chlamydial egress forms were described in the past: Lytic egress and *Chlamydia*-specific, non-lytic extrusion formation.

In the first part of this study, the intracellular development of *C. psittaci* in HeLa cells was investigated. It was shown that EB to RB differentiation was completed at 12 hours post infection (h pi) and RB replication initiates. At 24 h pi, RB redifferentiation to EB started and at 34 h pi, similar amounts of EBs, RBs and intermediate forms were present in the inclusion. Starting at 42 h pi, most of the bacteria were in EB form and the infectivity reached a maximum, suggesting to perform egress studies at this time point.

In the following part of this study, it was shown that *C. psittaci* uses a previously not characterized egress pathway, the formation of *Chlamydia*-containing spheres (CCS). CCS formation is a sequential process starting with proteolytic cleavage of an Aspartate-Glutamate-Valine-Aspartate (DEVD) tetrapeptide-containing substrate that can be detected inside of the chlamydial inclusions, followed by an increase in the intracellular calcium concentration of the infected epithelial cell. Subsequently, blebbing of the plasma membrane begins, the inclusion membrane destabilizes and the proteolytic cleavage of a DEVD-containing substrate increases rapidly within the whole infected cell. Finally, infected, blebbing cells detach and leave the monolayer thereby forming CCS. CCS contain infectious progeny and morphologically impaired cellular organelles and are surrounded by a phosphatidyl serine exposing membrane with specific barrier functions for TrypanRed or SYTOX Green. Interestingly, no extrusion formation was observed for *C. psittaci* infections, while CCS formation was the predominating egress type. In addition, CCS formation was also observed for *C. trachomatis*.

Next, investigations about the inclusion membrane stabilization during intracellular development mediated by the human ceramide transport protein CERT and about the inclusion membrane destabilization during CCS formation were realized. It was shown that CERT is recruited to the bacterial inclusion during intracellular development, while at late infection timepoints before CCS formation, this recruitment was not observed. An early lack of CERT at the inclusion membrane drove the formation of premature CCS containing non-infectious bacteria.

Finally, the lipidome of *C. psittaci*-infected HeLa cells during intracellular development and before host cell egress was investigated. It was shown that both, during intracellular development and during egress, increased concentration of phospholipid species with saturated, odd chain fatty acids were found, suggesting that they are a general characteristic of chlamydial infection. Before egress, the amount of specific phospholipids species comprising shorter fatty acids was increased, suggesting that they are a specific characteristic of late infections.

Taken together, this study shows that egress by CCS formation is a relevant part of the chlamydial developmental cycle. CCS formation depends on both, bacterial and host cellular factors, as a putative bacterial DEVD-cleaving protease and a CERT-recruiting factor or as the ceramide transporter CERT, calcium signaling and lipid metabolism, respectively. The zoonic pathogen *C. psittaci* and the human-specific pathogen *C. trachomatis* apply different egress strategies with CCS formation being the predominant egress pathway of *C. psittaci*. This suggests that the different biology of the different *Chlamydia* spp. including host tropism, protection from host cell defense mechanisms or bacterial pathogenicity could possibly be linked to different egress strategies.

1 Introduction

1.1 The family of *Chlamydiacea* within the order of *Chlamydiales*

The group of *Chlamydiales* are an order of Gram-negative, obligate intracellular bacteria sharing a biphasic developmental cycle (Bachmann et al., 2014; Bayramova et al., 2018). Its members act as pathogens or symbionts of several eukaryotic species ranging from humans to amoeba (Bachmann et al., 2014; Bayramova et al., 2018). Beside an increasing number of families of *Chlamydia*-related bacteria, the family of *Chlamydiacea* is the currently best-studied family in the order of *Chlamydiale*s. It includes important human and animal pathogens as for example *Chlamydia trachomatis*, the causative agent of the most common sexually transmitted bacterial disease worldwide and the causing agent of blinding trachoma, or *Chlamydia psittaci*, the causative agent of the worldwide occurring zoonotic disease psittacosis (Bachmann et al., 2014; Bayramova et al., 2018; Knittler et al., 2014; Knittler & Sachse, 2015; S. M. Murray & McKay, 2021; Radomski et al., 2016; Stephens et al., 2009; Sturd & Rucks, 2023; World Health Organization, 2016).

1.1.1 Taxonomy of *Chlamydiacea*

Within the family of *Chlamydiacea*, 11 species are described which are currently grouped within one genus, the genus *Chlamydia*. However, in the past, *Chlamydiacea* were separated into two genera, *Chlamydia* and *Chlamydophila*, based on 16S ribosomal ribonucleic acid sequences (Everett et al., 1999), which were ten years later reunited based on genome comparisons (Stephens et al., 2009). The species within the genus of *Chlamydia* are pathogens of animals and humans, including species infecting a wide range of hosts, but also species-specific pathogens (see Table 1). In this study, the focus will be on *C. psittaci* and *C. trachomatis*.

Table 1: Overview of *Chlamydia*-species (Bachmann et al., 2014; Borel & Sachse, 2023). Between 1999 and 2009, species marked with an asteric (*) were grouped as *Chlamydophila* and species marked with a cross (†) were grouped as *Chlamydia* (Everett et al., 1999).

Chlamydia	**Host**	**Infection/Disease**
Human-specific pathogens		
C. trachomatis†	Humans	ocular and genital infections
Broad host-ranged pathogens		
*C. pneumoniae**	Mammals, reptiles	respiratory infections
*C. psittaci**	Avian species and mammals	respiratory infections
C. avium	Avian species, zoonotic potential under debate	asymptomatic infections
C. gallinacea	Avian species	asymptomatic infections

Chlamydia	Host	Infection/Disease
*C. pecorum**	Ruminants, swine, koala	respiratory and genital infections
*C. abortus**	Ruminants, swine, humans	abortion and fetal death
Animal-specific pathogens		
*C. caviae**	Guinea pigs, with zoonotic potential	ocular and genital infections
*C. felis**	Cats, with zoonotic potential	ocular and respiratory infections
C. muridarum†	Mice	ocular and genital infections
C. suis†	Swine, zoonotic potential under debate	ocular and respiratory infections

1.1.2 Relevance of *Chlamydia psittaci*

C. psittaci is the causative agent of the zoonotic disease psittacosis. Its primary host are avian species, which can transmit *C. psittaci* to mammal species including humans via direct contact or inhalation of infected material (Knittler et al., 2014; Knittler & Sachse, 2015; Radomski et al., 2016). In humans, infections with *C. psittaci* are typically established in the respiratory tract with symptoms ranging from asymptomatic cases over influenza-like symptoms including fever, chills, headache, coughing, and dyspnea to severe disease and even death (Knittler et al., 2014; Knittler & Sachse, 2015; Radomski et al., 2016). Beside of transmission from birds to humans, cases of human-to-human-transmission are reported (Dembek et al., 2023; Z. Zhang et al., 2022).

Psittacosis can be diagnosed by polymerase chain reaction (PCR) and/or serological testing including enzyme linked immunosorbent assay (ELISA), immunofluorescence tests and immune-peroxidase tests (Dembek et al., 2023). As laboratory tests are difficult and thus, often specialized laboratories need to perform those tests, definitive diagnosis is often not made in mild cases. However, this leads to an estimated misdiagnosis rate of psittacosis of 50-80% (Dembek et al., 2023; Liu et al., 2023).

Today, infections with *C. psittaci* can be treated with antibiotics, typically with doxycycline or tetracycline, which begins to regress the symptoms after 24 to 48 h (Dembek et al., 2023). Thus, the mortality rate of psittacosis is about 1%, as doxycycline or tetracycline resistance was not detected in *C. psittaci* in vivo until now (Binet & Maurelli, 2007; Borel et al., 2016; Vanrompay et al., 2018). However, the mortality rate of psittacosis was up to 50% in the 20th century prior to the introduction of antibiotics into clinical use (Dembek et al., 2023; Weston et al., 2023).

Due to the high mortality rates without antibiotic treatment, *C. psittaci* was studied as a potential bioweapon by different countries including the USA, the former Soviet Union and China (Dembek et al., 2023; Hay, 1999; Leitenberg, 2001). In the last years, methods to genetically modify *Chlamydia* spp. were established, including the generation of genetically modified *C. psittaci* using a plasmid shuttle vector system adapted from *C. trachomatis* (Shima et al., 2020; Wan et al., 2023). In a recent publication, Dembek et al. speculate that this technique could also be used to insert antimicrobial resistance genes to *C. psittaci* or to enhance infectivity or immune evasion, so they recommend disease recognition, improved laboratory testing methods and public health awareness (Dembek et al., 2023).

Interestingly, a psittacosis outbreak in Germany, but also in Austria, Denmark, Sweden and the Netherlands was reported recently (at the end of 2023 and at the beginning of 2024) (Singer et al., 2024; World Health Organization, 2024). During this outbreak, five deaths (four in Denmark and one in the Netherlands) were reported (World Health Organization, 2024). However, the reasons for this outbreak remain unclear (Singer et al., 2024).

1.1.3 Relevance of *Chlamydia trachomatis*

The human-specific pathogen *C. trachomatis* is the causative agent of three different kinds of diseases (C. Elwell et al., 2016; S. M. Murray & McKay, 2021; Sturd & Rucks, 2023). Based on the kind of disease they cause, *C. trachomatis* strains are grouped into three biovars: The trachoma biovar (serovar A-C) causes blinding trachoma, the leading cause of preventable blindness, the urogenital tract biovar B (serovars D-K) infects the genital tract and causes the most common sexually transmitted bacterial disease worldwide, and the lymphogranuloma venereum biovar (serovar L1-L3) causes invasive urogenital and anorectal infection (C. Elwell et al., 2016; S. M. Murray & McKay, 2021; Sturd & Rucks, 2023). The World Health Organization (WHO) estimated that 128.5 million new infections occur with *C. trachomatis* in 2020 worldwide among adults aged 15 to 49 years (World Health Organization, 2023).

The trachoma biovar of *C. trachomatis* is estimated by the WHO to cause over 40 million active cases of trachoma and 1.3 million blindness people (Faris et al., 2019; Hu et al., 2013). It is mainly found in poor areas of developing countries (Faris et al., 2019; Hu et al., 2013). There, in trachoma endemic regions, children experience repeating episodes of infection that can cause severe scarring complications in the conjunctiva of the eye which can end up in blindness (Hu et al., 2013).

The urogenital tract biovar of *C. trachomatis* causes different symptoms in the genital tract of men and woman. In men, it causes urethritis and epididymitis, but is not associated with infertility (Bébéar & de Barbeyrac, 2009; S. M. Murray & McKay, 2021). In contrast, up to 80% of infections in women are asymptomatic. However, if the upper genital tract is infected, severe complications can occur including pelvic inflammatory disease, infertility, ectopic pregnancy,

and chronic pelvic pain (Bébéar & de Barbeyrac, 2009; C. Elwell et al., 2016; S. M. Murray & McKay, 2021).

The lymphogranuloma venereum biovar of *C. trachomatis* is also sexually transmitted, but can infect macrophages and thus, disseminate to the lymph nodes, causing invasive urogenital or anorectal infections (Banhart et al., 2019; C. Elwell et al., 2016; Jury et al., 2023). It has become particularly associated with human immunodeficiency virus (HIV)-infected men who have sex with men (Childs et al., 2015; de Vrieze & de Vries, 2014; S. M. Murray & McKay, 2021).

Case numbers broken down into the urogenital tract biovar and the lymphogranuloma venereum biovar of *C. trachomatis* are not available as many countries including Germany do not report *C. trachomatis* infections. However, in Germany reporting of infections with the lymphogranuloma venereum biovar of *C. trachomatis* has started in 2022 (Robert Koch-Institut, 2023; World Health Organization, 2023).

C. trachomatis infections are normally diagnosed by nucleic acid amplification tests, which are highly sensitive and specific, can be automated and are commercially available (Bébéar & de Barbeyrac, 2009). Other tests as cell culture, antigen-based detection methods or nucleic acid hybridization tests are also available, but not common in routine diagnostics (Bébéar & de Barbeyrac, 2009). Similar to *C. psittaci* infections, *C. trachomatis* infections can be treated with antibiotics, preferentially with doxycycline or with azithromycin (S. M. Murray & McKay, 2021; Sturd & Rucks, 2023).

1.1.4 The developmental cycle of *Chlamydia*

All chlamydial species share a biphasic developmental cycle. During this developmental cycle, *Chlamydia* exist as infectious, osmotically stable, but mostly metabolically inactive EBs with about 0.3 µm in size or as non-infectious, osmotically instable, intracellular replicating RBs with about 1 µm in size (Banhart et al., 2019; Knittler & Sachse, 2015; Radomski et al., 2016).

The developmental cycle of *Chlamydia* spp. is shown in Figure 1. To infect a host cell, EBs attach to the host cell plasma membrane and invade into the host cell via the endocytosis or phagocytosis pathway (Banhart et al., 2019; C. Elwell et al., 2016). This entry process is driven by complex interactions of bacterial adhesins and host cell receptors. Of importance for the adhesion process are for example chlamydial polymorphic membrane proteins, outer membrane complex protein B and a lipid-dependent internalization promoting protein, which interact with host cell factors as glycosaminoglycans, epidermal growth factor receptors, or other receptors at the host cell membrane and are characterized especially for *C. trachomatis* and *C. pneumoniae* (Becker & Hegemann, 2014; Fadel & Eley, 2007; Favaroni & Hegemann, 2021; Galle et al., 2019; Luczak et al., 2016; Mölleken et al., 2013; Mölleken & Hegemann,

2008; Stephens et al., 2001). An unknown number of other currently uncharacterized bacterial adhesins seem to be involved in this process (Hegemann & Mölleken, 2012; Mehlitz & Rudel, 2013). In addition, *Chlamydia* spp. secrete effector proteins into the host cell by type 3 secretion that modulate the membrane and cytoskeleton of the host cell to facilitate endocytic EB uptake. For *C. trachomatis*, TarP (translocated actin recruiting protein) and TmeA (translocated membrane effector A) are well characterized key factors of this process, while for *C. pneumoniae*, Cpn0572, SemC and SemD fulfill similar functions (Aranjuez et al., 2022; Braun et al., 2019; Clifton et al., 2004; Faris et al., 2020; Hänsch et al., 2020; Höhler et al., 2024; Jewett et al., 2006, 2010; Kocher et al., 2024; Romero & Carabeo, 2024; Spona et al., 2023).

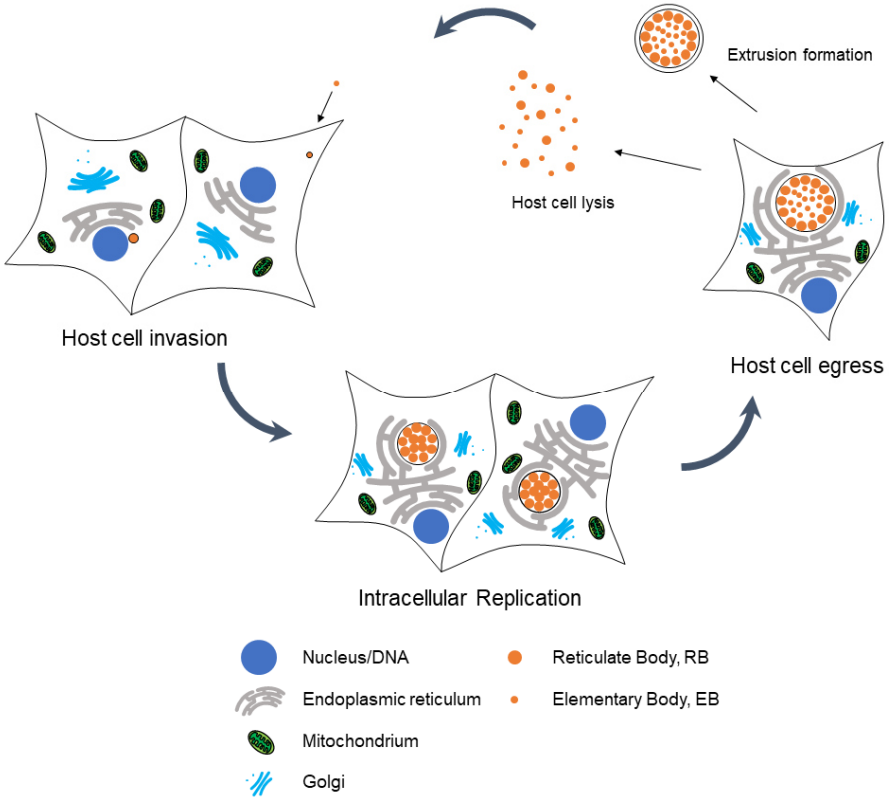

Figure 1. The developmental cycle of *Chlamydia* spp. Chlamydial elementary bodies (EBs) attach and invade into the host cell via endocytosis. Subsequently, inside of the chlamydial inclusion, they differentiate into reticulate bodies (RBs) and modify the host cell by the secretion of effector proteins. RBs replicate inside of the mature inclusion and then rediffeentiate to EBs. These infectious EBs egress from the host cell via extrusion formation or via host cell lysis to start a new round of infection. Modified from Scholz & Heuer, 2024.

Inside of the endocytic vesicle, *Chlamydia* establish their intracellular replication niche, the inclusion, by type 3 secretion of effector proteins into the host cell cytosol and into the inclusion membrane (Moore & Ouellette, 2014). These effector proteins manipulate the host cell metabolism and reorganize cellular organelles, as for example sphingolipids are taken up by the chlamydial inclusion and the host cell Golgi apparatus is fragmented (Christian et al., 2011; Heuer et al., 2009; Heymann et al., 2013; Koch-Edelmann et al., 2017; Rejman Lipinski et al., 2009). Simultaneously, EBs differentiate to RBs, which then metabolize and rapidly replicate (Abdelrahman et al., 2016). After massive RB replication, RBs redifferentiate into EBs. Finally,

EBs egress from the infected host cell either by host cell lysis or by non-lytic extrusion formation (C. Elwell et al., 2016; Hybiske & Stephens, 2007; Zuck et al., 2016).

The chlamydial egress mechanisms, host cell lysis and extrusion formation, are mainly studied for *C. trachomatis*. To perform host cell lysis, the inclusion membrane is destabilized with involvement of proteases, followed by calcium-dependent permeabilization of the host cellular plasma membrane (Hybiske & Stephens, 2007). In contrast, extrusion formation is described as a cytoskeleton-dependent packaged release process, where both, the inclusion membrane and the plasma membrane, remain intact and infectious bacteria are released without host cell death (Hybiske & Stephens, 2007; Lutter et al., 2013; Nguyen et al., 2018).

Compared to *C. trachomatis* egress, *C. psittaci* egress remains rarely studied (Knittler & Sachse, 2015; Moulder, 1991; Radomski et al., 2016). However, some findings were obtained in the past regarding late development and subsequent egress of *C. psittaci*. Prior to host cell egress, *C. psittaci* RBs redifferentiate to EBs (Bedson & Bland, 1932, 1934; Rockey et al., 1996). During *C. psittaci* lytic egress, lysosomal enzymes are released into the host cell cytosol, act as lytic agents and lyse both membranes, inclusion and plasma membrane (Kordová et al., 1971; Rockey et al., 1996; Todd & Storz, 1975). It was suggested that also apoptosis is involved into lysis of *C. psittaci*-infected cells (Gibellini et al., 1998). However, there are also indications that *C. psittaci* performs non-lytic egress (Doughri et al., 1972; Zuck et al., 2016). During *C. psittaci* infection of calves, Doughri et al. observed expulsion of whole infected cells into the intestinal lumen and extrusion formation beside lytic egress by electron microscopy of intestinal epithelial cells (Doughri et al., 1972). Accordingly, Zuck et al. observed extrusions in the supernatant of *C. psittaci*-infected HeLa cells (Zuck et al., 2016). Thus, it is crucial to continue research on egress, especially non-lytic egress of *C. psittaci* to get insights into pathogen spreading and pathogenicity mechanisms.

1.2 Egress of intracellular pathogens

1.2.1 Overview

Egress of intracellular pathogens is of general importance for the host because it usually induces the inflammatory response of the host (Flieger et al., 2018; Frischknecht & Pradel, 2024). In comparison to other life cycle phases of intracellular pathogens as host cell entry processes or intracellular development, host cell egress is still understudied as it was historically understood as a passive process (Frischknecht & Pradel, 2024). However, today it is known that for most pathogens egress is an orchestrated, temporally defined process driven by specific proteins and following defined mechanisms (Flieger et al., 2018; Frischknecht & Pradel, 2024). Thus, the identification and characterization of novel egress strategies continues and enables us to understand how pathogens interact with the inflammatory response of the host and to develop strategies to combat them (Flieger et al., 2018; Friedrich et al., 2012; Frischknecht & Pradel, 2024).

In principle, egress is defined as the release of progeny to infect a new host cell. This can be realized by different egress mechanisms. The best studied group of egress mechanisms is “host cell lysis” (Frischknecht & Pradel, 2024; Hybiske & Stephens, 2015). However, it is not even clearly defined which egress mechanisms belong to this group (Flieger et al., 2018; Friedrich et al., 2012; Frischknecht & Pradel, 2024; Hybiske & Stephens, 2015). In general, during lytic egress mechanisms, intracellular pathogens somehow destabilize and permeabilize their surrounding membrane, thereby forcing their release (Friedrich et al., 2012; Frischknecht & Pradel, 2024; Hybiske & Stephens, 2015). Thus, egress mechanisms where microbial molecules as pore-forming proteins or proteases perforate membranes are generally count as “host-cell lysis” (Frischknecht & Pradel, 2024). However, which further mechanisms should be included into this group is still controversially discussed (Flieger et al., 2018; Friedrich et al., 2012; Frischknecht & Pradel, 2024).

Friedrich et al. (2012) include egress mechanisms where the necrotic or pyroptotic cell death pathway are abused to destabilize and permeabilize the host cell membrane as “egress by damaging the host cell” next to pore-forming activities and proteases and in contrast to “egress by non-lytic mechanisms” and “egress by reversion into exocytic/exocytic-like pathways” (Friedrich et al., 2012). Similar, Hybiske and Stephens (2015) include egress mechanisms where the apoptotic or pyroptotic cell death pathway are abused as “egress by lysis of the host cell” beside pore-forming proteins and proteases (Hybiske & Stephens, 2015). In contrast, Flieger et al. (2018) defined a group of “egress by induction of programmed host cell death” separated from “egress by active (lytic) host cell destruction”, a classification that was taken over by Frischknecht and Pradel (Flieger et al., 2018; Frischknecht & Pradel, 2024).

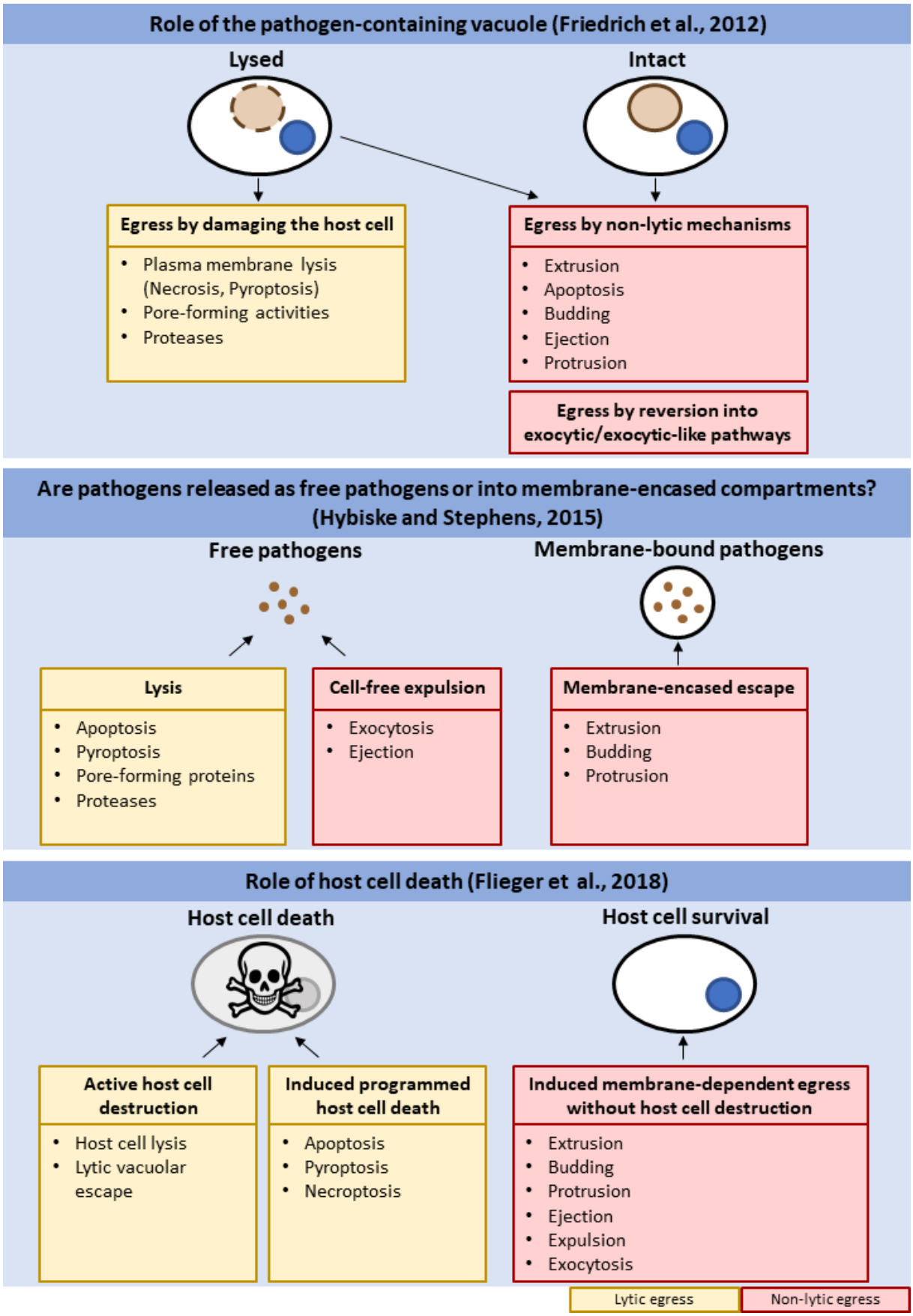

Figure 2. Different concepts to categorize lytic and non-lytic egress strategies of different intracellular pathogens. Friedrich et al. (2012) distinguished between strategies where the pathogens remain within a vacuole and those where the pathogens leave the vacuole before egress. Hybiske and Stephens (2015) asked whether the pathogens are released as free pathogens or within membrane-encased compartments. Flieger et al. (2018) distinguished between pathways where the host cell survives and those which end up in host cell death.

Beside host cell lysis, a diverse group of other egress mechanisms exist. As already described for the term “host cell lysis”, also the arrangement of these “non-lytic egress pathways” into groups is inconsistent and follows different concepts (Flieger et al., 2018; Friedrich et al., 2012; Frischknecht & Pradel, 2024; Hybiske & Stephens, 2015). An overview about the different concepts to categorize egress strategies is given in Figure 2.

1.2.2 Non-lytic egress

As it is not even clearly defined which egress mechanisms belong to the group of mechanisms counted as “egress by host cell lysis”, it is even more challenging to consider “non-lytic egress pathways” and to further categorize these egress mechanisms (Figure 2) (Flieger et al., 2018; Friedrich et al., 2012; Frischknecht & Pradel, 2024; Hybiske & Stephens, 2015).

An attempt by Friedrich et al. (2012) distinguish between egress by vacuole lysis followed by non-lytic egress from the cytosol on the one hand, including for example apoptosis related mechanisms, ejection or protrusion, and on the other hand egress while remaining within a vacuole without membrane damage, including reversion into exocytic/exocytic-like pathways or extrusion formation (Friedrich et al., 2012). This categorization based on the idea that key distinction factor is the question if the pathogen-containing vacuole is lysed before egress or not (Friedrich et al., 2012).

In contrast, to further categorize non-lytic egress Hybiske and Stephens (2015) asked the question whether the pathogens are released into membrane-encased compartments or as free pathogens (Hybiske & Stephens, 2015). Thus, they termed one group of non-lytic egress pathways “membrane encased escape”, including extrusion, actin-based protrusion, and budding, while the other group was termed “egress by cell-free expulsion”, including exocytosis and ejection (Hybiske & Stephens, 2015). This categorization shifts the focus away from the egress mechanism itself towards the following aspects regarding the inflammatory response of the host and the following infection of neighboring host cells. During egress by “cell-free-expulsion”, the intracellular pathogens are released to the extracellular space. In contrast, during “membrane encased escape”, pathogens are released into a membranous compartment to spread between cells without contact to the extracellular environment. This could protect the pathogen from extracellular immune defense mechanisms (Flieger et al., 2018; Friedrich et al., 2012; Hybiske & Stephens, 2015).

Another different categorization was made by Flieger et al. (2018). They highlighted the role of induced programmed host cell death as group of egress mechanisms, including apoptosis, pyroptosis and necroptosis. Other non-lytic egress mechanisms were put into one group named “induced membrane-dependent egress without host cell destruction”, which includes extrusion, budding, actin-mediated protrusion, ejection, expulsion, and exocytosis (Flieger et al., 2018).

Taken together, the challenges during categorization of especially non-lytic egress mechanisms demonstrates the need of further research on this topic.

1.2.3 Egress by apoptotic host cell death

Interestingly, 25 years ago it was reported that *C. psittaci* infection causes the induction of apoptosis at late infection time points (Gibellini et al., 1998). However, a link of *Chlamydia*-induced apoptosis to *C. psittaci* egress was not proposed. In general, the findings about the role of different cell death pathways during chlamydial infections is still controversial and the role of apoptosis during chlamydial infections is still under investigation (Z. He et al., 2022; Kerr et al., 2017; Matsuo et al., 2019; Sixt, 2021; Sixt et al., 2019; Waguia Kontchou et al., 2022; Weber et al., 2017).

Nevertheless, apoptosis-related egress mechanisms have been reported for other intracellular pathogens as for example for the Gram-positive bacterium *Mycobacterium marinum*, for the protozoan parasite *Leishmania* spp., for the fungal pathogen *Cryptococcus neoformans* and for the Gram-negative bacterium *Coxiella burnetii* (Davis & Ramakrishnan, 2009; De Leon-Rodriguez et al., 2018; Schulze-Luehrmann et al., 2024; van Zandbergen et al., 2004).

Several of these strategies are associated with masking pathogens by encapsulating them within apoptotic bodies, which supports their subsequent uptake by macrophages (Davis & Ramakrishnan, 2009; van Zandbergen et al., 2004). This strategy is used by *M. marinum* for egress from macrophages and by *L. major* for egress from polymorphonuclear neutrophil granulocytes (Davis & Ramakrishnan, 2009; van Zandbergen et al., 2004). Interestingly, *C. trachomatis* follows a similar strategy during egress by extrusion formation, which also present phosphatidyl serine (PS) and thereby force extrusion uptake by macrophages (Zuck et al., 2017).

In addition, apoptosis-related egress strategies exist where pathogens are released without being covered by a membrane (De Leon-Rodriguez et al., 2018; Schulze-Luehrmann et al., 2024). This is the case for egress of *C. neoformans* from infected macrophages by phagolysosomal membrane permeabilization (PMP) and *C. burnetii* egress from epithelial and endothelial cells (De Leon-Rodriguez et al., 2018; Schulze-Luehrmann et al., 2024). In both cases, apoptosis is related with pathogen egress, but apoptosis is not completed and also other mechanisms seem to be involved.

1.3 Lipids during chlamydial infections

During infections with bacterial pathogens, lipids are important for the bacteria as energy source, metabolites, and signaling molecules, but also as parts of membranes that they have to overcome or that they modify (Banhart et al., 2019; Prado et al., 2023). In contrast to other bacterial pathogens, *Chlamydia* spp. are able to obtain sphingolipids from the host cell (Hackstadt et al., 1995, 1996). Thus, during lipid studies of chlamydial infections, there was a reasonable focus on sphingolipids and on the interaction with the host cellular sphingolipid metabolism in the past, which promoted the general understanding of sphingolipid metabolism and transport in infected as well as uninfected human cells (Banhart et al., 2019).

1.3.1 Sphingolipid metabolism of eukaryotic cells

Sphingolipids are a structurally diverse group of polar lipids and an important component of eukaryotic cell membranes (Banhart et al., 2019; Quinville et al., 2021). They contribute to different cellular functions including cell–cell interaction, cell adhesion, cell proliferation and migration, and cell death (Breslow, 2013; Breslow & Weissman, 2010; Quinville et al., 2021).

The principle building block of all sphingolipids is a sphingoid base backbone that is linked via an amide bond to various fatty acid chains (Chen et al., 2010; Quinville et al., 2021). This backbone can be linked to different head groups (Castro et al., 2014; Chen et al., 2010; Quinville et al., 2021). The major groups of mammalian sphingolipids are based on a sphingosine backbone as sphingoid base, which can be linked for example to a hydroxy group and is then named ceramide, to a phosphatidyl choline (PC) and is then named sphingomyelin (SM), or to different sugar residues to build the diverse group of glycosphingolipids (Castro et al., 2014; Chen et al., 2010; Quinville et al., 2021). The principle sphingolipid structure is shown in Figure 3.

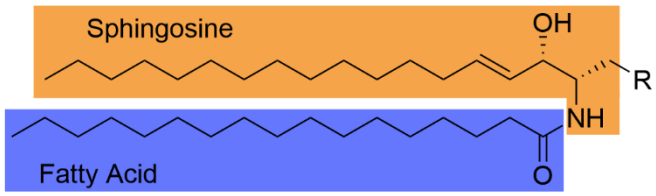

Figure 3. Structure of sphingolipids. Sphingolipids are built of a sphingoid base backbone, in mammalian cells typically a sphingosine, which is linked to a fatty acid, here palmitate, with an amide bound. The head group (R) can be (1) a hydroxy group (ceramide), (2) phosphatidyl choline (sphingomyelin) or (3) sugar residues (glycosphingolipids).

Sphingolipids are synthesized by three distinct pathways: *de novo* synthesis, sphingomyelinase pathway, and salvage pathway (Banhart et al., 2019; Sasset et al., 2016). *De novo* synthesis starts within the endoplasmic reticulum (ER) with the decarboxylating condensation of L-serine and a fatty acid activated by the esterification with coenzyme A (CoA), typically with palmitoyl-CoA, to form 3-ketosphinganine, catalyzed by the enzyme serine palmitoyltransferase (SPT) (Quinville et al., 2021; Sasset et al., 2016). 3-ketosphinganine is

further metabolized within the ER to form a ceramide (Banhart et al., 2019; Quinville et al., 2021; Sasset et al., 2016). This ceramide is then transported to the Golgi apparatus by the cellular ceramide transporter CERT (Banhart et al., 2019; Chung et al., 2021; Quinville et al., 2021). In the Golgi apparatus, ceramide can be further modified at the head group position to form SM or glycosphingolipids (Quinville et al., 2021; Sasset et al., 2016). Subsequently, sphingolipids are transported to the plasma membrane via the secretory pathway (Banhart et al., 2019; Quinville et al., 2021). *De novo* synthesis of sphingolipids is summarized in Figure 4.

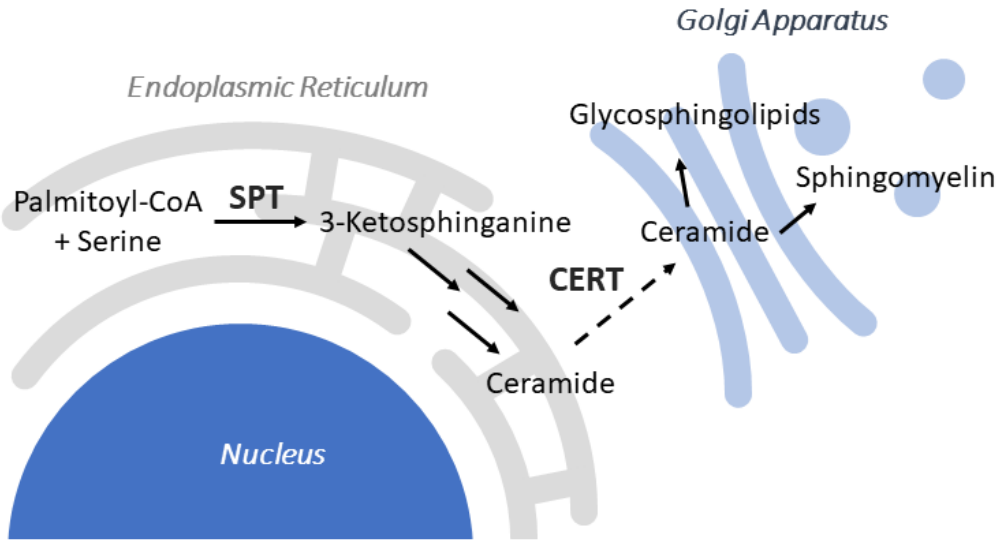

Figure 4: *De novo* synthesis of sphingolipids. *De novo* synthesis of sphingolipids starts in the endoplasmic reticulum with the condensation of palmitoyl-CoA and serine to form 3-ketosphinganine, catalyzed by the serine palmitoyltranserase (SPT). 3-ketosphinganine is further metabolized within the endoplasmic reticulum to form a ceramide. This ceramide is then transported to the Golgi apparatus by CERT. There, it is used to form glycosphingolipids and sphingomyelin.

SM from the plasma membrane can be reused to form other sphingolipids via the sphingomyelinase pathway. Here, SM is degraded to ceramides and PC at the plasma membrane or within lysosomes (Banhart et al., 2019; Yamaji & Hanada, 2015). Released ceramides and PC can be processed by SM synthase 2 to synthesize SM at the plasma membrane (Banhart et al., 2019; Kitatani et al., 2008). Similar, the salvage pathway reuses complex sphingolipids from the plasma membrane. Here, sphingolipids are degraded to sphingosine, which can enter different compartments and thus, being reused for the synthesis of different sphingolipids (Kitatani et al., 2008; Quinville et al., 2021).

1.3.2 Sphingolipid acquisition of *Chlamydia*

Chlamydia spp. acquire SM from the host cell by using different vesicular and non-vesicular transport pathways. Acquisition of SM is best studied for *C. trachomatis* (Banhart et al., 2019).

C. trachomatis is able to accumulate fluorescently labeled ceramide rather than fluorescently labeled SM, indicating that sphingolipids are derived from the Golgi apparatus, not from the

plasma membrane (Hackstadt et al., 1995, 1996). This sphingolipid acquisition seems to be crucial for the intracellular development as decreasing the uptake of fluorescently labeled ceramide by knock down of Rab6A and Rab11A decreases infectious progeny (Rejman Lipinski et al., 2009). In addition, sphingolipid acquisition depends on the conversation of ceramide to SM and treatment with not convertible ceramide species reduce *C. trachomatis* progeny formation (Banhart et al., 2014; Kumagai et al., 2022; Saied et al., 2015).

Vesicular transport of sphingolipids to the *C. trachomatis* inclusion occurs from Golgi mini-stacks or from multivesicular bodies (MVBs) (Beatty, 2006, 2008; Heuer et al., 2009). *C. trachomatis* (but also *C. psittaci*) infection induces fragmentation of the Golgi apparatus to Golgi mini-stacks, induced by the cleavage of golgin-84 (Heuer et al., 2009; Knittler et al., 2014). Inhibition of this process by inhibiting golgin-84 cleavage blocks sphingolipid acquisition and decreases *C. trachomatis* progeny formation (Heuer et al., 2009). MVBs are cellular organelles which play an important role for protein and lipid sorting (Bissig & Gruenberg, 2013; Gambarte Tudela et al., 2019). Different proteins and lipids of MVBs are recruited to *C. trachomatis* inclusions and inhibiting the biogenesis of MVBs disrupt inclusion maturation and the sphingolipid transport to *C. trachomatis* inclusions (Beatty, 2006, 2008).

1.3.3 The role of CERT for chlamydial sphingolipid acquisition

Beside vesicular transport of sphingolipids to the chlamydial inclusion, different chlamydial species including *C. trachomatis*, *C. psittaci* and *C. muridarum* recruit CERT to their inclusion and thereby facilitate sphingolipid acquisition (Derré et al., 2011; C. A. Elwell et al., 2011; Koch-Edelmann et al., 2017). During lipid transport in uninfected eukaryotic cells, CERT is linked to the ER with its central FFAT motif (two phenylalanines (FF) in an acidic tract) and interacts there with ER localized VAP proteins (vesicle-associated membrane protein-associated proteins) (Banhart et al., 2019; Chung et al., 2021). At the ER, the C-terminal START domain (steroidogenic acute regulatory protein-related lipid-transfer domain) binds ceramides, which are then transported to the Golgi apparatus via binding of the N-terminal PH (pleckstrin homology) domain to phosphatidyl inositol-4-phosphate (PI4P) at the Golgi membrane (Banhart et al., 2019; Chung et al., 2021). The functional domains of CERT are depicted in Figure 5.

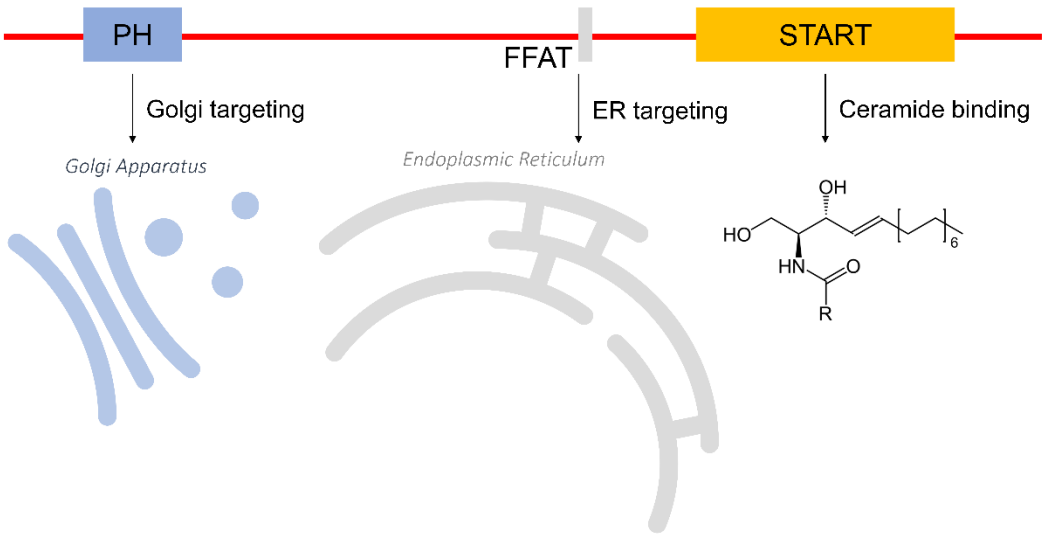

Figure 5. Functional domains of the ceramide transport protein CERT. The N-terminal PH domain of CERT targets the Golgi apparatus, the central FFAT motif targets the endoplasmic reticulum and the C-terminal START domain is responsible for ceramide binding. Modified from Scholz et al., 2024a.

In infected cells, *Chlamydia* spp. impair the ER-Golgi ceramide transport by CERT by recruiting CERT over its PH domain (Derré et al., 2011; C. A. Elwell et al., 2011; Koch-Edelmann et al., 2017). For *C. trachomatis*, the inclusion membrane protein (Inc-protein) IncD mediates the recruitment of CERT (Derré et al., 2011). However, no IncD analog has been identified in *C. psittaci* so far. Thus, the recruitment mechanism of CERT to *C. psittaci* inclusion is still under investigation (Koch-Edelmann et al., 2017).

CERT depletion decreases infectious progeny of *C. trachomatis*, *C. psittaci* and *C. muridarum*, demonstrating the crucial role of sphingolipids and CERT for chlamydial development (Derré et al., 2011; C. A. Elwell et al., 2011; Koch-Edelmann et al., 2017). Interestingly, ceramide transport to the *C. psittaci* inclusion is increased after CERT knock out (KO), which is counterintuitive and in contrast to *C. trachomatis* (Koch-Edelmann et al., 2017). This suggests another sphingolipid transport mechanism to *C. psittaci* inclusions and underlines our lack of understanding about sphingolipid transport and the role of CERT in *C. psittaci* infections (Banhart et al., 2019; Koch-Edelmann et al., 2017).

1.3.4 CERT-stabilized ER-inclusion-membrane contact sides

Beside its functional role as a sphingolipid transporter, CERT has also a mechanistic role during chlamydial infections in stabilizing ER-inclusion membrane contact sides (MCS) (Derré, 2015; Derré et al., 2011). MCS between the ER and chlamydial inclusions were at first characterized for *C. trachomatis*, being composed of the bacterial Inc-protein IncD that is localized in the inclusion membrane and that interacts with CERT that localizes in the ER membrane (Derré et al., 2011). Beside the inclusions of *C. trachomatis*, also *C. psittaci*, *C. muridarum*, and *C. pneumoniae* inclusions interact with CERT or the ER membrane, indicating that ER-inclusion membrane contact sides are a conserved strategy of *Chlamydia* spp. (Derré, 2015; C. A. Elwell et al., 2011; Koch-Edelmann et al., 2017). In addition, it was

suggested that CERT can indirectly support the recruitment of Golgi mini-stacks to the vicinity of the inclusion by ER-Golgi MCS (C. A. Elwell et al., 2011; Heuer et al., 2009).

In addition to CERT, the ER-resident proteins VAPA/B localize in the ER membrane within ER-inclusion MCS of *C. trachomatis*, interacting with the FFAT domain of CERT and with the chlamydial Inc-protein IncV (Agaisse & Derré, 2014; R. Murray et al., 2017). IncV was shown to contain two FFAT motifs, a canonical and a noncanonical one, that both interact with VAPA/B in ER-inclusion MCS and deletion of IncV reduces the formation of ER-inclusion MCS (R. Murray et al., 2017). The recruitment of VAPA/B by IncV depends on the IncV phosphorylation state, regulated by casein kinase 2 and additional kinases and phosphatases, suggesting that the ER-inclusion MCS are dynamically regulated by host cell kinases and phosphatases (Ende et al., 2022).

Another ER localizing component of the *C. trachomatis* ER-inclusion MSC is Stromal Interaction Molecule 1 (STIM1) (Agaisse & Derré, 2015). STIM1 is an ER calcium sensor that plays a central role during store-operated calcium entry (Gudlur et al., 2018; Stiber et al., 2008). During *C. trachomatis* infections, it colocalizes with CERT and VAPA/B at the inclusion membrane through the whole developmental cycle and its recruitment impairs the cellular store-operated calcium entry (Agaisse & Derré, 2015; Chamberlain et al., 2022). Interestingly, STIM1 depletion inhibits egress of *C. trachomatis* by extrusion formation (Nguyen et al., 2018). Recently, the Inc-protein IncS was characterized and identified as the bacterial interaction partner of STIM1, also being part of the ER-inclusion MCS of *C. trachomatis* (Cortina et al., 2022; Cortina & Derré, 2023). Similar to STIM1 depletion, also deletion of IncS of *C. trachomatis* enforces egress by host cell lysis. However, IncS and STIM1 do not interact at the inclusion membrane in *C. muridarum* infections (Cortina & Derré, 2023). The components of the ER-inclusion MCS of *C. trachomatis* are summarized in Figure 6.

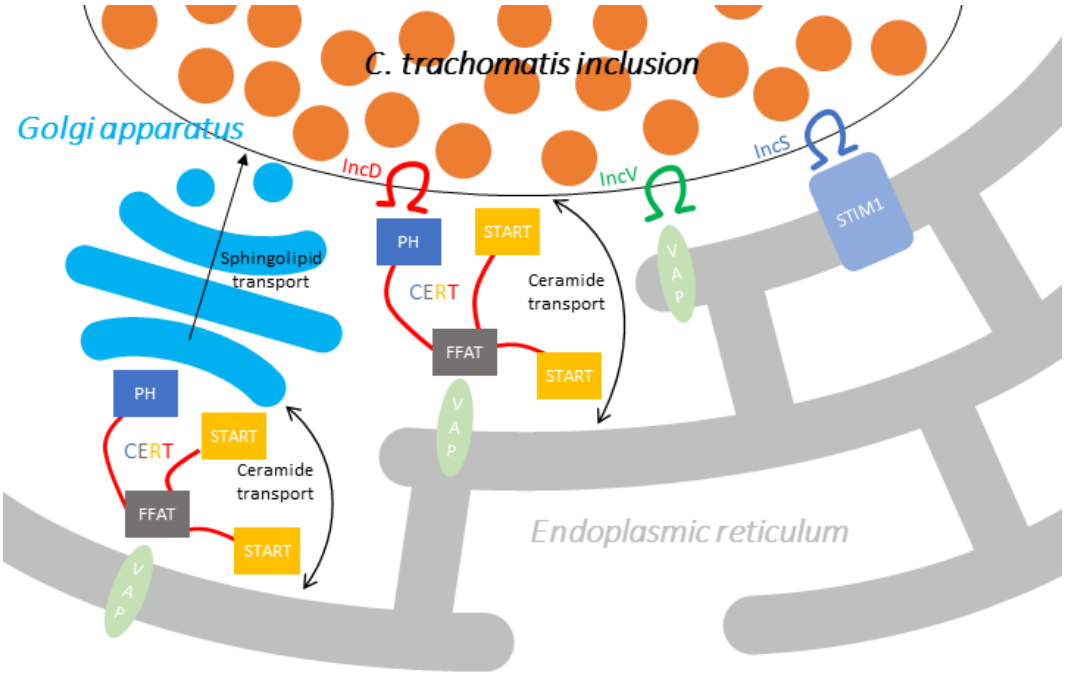

Figure 6. Schematic of ER-inclusion MCS of *C. trachomatis* (Agaisse & Derré, 2015; Derré, 2015; R. Murray & Derré, 2018; Subtil, 2011)**.** The bacterial Inc-proteins IncD, IncV, and IncS interact with the ER proteins CERT, VAP, and STIM1, respectively, thereby forming ER-inclusion MCS. CERT interact with VAP mediated by its FFAT motif and with chlamydial IncD mediated by the PH domain. CERT and VAP also participate in ER-Golgi MCS, where the PH domain mediates the interaction of CERT and the golgi apparatus. This ER-Golgi MCS can indirectly support the recruitment of Golgi mini-stacks to the vicinity of the inclusion.

1.3.5 The role of other lipids during chlamydial infections

In addition to sphingolipids, *Chlamydia* spp. are also able to acquire other host cellular lipids as glycerophospholipids in a vesicle-independent manner (C. A. Elwell & Engel, 2012; Hatch & McClarty, 1998; Scidmore, 2011; Wylie et al., 1997). Interestingly, it was shown that *C. trachomatis* replace the eukaryotic straight chain fatty acid at the sn-2 position of host-derived glycerophospholipids with a *Chlamydia*-derived branched chain fatty acid (C. A. Elwell & Engel, 2012; Su et al., 2004; Wylie et al., 1997). For *C. psittaci*, the role of other lipids than sphingolipids was only rarely studied. However, also for *C. psittaci* it was shown that branched chain fatty acids be contained in the lipids extracted from infected monkey kidney cells (Makino et al., 1970).

1.4 Aim of this study

Several human diseases are caused by human pathogenic microorganisms. To combat those diseases, it is crucial to get deeper insights into the biology of the pathogens. For intracellular pathogens as the zoonotic agent *C. psittaci*, egress from the host cell is of importance for their transmission, host tropism, and pathogenicity. Thus, the aim of this study was to understand the so far not characterized non-lytic egress of *C. psittaci* mechanistically and in the context of lipid acquisition and alteration. This includes in particular the role of apoptotic cell death, of the sphingolipid transporter CERT, and of cellular lipid concentrations.

Initially, the time course of the intracellular developmental cycle of *C. psittaci* was characterized. Subsequently, the end of the intracellular developmental phase could be further investigated regarding host cell egress. Lytic and non-lytic egress pathways of *C. psittaci* and egress pathways of *C. trachomatis* were comparatively characterized. By state-of-the-art imaging techniques including live cell imaging and electron microscopy, the different egress pathways of *C. psittaci* and *C. trachomatis* were examined. Especially, a novel non-lytic egress mechanism of *C. psittaci* named *Chlamydia*-containing sphere (CCS) formation was identified and further characterized regarding its relevance and bacterial and host cellular factors involved in its mechanism. In addition, the role of the ceramide transporter CERT for CCS formation was investigated by using a CRISPR/Cas9-generated KO cell line and KO complementation studies. Particularly, the role of CERT for the regulation of inclusion membrane stability and its destabilization during CCS formation was examined. Finally, the cellular lipid composition of *C. psittaci*-infected HeLa cells was investigated in comparison to the cellular lipid composition of uninfected HeLa cells. In addition, the cellular lipid composition of *C. psittaci*-infected HeLa cells before host cell egress at 48 h pi was compared to the cellular lipid composition of *C. psittaci*-infected HeLa cells during intracellular RB replication at 24 h pi. For this, a liquid chromatography (LC)- tandem mass spectrometry (MS/MS) based non-targeted lipidomics study was performed.

2 Material and Methods

2.1 Material

2.1.1 Organisms

The eukaryotic cell lines used in this study are listed in Table 2.

Table 2. Eukaryotic Cell Lines

Cell Line	Species	Tissue	Relevant Genetic Modifications	Source
HeLa	Human	Cervix carcinoma	-	ATCC CCL-2
HeLa DHE002	Human	Cervix carcinoma	Stably expressing eGFP (enhanced green fluorescent protein) in the cytosol	Heuer et al., 2009
HeLa ER-LAR-Geco G-Geco	Human	Cervix carcinoma	Dual calcium reporter cell line	Stelzner et al., 2020
HeLa EqtSM::Halo Tag	Human	Cervix carcinoma	Stably expressing a non-toxic, HaloTagged version of equinatoxin II	Niekamp et al., 2022
HeLa CERT-KO	Human	Cervix carcinoma	Stable knock out of the ceramide transporter CERT	Koch-Edelmann et al., 2017
HeLa CERT-KO Control	Human	Cervix carcinoma	Knock out control cells for the HeLa CERT-KO cells	Koch-Edelmann et al., 2017
A549	Human	Lung	-	ATCC CCL-185

The bacteria used in this study are listed in Table 3.

Table 3. Bacteria

Species	Strain	Characteristics	Source
C. psittaci	02DC15	Bovine isolate	Goellner et al., 2006
C. trachomatis	L2	lymphatic isolate 434 Bu	ATCC VR-902B
	L2-GFP	lymphatic isolate 434 Bu transformed with pGFP::SW2	kindly provided by Thomas Rudel
Escherichia coli	C2992	Used for cloning	New England Biolabs
	Rosetta 2	Used for recombinant gene expression	Novagen by Merck

2.1.2 Nucleic Acids

The primer used for cloning during this study are listed in Table 4.

Table 4. Primer used for Cloning

Gene product	Primer Sequence (3'-5')	Restriction Site	Direction
C. psittaci IncA C terminus	ATCGGCCGGCCGGCAGGATAGCACCCCCTCT	FseI	forward
C. psittaci IncA C terminus	TCTGCGGCCGCTTACTGTTCATATATTGG	NotI	reverse

Gene product	Primer Sequence (3'-5')	Restriction Site	Direction
C. psittaci IncA C terminus	ATTGGCGCGCCTCGGCCGGCCGG	AscI	forward
C. psittaci Cps0558 C terminus	ATCGGCCGGCCGGCGTATTCTTAAAAAGCCT	FseI	forward
C. psittaci Cps0558 C terminus	TCTGCGGCCGCTTATGATTCTTCTTCTTT	NotI	reverse
C. psittaci Cps0558 C terminus	ATTGGCGCGCCTCGGCCGGCCGG	AscI	forward

The primer used for qPCR during this study are listed in Table 5.

Table 5. Primer used for qPCR

Target sequence	Primer Sequence (3'-5')	Direction	Reference
c16S rDNA (ribosomal DNA, Deoxyribonucleic acid)	CCGCCAACACTGGGACT	forward	Lienard et al., 2011
c16S rDNA	GGAGTTAGCCGGTGCTTCTTTAC	reverse	Lienard et al., 2011

The sequencing primer used in this study are listed in Table 6.

Table 6. Sequencing primer

Target sequence	Primer Sequence (3'-5')	Direction	Backbone
pGEX-3x	GGGCTGGCAAGCCACGTTTGGTG	forward	pGEX-3x
pGEX-3x	CCGGGAGCTGCATGTGTCAGAGG	reverse	pGEX-3x

The plasmids used for this study are listed in Table 7.

Table 7. Plasmids

Plasmid name	Gene product	Backbone	Source	Reference
pJG009	GST-CT006 (N-terminus)-CT006 (C-terminus)	pGEX-3X	RKI, Jean-Marc Gensch	-
pJG030	Cps0558 (N-terminus)-eGFP-Cps0558 (C-terminus)	pEGFP-C1	RKI, Jean-Marc Gensch	-
pJG034	IncA (N-terminus)-eGFP-IncA (C-terminus)	pEGFP-C1	RKI, Jean-Marc Gensch	-
pJS002	GST-Cps0558 (C-terminus)	pGEX-3X	This work	-
pJS003	GST-IncA (C-terminus)	pGEX-3X	This work	-
pEGFP-N1	eGFP	pEGFP-N1	Clonetech	-
p5776	EqtSM-HaloTag	pLX304	Universität Osnabrück Michael Hensel,	Scharte et al., 2023

Plasmid name	Gene product	Backbone	Source	Reference
pAGH149	CERT-GFP	pEGFP-C1	RKI, Sophia Edelmann	Koch-Edelmann et al., 2017
pAGH158	CERT-GFPΔSTART	pEGFP-C1	RKI, Sophia Edelmann	-
pAGH160	CERT-GFPΔPH	pEGFP-C1	RKI, Sophia Edelmann	Koch-Edelmann et al., 2017
pAGH154	CERT-GFPΔFFAT	pEGFP-C1	RKI, Sophia Edelmann	-

2.1.3 Media, Buffers, and Solutions

The cell culture media used in this study are listed in Table 8.

Table 8. Cell culture media

Application	Composition	Manufacturer	Catalog Number
Cell growth (HeLa)	RPMI (Roswell Park Memorial Institute) 1640	Gibco	21875091
	10% (v/v) FBS (Fetal bovine serum), heat-inactivated	Sigma-Aldrich	F7524, Lot No. 19B123
	1 mM sodium pyruvate	Gibco	11360039
Cell growth (A549)	Ham's F-12K (Kaighn's) Medium	Gibco	21127022
	10% (v/v) FBS, heat-inactivated	Sigma-Aldrich	F7524, Lot No. 19B123
Infection (HeLa)	Dulbeccos Modified Eagle Medium (DMEM) high glucose (4.5 g/L)	Gibco	31053044
	5% (v/v) FBS, heat-inactivated	Sigma-Aldrich	F7524, Lot No. 19B123
	1 mM sodium pyruvate	Gibco	11360039
	5 mM L-glutamine	Gibco	25030024
Infection (A549)	Ham's F-12K (Kaighn's) Medium	Gibco	21127022
	5% (v/v) FBS, heat-inactivated	Sigma-Aldrich	F7524, Lot No. 19B123
	5 mM L-glutamine	Gibco	25030024
Calcium-free experiments	DMEM high glucose (4.5 g/L) w/o $CaCl_2$	Gibco	21068028
	1 mM sodium pyruvate	Gibco	11360039
	5 mM L-glutamine	Gibco	25030024
Lipidomics experiments	DMEM high glucose (4.5 g/L)	Gibco	31053044
	5 mM L-glutamine	Gibco	25030024
	1 mM sodium pyruvate	Gibco	11360039
Transfection	OptiMEM	Gibco	31985062
Washing	Phosphate-Buffered Saline (PBS)	Gibco	20012068
Passaging	Trypsin	Gibco	25200072

The media for cultivation of *E. coli* used in this study are listed in Table 9.

Table 9. Media for *E. coli* cultivation

Medium	Application	Composition	Manufacturer	Catalog Number
Lysogeny broth (LB) medium	Liquid culture	10 g/L Bacto Tryptone	Gibco	211705
		5 g/L Bacto Yeast Extract	Gibco	212750
		5 g/L NaCl	Supelco (Merck)	1.06404
Super optimal broth (SOB) medium	Transformation	20 g/L Bacto Tryptone	Gibco	211705
		5 g/L Bacto Yeast Extract	Gibco	212750
		0.58 g/L NaCl	Supelco (Merck)	1.06404
		0.19 g/L KCl	Supelco (Merck)	1.04936
LB agar plates	Solid culture	10 g/L Bacto Tryptone	Gibco	211705
		5 g/L Bacto Yeast Extract	Gibco	212750
		5 g/L NaCl	Supelco (Merck)	1.06404
		1.5% Oxoid Agar Bacteriological	Thermo Fisher Scientific	LP0011

The buffers and solutions used in this study are listed in Table 10.

Table 10. Buffers and Solutions

Buffer/Solution	Composition
10x TBE buffer	55 g boric acid, 108 g Tris, 40 mL EDTA (0.5 M) in 1 L distillated water, pH 8.0
5X Separating gel SDS-PAGE buffer	0.5 M Tris/HCl, 0.4% (w/v) SDS in distillated water, pH 8.8
5X Stacking gel SDS-PAGE buffer	1.5 M Tris/HCl, 0.4% (w/v) SDS in distillated water, pH 6.7
Annexin Binding Buffer (ABB)	400 mg/L $CaCl_2$ in PBS
AnnexinV staining solution	AnnexinV Alexa Fluor 568 diluted 1:10 in ABB
BODIPY FL C5-Ceramid complexed to BSA staining solution	0.5 mM BODIPY FL C5-Ceramid complexed to BSA diluted 1:1000 in infection medium
BODIPY FL C5-Sphingomyelin staining solution	0.5 mM BODIPY FL C5-Sphingomyelin in DMSO diluted 1:1000 in infection medium
Clinic Fixative	2.5% (w/v) glutaraldehyde and 1% (w/v) PFA in 50 mM HEPES buffer
Coomassie destaining solution	10% (v/v) acetic acid, 40% (v/v) ethanol in distillated water
Coomassie staining solution	0.1% (w/v) Coomassie Blue R-250, 10% (v/v) acetic acid in distillated water
Elution buffer	50 mM Tris-HCl, 10 mM reduced glutathione in distillated water, pH 8.0
Epon resin	Stock solution A (62 mL Glycidyl ether and 100 mL DDSA) and stock solution B (100 mL Glycidyl ether and 89 mL MNA) mixed in varying proportions together with 1.5% (v/v) DMP-30, polymerized for 20 h at 45°C and then for 24 h at 60°C
FM4-64 staining solution	10 mM FM4-64 in DMSO diluted 1:1000 in infection medium

Buffer/Solution	Composition
Harvesting Solution	10 µg/mL BHT in PBS
HEPES buffer	50 mM HEPES in distillated water
Hoechst 33342 staining solution	25 mg/mL Hoechst 33342 diluted 1:2000 in infection medium
Incucyte Caspase-3/7 Red Dye staining solution	0.83 µM Incucyte Caspase-3/7 Red Dye in infection medium or calcium-free infection medium
Janelia Fluor 585 HaloTag Ligand Staining solution	20 µM Janelia Fluor HaloTag Ligand 585 nm in DMSO diluted 1:100 in infection medium
Laemmli buffer	375 mM Tris/HCl, 48% (v/v) glycerol, 9% (v/v) β-mercaptoethanol, 6% (w/v) SDS, 0.03% (w/v) bromphenol blue in distillated water, pH 6.8
Lysis buffer	50 mM Tris, 0.1% (v/v) Triton X100, 100 µg/mL lysozyme, 500 U/µL nuclease in distillated water, pH 8.0, with Complete protease inhibitor cocktail
Mowiol mounting medium	2.4 g Mowiol 4-88, 6 g glycerol, 6 mL distillated water, 12 mL 0.2 M Tris/HCl, pH 8.5
PBS	137 mM NaCl, 2.7 mM KCl, 10 mM Na_2HPO_4, 1.76 mM KH_2PO_4 in distillated water, pH 7.4
Rhod-3 incubation buffer	250 µM Probenecid in infection medium or calcium-free infection medium
Rhod-3 loading buffer	1x PowerLoad concentrate, 10 µM Rhod-3 AM, 250 µM Probenecid in infection medium or calcium-free infection medium
SDS-PAGE buffer	25 mM Tris/HCl, 192 mM glycine, 0.1% (w/v) SDS in distillated water
SPG buffer	250 mM sucrose in PBS
Spiking solution	Each 150 ng/mL Cer d18:1-d7/16:0, PC 17:0_14:1-d5, PE 17:0_18:1-d5, SM d18:1/16:1-d9, PI 17:0_14:1-d5, LPC 17:0-d5, LPE 17:0-d5, LPG 17:0-d5, LPI 17:0-d5, LPS 17:0-d5 in methanol
SYTOX staining solution	5 mM SYTOX Green in DMSO diluted 1:2000 in infection medium
Trypan Red staining solution	100 mM Trypan Red Plus diluted 1:100 in PBS

2.1.4 Antibodies

The primary antibodies used in this study are listed in Table 11.

Table 11. Primary Antibodies

Antigen	Source species	Dilution	Source	Catalog Number
ACAD11	mouse	1:50	Abnova	H00084129-A01
C. psittaci Cps0558	rabbit	1:500	Self-made	-
C. psittaci IncA	rabbit	1:500	Self-made	-
CERT	rabbit	1:200	Invitrogen	PA5-103558
Chlamydial HSP60	mouse	1:600	Enzo Life Sciences	ALX-804-072
Cleaved caspase-3	rabbit	1:400	Cell Signaling Technology	9661
HaloTag	rabbit	1:500	Promega	G9281
STIM1	rabbit	1:50	Proteintech	11565-1-AP

The secondary antibodies used in this study are listed in Table 12.

Table 12. Secondary Antibodies

Antigen (Conjugate)	Source species	Dilution	Source	Catalog Number
mouse IgG (Alexa Fluor 488)	goat	1:100	Dianova	115-545-003
mouse IgG (Cy3)	goat	1:200	Dianova	115-165-146
rabbit IgG (Alexa Fluor 488)	goat	1:100	Dianova	111-545-144
rabbit IgG (Cy3)	goat	1:200	Dianova	111-165-144

2.1.5 Chemicals

The chemicals used in this study are listed in Table 13.

Table 13. Chemicals

Chemical	Manufacturer	Catalog Number
Acetic Acid	Roth	3738
Acetonitrile	Merck	100029
Acrylamide	Roth	3029
Agarose	VWR	436553W
Ammonium formate, LC-MS Grade	Merck	70221
Ammonium Persulfate (APS)	Roth	9592
Ampicillin	Sigma-Aldrich	A5354
AnnexinV	Molecular Probes	A13202
BAPTA-AM	Merck	196419
Blebbistatin	Sigma-Aldrich	B0560
BODIPY FL C5-Ceramide complexed to BSA	Invitrogen	B22650
BODIPY FL C5-Sphingomyelin	Invitrogen	D3522
Boric Acid	Roth	6943
Bovine Serum Albumin Fraction V (BSA)	Roth	8076
Bromphenol blue	Roth	A512
Butyl hydroxy toluene (BHT)	Sigma-Aldrich	B1215000
Calcium chloride ($CaCl_2$)	Roth	CN93
Cer d18:1-d7/16:0	Avanti Polar Lipids	860676
Chloroform, LC-MS Grade	Merck	102444
Coomassie blue R-250	Roth	3862
4′,6-Diamidino-2-Phenylindole (DAPI)	Roth	6335
Dimethyl sulfoxide (DMSO)	Roth	HN47
Disodium hydrogen phosphate dihydrate ($Na_2HPO_4 \cdot 2H_2O$)	Roth	P030
Dodecenyl succinic anhydride (DDSA)	Serva	20755
Ethanol	Roth	9065
Ethanol LC-MS Grade	Honeywell	34852

Chemical	Manufacturer	Catalog Number
Ethylenediaminetetraacetic acid (EDTA)	Roth	8043
FM4-64	Sigma-Aldrich	SCT127
Formic Acid, LC-MS Grade	Merck	159013
Glutaraldehyde	TAAB Laboratory and Microscopy	G011
Glycerol	Roth	3783
Glycidyl ether	Serva	21045
4-(2-hydroxyethyl)-1-piperazineethanesulfonic acid (HEPES)	Sigma-Aldrich	PHG001
Hoechst 33342	Sigma-Aldrich	14533
Hydrochloric acid (HCl)	Roth	X896
Isopropyl β-D-1-thiogalactopyranoside (IPTG)	Roth	CN08
Janelia Fluor 585 HaloTag Ligand	Promega	CS315118
Jasplakinolide	Santa Cruz	sc-202191
Kanamycin sulfate	Sigma-Aldrich	T832
Latrunculin B	Merck	428020
Lead citrate	Serva	15158
Lipofectamine 2000 Transfection Reagent	Invitrogen	11668019
Low-melting point agarose	Sigma Aldrich	A9414
LPC 17:0-d5	Avanti Polar Lipids	855679
LPE 17:0-d5	Avanti Polar Lipids	856710
LPG 17:0-d5	Avanti Polar Lipids	858130
LPI 17:0-d5	Avanti Polar Lipids	850108
LPS 17:0-d5	Avanti Polar Lipids	858148
Methanol	Roth	4627
Methanol, LC-MS Grade	Merck	106035
Methyl tert-butyl ether (MTBE), LC-MS Grade	Merck	101845
Methylnadic anhydride (MNA)	Serva	29452
Milk Powder	Roth	T145
Monopotassium phosphate (KH_2PO_4)	Roth	P748
Mowiol 4-88	Roth	0713
Nocodazole	Sigma-Aldrich	M1404
Osmium tetroxide	Sigma Aldrich	251755
Paraformaldehyde (PFA)	Roth	0335
PC 17:0_14:1-d5	Avanti Polar Lipids	855683
PE 17:0_18:1-d5	Avanti Polar Lipids	856719
PI 17:0_14:1-d5	Avanti Polar Lipids	850109

Chemical	Manufacturer	Catalog Number
Pierce Bovine Serum Albumin Standard	Thermo Fisher Scientific	23209
Potassium chloride (KCl)	Roth	6781
2-Propanol, LC-MS Grade	Merck	102781
Reduced L-glutathione	Sigma-Aldrich	G4251
SM d18:1/16:1-d9	Avanti Polar Lipids	860741
Sodium chloride (NaCl)	Roth	3957
Sodium Dodecyl Sulfate (SDS)	Roth	CN30
Staurosporine	Biomol	LKT-S7600
Sucrose	Roth	4621
SYTOX Green Nucleic Acid Stain - 5 mM Solution in DMSO	Invitrogen	S7020
Tannic acid	Mallinkrodt	1746
tert-Butylmethylether,	Roth	T175
Tetramethyl-ethylenediamine (TEMED)	Roth	2367
Triethylamine, LC-MS Grade	Merck	81101
Tris	Roth	4855
2,4,6-Tris(dimethylaminomethyl)phenol (DMP-30)	Serva	36975
Triton X-100	Roth	3051
Trypan Red	Biomol	ABD-2456
Tween20	Roth	9127
Uranyl acetate	Serva	77870
Water, LC-MS Grade	Merck	106035
Wiskostatin	Sigma-Aldrich	W2270
Z-DEVD-FMK	Santa Cruz	sc-311558
Z-VAD-FMK	Santa Cruz	sc-3067
β-Mercaptoethanol	Roth	4227

2.1.6 Kits and Enzymes

The kits and enzymes used in this study are listed in Table 14.

Table 14. Kits and Enzymes

Kit/Enzyme	Manufacturer	Catalog Number
6X DNA Loading Dye	Thermo Fisher Scientific	R0611
Antarctic Phosphatase (1000 U/mL)	New England Biolabs	M0289
Asc I	New England Biolabs	R0558
BCA Kit	Thermo Fisher Scientific	23225
BigDye Terminator v3.1 Cycle Sequencing Kit	Thermo Fisher Scientific	4337455

Kit/Enzyme	Manufacturer	Catalog Number
cOmplete, Mini, EDTA-free Protease Inhibitor Cocktail	Sigma-Aldrich	11836170001
GeneJET Plasmid-Miniprep-Kit	Thermo Fisher Scientific	K0503
GeneRuler 1 kb	Thermo Fisher Scientific	SM0312
GeneRuler 100 bp	Thermo Fisher Scientific	SM0241
Glutathion-Sepharose 4B	Sigma-Aldrich	GE17-0756-01
Incucyte Caspase-3/7 Red Dye for Apoptosis	Sartorius	4704
Luna Universal Probe qPCR Master Mix	New England Biolabs	M3004
Lysozyme	Roth	8259
MasterPure Gram Positive DNA Purification Kit	Biozym	MPG04100
Midori Green Advance	NIPPON Genetics	MG04
Not I-HF	New England Biolabs	R3189
PageRuler Unstained Broad Range Protein Ladder	Thermo Fisher Scientific	26630
Phusion High-Fidelity PCR Master Mix with HF Buffer	New England Biolabs	M0531
Pierce 660 nm protein assay reagent	Thermo Fisher Scientific	22660
Pierce Universal Nuclease for Cell Lysis	Thermo Fisher Scientific	88701
rCutSmart Buffer	New England Biolabs	B6004
Rhod-3 Calcium Imaging Kit	Thermo Fisher Scientific	R10145
T4 DNA Ligase Buffer (10X)	Thermo Fisher Scientific	B69
T4 DNA Ligase, LC (1 U/µL)	Thermo Fisher Scientific	EL0016
Wizard SV Gel and PCR Clean-Up System	Promega	A9282

2.1.7 Consumables

The consumables used during this study are listed in Table 15.

Table 15. Consumables

Consumable	Manufacturer	Catalog Number
µ-Slide 15 Well	Ibidi	81506
12 well plates	TPP	92412
18G needle	Roth	C724
24 well plates	TPP	92424
26G needle	Roth	C718
35 mm Dish	Mattek	P35GC-1.0-14-C
6 well plates	TPP	92406

Consumable	Manufacturer	Catalog Number
8 well chambered slide IbiTreat	Ibidi	80826
8 well chambered slide poly-L-lysin coated	Ibidi	80824
96 well plates	TPP	92696
Cell scraper 24 cm	TPP	99002
Cell scraper 30 cm	TPP	99003
Cover slips 12 mm	Roth	P231
Cover slips 15 mm	Roth	P232
Culture flask 1 L	Roth	L187
Culture flask 250 mL	Roth	L184
Eppendorf tube 0.5 mL	Roth	7096
Eppendorf tube 1.5 mL	Roth	7080
Eppendorf tube 2 mL	Roth	7083
Falcon Tube 15 mL	TPP	91015
Falcon Tube 50 mL	TPP	91050
Filter tips 0.1-10 µL	Thermo Fisher Scientific	2149
Filter tips 100-1000 µL	Thermo Fisher Scientific	2079
Filter tips 2-100 µL	Eppendorf	10531
Glass beads	Roth	A557
Microscope slide	Roth	H868
Parafilm	Brand	701620
Pierce Disposable Column	Thermo Fisher Scientific	29922
Pipet tips 0.5-20 µL	Roth	9260
Pipet tips 100-1200 µL	Roth	2679
Pipet tips 1-200 µL	Roth	1LP1
Polyvinylidene difluoride (PVDF)-membrane	Millipore	T831
Scalpel	Roth	X004
Serological pipets 10 mL	TPP	94010
Serological pipets 2 mL	TPP	94002
Serological pipets 25 mL	TPP	94024
Serological pipets 5 mL	TPP	94005
Stainless steel beads (2.8 mm)	Precellys	P000925-LYSK0-A
Syringe 5 mL	Roth	0057
T150 cell culture flasks	TPP	90151
T25 cell culture flasks	TPP	90026
T75 cell culture flasks	TPP	90076
X-Ray films	Cytiva Amersham	28-9068-36
µ-Dish 35 mm high	Ibidi	81156

2.1.8 Equipment

Experiments were performed in standard modern laboratories equipped with the instruments listed in Table 16.

Table 16. Equipment

Equipment	Model	Manufacturer
Benchtop centrifuge	Allegra X-15 R	Beckman Coulter
Benchtop centrifuge	Avanti J-15 R	Beckman Coulter
CMOS-camera	Phurona,	EMSIS GmbH
Confocal laser scanning microscope	LSM 780	Zeiss
Confocal laser scanning microscope	Stellaris 8	Leica
Electrophoresis cell	Mini-Protean Tetra	BioRad
Fluorescence Microscope	Axiovert 40 CFL	Zeiss
High-performance liquid chromatography (HPLC) column	Luna Omega C18 (100 Å × 2.1 mm × 1.6 µm)	Bruker Daltonics
Incubator	Ecotron	Infors HT
Incubator	CB 150	Binder
Microfuge	Centrifuge 5417 R	Eppendorf
Microplate reader	Infinite 200 Pro	Tecan
NanoPhotometer	N120	Implen
PCR thermocycler	FlexCycler	Analytik Jena
Phase contrast microscope	Axiovert 40 CLF	Zeiss
qPCR thermocycler	AriaMx real-time PCR system	Agilent Technologies
Safety cabinet	HS2020	Thermo Fisher Scientific
Thermo shaker	Biometra TS1	Analytik Jena
Transmission electron microscope	Tecnai 12	FEI Company
Trapped Ion Mobility Spectrometry-quadrupole Time-of-Flight (TIMS-qToF) mass spectrometer	Pro	Bruker Daltonics
Ultra(U)HPLC system	Elute	Bruker Daltonics
Ultracentrifuge	Optima XPN-1000	Beckman Coulter
Ultramicrotome	UC7	Leica
Vacuum concentrator	Speed Vac	Thermo Fisher Scientific

2.1.9 Software

The software used in this study are listed in Table 17.

Table 17. Software

Software	Version	Manufacturer
Adobe Photoshop	CS5	Adobe
ChemDraw Professional	17.0	PerkinElmer

Software	Version	Manufacturer
Compass DataAnalysis	4	Bruker Daltonics
CoreDraw Graphics Suite	X6	Corel GmbH
Fiji	1.53a	US National Institute of Health, Bethesda
Geneious Prime	2021.2.2	Invitrogen
Graph Pad Prism	9	GraphPad Software
LasX	1.4.6	Leica
Metaboscape	2021b	Bruker Daltonics
Compass Hystar	6.2	Bruker Daltonics
Microsoft Image Composite Editor	2.03	Microsoft
Microsoft Office	Professional Plus 2019	Microsoft
Radius – EM Imaging Software	2.1	EMSIS GmbH
timsControl	2	Bruker Daltonics
ZEN (black edition)	2.3	Zeiss
ZEN (blue edition)	3.4	Zeiss

2.2 Methods

2.2.1 Cell culture methods

All cell culture experiments were performed under sterile conditions.

2.2.1.1 Cell culture of eukaryotic cells

Cell culture of eukaryotic cells was performed as described previously (Koch-Edelmann et al., 2017). Briefly, cells were cultivated at 37°C and 5% CO_2 in T75 cell culture flasks in 12 mL of the respective medium (see Table 8) and passaged every 2 to 3 days for up to ten passages. For passaging cells, cells were washed with 10 mL PBS and subsequently treated with 2 mL trypsin solution. After incubation for 5 min at 37°C and 5% CO_2, 10 mL of the respective medium were added to the detached cells to stop the trypsin digest. Cells were further diluted and seeded onto new culture vessels including cell flasks, 6 well, 12 well, 24 well or 96 well plates and 8 well chambered coverslips.

2.2.1.2 Preparation of *Chlamydia* stock solutions

To prepare *Chlamydia* stocks, HeLa cells were grown in two T75 cell culture flasks and infected with the respective *Chlamydia* strain (see Table 3) (multiplicity of infection (MOI) 5). Infected cells were incubated at 35°C and 5% CO_2. For the *C. psittaci* strain, infection was performed in 2 mL infection medium and 0.5 h pi, infected cells were centrifuged (30 min, 600 x *g*, room temperature (RT)). After centrifugation, 4 mL of infection medium per flasks were added and infected cells were incubated for another 60 min. Subsequently, cells were washed with infection medium and 12 mL of fresh infection medium/cell flask were added. For the *C. trachomatis* strains, infection was performed in 6 mL infection medium. At 2 h pi, cells were washed with infection medium and 12 mL of fresh infection medium/cell flask were added. For all strains, after approximately one ideal developmental cycle at 48 h pi, cells were detached by cell scraping. To release bacteria, cells were transferred into glass beads containing falcon tubes and glass bead lysis was performed by vortexing for 3 min. Supernatants were transferred to new falcon tubes and bacteria were separated from cell debris by centrifugation (10 min, 500 x *g*, RT). The supernatant was used as inoculum to infect further 16 T75 cell culture flasks of HeLa cells as described above for the different *Chlamydia* strains. At 48 h pi, *Chlamydia* stock solutions were prepared on ice/at 4°C. For this, cells were detached by cell scraping, bacteria were released by glass bead lysis, and bacteria were separated from cell debris by centrifugation as described above. Bacteria were enriched by centrifugation of the bacteria-containing supernatant (60 min, 48,000 x *g*, 4°C) and the pelleted bacteria were resuspended in 40 mL SPG buffer for washing. Again, bacteria were enriched by centrifugation (60 min, 48,000 x *g*, 4°C) and resuspended in 5 mL SPG buffer. Suspensions were homogenized by syringing through 26G and 18G needles and aliquots of 25 µL and 50 µL of

bacteria suspension were stored at -80°C until use. For titer determination, please see section 2.2.1.7 (Reinfection assays).

2.2.1.3 *Chlamydia* infection assays

Infection assays were performed as described previously (Koch-Edelmann et al., 2017). For infection assays, subconfluent eukaryotic cells were washed with the respective infection medium (see Table 8) and incubated at 35°C and 5% CO_2 using the indicated MOI with the respective *Chlamydia* strain (see Table 3). *C. psittaci*-infected cell cultures were centrifuged (30 min, 600 x *g*, RT) at 0.5 h pi. *C. psittaci* and *C. trachomatis* L2-infected cell cultures were washed with infection medium at 2 h pi.

2.2.1.4 Transient transfection

Transient transfection of HeLa cells was performed 4 h prior to infection with Lipofectamine 2000 reagent according to manufacturer's instructions. Briefly, a dilution of 1-2 µL Lipofectamine2000 per 50 µL OptiMEM and a dilution of 0.4-0.8 µg plasmid DNA per 50 µL OptiMEM were prepared, mixed and incubated at RT for 5 min. Subsequently, both dilutions were mixed and incubated for another 20 min. 20-50 µL of the mixture per 1 cm^2 cell surface area were added dropwise into the medium on previously washed HeLa cells.

2.2.1.5 Induction of apoptosis

To compare CCS with apoptotic cells, chemical apoptosis of uninfected HeLa cells was induced by treatment with 10 µM staurosporine. For this, a 1 mM stock solution of staurosporine in DMSO was prepared and diluted into infection medium. Cells were washed once with infection medium and staurosporine-containing medium was added. At 42 h post treatment, apoptotic cells in the supernatant were collected by centrifugation (5 min, 300 x *g*, RT). Staining of apoptotic cells and preparation for transmission electron microscopy was performed as described for CCS (please see section 2.2.2.3, staining of CCS and section 2.2.2.8, transmission electron microscopy).

2.2.1.6 Separation of CCS from free bacteria

To separate CCS and free bacteria, HeLa cells were initially infected with *C. psittaci* and incubated for 48 h. Then, supernatants were collected and centrifuged at low speed (5 min, 300 x *g*, RT) to pellet CCS and separate them from free bacteria in the remaining supernatant.

2.2.1.7 Reinfection assays

Reinfection assays were performed for titer determination and for determining the infectivity of lysates of infected cells, CCS or free bacteria. For both applications, reinfection assays were performed by infecting HeLa cells grown on glass coverslips, either with serial dilutions of the prepared *Chlamydia* stock solutions or with serial dilutions of glass bead lysed cells, CCS or

free bacteria. Cells were fixed at 24 h pi, stained for HSP60 (please see section 2.2.2.2, immunofluorescence staining), and numbers of infection forming units (IFU) per mL were calculated from average inclusion counts in 10 fields of view per condition using a Zeiss Axiovert 40 CFL microscope with 40x magnification.

2.2.1.8 Determination of the working concentrations of the caspase inhibitors

To determine the working concentration of the caspase-3 inhibitor Z-DEVD-FMK and the pan caspase inhibitor Z-VAD-FMK in my cell culture model, HeLa cells were seeded in 8 well chambered coverslips. Cells were treated with inhibitors diluted into RPMI in concentrations of 0 µM, 2 µM, 20 µM, and 50 µM. At 4 h post treatment, apoptosis was induced by addition of 5 µM staurosporine and caspase-3 activity was monitored using Incucyte Caspase-3/7 Red Dye for Apoptosis in a final assay concentration of 833 nM. At 16 h post staurosporine treatment, samples were analyzed by confocal laser scanning microscopy (please see section 2.2.2.1, confocal laser scanning microscopy).

2.2.1.9 Inhibitor treatment and quantification of CCS or extrusions

The number of CCS or extrusions in *C. psittaci*- or *C. trachomatis*-infected cell cultures, respectively, was determined under different inhibitory and medium conditions. Inhibitor-containing medium was prepared by diluting the following inhibitors in the given concentrations in infection medium: blebbistatin (50 µM), jasplakinolide (1 µM), latrunculin B (0.5 µM), nocodazole (30 µM), wiskostatin (50 µM), Z-VAD-FMK (2 µM), Z-DEVD-FMK (2 µM), and BAPTA-AM (10 and 20 µM). In addition, experiments with calcium- and FBS-free infection medium supplemented with the indicated concentrations of calcium chloride were performed. At indicated time points, cell cultures were washed with PBS and medium was changed to conditional medium and cultivation was continued for additional 4 h. To quantify the number of CCS or extrusions, supernatant of the infected cell cultures was transferred to a new 12 well plate. The average number of CCS or extrusions of at least five visual fields was determined using a Zeiss Axiovert 40 CFL microscope with 20x magnification and normalized to the infected cell area.

2.2.2 Microscopy analysis

2.2.2.1 Confocal Laser scanning microscopy (CLSM)

Confocal laser scanning microscopy was used to analyze immunofluorescence stained samples, stained CCS and for live cell imaging. Two confocal laser scanning microscopes were used: a Zeiss LSM 780 laser scanning confocal microscope equipped with Zeiss Zen software and a Leica Microsystems Stellaris 8 confocal microscope platform equipped with LAS X navigator software. Image processing was performed using Fiji software.

2.2.2.2 Immunofluorescence staining

For immunofluorescence assays, eukaryotic cells were seeded onto cover slips and infected with *C. psittaci*, *C. trachomatis* or left uninfected. At indicated time points, culture medium was removed and cells were fixed with 4% paraformaldehyde in PBS (30 min, RT). After washing with PBS, samples were blocked and permeabilized using 0.2% Triton X-100 and 0.2% BSA in PBS (20 min, RT). Incubation with primary antibodies for 1 h at RT was followed by washing and incubation with secondary antibodies and DAPI (25 µg/mL) for 1 h at RT. All antibodies were diluted using 0.2% BSA in PBS. The used primary antibodies and their working concentrations are listed in Table 11, the used secondary antibodies and their working concentrations are listed in Table 12.

2.2.2.3 Staining of CCS

Separated CCS (please see section 2.2.1.6, separation of CCS from free bacteria) or apoptotic cells as control (please see section 2.2.1.5, induction of apoptosis) were analyzed by immunofluorescence staining and live staining. For immunofluorescence staining, pelleted CCS were mixed with 4% paraformaldehyde in PBS and transferred into a poly-L-lysine coated 8 well chambered coverslip. After 30 min of incubation at RT, staining was continued as described for immunofluorescence assays (please see section 2.2.2.2, immunofluorescence staining).

Live staining was performed to analyze CCS and apoptotic cells using different dyes for different characteristics. FM4-64 and Hoechst 33342 were used to stain the membrane and nucleic acids, respectively. SYTOX Green and Trypan Red Plus are both impermeable to intact cellular membranes but can permeate the compromised membranes of dead cells and were used to study the membrane integrity of CCS. While SYTOX Green is a nucleic acid dye, Trypan Red Plus stains the whole damaged cell. AnnexinV is a protein binding PS with high affinity and is used to detect the exposure of PS to the outer leaflet of CCS membrane. For live staining, pelleted CCS were mixed with the indicated staining solutions (please see Table 10 for preparation of the staining solutions). Samples were transferred into a 15 well chambered coverslip and either examined directly (FM4-64, Hoechst, SYTOX and Trypan Red Plus staining) or examined after 15 min of incubation at RT (AnnexinV staining) by confocal laser scanning microscopy (please see section 2.2.2.1, confocal laser scanning microscopy).

2.2.2.4 Monitoring of *Chlamydia* egress by Live cell imaging

To monitor *C. psittaci* or *C. trachomatis* egress, live cell imaging of *Chlamydia*-infected cells stably expressing eGFP was performed. HeLa cells stably expressing eGFP were cultured and infected in 8 well chambered coverslips. Live cell microscopy was performed at a Stellaris 8 Confocal Microscope equipped with a live cell chamber at 35°C. Z-stacks of 12 slices with each 3 µm distance covering both adherent cells and the supernatant containing CCS and

extrusions were acquired every 2:10 min for a total of 32.5 h starting 42 h pi. For live cell imaging of *C. psittaci* egress under calcium-free conditions, cell cultures were washed with PBS at 42 h pi and calcium- and FBS-free infection medium was added for live imaging. Live cell imaging data was visually analyzed for the type of egress pathway (CCS formation, lysis, extrusion formation or no egress) and time point. In total, for *C. psittaci* egress, *C. trachomatis* egress, and *C. psittaci* egress under calcium-free conditions, 410, 391, and 427 infected cells were analyzed, respectively.

To monitor early CERT-KO-induced egress of *C. psittaci*, live cell imaging of *Chlamydia*-infected HeLa CERT-KO cells transiently expressing eGFP was performed (please see section 2.2.1.4, transient transfection, for detailed information on the transfection procedure and Table 7 for information about the used plasmid for cytosolic expression of eGFP). Cultivation and live cell imaging were performed as described above, images were acquired every 2 min to 2.5 min from 20 h pi to 24 h pi.

2.2.2.5 Imaging of cytosolic SM exposure

To monitor the cytosolic SM exposure at the inclusion membrane, I used a HeLa cell line stably expressing a non-toxic, Halo-tagged variant of equinatoxin II (EqtSM-HaloTag) (Niekamp et al., 2022). Cytosolic exposure of SM was determined by immunofluorescence assays at middle and late infection time points. For this, cells were fixed at 24 h pi and 48 h pi and stained as described for immunofluorescence staining using a rabbit anti-HaloTag antibody (see Table 11) for EqtSM-HaloTag detection (please see section 2.2.2.2, immunofluorescence staining). To determine cytosolic exposure of SM under caspase inhibition, the caspase inhibitors Z-VAD-FMK and Z-DEVD-FMK were both used in concentrations of 2 µM. In addition, experiments with calcium- and FBS-free infection medium supplemented with the 0 mM or 1.8 mM of calcium chloride were performed. At 44 h pi, cell cultures were washed with PBS and medium was changed to the described medium conditions. Cultivation was continued for additional 4 h and subsequently, cells were fixed and stained as described for immunofluorescence staining (please see section 2.2.2.2, immunofluorescence staining). In addition, live cell imaging experiments were performed. For this, cell culture, transient transfection and infection were performed in 8 well chambered coverslips. HeLa cells stably expressing EqtSM-HaloTag were transiently transfected with a plasmid for cytosolic expression of eGFP (see Table 7) or HeLa CERT-KO cells were transiently transfected with a plasmid for cytosolic expression of EqtSM-HaloTag (see Table 7) and infected with *C. psittaci* (MOI 2). At 43.5 h pi, cells were labeled with 200 nM Janelia Fluor 585 HaloTag Ligand in infection medium for 30 min, washed with infection medium and live cell imaging was performed at a Stellaris 8 Confocal Microscope equipped with a live cell chamber at 35°C. Z-stacks of 12 slices with each 3 µm distance were acquired every 2.5 min for a total of 4 h.

2.2.2.6 Determination of proteolytic DEVD cleaving activity

Proteolytic DEVD cleaving activity was determined using the Incucyte Caspase-3/7 Red Dye for Apoptosis. Inert Incucyte Caspase-3/7 Red Dye for Apoptosis is a membrane permeable, non-fluorescent reagent consisting of the activated caspase-3/7 recognition motif DEVD coupled to a DNA intercalating dye. Cleavage of the DEVD motif by caspase-3/7 or other DEVD cleaving proteases releases the DNA intercalating dye and results in red DNA staining. To determine proteolytic DEVD cleaving activity, cells were cultured and infected in 8 well chambered coverslips. Proteolytic DEVD cleaving activity was determined using the Incucyte Caspase-3/7 Red Dye for Apoptosis as described in the manufacturer's protocol. Briefly, Incucyte Caspase-3/7 Red Dye was diluted in infection medium to a final assay concentration of 833 nM and added to *C. psittaci*-infected cell cultures at indicated time points. After further cultivation (35°C, 5% CO_2), samples were analyzed by confocal laser scanning microscopy (please see section 2.2.2.1, confocal laser scanning microscopy).

2.2.2.7 Calcium imaging

Imaging of intracellular calcium levels and distribution was performed by either Rhod 3 staining or live cell imaging of the dual calcium reporter cell line HeLa ER-LAR-Geco G-Geco (Stelzner et al., 2020).

The red-fluorescent Rhod-3 AM dye is a plasma membrane permeable dye that shows hardly no uptake to cellular organelles and thus localizes in the cytosol. After calcium-binding, the red fluorescence of Rhod-3 strongly increases. For Rhod 3 staining, cell culture and infection were performed in 8 well chambered coverslips. Rhod-3 staining was performed using the Rhod-3 Calcium Imaging Kit as described in the manufacturer's protocol. In brief, cells were washed with PBS twice and 150 µL per well of freshly prepared Rhod-3 loading buffer (see Table 10) were added. After incubation (60 min, 35°C, 5% CO_2), cells were washed three times with PBS and 150 µL per well of Rhod-3 incubation buffer (see Table 10) were added. After incubation (60 min, 35°C, 5% CO2), cells were washed with PBS and 150 µL per well of 25 mg/mL Hoechst 33342 diluted 1:2000 in infection medium were added for confocal laser scanning microscopy which was performed as described in section 2.2.2.1, confocal laser scanning microscopy.

For live cell calcium imaging, the dual calcium reporter cell line HeLa ER-LAR-Geco G-Geco (Stelzner et al., 2020) was cultured and infected in 8 well chambered coverslips. This cell line stably expresses a red fluorescent ER-targeted fluorescent calcium sensor (ER-LAR-Geco) in addition to a green fluorescent cytosolic calcium indicator (G-Geco). For imaging of cytosolic calcium levels, the green channel was monitored using a Stellaris 8 Confocal Microscope equipped with a live cell chamber at 35°C. Z-stacks of 13 slices with each 2.5 µm distance covering both adherent cells and CCS were acquired every 2.5 min for a total of 4 h. For

imaging of cytosolic calcium levels in combination with determination of the proteolytic DEVD cleaving activity, cells were stained with Incucyte Caspase-3/7 Red Dye for Apoptosis as described. Live imaging was performed using an LSM 780 CLSM equipped with a live cell chamber at 35°C. Z-stacks of 12 slices with each 2.5 µm distance covering both adherent cells and CCS were acquired every 2.5 min for a total of 4 h.

2.2.2.8 Transmission electron microscopy (TEM)

Adherent HeLa cells, which were infected with *C. psittaci* (MOI 2) for 48 h, the culture supernatant of *C. psittaci*-infected cell cultures (sedimented by centrifugation for 5 min at 300 x *g*) and adherent uninfected HeLa cells (42 h after apoptosis induction) were fixed with clinic fixative. All further sample preparation and imaging was performed in the group of Michael Laue, RKI, Berlin. After incubation for 2 h at RT, cells were scraped from the dishes and collected in HEPES buffer. All suspensions were centrifuged (6000 x *g*, 10 min) and sediments were embedded in low-melting point agarose. Small sample blocks were extracted from the solidified agarose, post fixed in osmium tetroxide (1% in distilled water) followed by block contrasting with tannic acid (0.1% in 50 mM HEPES buffer) and uranyl acetate (2% in distilled water). Subsequently, samples were dehydrated by incubation in a graded ethanol series and embedded in epon resin. After polymerization for 48 h at 60°C, ultrathin sections (approximately 70 nm) were prepared using an ultramicrotome UC7 and stained with uranyl acetate (2% in distilled water, 20 min) followed by lead citrate (2 min) to increase contrast. Sections were examined with a Tecnai 12 transmission electron microscope at 120 kV. Images were recorded using a CMOS-camera.

2.2.3 Nucleic acid techniques

2.2.3.1 qPCR

To quantify chlamydial replication, the amount of chlamydial DNA was determined using qPCR as described previously (Lienard et al., 2011) using the MasterPure Gram Positive DNA Purification Kit for DNA extraction and the Luna Universal Probe qPCR Master Mix kit for qPCR (see Table 14). Reactions were run on an AriaMx real-time PCR system (see Table 16).

2.2.3.2 Amplification PCR

To amplify DNA fragments for cloning, PCR reactions using the Phusion High-Fidelity PCR Master Mix with HF Buffer (see Table 14) were performed. The standard reaction mixtures were prepared as shown in Table 18 and run on a FlexCycler (see Table 16) using the standard cycling protocol shown in Table 19.

Table 18. Standard reaction mixture for PCR

Reagent	20 µL reaction	Final concentration
2x Phusion Master Mix	10 µL	1x
10 µM Forward Primer	1 µL	0.5 µM
10 µM Reverse Primer	1 µL	0.5 µM
50 ng/µL Template DNA	1 µL	2.5 ng/µL
Nuclease free water	7 µL	-

Table 19. Standard cycling protocol for PCR

Reaction step	Time	Temperature	Cycle
Initial denaturation	5 min	98°C	
Denaturation	30 s	98°C	
Annealing	30 s	51°C–70°C	30x
Elongation	30 s	72°C	
Final Elongation	5 min	72°C	

2.2.3.3 Agarose gel electrophoresis

Agarose gel electrophoresis was used to separate PCR products or digested DNA fragments. Agarose gels were prepared using 1.5 g agarose and 8 µL Midori Green Advanced per 100 mL TBE buffer. PCR products or digested DNA fragments were mixed with 6x DNA loading dye, applied onto the agarose gel and framed by GeneRuler 100 bp or GeneRuler 1 kb. Agarose gel run was performed at 110 V for 20 min to 35 min.

2.2.3.4 Nucleic acid isolation

DNA was isolated from agarose gels using the Wizard SV Gel and PCR Clean-Up System according to the manufacturer's instructions. In brief, excised band from agarose gel was incubated with membrane binding solution at 60°C until the gel was dissolved. Dissolved gel including DNA was loaded on an SV Binding Column (1 min, RT), washed two times with Membrane Wash Solution and eluted with DNAse free water.

2.2.3.5 Cloning by restriction enzyme digestion and ligation

For cloning by restriction enzyme digest and ligation, purified PCR product or vector were digested with restriction enzymes at 37°C for 1 h. For vector digest, linearized vector was subsequently incubated with Antarctic phosphatase at 37°C for 30 min to prevent religation. Enzymes were heat inactivated at 80°C for 20 min. After DNA purification by agarose gel electrophoresis (please see section 2.2.3.3, Agarose gel electrophoresis), vector and insert were digested using the T4 DNA ligase at RT for 15 min in a molar ratio of 1:3. Enzymes were heat inactivated at 70°C for 5 min.

2.2.3.6 Transformation of constructs into competent bacteria

Chemically competent *E. coli* (C2992) were transformed with the ligation product. After incubation for 30 min on ice, heat shock for 30 s at 42°C was performed and bacteria were again incubated for 5 min on ice. Bacteria were taken up in 1 mL SOB medium and incubated for 1 h at 37°C in a shake incubator. Subsequently, they were plated on ampicillin containing LB agar plates and incubated at 37°C overnight. The same transformation protocol was used to transform competent *E. coli* (Rosetta 2) with one of the expression plasmids pJS002 or pJS003.

2.2.3.7 Colony PCR

Colony PCR was performed as control for uptake of the correct ligated vector. For this, colonies were picked and diluted into 20 µL nuclease free water. The standard reaction mixtures were prepared as shown in Table 20 and run on a FlexCycler (see Table 16) using the standard cycling protocol shown in Table 21.

Table 20. Standard reaction mixture for Colony PCR

Reagent	20 µL reaction	Final concentration
2x Phusion Master Mix	10 µL	1x
10 µM Forward Primer pGEX	1 µL	0.5 µM
10 µM Reverse Primer pGEX	1 µL	0.5 µM
Colony	5 µL	-
Nuclease free water	3 µL	-

Table 21. Standard cycling protocol for Colony PCR

Reaction step	Time	Temperature	Cycle
Initial denaturation	5 min	95°C	
Denaturation	30 s	95°C	30x
Annealing	30 s	52°C	
Elongation	1 min	72°C	
Final Elongation	5 min	72°C	

PCR products were analyzed by agarose gel electrophoresis (please see section 2.2.3.3, Agarose gel electrophoresis).

The remaining 15 µL of the colonies were inoculated into 5 mL LB Medium with ampicillin and incubated at 37°C in a shake incubator overnight.

2.2.3.8 Plasmid DNA preparation

Plasmid DNA was prepared using the GeneJET Plasmid-Miniprep-Kit according to the manufacturer's instructions. In brief, *E. coli*-culture was transferred to a microcentrifuge tube and bacteria were pelleted (1 min, 16.000 x *g*, RT). Pelleted bacteria were resuspended in 250 µL resuspension buffer, 250 µL lysis buffer were added and lysis was performed for 5 min

at RT. Subsequently, 250 µL neutralization solution were added and dissolved DNA was separated from cell debris by centrifugation (5 min, 16.000 x *g*, RT). The supernatant including dissolved DNA was loaded onto a Spin Column. After two washing steps using Wash Solution, DNA was eluted with 50 µL DNAse free water.

2.2.3.9 Sanger sequencing

DNA sequences of final constructs were verified by Sanger sequencing using Big Dye according to manufacturer's instructions in the Robert Koch Institute sequencing facility.

2.2.4 Protein techniques

2.2.4.1 Protein Expression

Protein expression was preformed to generate antigen for *C. psittaci*-IncA or *C. psittaci*-Cps0558 antibody production. *E. coli* (Rosetta 2) were transformed with pJS003 or pJS002, respectively (please see section 2.2.3.6, transformation of constructs into competent bacteria). Single colonies were picked and used for inoculation of liquid preculture in 50 µL LB medium with ampicillin. Preculturing was performed at 37°C and 220 rpm overnight. 200 mL liquid culture were inoculated by transferring the preculture into 150 mL LB medium with ampicillin and cultivation was performed at 37°C and 220 rpm for approximately 2 h until an optical density at 600 nm (OD600) of ≥0.5 was reached. Expression of Glutathione *S*-transferase (GST)-IncA fusion protein was induced by cold shock (1 min on ice) and addition of 0.5 µM IPTG. Expression was performed at 16°C and 220 rpm overnight. Expression of GST-Cps0558 fusion protein was induced by addition of 1 µM IPTG. Expression was performed at 37°C and 220 rpm for 4 h.

2.2.4.2 Protein Purification

For protein purification, bacteria were pelleted after protein expression and the pellets were incubated with lysis buffer (see Table 10) for 30 min on ice, followed by 5x 30 s sonification interrupted by incubation on ice for 30 s to lyse bacteria and thereby release the GST-Inc fusion protein. After centrifugation (20 min, 12.000 x *g*, 4°C), the supernatant containing the soluble fraction of the GST-Inc fusion protein was added to a 5 mL disposable plastic column filled with prewashed Glutathion-Sepharose 4B and incubated at 4°C under rotation to bind the GST-Inc fusion protein to the glutathione sepharose beads. The beads were washed three times with PBS and the GST-Inc fusion protein was eluted from the beads by incubation with elution buffer at RT for 20 min three times.

2.2.4.3 SDS-PAGE

To analyze protein expression and protein Sodium Dodecyl Sulfate – PolyAcrylamid Gel Electrophoresis (SDS-PAGE) was performed. Protein separation depending on the molecular weight of proteins by gel electrophoresis was performed according to standard procedures

based on Laemmli (1970). In brief, samples were mixed with Laemmli buffer and incubated at 95°C for 5 min. Subsequently, samples were applied onto 10% to 15% separating gels with 5% stacking gel and framed by PageRuler Unstained Broad Range Protein Ladder. SDS-PAGE run was performed at 80 V for 20 min (stacking) and subsequently at 140 V for 60 min (separation).

2.2.4.4 Coomassie Blue Staining

Coomassie blue staining of SDS-PAGE gels was performed to visualize the separated proteins. After running SDS-PAGE, the gel was rinsed with distillated water and covered with Coomassie staining solution. Staining was performed under slight shaking at RT overnight. To remove background staining, staining solution was removed and the gel was covered with destaining solution under slight shaking at RT for at least 1 h. After a second destaining step, the gel was rinsed with distillated water for at least 1 h and pictures of the gels were taken.

2.2.4.5 Protein quantification by Pierce 660 nm Protein Assay

Protein concentrations of purified antigen (please see section 2.2.4.2, protein purification) were measured by Pierce 660 nm Protein Assay according to the manufacturer's instructions. In brief, 10 µL of protein samples and BSA standard in concentrations ranging from 0 µg/mL to 2000 µg/mL were mixed with 150 µL Protein Assay Reagent in 96-Well-Plates. After mixing on a plate shaker for 1 min and incubation at RT for 5 min, absorbance at 660 nm was measured using a microplate reader.

2.2.4.6 Antibody production and Affinity purification

Polyclonal rabbit anti-IncA and anti-Cps0558 antibodies were produced by immunization of rabbits with the C-terminal cytoplasmic fragment of IncA or Cps0558 fused to GST. All animal handling and antibody purification was performed by Biogenes, Berlin.

2.2.5 Lipid techniques

2.2.5.1 Sample collection for untargeted 4D cell lipidomic profiling

To generate samples for untargeted 4D cell lipidomic profiling, HeLa cells were cultivated in 6 well plates and infected with *C. psittaci* (MOI 2). At 20 h pi or 44 h pi, cells were washed with PBS and 2 mL FBS-free medium was added. After further cultivation for 4 h, cells were harvested on ice. Medium was removed and cells were scraped into 1 mL of harvesting solution and transferred into 2 mL reaction tubes. After centrifugation (5 min, 5000 x *g*, 4°C), supernatant was removed and pellets were stored at -80°C.

2.2.5.2 Sample preparation and shipping for untargeted 4D cell lipidomic profiling

For lipidomics analysis, cell pellets were resuspended in 200 µL ice-cold methanol to lyse cells and denature cellular proteins. Subsequently, methanol was evaporated using a vacuum

concentrator. Samples were shipped on dry ice for lipid extraction and LC-MS/MS measurements to the Integrated Proteomics and Lipidomics platform of the SPP2225, Johannes Gutenberg-Universität, Mainz, to the group of Laura Bindila.

2.2.5.3 Liquid-liquid extraction for untargeted 4D cell lipidomic profiling

Lipid extraction was performed in the group of L. Bindila, Johannes Gutenberg-Universität, Mainz. All steps of the liquid-liquid extraction (LLE) procedure were carried out at 4°C on ice, using a slightly modified in-house developed extraction protocol for lipid extraction from low-amount cell samples (del Barrio Calvo & Bindila, 2024; Post et al., 2022).

At first, samples were spiked with 5-7 pre-cooled stainless steel beads, then 800 µL of ice-cold MTBE/MeOH (10:3; v/v) containing spiking solution (a mixture of deuterated internal standards (ISTDs)) and 250 µL of ice-cold 0.1 M formic acid were added to the samples. Next, the tubes were placed into the tissue disrupter for 30 s of homogenization at maximal speed. Homogenates (without steel balls) were then transferred into new pre-cooled 1.5 mL Eppendorf tubes. Next, samples were vortexed in a Thermo Shaker (maximum speed, 15 min, 4°C), followed by centrifugation (10 min, 5000 x *g*, 4°C). The resulting upper organic phase was transferred in new 1.5 mL Eppendorf tubes and evaporated under a gentle stream of N_2 at 37°C for 5 min. Dried extracts were then stored at -80°C for further processing.

2.2.5.4 Untargeted 4-dimensional trapped ion mobility mass spectrometry cell lipid profiling

Lipidomics analysis was performed in the group of L. Bindila, Johannes Gutenberg-Universität, Mainz. For lipid separation, an UHPLC system with a C18 Luna Omega column (100 Å × 2.1 mm × 1.6 µm) was used to perform reversed-phase (RP) chromatographic separation of samples. The column was thermostated at 45°C. The separation solvent and gradient system used for the lipidomic and metabolomic approach in negative and positive ion mode, as well as the LC lipidomic gradient, is the same as described previously (Lerner et al., 2023).

This gradient was run at a flow rate of 0.2 mL/min. In positive mode, the injection volume onto the column was 10 µL, whereas in negative mode, it was 20 µL. Throughout the analysis, the auto-sampler remained consistently at 4°C. The experiments were conducted in a hybrid TIMS-qToF mass spectrometer coupled to the UHPLC system for both negative ion mode and positive ion mode. For fragmentation analysis, the scan mode was set to PASEF with the mass scan range of 100–1,350 Da for both MS1 and MS2 acquisition. The acquisition cycle consisted of 0.1 s with the mobility scan range of 0.55–1.87 V*s/cm^2 for the positive mode and 0.55–1.86 V*s/cm^2 for the negative mode.

Throughout data acquisition, Compass Hystar 6.2 and timsControl2 application (Bruker Daltonics in Bremen, Germany) are used to control the LC- and the timsTOF instrument. Data

assessment and processing, such as verification of lipid annotations, evaluation of specifically extracted ion chromatograms or fragmentation patterns of interest, as well as standardized performance- and quality- checking's, were done using Compass DataAnalysis. Additionally, Metaboscape 2021b was used to verify lipid annotation, to extract the 4D-lipid features, and for further lipid identification and curation using internal and external reference lipid databases. For semi-quantification, analyte peak areas were normalized to those of class-specific ISTDs, molecular weights, and protein content (BCA kit standard procedure according to the manual provided with the kit). Lipid levels were then calculated based on spiked amounts of ISTDs and given in nmol/mL. Relative amounts of lipid levels were calculated and given in mol% of total lipids.

2.2.6 Computational methods

2.2.6.1 In silico cloning, sequence alignment

For in silico cloning the software Geneious Prime was used. DNA sequences were imported from NCBI databases and oligo design, alignments and cloning steps were performed using Geneious built-in algorithms. Sequence alignments were performed with the Geneious Alignment option using the type of global alignment with free end gaps.

2.2.6.2 Image analysis

For quantification of AnnexinV, TrypanRed and SYTOX Green staining, the software Fiji was used. Particle identification of membranes and nuclei was performed using Otsu's threshold clustering algorithm based on AnnexinV staining or Hoechst staining channel, respectively, and CCS were identified by phase contrast images. Mean intensity of AnnexinV staining at membranes, SYTOX Green staining at nuclei or TrypanRed staining of CCS or apoptotic cells was determined. The distribution of the mean intensities of CCS and apoptotic cell structures was visualized as violin plot using GraphPad Prism.

2.2.7 Statistical Analysis

Data from at least two biological independent experiments were taken and technical replicates were included to correct for internal variations. If not noted otherwise, mean values and standard errors of the mean are plotted in the diagrams (mean ± SEM). Statistical significance was determined by indicated statistical test (*: p-value < 0.05; **: p-value < 0.01; ***: p-value < 0.005). Principal component analysis was computed using GraphPad Prism.

3 Results

3.1 Analysis of intracellular development of *C. psittaci* indicates that massive infectious EB release can initiate at 40 h pi

Egress of *Chlamydia* spp. completes their intracellular development with the release of a high number of infectious bacteria (Banhart et al., 2019; Hybiske & Stephens, 2007; J. K. Lee et al., 2018; Zuck et al., 2017). Thus, the outcome of egress depends on the one hand on the previous success during RB replication to ensure that high numbers of bacteria can egress. On the other hand, it depends on the redifferentiation of RBs to EBs and on the timing of egress subsequent to EB accumulation to ensure that the present bacteria are infectious. Hence, in the first part of this study, I investigated the timing of RB replication, RB redifferentiation to EB and EB accumulation during the intracellular developmental cycle of *C. psittaci* in HeLa cells.

3.1.1 Infectious progeny formation during the intracellular development of *C. psittaci* starts at 26 h pi and reaches its maximum between 40 h pi and 48 h pi

At first, I determined the number of bacteria by genome copy and formation of infectious progeny of *C. psittaci* at different time points during infection of HeLa cells (MOI 2).

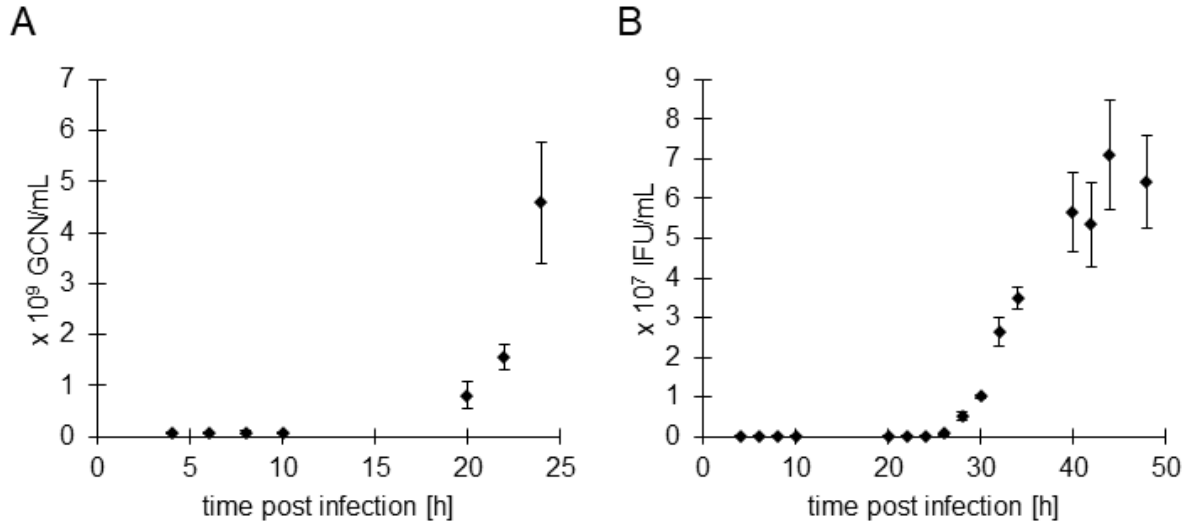

Figure 7. Time course of replication and progeny formation of *C. psittaci* during the infection of HeLa cells. HeLa cells were infected with *C. psittaci* (MOI 2) and at the indicated time points, samples of infected cells were taken for **(A)** the determination of the genome copy number (GCN) by qPCR or **(B)** the determination of infection forming units (IFU) by reinfection assays. Data show mean ± SEM; n = 3. *GCN and progeny determination was performed by Andrea Martini, RKI, Berlin*

The genome copy number (GCN) of *C. psittaci* remained relatively constant between 4 h pi and 10 h pi with approximately 0.06 to 0.08 x 10^9 GCN/mL, marking the lag phase of bacterial development, where the bacteria are endocytosed and differentiate to RBs and do not replicate. Between 10 h pi and 20 h pi, the GCN increased to 0.81 x 10^9 GCN/mL, marking the start of rapid RB replication and the beginning of the exponential growth phase. The GCN

further increased to 1.57 and 4.59 x 10^9 GCN/mL at 22 h pi and 24 h pi, respectively, showing that RB replication continued (Figure 7 A). The infectious progeny remained at 0.01 x 10^7 IFU/mL between 4 h pi and 24 h pi. Between 24 h pi and 26 h pi, the infectious progeny started to increase exponentially. This exponential increase of infectious progeny continued until 40 h pi, where the infectious progeny was increased up to 5.65 x 10^7 IFU/mL. Between 40 h pi and 48 h pi, the infectious progeny remained stationary, varying between 5.34 and 7.11 x 10^7 IFU/mL (Figure 7 B).

This data show that RB replication started between 10 h pi and 20 h pi, RBs started to redifferentiate to EBs between 24 h pi and 26 h pi, and this redifferentiation phase ended with EB accumulation between 40 h pi and 48 h pi.

3.1.2 RB-to-EB redifferentiation of *C. psittaci* starts at 24 h pi and EBs accumulate within the inclusion at 42 h pi

To investigate the developmental stages of *C. psittaci* during the time course of infection, *C. psittaci*-infected HeLa cells were analyzed by TEM at the beginning of RB replication, at the beginning of RB redifferentiation to EB, during RB to EB redifferentiation, and during EB accumulation at 12 h pi, 24 h pi, 34 h pi, and 42 h pi, respectively.

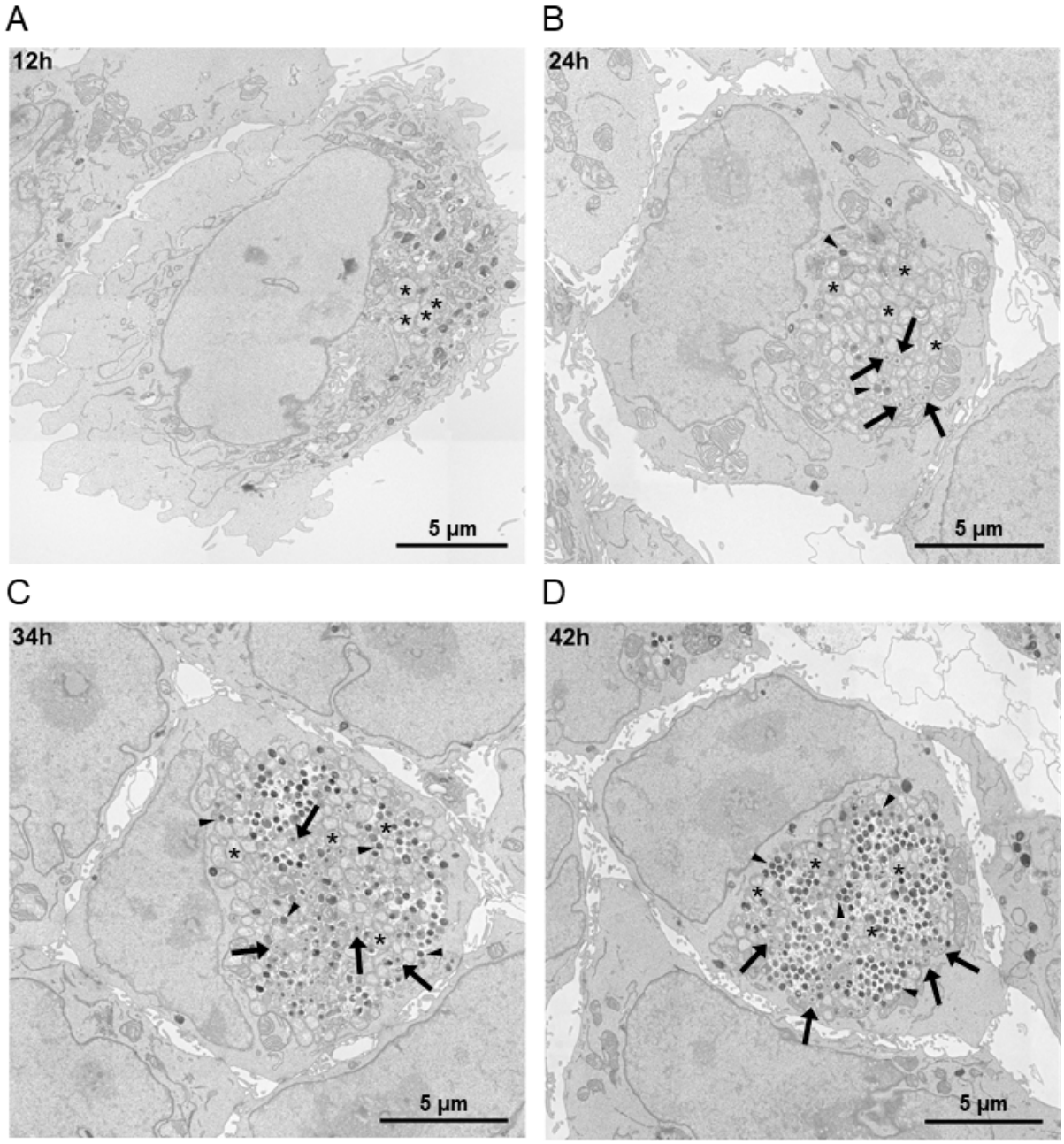

Figure 8. Time course of *C. psittaci* differentiation stages during the time course of infection of HeLa cells. HeLa cells were infected with *C. psittaci* (MOI 2). At **(A)** 12 h pi, **(B)** 24 h pi, **(C)** 34 h pi, and **(D)** 42 h pi, cells were chemically fixed, embedded, and thin sections were prepared. Panels show representative transmission electron microscopy images with *C. psittaci* reticulate bodies, intermediated bodies and elementary bodies marked with an asterisk, arrow, or arrowhead, respectively; n = 3. *Electron microscopy was performed in the group of M. Laue, RKI, Berlin.*

At 12 h pi, single RBs were observed in inclusions in the vicinity of the host cell nucleus that started to replicate (Figure 8 A). At 24 h pi, the inclusion increased in size and was filled with RBs, some intermediate bodies (IBs) and single EBs (Figure 8 B). At 34 h pi, the size of the inclusion was further increased and EBs, IBs, and RBs were found in similar proportions within the inclusion (Figure 8 C). At 42 h pi, the size of the inclusion remained constant, but the proportion of EBs increased, while the proportion of RBs decreased (Figure 8 D).

TEM analysis supports that during *C. psittaci* infection of HeLa cells, RB replication starts at 12 h pi, redifferentiation of RB to EB starts at 24 h pi, and EBs accumulate at 42 h pi,

suggesting that egress of *C. psittaci* in HeLa cells takes place after 42 h pi to release a high number of infectious bacteria.

3.1.3 Localization of chlamydial HSP60 and IncA during the intracellular development of *C. psittaci* confirms that at 42 h pi egress could initiate

To further describe the different stages of intracellular development of *C. psittaci*, I analyzed *C. psittaci*-infected HeLa cells by confocal laser scanning microscopy for the localization of two chlamydial model proteins, HSP60 and IncA. While HSP60 is a chlamydial heat-shock protein that localizes inside of the bacteria, Inc A is a type III secreted protein that localizes in the inclusion membrane after 18 h pi during RB replication, redifferentiation and EB accumulation (Borth et al., 2011; Rockey et al., 1995, 1997; Yuan et al., 1992).

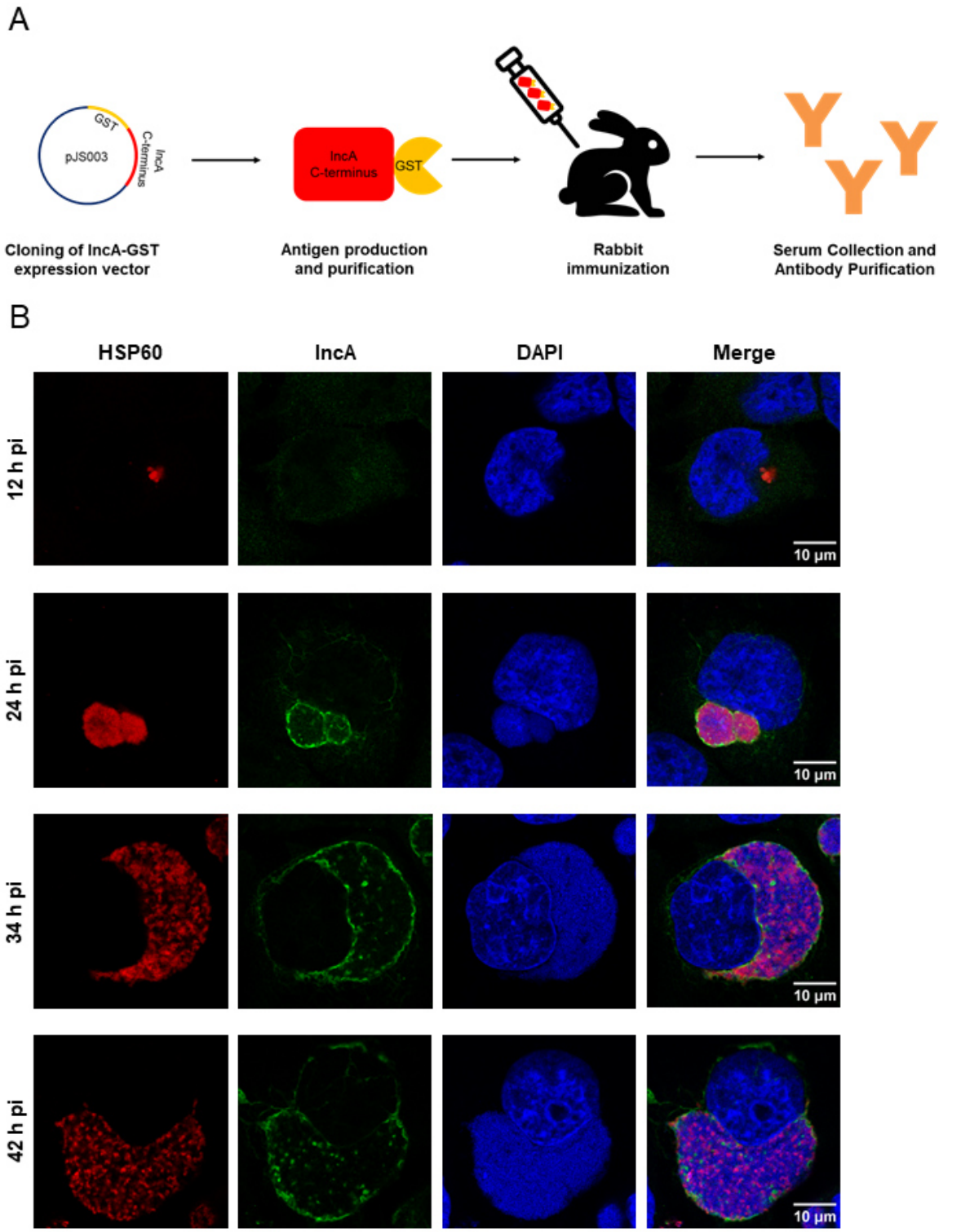

Figure 9. HSP60- and IncA-immunofluorescent staining is characteristic for the different phases of intracellular development of *C. psittaci*. (A) Schematic showing the generation of antibodies against IncA. IncA-GST expression vectors were cloned (see Supplemental Figure S1 for more details) and the protein was recombinantly expressed in *E. coli* and purified for antigen production (see Supplemental Figure S2 for more details). Rabbits were immunized with the purified antigen. Animal serum was collected and antibodies were purified. *All animal handling and antibody purification was performed by Biogenes, Berlin. Generation of antibodies against Cps0558 was performed following an analogical strategy.* **(B)** Localization of HSP60 and IncA during *C. psittaci* infection. HeLa cells were infected with *C. psittaci* (MOI 2) and at the indicated time points, cells were fixed with PFA. HSP60 and IncA were detected using a mouse-anti-HSP60 (Cy3) and a rabbit-anti-IncA (AF488) antibody, respectively. The DNA was counterstained using DAPI; n = 3.

To analyze the localization of IncA and HSP60, I performed immunofluorescent staining using antibodies against these targets. While anti-HSP60 antibodies are commercially available, anti-IncA antibodies were generated in-house. For this, I cloned an expression vector for the C-terminal cytosolic domain of IncA fused to GST. Vector expression and purification of the IncA-GST fusion protein as antigen for the subsequent immunization of rabbits was performed and antibody-containing rabbit serum was collected and purified (Figure 9 A). All animal handling and antibody purification was performed by Biogenes, Berlin. More detailed information on molecular cloning and antigen expression and purification is given in Supplemental Figure S1 and Supplemental Figure S2, respectively.

I examined *C. psittaci*-infected HeLa cells at the beginning of RB replication, at the beginning of RB redifferentiation to EB, during RB to EB redifferentiation, and during EB accumulation at 12 h pi, 24 h pi, 34 h pi, and 42 h pi, respectively. At 12 h pi, a small inclusion filled with HSP60-positive bacteria localized next to the nucleus. IncA in the inclusion membrane was not detected by immunofluorescence microscopy (Figure 9 B). In contrast, at 24 h pi, the enlarged HSP60-positive inclusion was surrounded by an IncA-positive inclusion membrane, characteristic for the continuing massive RB replication at the beginning of RB redifferentiation to EB. At 34 h pi, the inclusion further increased in size and only subsections of the inclusion were still filled with HSP60, characterizing the continuing redifferentiation to EB, while some RB still replicate. At 42 h pi, the inclusion remained at the same size, while the HSP60-staining within the inclusion was even more fragmented, showing the ongoing EB accumulation (Figure 9 B). At 34 h pi and 42 h pi, the inclusion membrane remained IncA-positive.

This data points out that during *C. psittaci* infection in HeLa cells, HSP60 and IncA show a characteristic localization at the beginning of RB replication, at the beginning of RB redifferentiation to EB, during RB to EB redifferentiation, and during EB accumulation. This staining pattern could be used to analyze the time course of infection of *C. psittaci* in other host cells.

3.2 *Chlamydia*-containing spheres (CCS) are a novel and predominant form of egress by the pathogen *C. psittaci*

Host cell egress is an essential step in the life cycle of intracellular pathogens, in addition to host cell invasion and intracellular replication (Flieger et al., 2018). Chlamydial egress has been mainly described for *C. trachomatis* and occurs through host cell lysis or non-lytic extrusion formation (Hybiske & Stephens, 2007; Zuck et al., 2016). However, the egress pathways of the zoonotic pathogen *C. psittaci* are not well understood. Therefore, in the second part of this study, I aimed to investigate *C. psittaci* egress in greater detail.

3.2.1 *C. psittaci* egresses from the cellular monolayer through formation of *Chlamydia*-containing spheres (CCS)

To investigate *C. psittaci* egress in greater detail, I monitored HeLa cells that stably expressed eGFP in the cytosol after infection with *C. psittaci* using fluorescence live cell microscopy, starting during EB accumulation at 42 h pi. Initially, the bacterial inclusion did not contain any eGFP as indicated by a black hole in the eGFP-detecting channel (Figure 10 A). Then blebbing of the cellular plasma membrane was observed, followed by the influx of eGFP into the inclusion lumen, demonstrating loss of inclusion membrane integrity. Subsequently, the plasma membrane blebs enlarged, and the entire host cell detached, forming spherical, low phase-contrast structures in the supernatant of the infected cell cultures. I named these structures *Chlamydia*-containing spheres (CCS) (Figure 10 A).

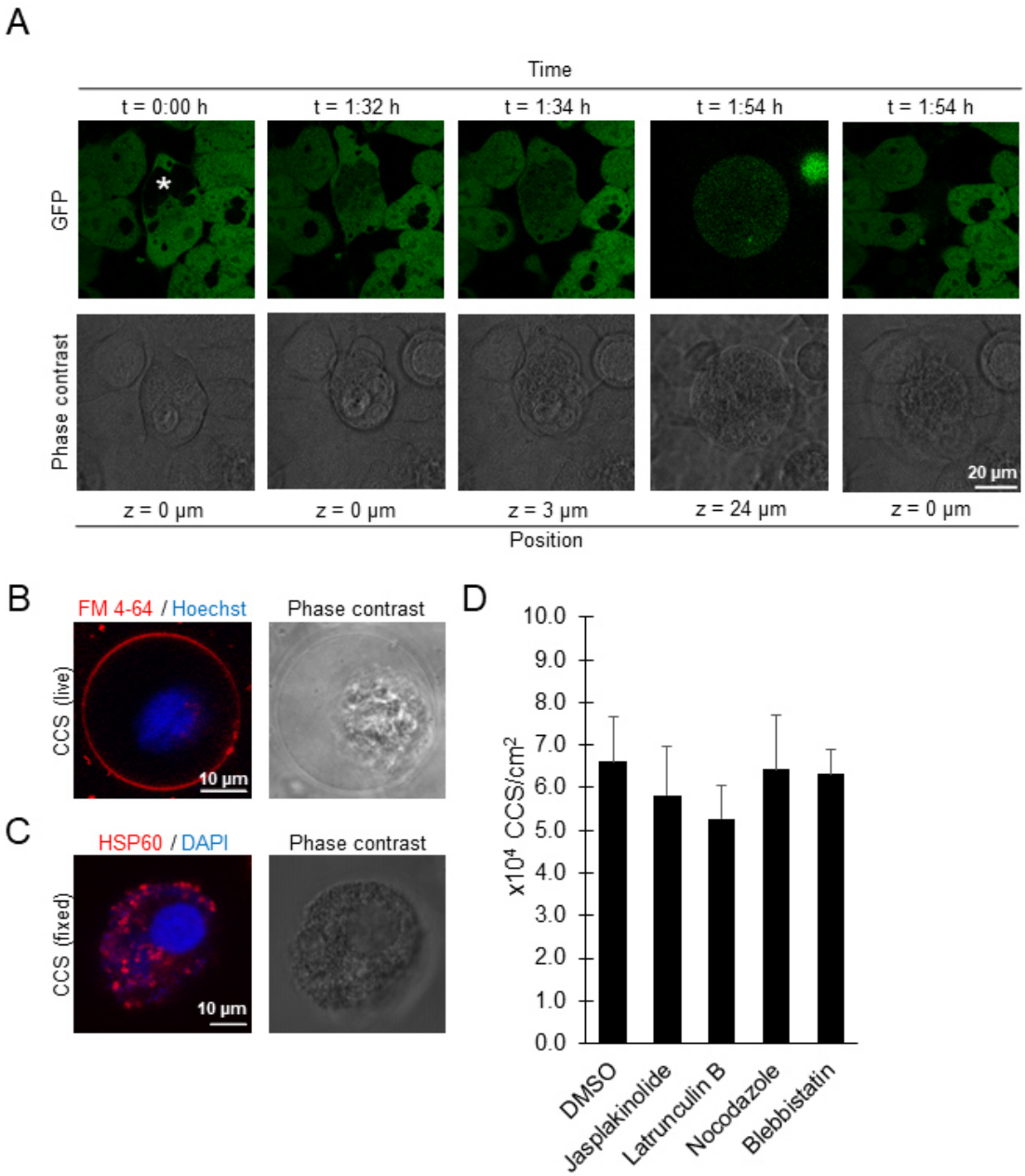

Figure 10. CCS formation represents the predominate *C. psittaci* egress pathway and is characterized by membrane blebbing and destabilization of the inclusion membrane. (A) Time course of CCS formation. *C. psittaci*-infected HeLa cells (MOI 2) stably expressing GFP were monitored from 42 h pi to 74.5 h pi using a CLSM equipped with a live-cell chamber. Panels show representative images of a section plane of a CCS forming HeLa cell; n = 2. Asterisk indicates *C. psittaci* inclusion. **(B)** Representative fluorescence images of a live CCS isolated of the supernatant of *C. psittaci*-infected HeLa cells (MOI 2, 48 h pi). The surrounding membrane was visualized using the membrane marker FM 4-64 and DNA was counterstained by Hoechst; n = 3. **(C)** Representative fluorescence images of a PFA-fixed CCS isolated from *C. psittaci*-infected HeLa cells (MOI 2, 48 h pi). Bacteria inside the CCS were detected using a chlamydial HSP60 (Cy3) antibody and the DNA was counterstained using DAPI; n > 3. **(D)** CCS formation is not influenced by inhibitors of host cell cytoskeleton elements. HeLa cells were infected with *C. psittaci* at MOI 2, washed with PBS at 44 h pi and treated with 1 µM jasplakinolide, 0.5 µM latrunculin B, 30 µM nocodazole, 50 µM blebbistatin or DMSO (negative control) and stained with Hoechst. *C. psittaci* CCS in the supernatant were quantified at 48 h pi. Data show mean ± SEM; n ≥ 3; *p < 0.05; (Student's t-test). Modified from Scholz et al., 2024b.

To describe the morphology of *C. psittaci* CCS, I stained CCS with different markers and analyzed stained CCS by CLSM. CCS were stained with FM 4-64, a dye that stains the plasma membrane and then integrates into the cellular vesicular network, and Hoechst. Fluorescence live cell confocal microscopy of stained CCS showed that CCS were surrounded by a

membrane and contained concentrated DNA, suggesting the presence of the cell nucleus (Figure 10 B). CLSM was used to examine immunofluorescence staining of fixed CCS. Antibodies specific for bacterial HSP60 were used, along with the DNA marker DAPI, showing that bacteria positive for both markers were dispersed throughout the CCS, while concentrated, HSP60-negative DNA next to the bacteria support the presence of a host cell nucleus within CCS (Figure 10 C).

The formation of *C. trachomatis* extrusions depends on different parts of the host cell cytoskeleton (Hybiske & Stephens, 2007). To investigate the requirement of the host cell cytoskeleton for CCS formation, I treated *C. psittaci*-infected cell cultures between 44 h pi and 48 h pi with the previously described inhibitors jasplakinolide, latrunculin B, nocodazole and blebbistatin as inhibitors of actin depolymerisation, actin polymerisation, microtubules, neural Wiskott-Aldrich syndrome protein (N-WASP) and myosin II, respectively. I observed no significant difference in the number of CCS formed between DMSO-treated controls (6.6×10^4 CCS/cm^2) and jasplakinolide-, latrunculin B-, nocodazole- and blebbistatin-treated samples (5.8, 5.3, 6.4 and 6.3×10^4 CCS/cm^2, respectively) (Figure 10 D).

Collectively, these data demonstrate that *C. psittaci* egresses from cell culture monolayers by CCS formation, a novel non-lytic egress pathway.

3.2.2 *C. psittaci* CCS formation is fundamentally different to *C. trachomatis* extrusion formation

Next, I performed a side-by-side comparison between *C. trachomatis* extrusion formation and *C. psittaci* CCS formation to show that CCS formation clearly differs from extrusion formation on a morphological and mechanistical level.

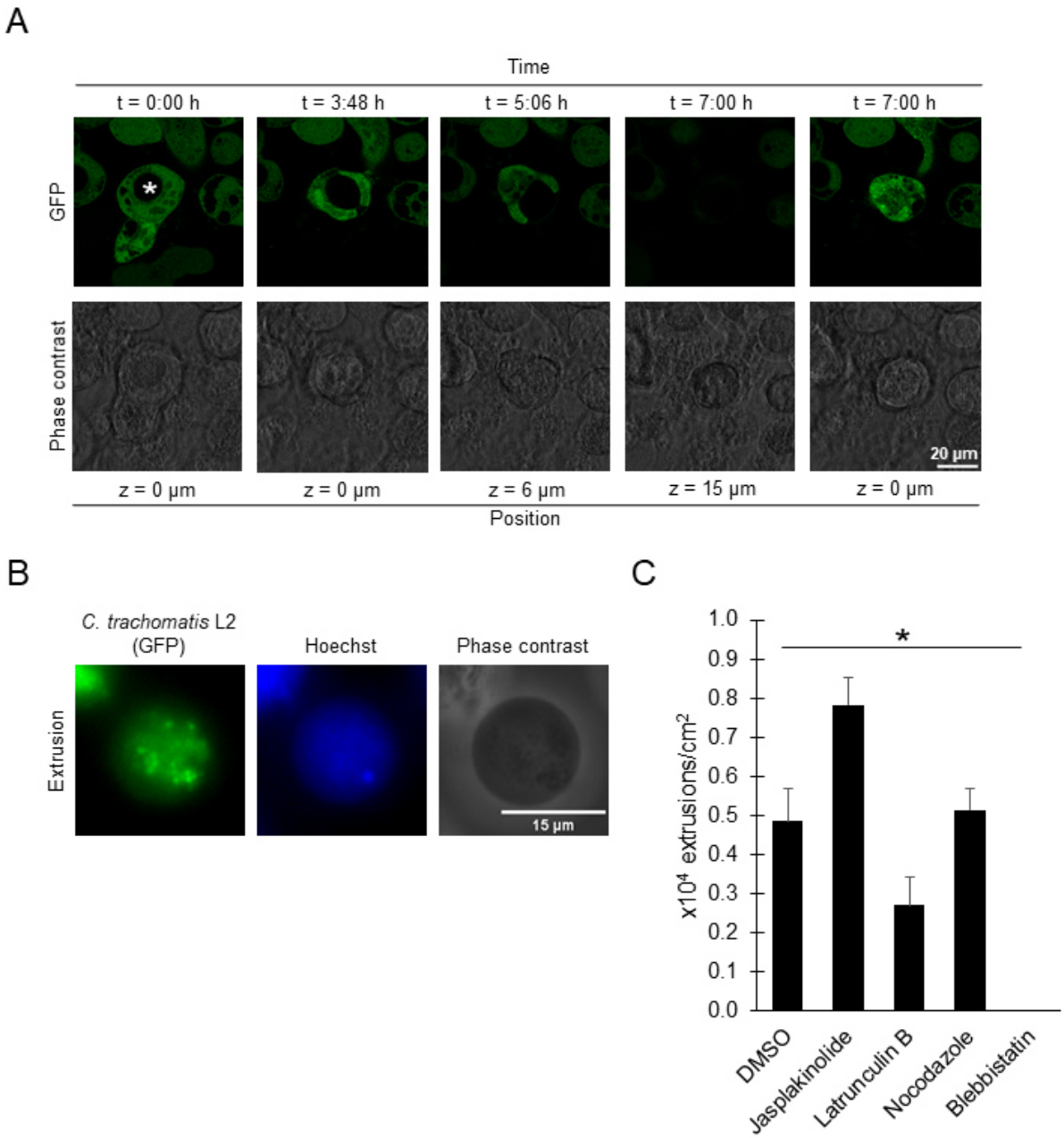

Figure 11. Extrusion formation of *C. trachomatis* is characterized by a stabilized inclusion membrane, surviving of the host cell and dependency on the host cell cytoskeleton. (A) Time course of extrusion formation. *C. trachomatis* L2-infected HeLa cells (MOI 2) stably expressing GFP were monitored from 42 h pi to 74.5 h pi using a CLSM equipped with a live-cell chamber. Panels show representative images of a section plane of an extrusion forming HeLa cell; n = 2. Asterisk indicates *C. trachomatis* inclusion. **(B)** Representative fluorescent image of a *C. trachomatis* L2 extrusion. HeLa cells were infected with GFP-expressing *C. trachomatis* L2 (MOI 2) and at 70 h pi, cells were stained with Hoechst. At 74 h pi, supernatants were microscopically analyzed; n = 3. **(C)** *C. trachomatis* L2 extrusion formation is influenced by inhibitors of host cell cytoskeleton elements. HeLa cells were infected with GFP-expressing *C. trachomatis* L2 at MOI 2, washed with PBS at 70 h pi, treated with 1 µM jasplakinolide, 0.5 µM latrunculin B, 30 µM nocodazole, 50 µM blebbistatin or DMSO (negative control) and stained with Hoechst. *C. trachomatis* L2 extrusions in the supernatant were quantified at 74 h pi. Data show mean ± SEM; n ≥ 3; *p < 0.05; (Student's t-test). Modified from Scholz et al., 2024b.

At first, I conducted fluorescence live-cell microscopic analysis using HeLa cells stably expressing cytosolic eGFP that were infected with *C. trachomatis* L2. Unlike CCS formation, the release of *C. trachomatis* L2 through extrusions resulted in the inclusion remaining eGFP negative throughout the process, supporting previous observations that the inclusion

membrane remains intact in extrusions (Hybiske & Stephens, 2007). Additionally, during extrusion formation, the host cell remained intact and did not detach (Figure 11 A).

Next, I analyzed *C. trachomatis* extrusions for the presence of a host cell nucleus. In contrast to CCS, extrusions formed by *C. trachomatis* L2 expressing eGFP and stained with Hoechst were filled with bacteria that were positive for both eGFP and Hoechst, but no other host cell structures were detected by Hoechst staining (Figure 11 B), supporting the absence of a host cell nucleus within extrusions.

While CCS formation is independent from the host cell cytoskeleton (Figure 10 D), it was previously shown that the formation of *C. trachomatis* extrusions depends on different parts of the host cell cytoskeleton (Hybiske & Stephens, 2007). I was able to reproduce this dependency on the host cell cytoskeleton of *C. trachomatis* extrusion formation as I observed an increase in extrusion formation for jasplakinolide and nocodazole treated samples (0.78 and 0.51 x 10^4 extrusions/cm^2, respectively) compared to DMSO treated controls (0.49 x 10^4 extrusions/cm^2) and a decrease in extrusion formation for latrunculin B and blebbistatin treated samples (0.27 and 0.00 x 10^4 extrusions/cm^2, respectively) (Figure 11 C), consistent with the findings of Hybiske & Stephens (2007).

These results indicate that *Chlamydia*-containing spheres (CCS) are clearly distinguishable from *C. trachomatis* extrusions both morphologically and in their formation.

3.2.3 Ultrastructural characterization of *C. psittaci* egress by TEM

I next characterized CCS by TEM to resolve CCS morphology at the ultrastructural level.

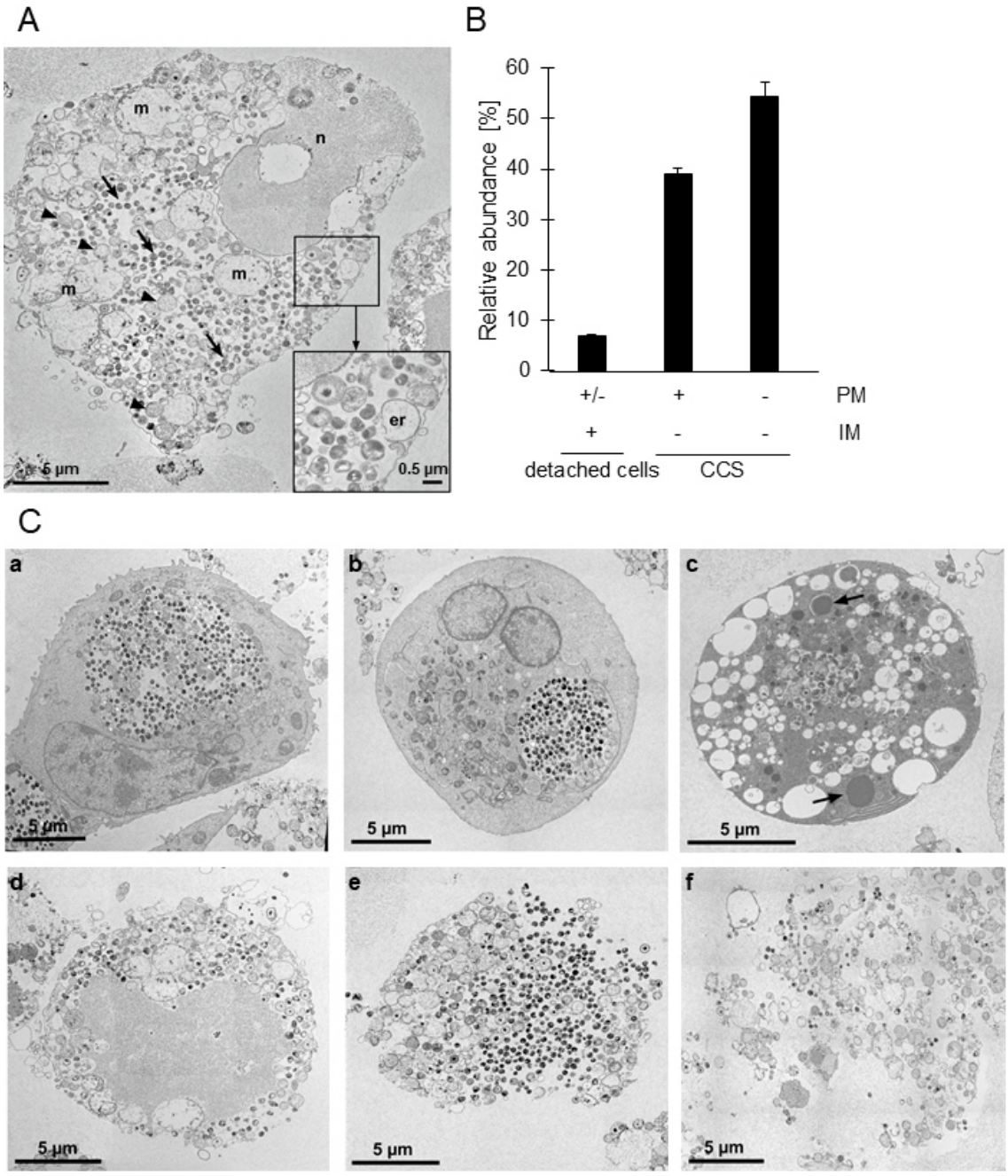

Figure 12. CCS are distinct from infected adherent cells, apoptotic cells and extrusions on an ultrastructural level. (A) Transmission electron microscopy (TEM) of a thin section through a chemically fixed CCS isolated from the supernatant of *C. psittaci*-infected HeLa cells (MOI 2, 48 h pi). The CCS is almost entirely surrounded by an intact membrane and reveals many RBs (arrowheads) and EBs (arrows) besides structurally impaired cell organelles, such as mitochondria (m) or the nucleus (n). The inset shows a small region from the center of the CCS at higher magnification with bacteria at different stage of differentiation; n = 3. **(B)** Quantification of the CCSs and detached cells found in the supernatant of *C. psittaci*-infected HeLa cell cultures. TEM images of thin sections through fixed and embedded supernatants of *C. psittaci*-infected HeLa cells (MOI 2, 48 h pi) were analyzed for the different structures present (see Figure 12 C for an overview of some of the structures). IM, inclusion membrane; PM, plasma membrane. Data shows mean ± SEM; n = 3. **(C)** Representative transmission electron microscopy images of thin sections through chemically fixed *C. psittaci*-infected HeLa cells (MOI 2, 48 h pi) **(a-c)** and *C. psittaci* containing cellular structures found in the supernatant above these cells **(d-f)**. **(a, b)** Section profiles of intact HeLa cells with intact inclusion bodies. The cell in (a) was fixed while adhered at the substrate (note the flat cell bottom) and the cell with the round profile in (b) was fixed in the supernatant. **(c)** Round cell profile of an apoptotic cell with a bacterial inclusion fixed in the supernatant. Note the profiles of the fragmented nucleus (arrow) which are surrounded by cisternae of the rough endoplasmic reticulum and the many profiles of larger vesicles. **(d-e)** Section profile of CCSs fixed in the supernatant with either visible (d) or invisible (e) plasma membrane. **(f)** Profiles of bacteria and cell organelles dispersed in low-melting point agarose used for stabilizing the sediment after fixation of the supernatant. *Electron microscopy was performed in the group of M. Laue, RKI, Berlin.* Modified from Scholz et al., 2024b.

TEM showed that CCS are bounded by a more or less intact plasma membrane and contain *C. psittaci* EBs and fewer RBs, which are dispersed throughout the CCS. The bacteria intermingle with morphologically impaired cell organelles such as mitochondria, endoplasmic reticulum and nucleus and are not separated from them by an inclusion membrane (Figure 12 A).

Quantification of *C. psittaci*-containing cellular structures found in the supernatant of *C. psittaci*-infected cell cultures showed that 93% of the structures were CCS, while 7% were detached cells (Figure 12 B).

In the detached cells bacteria were surrounded by an inclusion membrane and 84% of the cells showed signs of cell death (apoptosis or necrosis) with or without preserved plasma membrane. No inclusion membrane was found in any of the CCS detected and the CCS showed no signs of apoptosis. 39% of the CCS were surrounded by a plasma membrane, while 54% revealed only fragments of the plasma membrane around the CCS, suggesting that the stability of the plasma membrane was affected by CCS formation (Figure 12 B, C). Besides the structures described above, the supernatant showed detached cells without any bacteria and aggregates of cellular debris with and without bacteria (Figure 12 C).

The data presented indicate that CCS are distinct from extrusions in terms of their structural and ultra-structural characteristics.

3.2.4 CCS formation as egress form of *C. psittaci* occurs in lung cell infections

In humans, *C. psittaci* predominantly infects the respiratory tract (Knittler & Sachse, 2015; Radomski et al., 2016).

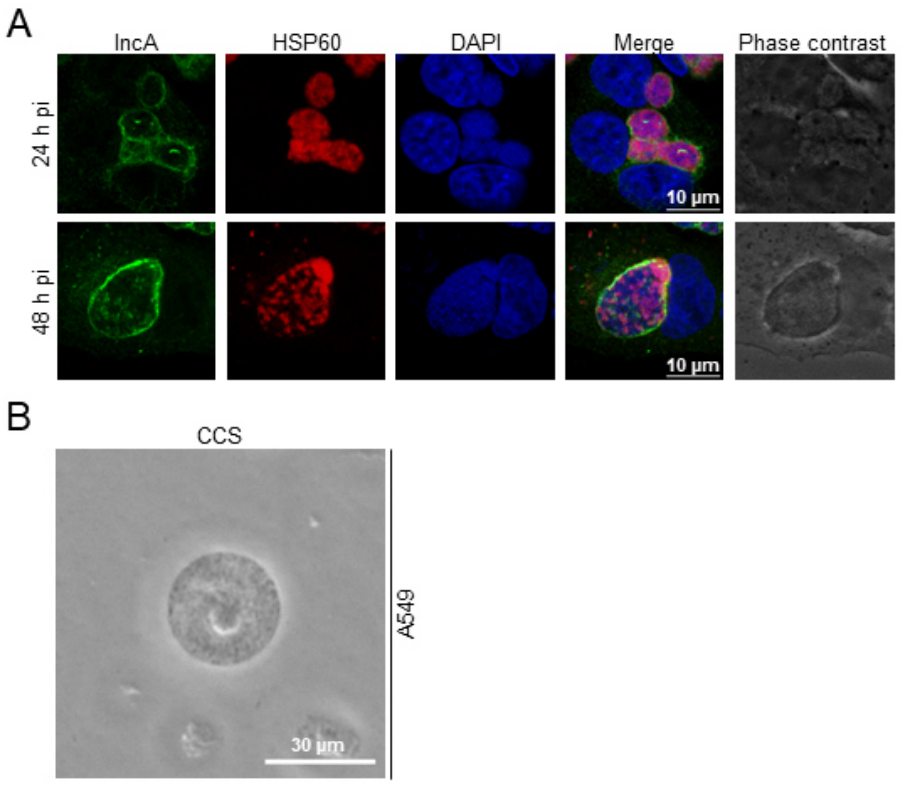

Figure 13. CCS are formed in *C. psittaci*-infected A549 cells. (A) Representative fluorescence images of *C. psittaci*-infected A549 cells (MOI 2, 24 h pi). PFA-fixed cells were stained for *C. psittaci* and the inclusion membrane using a mouse-anti-HSP60 (Cy3) and a rabbit-anti-IncA (AF488) antibody, respectively. DNA was counterstained using DAPI. n = 2. **(B)** Representative image of a CCS in the supernatant of infected A549 cells (MOI 2, 48 h pi); n = 3. Modified from Scholz et al., 2024b.

To investigate whether CCS are also formed after infection of lung tissue cell lines or not, I studied *C. psittaci* infections in the lung tissue cell line A549. At first, I showed that A549 cells can be infected with *C. psittaci* by detecting inclusions using immunofluorescence staining for the chlamydial antigens HSP60 and *C. psittaci*-specific IncA. *C. psittaci* inclusions were filled with HSP60 stained *Chlamydia* and surrounded by an IncA stained inclusion membrane at 24 h pi and 48 h pi (Figure 13 A). Microscopical analysis of supernatants of infected A549 cells at 48 h pi revealed spherical structures with a diameter of 25-30 µm that I identified as CCS (Figure 13 B).

These data show that CCS formation occurs after lung cell infections, indicating that CCS formation is a relevant egress type that occurs in different cell lines.

3.2.5 CCS formation is the predominant egress pathway of *C. psittaci* and is also present, but less frequent for *C. trachomatis*

During *C. trachomatis* infection of HeLa cell culture monolayers, host cell lysis and extrusion formation occur at nearly identical frequencies at 72 h pi (Hybiske & Stephens, 2007). To compare this later time point of infection with *C. psittaci* infections, I monitored HeLa cells infected with *C. psittaci* that stably expressed eGFP in the cytosol by live cell microscopy from 42 h pi to 74.5 h pi. The frequencies of CCS formation, extrusion formation, and host cell lysis

were quantified at each time point pi (Figure 14 A). Throughout the observation period, I observed a nearly linear increase of egress events over time with 63% of bacteria egressed at the end of the observation period. CCS formation and host cell lysis were constantly observed, while extrusion formation was not observed in *C. psittaci* infections. At the end of the observation period, 41.2% of the infected cells formed CCS and 21.5% underwent host cell lysis (for a representative panel of a *C. psittaci*-infected cell undergoing host cell lysis, see Supplemental Figure S3 A).

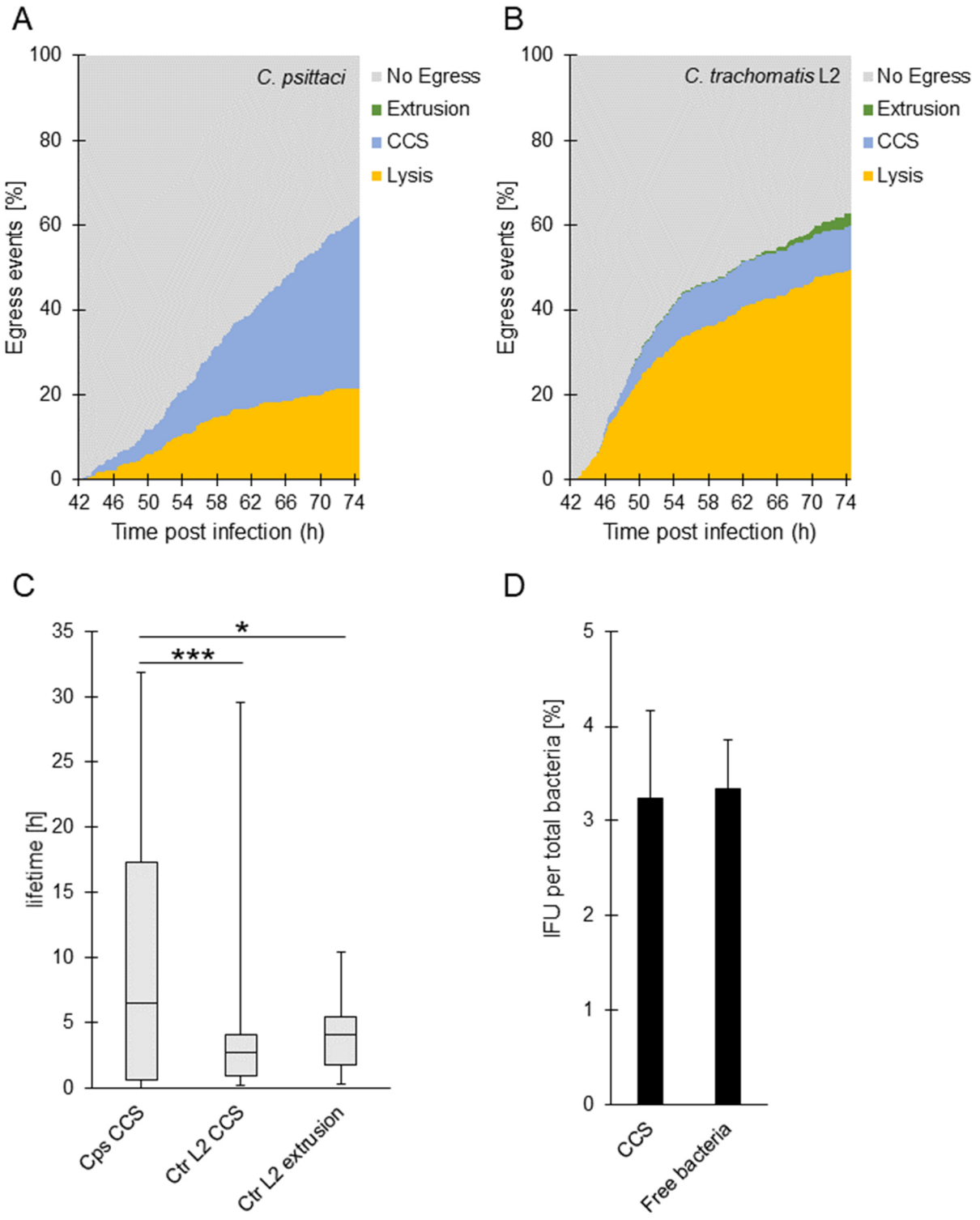

Figure 14. CCS formation is the predominant egress pathway of *C. psittaci* and is also present, but less frequent for *C. trachomatis*. (A) Frequency and time dependence of different *C. psittaci* egress pathways. HeLa cells stably expressing GFP were infected with *C. psittaci* (MOI 2) and at 42 h pi, Z-stack images were acquired using a CLSM equipped with a live-cell chamber for 32.5 h. The type of egress pathway (CCS formation, lysis, extrusion formation or no egress) and time point of a total of 410 cells (n = 2 biological replicates) were analyzed. Data shows the part of each egress pathway type on the total amount of infected cells at each given time point. **(B)** Frequency and time dependence of different *C. trachomatis* L2 egress pathways. HeLa cells stably expressing GFP were infected with *C. trachomatis* L2 (MOI 2) and at 42 h pi, Z-stack images were acquired using a CLSM equipped with a live-cell chamber for 32.5 h. The type of egress pathway (CCS formation, lysis, extrusion formation or no egress) and time point of 391 cells (n = 2 biological replicates) were analyzed. Data shows the part of each egress pathway type on the total amount of infected cells at each given time point. **(C)** Stability of *C. psittaci* and *C. trachomatis* L2 CCS and extrusions. Lifetime of all observed *C. psittaci* and *C. trachomatis* L2 CCS and extrusions (see Figure 2 A, B) was determined. Data shows the median lifetime as box and whisker plot. n = 3;

*p < 0.05; (Student's t-test). **(D)** CCS preserve infectivity of *C. psittaci*. CCS in the supernatant of *C. psittaci*-infected HeLa cells (MOI 2) were separated from free bacteria by centrifugation (5 min, 300 x *g*, RT) at 48 h pi. Infectious progeny was titrated after glass bead lysis and numbers were normalized to genome copy numbers determined by qPCR. Data show mean ± SEM; n = 3. Modified from Scholz et al., 2024b.

To investigate whether CCS formation is specific to *C. psittaci* or also occurs during *C. trachomatis* infections, I used live cell microscopy of *C. trachomatis* L2-infected, eGFP expressing HeLa cells from 42 h pi to 74.5 h pi. Interestingly, I observed *C. trachomatis*-infected cells forming a CCS at the end of the developmental cycle (Supplemental Figure S3 B). However, CCS formation was less frequent for *C. trachomatis* compared to *C. psittaci* with only 10.5% of the observed infected cells formed a CCS. In addition, CCS formation of *C. trachomatis*-infected cells mainly occurs between 45 h pi and 55 h pi (Figure 14 B). By 74.5 h pi, 63% of the *C. trachomatis* had egressed. Of the infected cells, 10.5% formed CCS, 49.4% underwent host cell lysis (for a representative panel of a *C. trachomatis*-infected cell undergoing host cell lysis, see Supplemental Figure S3 C), and 3.1% formed an extrusion.

Live cell imaging was used to track the stability of both CCS and extrusions in eGFP-expressing HeLa cells following their formation. For *C. psittaci*, approximately one third of the formed CCSs underwent lysis at the end of the observation period, while two thirds remained stable (data not shown). The median time to lysis for *C. psittaci* CCSs was approximately 6.5 h with an interquartile range (IQR) of 0.7-17.3 h (Figure 14 C). For *C. trachomatis* L2 extrusions, approximately one third of the formed extrusions underwent lysis at the end of the observation period, with a median lifetime of approximately 4.1 h (IQR: 1.8-5.5 h) (Figure 2 C). In contrast, CCS from *C. trachomatis* L2-infected cells underwent lysis more frequently, with approximately 99.7% of them being lysed at the end of the observation period. The stability of *C. trachomatis* L2 CCS was lower than that of *C. psittaci*, with a median time to lysis of 2.7 h (IQR: 1.0-4.1 h) (Figure 14 C).

To determine if CCS contain infectious bacteria capable of infecting new host cells, I collected the supernatant from infected cells and isolated CCS from free bacteria released by host cell or CCS lysis using differential centrifugation. I then quantified the infectious progeny after glass bead lysis and normalized the IFU counts to bacterial genome copy numbers. The percentage of infectious progeny in CCS was 3.2 ± 0.9%, which was comparable to that of free bacteria (3.3 ± 0.5%) (Figure 14 D).

In summary, these data show that CCS formation is the predominant non-lytic egress pathway of *C. psittaci*. Additionally, CCS formation is also present but less frequent for *C. trachomatis* L2. The CCS in the supernatant contain infectious bacteria and are stable for several hours, indicating that CCS are relevant non-lytic egress structures of *C. psittaci* and *C. trachomatis*.

3.2.6 The occurrence and the frequency of CCS formation and extrusion formation as non-lytic egress pathways *C. trachomatis* are time-dependent

In a previous study performed by Hybiske & Stephens (2007), it was shown that for *C. trachomatis* L2 extrusion formation and host cell lysis occurs in similar frequencies (53 and 47%, respectively) (Hybiske & Stephens, 2007). However, this study was performed at 72 h pi. Thus, I analyzed my data in terms of the frequencies of egress pathways in different time ranges.

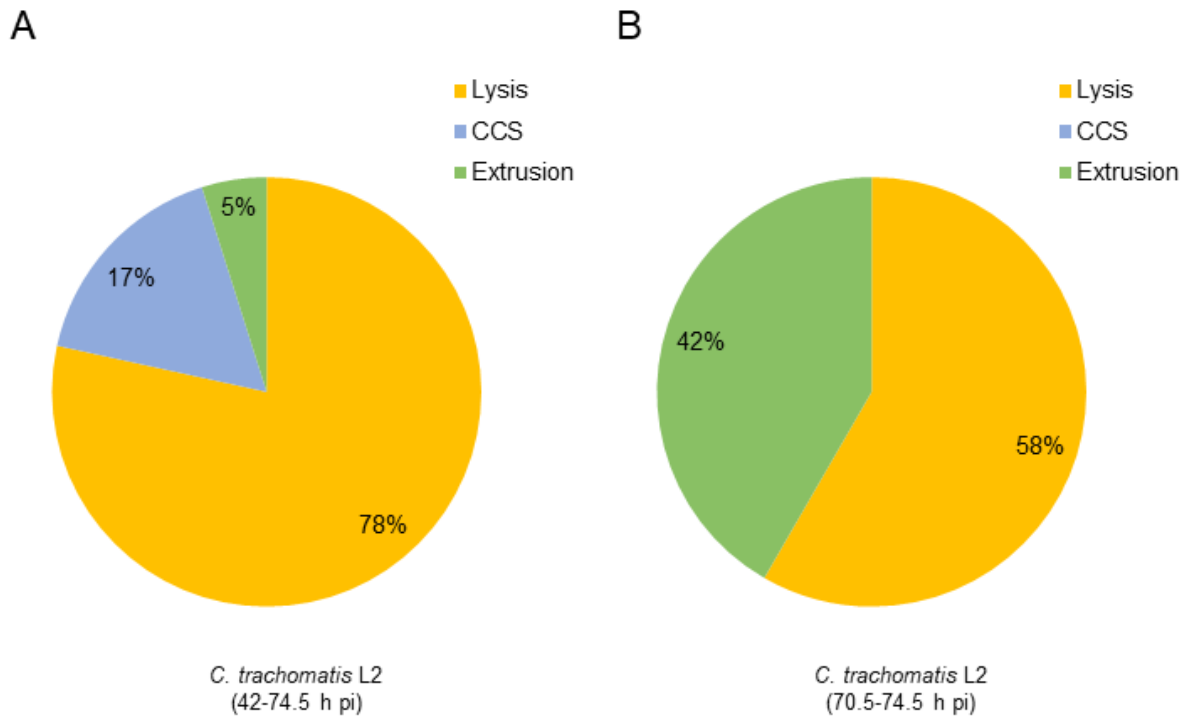

Figure 15. Distribution of egress pathways of *C. trachomatis* L2. *C. trachomatis* L2 egress events of all egressing *C. trachomatis* L2-infected cells between 42 h pi and 74.5 h pi **(A)** or within the last 4 h of observation between 70.5 h pi and 74.5 h pi **(B)** were quantified; n = 2. Modified from Scholz et al., 2024b.

Between 42 h pi and 74.5 h pi, 78% of the egressing cells performed host cell lysis, 17% performed CCS formation and 5% performed extrusion formation (Figure 15 A). At late infections time points, between 70.5 h pi and 74.5 h pi, I observed that 42% of *C. trachomatis* exited the host cell through extrusion formation, while 58% of infected cells lysed. At this time point, I did not detect any CCS formation, which supports previous findings by Hybiske & Stephens (2007) (Hybiske & Stephens, 2007) (Figure 15 B).

Taken together, this shows that for *C. trachomatis* L2, the egress pathways are temporally regulated.

3.2.7 The exposure of sphingolipids in the *C. psittaci* inclusion membrane to the cytosol precedes its destabilization and subsequent CCS formation

One important feature of the formation of extrusions in *C. trachomatis* L2 is the consistent stability of the inclusion membrane, which contrasts with the destabilization of the inclusion

membrane during host cell lysis (Hybiske & Stephens, 2007). Notably, I observed the influx of eGFP into the inclusion lumen during CCS formation (Figure 10 A). Therefore, I further examined changes of the inclusion membrane during CCS formation. To achieve this, I utilized EqtSM, a recently established reporter for SM. EqtSM has previously been used to investigate membrane damage induced by pathogens and the vacuolar escape of *M. marinum* and *Salmonella enterica* (Deng et al., 2016; Niekamp et al., 2022; Scharte et al., 2023). The recruitment of EqtSM to the pathogen-containing vacuole is linked to SM rearrangements in the vacuolar membrane, which is then followed by its lysis.

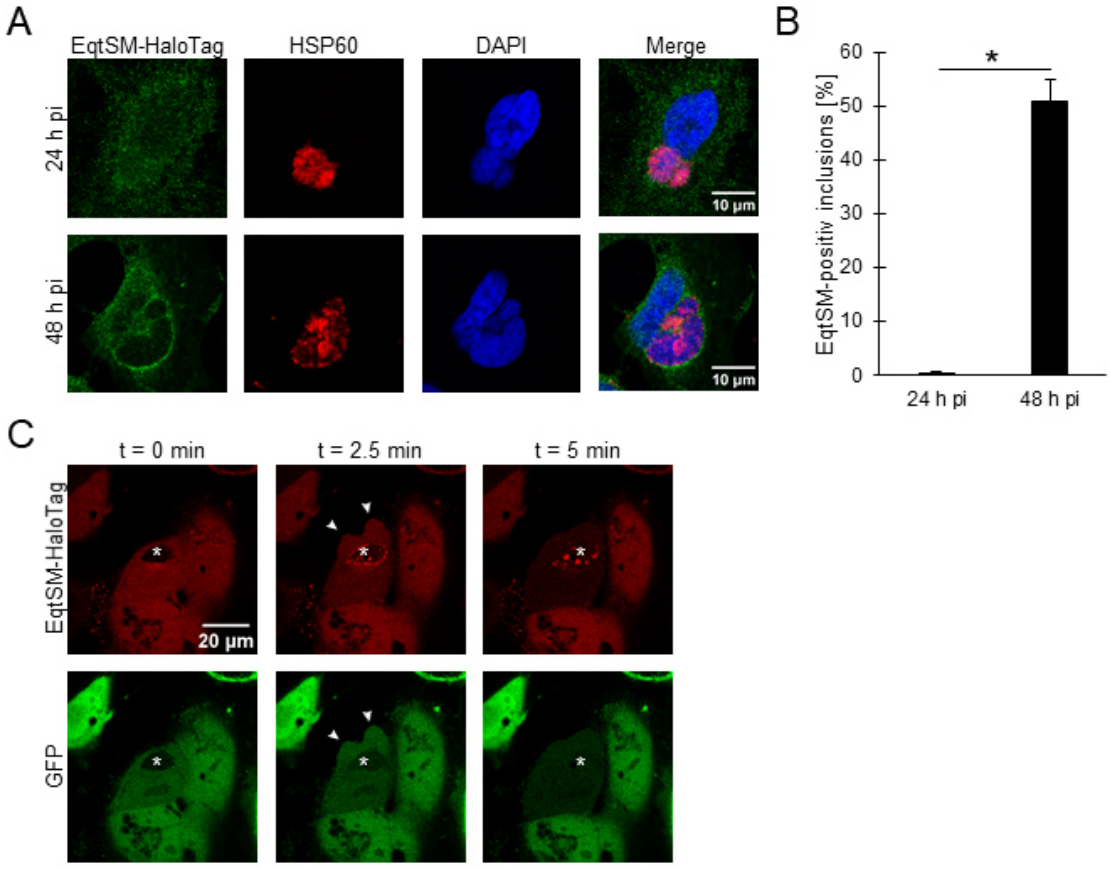

Figure 16. During CCS formation, sphingolipids in the *C. psittaci* inclusion membrane are reorganized, followed by its destabilization and CCS formation. (A) Recruitment of EqtSM-HaloTag to the *C. psittaci* inclusion occurs at 48 h pi. Representative fluorescent images of *C. psittaci*-infected HeLa cells stably expressing EqtSM-HaloTag at 24 h pi and 48 h pi. HeLa cells stably expressing EqtSM-HaloTag were infected with *C. psittaci* (MOI 2) and fixed at 24 h pi or 48 h pi with PFA. *C. psittaci* and EqtSM-HaloTag were detected using a mouse-anti-HSP60 (Cy3) and a rabbit-anti-HaloTag (AF488) antibody, respectively. The DNA was counterstained using DAPI; n = 4. **(B)** EqtSM-HaloTag is recruited to approx. 51% of the *C. psittaci* inclusions at 48 h pi, but hardly not at 24 h pi. Immunofluorescent images of *C. psittaci*-infected HeLa cells stably expressing EqtSM-HaloTag (MOI 2) at 24 h pi or 48 h pi were analyzed for recruitment of EqtSM-HaloTag to the *C. psittaci* inclusion. Data show mean ± SEM; n = 4; *p < 0.05 (Student's t-test). **(C)** EqtSM recruitment is followed by permeabilization of the inclusion membrane and CCS formation. HeLa cells stably expressing EqtSM-HaloTag were transiently transfected with a plasmid for cytosolic expression of eGFP and infected with *C. psittaci* (MOI 2). At 44 h pi, were labeled with 200 nM Janelia Fluor 585 HaloTag Ligand (Promega) and monitored using a CLSM equipped with a live-cell chamber. Panels show representative images of an EqtSM-HaloTag recruiting *C. psittaci* inclusion during CCS formation, which subsequently gets permeable for eGFP; n = 3. Asterisks mark *C. psittaci* inclusion, arrowheads indicate blebbing of host cell plasma membrane. Modified from Scholz et al., 2024b.

Therefore, I analyzed the recruitment of EqtSM-HaloTag in HeLa cells to *C. psittaci* inclusions at 24 h pi and 48 h pi, respectively, as an indicator of inclusion membrane instability. Using

immunofluorescence staining with a HaloTag antibody, I observed the recruitment of EqtSM-HaloTag to approximately 51.0% of *C. psittaci* inclusions at 48 h pi, but hardly any at 24 h pi (Figure 16 A, B).

I investigated whether EqtSM-HaloTag recruitment correlates in time with inclusion membrane destabilization and CCS formation. To do this, I infected HeLa cells that stably express EqtSM-HaloTag and transiently express eGFP with *C. psittaci*. At 44 h pi, I labeled the cells with Janelia Fluor 585 HaloTag Ligand and performed live cell imaging. I observed recruitment of EqtSM-HaloTag just before host cell plasma membrane blebbing (arrowheads) was detected and eGFP influx into the inclusion lumen occurred (Figure 16 C).

Taken together, these data indicate that sphingolipids in the inclusion membrane of *C. psittaci* undergo reorganization and this reorganization correlates in time with inclusion membrane destabilization and the onset of CCS formation.

3.2.8 Similar to apoptotic cells, CCS expose PS to the outer membrane leaflet

I aimed to better characterize the molecular mechanisms leading to CCS formation. About twenty years ago, it has been shown that an atypical form of apoptosis gets activated during late *C. psittaci* infection, but the function of this form of apoptosis for *C. psittaci* infection remains unclear (Gibellini et al., 1998). By live cell microscopy, I detected plasma membrane blebbing during CCS formation, which is described as a characteristic feature of apoptosis (Aoki et al., 2020; D'Arcy, 2019). Thus, I asked whether CCS formation is linked to activation of apoptosis.

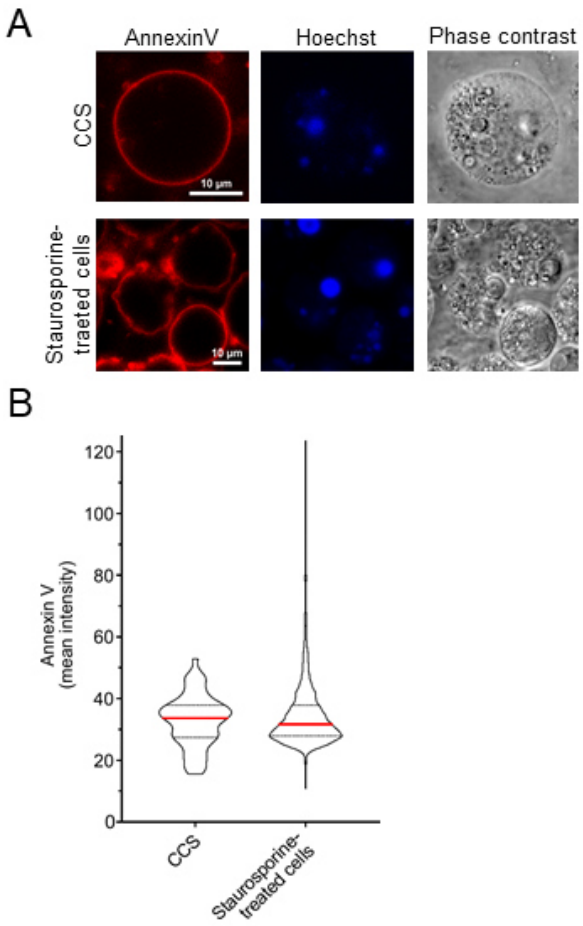

Figure 17. CCS show a similar AnnexinV staining pattern compared to apoptotic cells. (A) Representative images of a CCS positive for AnnexinV (Alexa Fluor 568) in comparison to staurosporine-treated, apoptotic cells. CCS were collected from the supernatant of *C. psittaci*-infected HeLa cells (MOI 2, 48 h pi), while apoptotic cells were collected from the supernatant of uninfected, staurosporine-treated HeLa cells (10 µM staurosporine, 42 h post treatment). PS was visualized using AnnexinV (Alexa Fluor 568) and DNA was counterstained using Hoechst. **(B)** Quantification of PS exposure of CCS and staurosporine-treated, apoptotic cells. Mean intensities of the AnnexinV staining of individual Hoechst-positive CCSs and of apoptotic cell structures of at least 2 µm^2 were determined and the distribution of the mean intensities of 54 CCS and 2213 apoptotic cell structures was visualized as violin plot; n = 3. Modified from Scholz et al., 2024b.

During early apoptosis, PS is exposed to the outer leaflet of the plasma membrane (S.-H. Lee et al., 2013; Mariño & Kroemer, 2013). Thus, I stained CCS and staurosporine-treated apoptotic cells as control with AnnexinV as PS marker. CCS showed a clear membrane staining with AnnexinV in a similar way as staurosporine-treated apoptotic cells (Figure 17 A).

Next, I investigated the distribution of the marker intensities between the populations of CCS and apoptotic cells. For this, I visualized the mean intensities of the AnnexinV staining of individual CCS and of apoptotic cell structures as violin plot. Both populations were distributed around a median of 33.7 and 31.7 for CCS and staurosporine-treated cells, respectively, with similar quartiles of 27.5 and 37.6 for CCS and 27.8 and 37.7 for apoptotic cells (Figure 17 B).

These results show that CCS expose PS on their outer membrane leaflet in similar quantities as apoptotic cells.

3.2.9 CCS differ from late apoptotic cells by retaining their membrane barrier function for different non-permeable dyes

In addition to PS exposure of early apoptotic cells, at late stages of apoptosis secondary necrosis can be induced, leading to the loss of plasma membrane integrity (Rogers et al., 2017; Y. Zhang et al., 2018). Thus, I stained CCS and staurosporine-treated apoptotic cells as control with TrypanRed Plus and SYTOX Green as markers of plasma membrane integrity. However, no TrypanRed Plus staining was observed within CCS (Figure 18 A), which was also confirmed by SYTOX Green staining (Figure 18 B). In contrast, staurosporine-treated apoptotic cells were positive for all indicated markers (Figure 18 A, B).

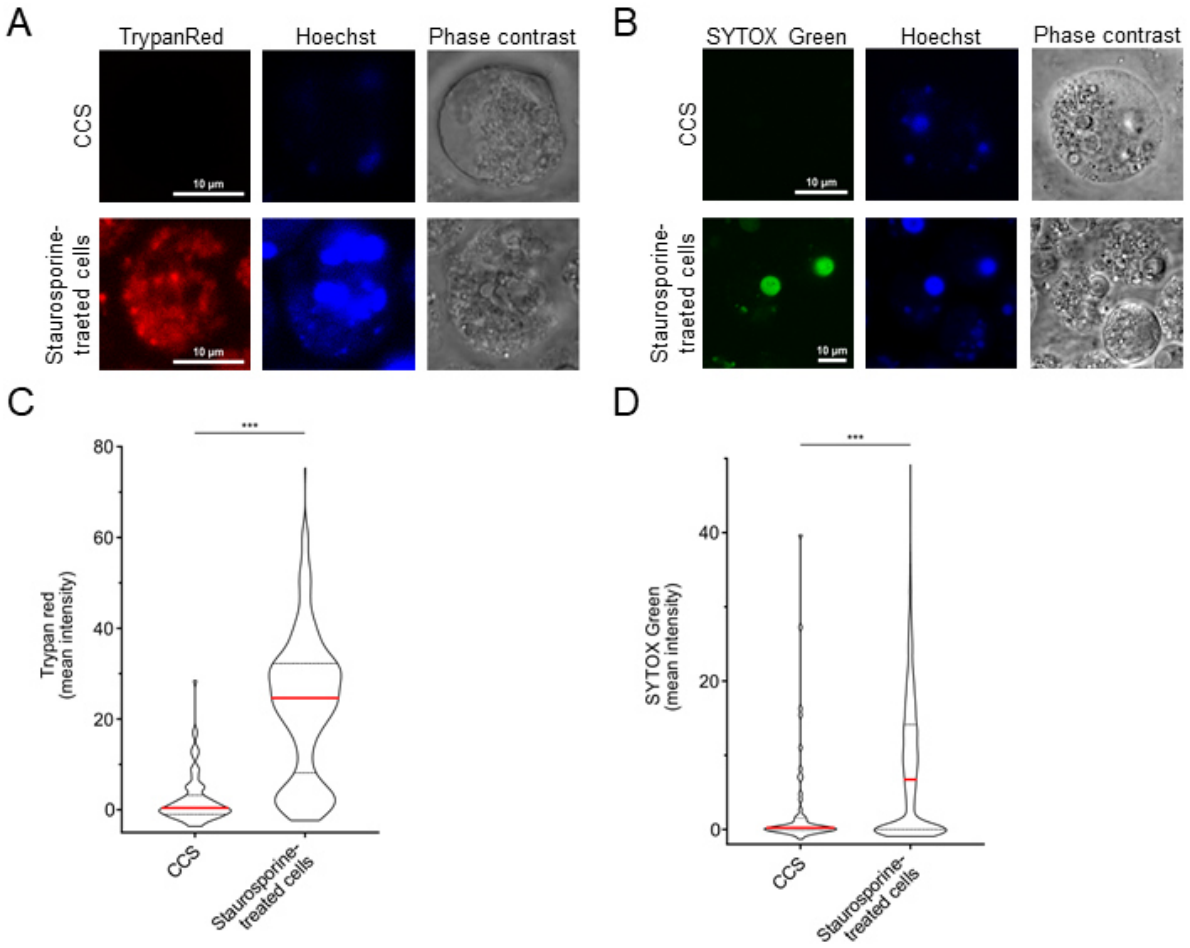

Figure 18. In contrast to apoptotic cells, CCS retain their membrane integrity. (A, B) Representative images of a CCS negative for TrypanRed Plus **(A)** and negative for SYTOX Green **(B)** in comparison to staurosporine-treated, apoptotic cells positive for both. CCS were collected from the supernatant of *C. psittaci*-infected HeLa cells (MOI 2, 48 h pi), while apoptotic cells were collected from the supernatant of uninfected, staurosporine-treated HeLa cells (10 µM staurosporine, 42 h post treatment). Structures with damaged or compromised membranes were stained with TrypanRed Plus **(A)** or SYTOX Green **(B)** and DNA was counterstained using Hoechst; n = 3. **(C)** Quantification of membrane integrity of CCS and staurosporine-treated, apoptotic cells. Mean intensities of the TrypanRed Plus staining of individual CCSs and of single apoptotic cells were determined and the distribution of the mean intensities of 83 CCS and 404 apoptotic cells was visualized as violin plot; n = 3; ***p < 0.005 (Student's t-test). **(D)** Quantification of membrane integrity of CCS and staurosporine-treated, apoptotic cells. Mean intensities of the SYTOX Green staining in Hoechst-positive nuclei of CCS and of Hoechst-positive structures in apoptotic cells were determined and the distribution of the mean intensities of 54 CCS and 5515 apoptotic cell structures was visualized as violin plot; n = 3; ***p < 0.005 (Student's t-test). Modified from Scholz et al., 2024b.

Additionally, I visualized the mean intensities of the TrypanRed Plus staining of individual CCSs and apoptotic cells as violin plot. The median for CCS of 0.4 was significantly lower than the median for apoptotic cells of 24.6 with quartiles of -0.9 and 3.2 for CCS and 8.3 and 32.1 for apoptotic cells (Figure 18 C). Similar to TrypanRed Plus staining, quantification of the SYTOX Green intensities showed that the median for CCS of 0.2 was significantly lower than the median for apoptotic cells of 6.7 with quartiles of -0.1 and 1.4 for CCS and 0.0 and 14.1 for apoptotic cells (Figure 18 D).

Taken together, these results demonstrate that CCS are morphologically different from apoptotic cells in terms of their membrane integrity.

3.2.10 CCS differ from apoptotic cells by lacking fragmentation of the nucleus

Next, I compared the ultrastructure of CCS and staurosporine-treated apoptotic cells by TEM.

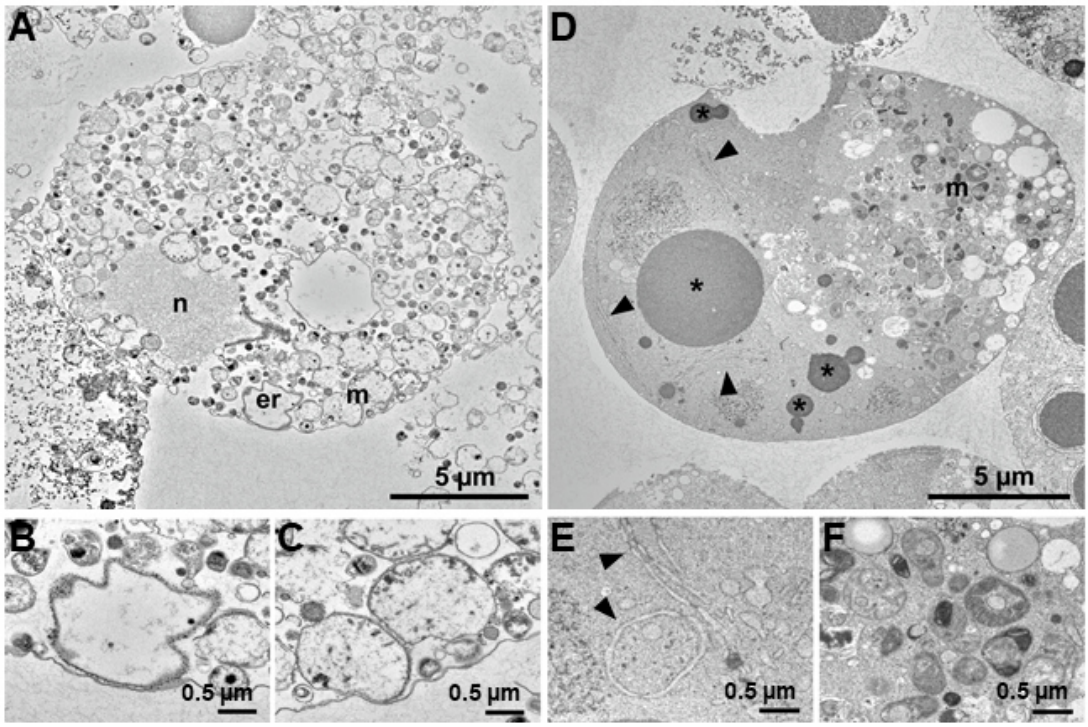

Figure 19. In CCS, the nucleus and the mitochondria are not condensed in contrast to apoptotic cells. Representative transmission electron microscopy images of thin sections through a CCS isolated from the supernatant of *C. psittaci*-infected HeLa cells (MOI 2, 48 h pi) **(A, B, C)** and a staurosporine-treated, apoptotic cell **(D, E, F)**. **(A)** The CCS shows many bacterial profiles at different stages (RBs, EBs, intermediate forms) and cellular organelles, such as nucleus (n), mitochondria (m) and endoplasmic reticulum (er), that appear extracted and dilated (see **B** and **C** for a higher magnification). **(D)** The apoptotic cell reveals a dense cytoplasm with one larger and few smaller profiles of the fragmented nucleus (asterisk). The matrix of the nuclear fragments appears dense and homogenous. Nuclear membranes (arrowheads), with typical nuclear pore structures, are detached and located in the adjacent cytoplasm **(E)**. The mitochondria reveal an aberrant internal structure, with condensed matter and/or vesicular structures **(F)**. *Electron microscopy was performed in the group of M. Laue, RKI, Berlin.* Modified from Scholz et al., 2024b.

CCSs contained lysed and dilated cell organelles (Figure 19 A). Especially, the contained endoplasmic reticulum (Figure 19 B) and mitochondria (Figure 19 C) were morphologically impaired, lysed or dilated. In contrast, apoptotic cells showed a dense cytoplasm with

fragmented nuclei and aberrant mitochondria (Figure 19 D). In addition, they contain detached nuclear membranes (Figure 19 E) and aberrant, condensed mitochondria (Figure 19 F).

In sum, this further supports that CCS are morphologically different from apoptotic cells, also in terms of their ultrastructure.

3.2.11 CCS formation correlates in time with a proteolytic activity specific for a DEVD-containing substrate, but not with caspase-3 activation

The intrinsic and extrinsic pathways of apoptosis converge in caspase-3 activation (D'Arcy, 2019).

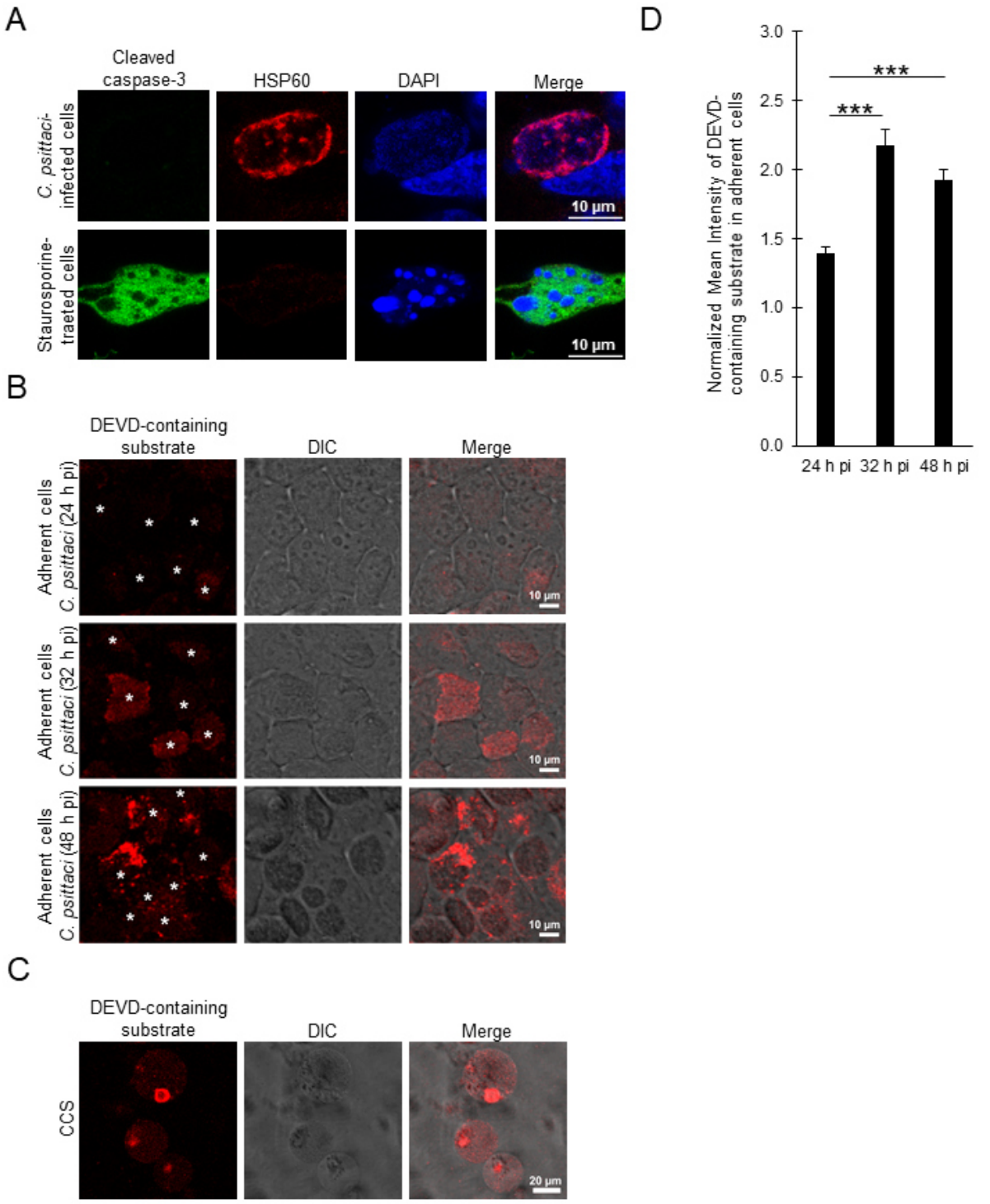

Figure 20. CCS formation is independent of caspase-3 activation, while a DEVD-containing substrate is proteolytically cleaved during CCS formation. (A) No cleavage of caspase-3 is detectable at late *C. psittaci* infections. Representative fluorescence images of *C. psittaci*-infected HeLa cells (MOI 2, 48 h pi) and staurosporine-treated uninfected HeLa cells as positive control. Cells were fixed with PFA and *C. psittaci* and cleaved caspase-3 were detected using a mouse-anti-HSP60 (Cy3) and a rabbit-anti-cleaved caspase-3 (AF488) antibody, respectively. The DNA was counterstained using DAPI; n = 2. **(B, C)** *C. psittaci* infection leads to activation of the caspase detection reagent by proteolytic cleavage of a DEVD containing substrate. HeLa cells were infected with *C. psittaci* (MOI 2) and at 40 h pi, the cells were stained with Incucyte Caspase-3/7 Dye for Apoptosis. Representative images of the infected, adherent cells at 24 h pi, 32 h pi, and 48 h pi **(B)** and of CCS in the supernatant at 48 h pi **(C)** are shown; n = 3. **(D)** Quantification of the proteolytic activity during CCS formation. *C. psittaci*-infected HeLa cells (MOI 2) were stained with Incucyte Caspase-3/7 Dye for Apoptosis at 16 h pi, 24 h pi or 40 h pi for 8 h. Z-stack images were acquired at a CLSM. Data were normalized to mean fluorescence intensity of uninfected cells at respective time points. Data show mean ± SEM; n = 3; ***p < 0.005 (Student's t-test). Modified from Scholz et al., 2024b.

Therefore, I analyzed the presence of cleaved caspase-3 in *C. psittaci*-infected cells at 48 h pi by immunofluorescence staining using an antibody specific for activated caspase-3. However, I did not detect activated caspase-3 in the cytosol of *C. psittaci*-infected host cells at 48 h pi, whereas uninfected, staurosporine-treated cells showed clear staining of activated caspase-3 (Figure 20 A).

Interestingly, I observed cleavage of the DEVD-containing substrate at 32 h pi mainly in *C. psittaci* inclusions using a fluorescent caspase-3/7 detection reagent that detects proteolytic cleavage of the substrate. The substrate was less present at 24 h pi (Figure 20 B). At 48 h pi, the cleavage of the DEVD-containing substrate was mainly observed in the cytosol of infected cells (Figure 20 B) and in CCS (Figure 20 C), indicating the involvement of a DEVD-containing substrate cleaving protease in CCS formation.

I also quantified the proteolytic cleavage of DEVD in adherent cells. Towards the end of the chlamydial developmental cycle, I observed a significant increase in intensity. At 24 h pi, the intensity was 1.4-fold higher compared to uninfected cells. At 32 h pi and 48 h pi, the intensity was 2.2- and 1.9-fold higher, respectively, compared to uninfected cells (Figure 20 D).

These data show that a DEVD-containing substrate is cleaved within *C. psittaci* inclusions prior to CCS formation, but no caspase-3 activation could be detected at this timepoint, indicating that a potential bacterial protease is involved in CCS formation independent of classical apoptosis.

3.2.12 Caspase inhibitors do not block CCS formation and the proteolytic cleavage of the DEVD-containing substrate

Next, I aimed to test my hypothesis that a currently unknown bacterial DEVD-cleaving protease is involved in CCS formation, that is independent of classical apoptotic caspases, especially of caspase-3.

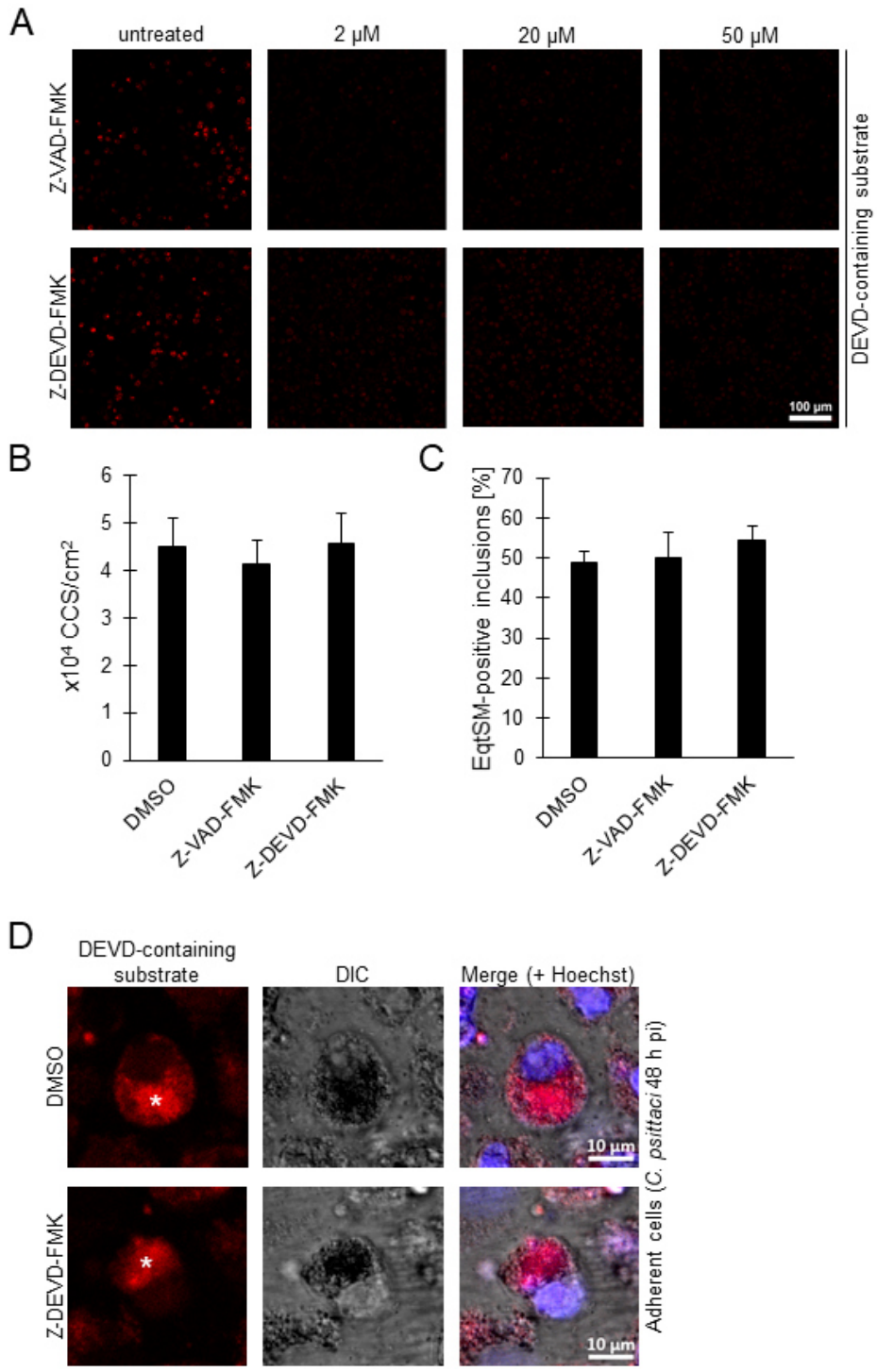

Figure 21. The caspase-3 inhibitor Z-DEVD-FMK blocks neither CCS formation nor the proteolytic cleavage of the DEVD-containing substrate. (A) Z-VAD-FMK and Z-DEVD-FMK inhibit caspase-3 during staurosporine-induced apoptosis of HeLa cells in concentrations between 2 µM and 50 µM. HeLa cells were washed with PBS, treated with Z-VAD-FMK and Z-DEVD-FMK in concentrations of 2 µM, 20 µM, and 50 µM or left untreated. At 4 h post treatment, apoptosis was induced by addition of 5 µM staurosporine and caspase-3 activity was monitored using Incucyte Caspase-3/7 Red Dye for apoptosis. Representative fluorescence images of each condition are shown; n = 2. **(B)** CCS formation is not affected by caspase inhibition. *C. psittaci*-infected HeLa cells (MOI 2) were washed with PBS at 44 h pi and treated with 2 µM Z-VAD-FMK, 2 µM Z-DEVD-FMK or DMSO (negative control). CCS in the supernatant were quantified at 48 h pi. Data show mean ± SEM; n = 3. **(C)** EqtSM-HaloTag recruitment is not affected by caspase inhibition. *C. psittaci*-infected HeLa cells stably expressing EqtSM-HaloTag (MOI 2), washed with PBS at 44 h pi and treated with 2 µM Z-VAD-FMK, 2 µM Z-DEVD-FMK or DMSO (negative control) and cells were fixed at 48 h pi with PFA. *C. psittaci* and EqtSM-HaloTag were detected using a mouse-anti-HSP60 (Cy3) and a rabbit-anti-HaloTag (AF488) antibody, respectively. The DNA was counterstained using DAPI. *C. psittaci* inclusions were analyzed for recruitment of EqtSM-HaloTag. Data show mean ± SEM; n = 3. **(D)** Proteolytic cleavage of DEVD can be observed in *C. psittaci*-infected cells after treatment with Z-DEVD-FMK. *C. psittaci*-infected HeLa cells (MOI 2, 40 h pi) were treated with 2 µM Z-DEVD-FMK to inhibit caspase-3 or left

untreated (DMSO control). Between 44 h pi and 48 h pi, proteolytic cleavage of DEVD was monitored using Incucyte Caspase-3/7 Red Dye for Apoptosis. Representative fluorescence images of both conditions at 48 h pi are shown; n = 2. Modified from Scholz et al., 2024b.

To do this, I performed inhibitor experiments using Z-VAD-FMK as a pan-caspase inhibitor and Z-DEVD-FMK as a specific caspase-3 inhibitor. At first, I aimed to identify the inhibitor concentrations to prevent caspase-3 activation during staurosporine-induced apoptosis. Treatment with Z-VAD-FMK and Z-DEVD-FMK in concentrations ranging from 2 µM to 50 µM showed that both inhibitors can be used at a concentration of 2 µM to prevent caspase-3 activation during staurosporine-induced apoptosis (Figure 21 A).

Next, I investigated whether inhibiting caspase-3 activation affects CCS formation. After treatment with 2 µM Z-VAD-FMK and 2 µM Z-DEVD-FMK for 44 h pi to 48 h pi, there was no significant difference in the number of CCS between the DMSO-treated controls (4.5×10^4 CCS/cm^2) and the Z-VAD-FMK and Z-DEVD-FMK treated samples (4.1 and 4.6×10^4 CCS/cm^2, respectively) (Figure 21 B).

Additionally, I analyzed EqtSM-HaloTag recruitment after treatment with 2 µM Z-VAD-FMK and 2 µM Z-DEVD-FMK for 44 h pi to 48 h pi. I did not observe a significant difference in the proportion of EqtSM-HaloTag recruiting *C. psittaci* inclusions between DMSO treated controls (48.9% of inclusions) and Z-VAD-FMK and Z-DEVD-FMK treated samples (50.2% and 54.5% of inclusions, respectively) (Figure 21 C).

As Z-DEVD-FMK treatment does not affect CCS formation, I analyzed the consequence of the treatment on DEVD cleavage in the *C. psittaci* inclusion, asking if protease activity in the inclusion is required for CSS formation. After treatment with Z-DEVD-FMK, proteolytic cleavage of DEVD was still observed in the inclusions of *C. psittaci*-infected cells similar as in untreated controls (Figure 21 D).

These data show that inhibition of caspase-3 does not affect CCS formation and cleavage of a DEVD-containing substrate within *C. psittaci* inclusions prior to CCS formation. Thus, I speculate that a currently unknown protease activity inside of the inclusion is required for CSS formation.

3.2.13 CCS formation depends on extracellular calcium concentration

Calcium is an important signaling molecule involved in diverse cellular processes (Mattson & Chan, 2003; Pinton et al., 2008; Sukumaran et al., 2021). Furthermore, calcium has been described to regulate the egress of *C. trachomatis* (Hybiske & Stephens, 2007; Nguyen et al., 2018). Therefore, I investigated the role of calcium in the formation of CCS.

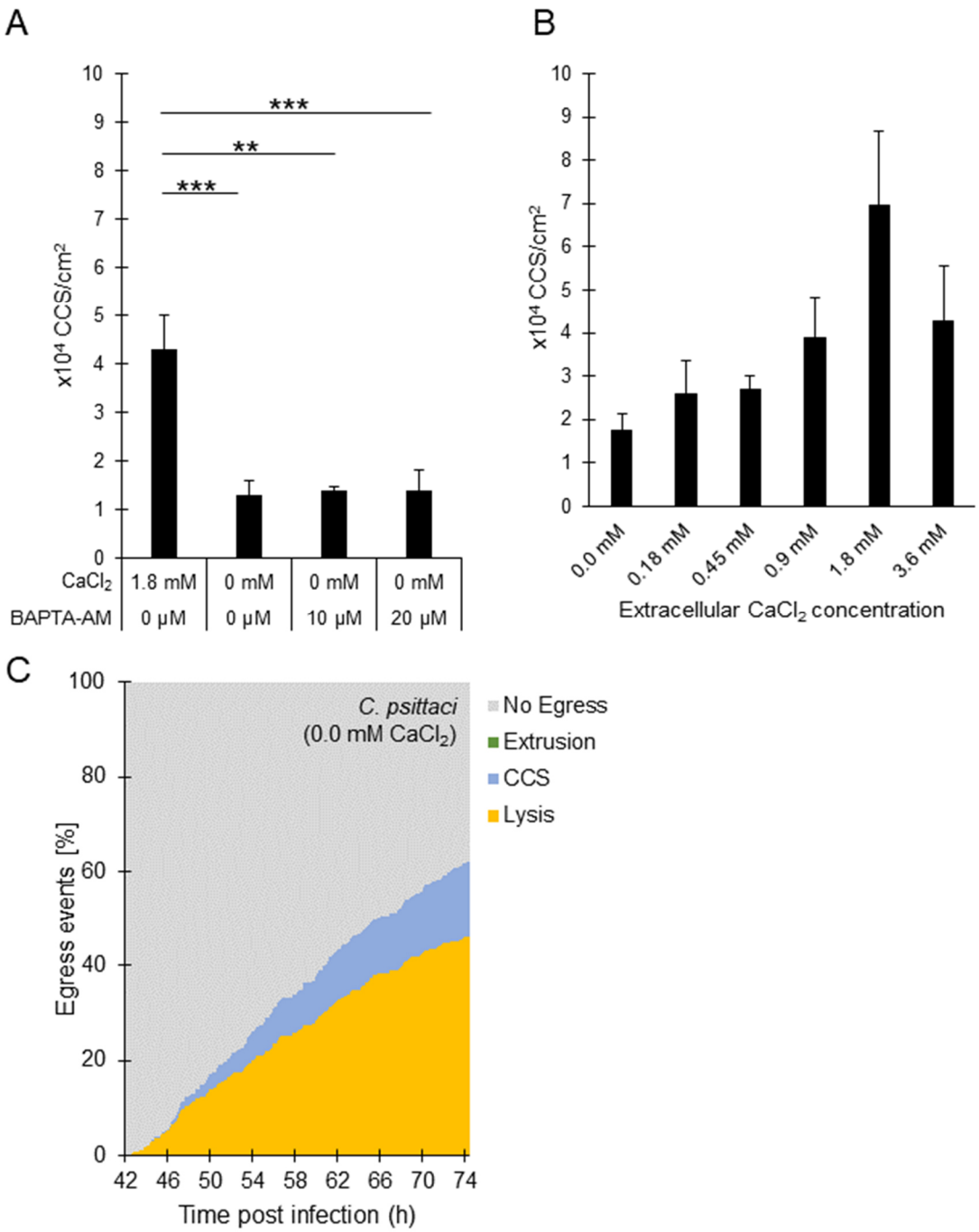

Figure 22. Variations in the extracellular calcium concentration affect CCS formation. (A) CCS formation is decreased under calcium chloride depleting conditions in the culture medium, but not further decreased by addition of the cellular calcium chelator BAPTA-AM. HeLa cells were infected with *C. psittaci* (MOI 2) and at 44 h pi, culture medium was replaced by serum-free medium supplemented with the indicated concentrations of calcium chloride and BAPTA-AM. CCS in the supernatant were visually quantified at 48 h pi. Data show mean ± SEM; n = 3; **p < 0.01; ***p < 0.005 (Student's t-test). **(B)** CCS formation depends on the extracellular calcium concentration. HeLa cells were infected with *C. psittaci* (MOI 2). At 44 h pi, culture medium was replaced by serum-free medium supplemented with the indicated concentrations of calcium chloride. CCS in the supernatant were visually quantified at 48 h pi. Data show mean ± SEM; n = 4. **(C)** Frequency and time dependence of different *C. psittaci* egress pathways under calcium depletion. HeLa cells stably expressing GFP were infected with *C. psittaci* (MOI 2) and at 42 h pi, culture medium was replaced by serum-free and calcium chloride-free medium and Z-stack images were acquired using a CLSM equipped with a live-cell chamber for 32.5 h. The type of egress pathway (CCS formation, lysis, extrusion formation or no egress) and time point of a total of 427 cells (n = 2 biological replicates) were analyzed. Data shows the part of each egress pathway type on the total amount of infected cells at each given time point. Modified from Scholz et al., 2024b.

Initially, I investigated the impact of reducing extracellular and intracellular calcium levels on CCS formation. I cultured cells infected with *C. psittaci* in medium containing calcium chloride or in calcium chloride-free medium. I then introduced the cell-permeable calcium chelator BAPTA-AM at varying concentrations between 44 h pi and 48 h pi. Reducing the extracellular calcium concentration from 1.8 mM (a concentration identical to my standard infection medium) to 0.0 mM decreased CCS formation from 4.3 to 1.3 x 10^4 CCS/cm^2, respectively (Figure 22 A). Additional use of BAPTA-AM in concentrations of 10 and 20 µM to the calcium chloride-free medium did not further decrease CCS formation (1.4 and 1.4 x 10^4 CCS/cm^2, respectively).

In addition, I cultivated *C. psittaci*-infected cells with calcium chloride concentrations ranging from 0 mM to 1.8 mM from 44 h pi to 48 h pi. I observed a dose-dependent increase in CCS formation until 1.8 mM calcium chloride (from 1.8 to 7.0 x 10^4 CCS/cm^2), while CCS numbers decreased at 3.6 mM calcium chloride to 4.3 x 10^4 CCS/cm^2 (Figure 22 B).

I next asked whether the decrease in the extracellular calcium concentration shifts egress towards host cell lysis or prevents egress in general. To address this question, I monitored *C. psittaci*-infected HeLa cells stably expressing eGFP in the cytosol in calcium chloride-free medium by live cell microscopy from 42 h pi to 74.5 h pi and determined frequencies of the different egress pathways (Figure 22 C). Compared to calcium-chloride containing conditions (Figure 14 A), the frequency of CCS formation decreased from 41.2% to 15.9%, while the frequency of host cell lysis increased from 21.5% to 46.6%. The frequency of *C. psittaci*-infected cells showing no sign of egress was similar with 37.5% compared to 37.3% for calcium-containing conditions, indicating that *C. psittaci*-infected cells underwent host cell lysis instead of CCS formation under calcium-chloride free conditions.

In summary, my data support that extracellular calcium signaling is an important regulator of egress pathways of *C. psittaci*.

3.2.14 Varying extracellular calcium concentrations affect intracellular calcium increase and proteolytic DEVD-cleavage in late infections

To better understand the impact of varying extracellular calcium concentrations on intracellular calcium levels, I examined the intracellular calcium concentration during the late stages of *C. psittaci* infection.

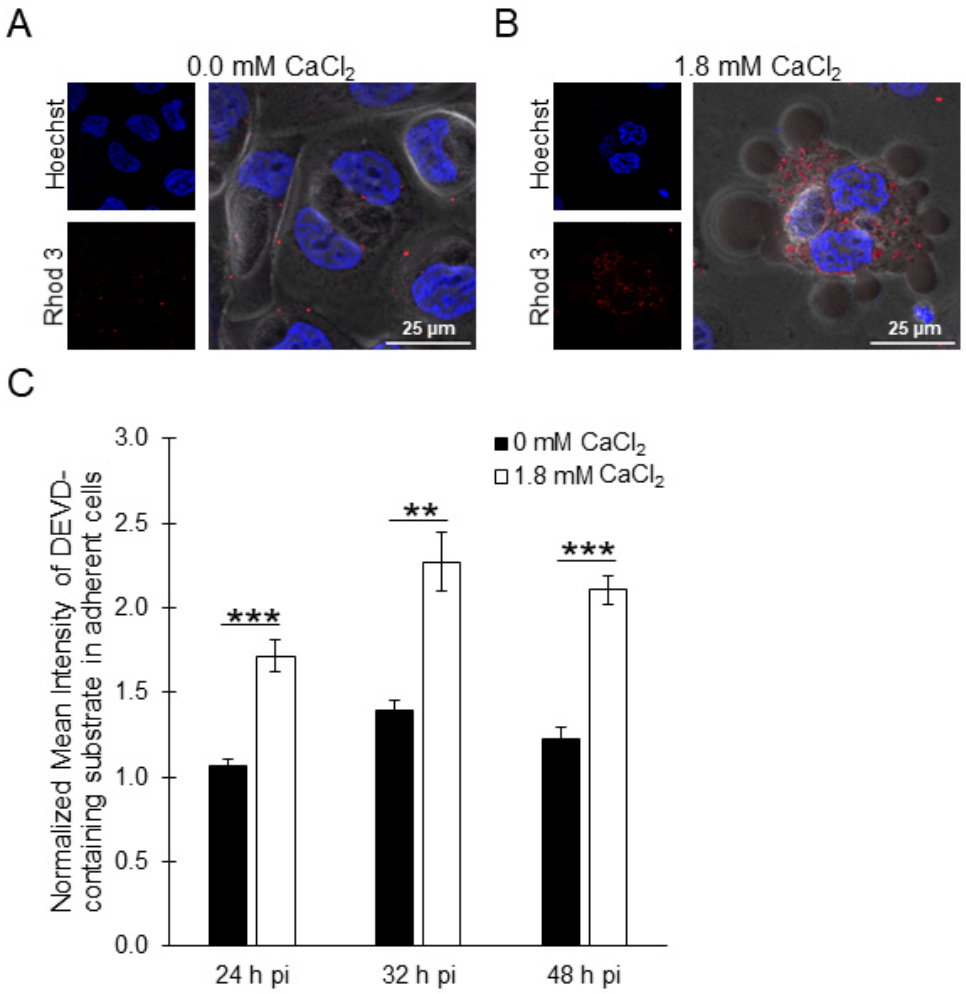

Figure 23. Intracellular calcium increase in late infections and proteolytic DEVD-cleavage are depending on extracellular calcium. (A, B) HeLa cells were infected with *C. psittaci* (MOI 2). At 44 h pi, medium was replaced by serum-free medium supplemented with 0 mM calcium chloride **(A)** or 1.8 mM calcium chloride **(B)**. At 46 h pi, cells were labeled with the calcium sensor Rhod-3 for 1 h. At 48 h pi, DNA was counterstained using Hoechst and images were acquired. Representative images of intact cells (0.0 mM $CaCl_2$) and CCS formation (1.8 mM $CaCl_2$) are shown; n = 2. **(C)** Proteolytic DEVD cleaving-activity in *C. psittaci*-infected HeLa cells depends on the extracellular calcium concentration. Culture medium of *C. psittaci*-infected HeLa cells (MOI 2) was replaced by serum-free medium supplemented with indicated concentrations of calcium chloride at 20 h pi, 28 h pi and 44 h pi and cells were stained with Incucyte Caspase-3/7 Dye for Apoptosis for 4 h. Z-stack images were acquired using a CLSM. Data were normalized to mean fluorescence intensity of uninfected cells without calcium chloride at respective time points. Data show mean ± SEM; n = 3; **p < 0.01; ***p < 0.005 (Student's t-test). Modified from Scholz et al., 2024b.

I used the Rhod-3 membrane-permeant cytosolic calcium sensor under conditions containing 0.0 mM and 1.8 mM calcium chloride. At 0.0 mM calcium chloride, I did not detect an increase in cytosolic calcium concentration in *C. psittaci*-infected cells at 48 h pi. However, at 1.8 mM calcium chloride, I observed *C. psittaci*-infected cells with blebbing membranes and an increased cytosolic calcium concentration (Figure 23 A, B).

Next, I addressed if extracellular calcium concentration affected cleavage of the DEVD-containing substrate late in *C. psittaci*-infected cells. For this, I compared the DEVD cleaving activity at 1.8 mM calcium chloride containing conditions to calcium-free conditions using the caspase-3/7 detection reagent. At all examined time points (24 h pi, 32 h pi, and 48 h pi), I

observed a decrease in the intensity from 1.7- to 1.1-fold, 2.3- to 1.4-fold, and 2.1- to 1.2-fold, respectively (Figure 23 C).

Taken together, my data indicate that extracellular calcium is a requisite for an intracellular calcium increase during CCS formation, which also regulates the activity of the DEVD-cleaving bacterial protease.

3.2.15 A peak in the cytosolic calcium concentration is followed by a rapid increase in DEVD-cleaving activity and CCS formation

I aimed to understand how the intracellular calcium increase is connected with CCS formation and with the activation of the DEVD-cleaving protease.

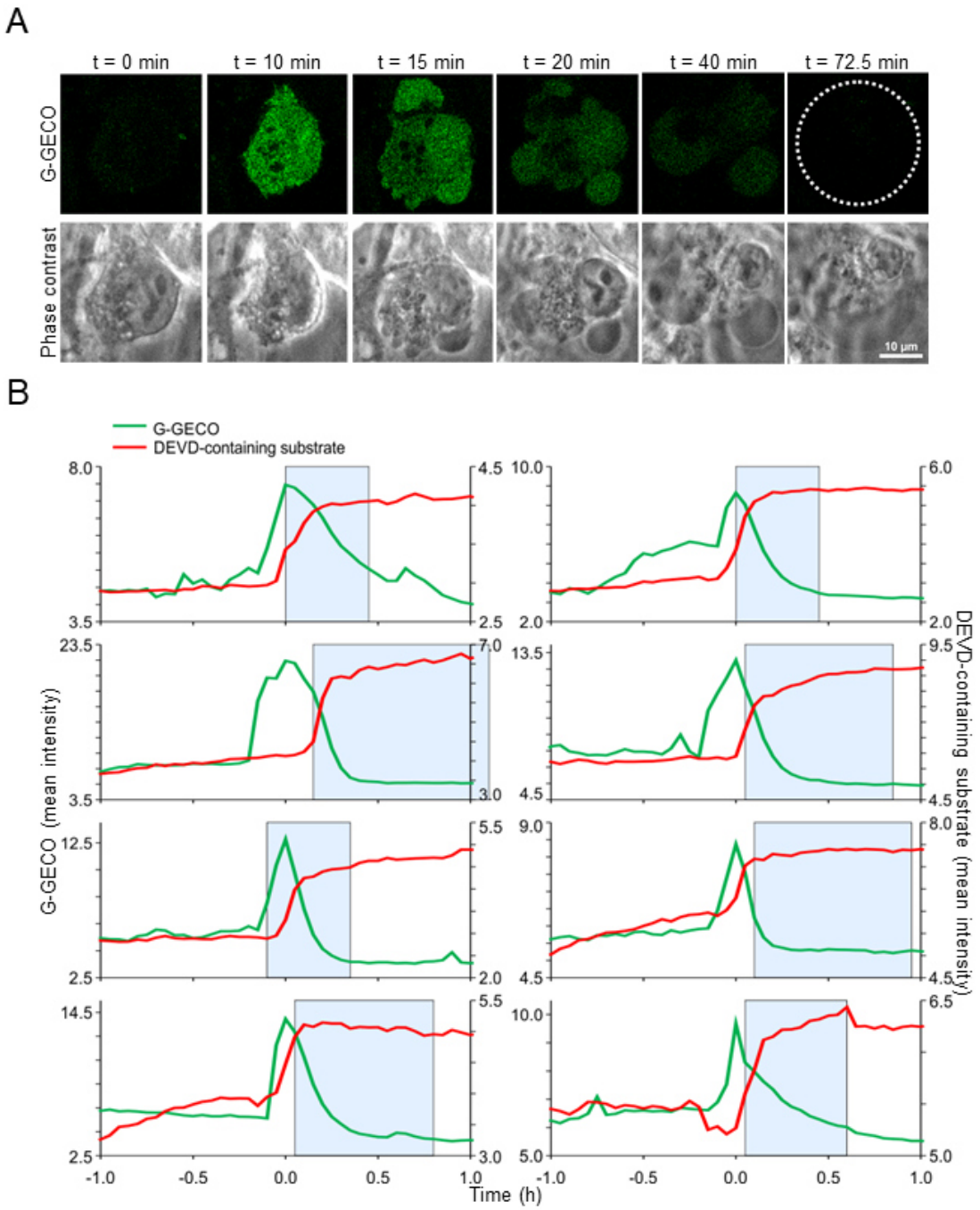

Figure 24. The cytosolic calcium concentration and the DEVD-cleaving activity increase before CCS formation. (A) Intracellular calcium concentration increases during CCS formation. Dual calcium reporter HeLa ER-LAR-Geco G-Geco cells were infected with *C. psittaci* (MOI 2). At 44 h pi, cells were monitored at a CLSM equipped with a live-cell chamber. Panels show representative images of a CCS forming cell. Dashed line indicates CCS; n = 3. **(B)** During CCS formation, proteolytic DEVD cleaving-activity rapidly increases after increase of the intracellular calcium concentration. Dual calcium reporter HeLa ER-LAR-Geco G-Geco cells were infected with *C. psittaci* (MOI 2). At 44 h pi, culture medium was replaced by serum-free medium supplemented with 1.8 mM calcium chloride and cells were stained with Incucyte Caspase-3/7 Dye for Apoptosis. Cells were monitored at a CLSM equipped with a live-cell chamber for 4 h. Data show the cytosolic calcium concentration and proteolytic DEVD cleaving-activity of 8 individual CCS forming cells of two biological replicates. Start and end of membrane blebbing is indicated by a blue box; n = 2. Modified from Scholz et al., 2024b.

At first, I analyzed the chronological order of membrane blebbing and calcium influx. For this, I visualized intracellular calcium levels during CCS formation using a genetically encoded calcium sensor (Stelzner et al., 2020). In HeLa cells that stably express G-Geco, an increase in intracellular calcium concentration was detected during CCS formation before the initiation

of the CCS characteristic membrane blebbing. This increased calcium concentration is subsequently slowly reduced during CCS formation, leading to a CCS with basal calcium level again (Figure 24 A).

Next, I aimed to further link the observed increase of cytosolic calcium concentration with the events of CCS formation, membrane blebbing and cleavage of the DEVD-containing substrate. For this, I measured the DEVD cleaving activity using the caspase-3/7 detection reagent in G-Geco cells simultaneously with the cytosolic calcium concentration at 1.8 mM calcium chloride containing medium conditions. Analysis of individual CCS-forming cells revealed that after a rapid increase in the cytosolic calcium concentration, DEVD cleaving activity also rapidly increased (Figure 24 B), showing that an increase of cytosolic calcium concentration precedes activation of a DEVD-containing protease. Interestingly, while the increase in cytosolic calcium concentration was rather transient, DEVD cleaving activity remained stable for a longer time period.

In summary, my data support that the increase in intracellular calcium activates the bacterial DEVD-cleaving protease, which initiates plasma membrane blebbing and CCS formation, indicating that calcium is an important regulator in *Chlamydia* biology, particularly in controlling the egress pathways of *C. psittaci*.

3.3 Recruitment of the cellular lipid transport protein CERT to *C. psittaci* inclusions regulates the timing of bacterial egress

In the previous part of this study, *C. psittaci* egress by CCS formation was characterized and the role of the host cell cytoskeleton, of host cell death, of a bacterial DEVD-cleaving protease and of extracellular and intracellular calcium was investigated. However, especially data on the regulation of the egress time point is missing. Thus, in the third part of this study, I particularly examined the role of CERT for the regulation of inclusion membrane stability and its temporarily coordinated destabilization during CCS formation.

3.3.1 CCS formation of *C. psittaci* temporally correlates with a reduction in CERT recruitment

The recruitment of CERT to *C. psittaci* inclusions was exclusively studied for early and middle infections, and not for late infections (Koch-Edelmann et al., 2017). Therefore, this study concentrated on the localization of CERT during late *C. psittaci* infections in the context of egress by CCS formation. At first, I analyzed CERT recruitment to *C. psittaci* inclusions by performing immunofluorescence staining using antibodies specific for CERT, bacterial HSP60, and the DNA marker DAPI. HSP60-positive *C. psittaci*-inclusions strongly recruit CERT at 24 h pi. However, this recruitment was reduced to weak or no recruitment at 48 h pi (Figure 25 A, right and left inclusion, respectively). Similar to this, ectopically expressed eGFP-CERT localized in close proximity to *C. psittaci* inclusions at 24 h pi, but not at 48 h pi (Figure 25 B).

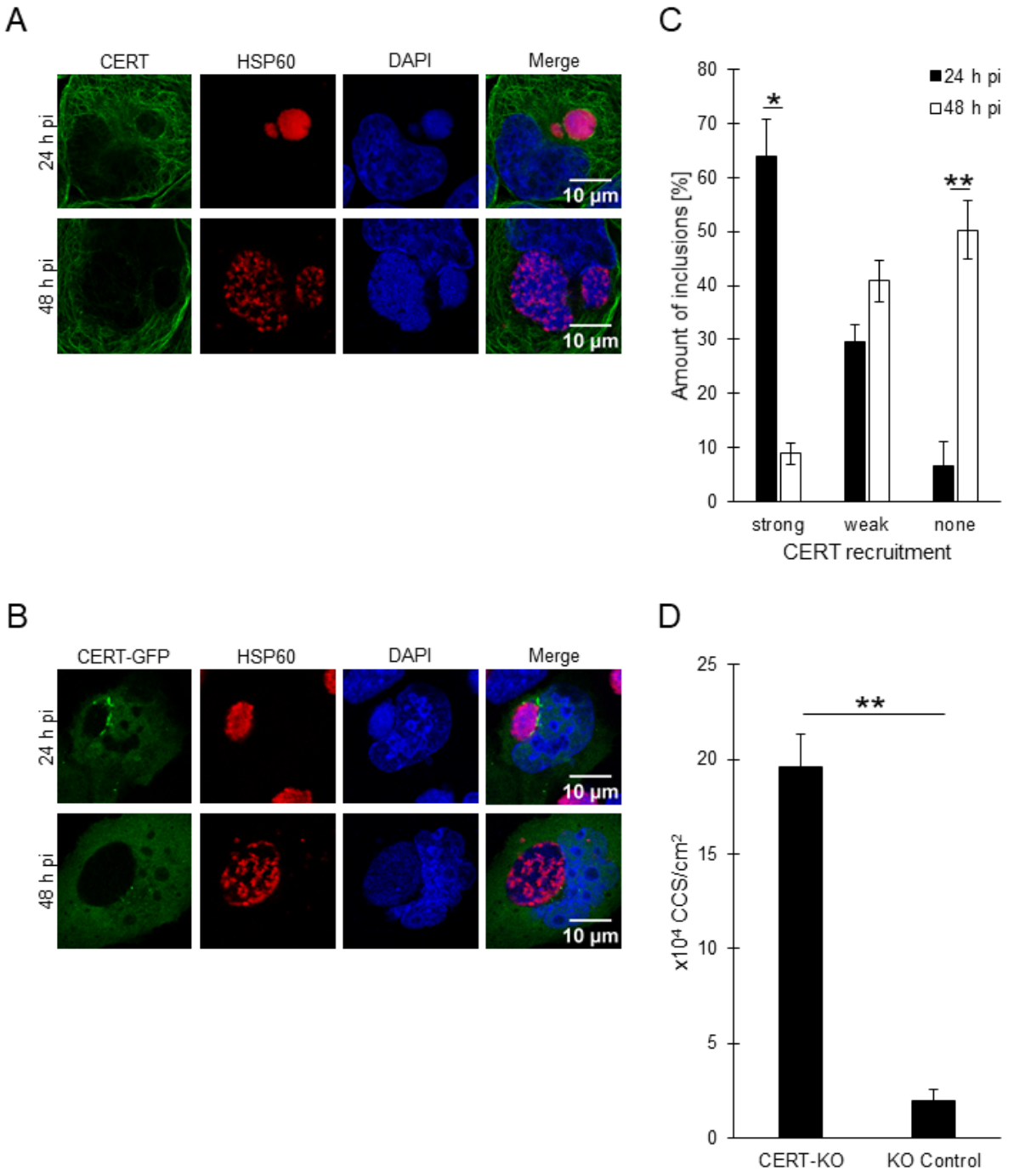

Figure 25. In late infections, CERT recruitment to *C. psittaci* inclusions is reduced and CERT-KO induce early egress of *C. psittaci* by CCS formation at 24 h pi. (A) Representative immunofluorescence images of *C. psittaci*-infected HeLa cells (MOI 2) at 24 h pi and 48 h pi. PFA-fixed cells were stained for *C. psittaci* and endogenous CERT using a mouse-anti-HSP60 (Cy3) and a rabbit-anti-CERT (AF488) antibody, respectively. DNA was counterstained using DAPI. n = 3. **(B)** Representative fluorescence images of HeLa cells transiently expressing eGFP-CERT infected with *C. psittaci* (MOI 2) at 24 h pi and 48 h pi. Cells were PFA-fixed and immunostained for *C. psittaci* using a mouse-anti-HSP60 (Cy3) antibody and DNA was counterstained using DAPI. n = 3. **(C)** Quantification of CERT recruitment to *C. psittaci* inclusions at 24 h pi and 48 h pi. Based on immunofluorescence images of *C. psittaci*-infected HeLa cells (MOI 2) at 24 h pi and 48 h pi, the number of inclusions showing strong, weak or no CERT recruitment was determined and normalized to the total number of inclusions. At least 60 inclusions per condition were analyzed. Data show mean ± SEM; n = 3; *p < 0.05, **p < 0.01 (Student's t-test). **(D)** CCS formation in HeLa CERT-KO and KO control cells. Cells were infected with *C. psittaci* (MOI 2), medium was replaced at 20 h pi and CCS in the supernatant were visually quantified at 24 h pi. Data show mean ± SEM; n = 3; **p < 0.01 (Student's t-test). Modified from Scholz et al., 2024a.

Subsequently, the recruitment of CERT was quantified in relation to the inclusions at 24 h pi and 48 h pi. At 24 h pi, the majority of the inclusions exhibited strong recruitment of CERT (63.8%), 29.6% demonstrated weak CERT recruitment, and only 6.6% were devoid of CERT recruitment (Figure 25 C). In contrast, at 48 h pi, the majority of the inclusions did not recruit CERT (50.2%), 40.9% showed a weak CERT-recruitment, and only 8.9% strongly recruited CERT (Figure 25 C).

I therefore sought to determine whether the loss of CERT at the inclusion membrane is associated with egress by CCS formation. To this end, HeLa CERT-KO cells were infected with *C. psittaci*. To ascertain whether CERT-KO induces the early egress of *C. psittaci* by formation of CCS, I quantified CCS in the supernatant of *C. psittaci*-infected cells under CERT-KO and KO control conditions at 24 h pi. A significant increase in formed CCS was observed, from 2.0 x 10^4 CCS/cm^2 in KO control cells to 19.6 x 10^4 CCS/cm^2 in CERT-KO cells at 24 h pi (Figure 25 D).

In conclusion, the data demonstrate that the absence of CERT at the inclusion membrane of *C. psittaci* correlates temporally with egress by CCS formation, indicating that alterations in CERT recruitment to *C. psittaci* inclusions regulate CCS formation.

3.3.2 Localization of CERT regulates CCS formation

CERT is composed of three functional domains: The N-terminal PH domain, mediating Golgi targeting in uninfected cells, the central FFAT motif, mediating ER targeting, and the C-terminal START-domain, that is a ceramide-specific lipid binding domain (Figure 5). During *C. trachomatis*, *C. muridarum*, and *C. psittaci* infections CERT is recruited to the inclusion by its PH domain (Derré et al., 2011; C. A. Elwell et al., 2011; Koch-Edelmann et al., 2017).

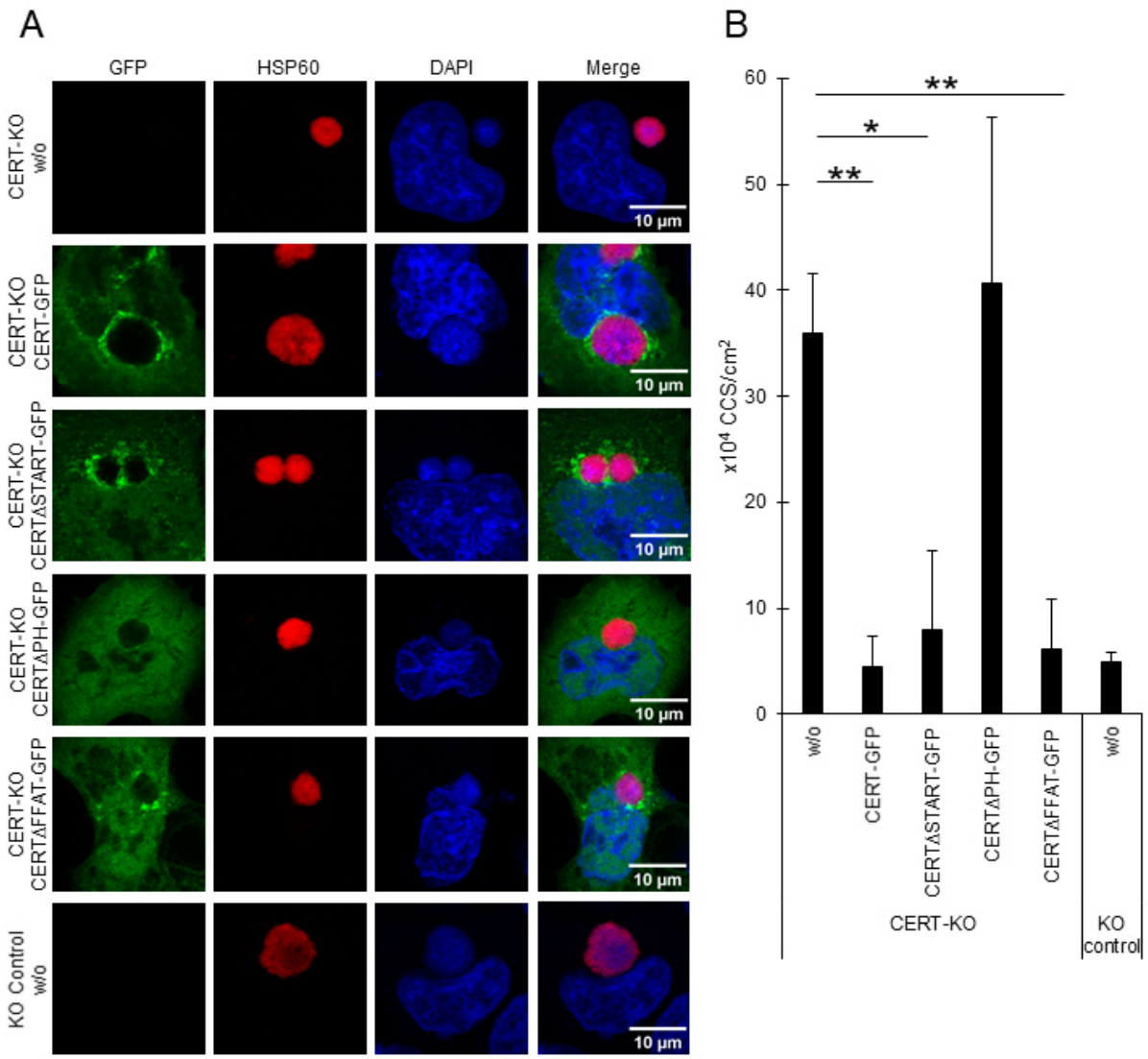

Figure 26. In contrast to full CERT and CERT variants lacking the START- or FFAT-domain, a CERT variant lacking the PH domain is not recruited to *C. psittaci* inclusions and cannot prevent premature CCS formation. (A) Representative fluorescence images of HeLa CERT-KO cells transiently expressing eGFP-CERT or eGFP-CERT variants lacking the START, FFAT or PH domain and controls infected with *C. psittaci* (MOI 2) at 24 h pi. Cells were PFA-fixed and immunostained for *C. psittaci* using a mouse-anti-HSP60 (Cy3) antibody; DNA was counterstained using DAPI; n = 4**. (B)** CCS formation in HeLa CERT-KO cells transiently expressing eGFP-CERT or eGFP-CERT variants lacking the START, FFAT or PH domain and controls. Cells were infected with *C. psittaci* (MOI 2), medium was replaced at 20 h pi and CCS in the supernatant were visually quantified at 24 h pi. CCS number was normalized on the transfection efficiency. Data show mean ± SEM; n = 4; *p < 0.05, **p < 0.01 (Student's t-test). Modified from Scholz et al., 2024a.

Initially, I infected CERT-KO cells ectopically expressing distinct eGFP-CERT variants with *C. psittaci* and analyzed the localization of the eGFP-CERT variants by immunofluorescence staining at 24 h pi. In cells that had not been transfected with an eGFP-CERT construct, no GFP-signal was detected (Figure 26 A). In CERT-KO cells transfected with full length eGFP-CERT, the protein was in close proximity to *C. psittaci* inclusions (Figure 26 A), comparable to the findings in HeLa cells (Figure 25 B). A comparable staining pattern was observed after transfection with eGFP-CERT lacking the START or FFAT domain (Figure 26 A). As published, eGFP-CERT lacking the PH domain was not recruited to *C. psittaci* inclusions (Koch-Edelmann et al., 2017).

Next, I analyzed CCS formation after infecting CERT-KO cells ectopically expressing different eGFP-CERT variants with *C. psittaci*. In untransfected CERT-KO cells, 36.0 x 10^4 CCS/cm^2 were formed compared to 4.9 x 10^4 CCS/cm^2 in untransfected KO control cells (Figure 26 B). In the conditions in which the CERT variants were introduced by transient transfection, the CCS numbers were normalized to the transfection efficiencies. Upon transfection of CERT-KO cells with full length eGFP-CERT, the normalized CCS formation (4.5 x 10^4 CCS/cm^2) resembles that detected in the control cells, indicating that full length CERT can complement the premature egress phenotype seen in the CERT-KO cells. Similarly, transfection of CERT-KO cells with eGFP-CERT lacking the START or FFAT domain significantly decreased CCS formation to 7.9 x 10^4 and 6.1 x 10^4 CCS/cm^2, respectively. In contrast, transfection of CERT-KO cells with eGFP-CERT lacking the PH domain did not decrease CCS formation (40.7 x 10^4 CCS/cm^2) (Figure 26 B).

Taken together, expression of CERT variants revealed that the ability of CERT to be recruited to the inclusion correlates with its capacity to prevent premature egress and suggest that CERT recruitment to the inclusion controls CCS formation.

3.3.3 CERT-KO induces early CCS formation by a sequence of events analogous to mature CCS

Next, I asked if the absence of CERT changes other characteristics of *C. psittaci* CCS formation beside of the egress time point. Mature CCS are formed by a sequential process including plasma membrane blebbing and inclusion membrane destabilization, recruitment of EqtSM, and proteolytic cleavage of a DEVD tetrapeptide-containing substrate (see section 3.2.1, section 3.2.7, and section 3.2.11 for more details). Thus, I examined the sequence of events described for mature CCS during early CERT-KO induced CCS formation.

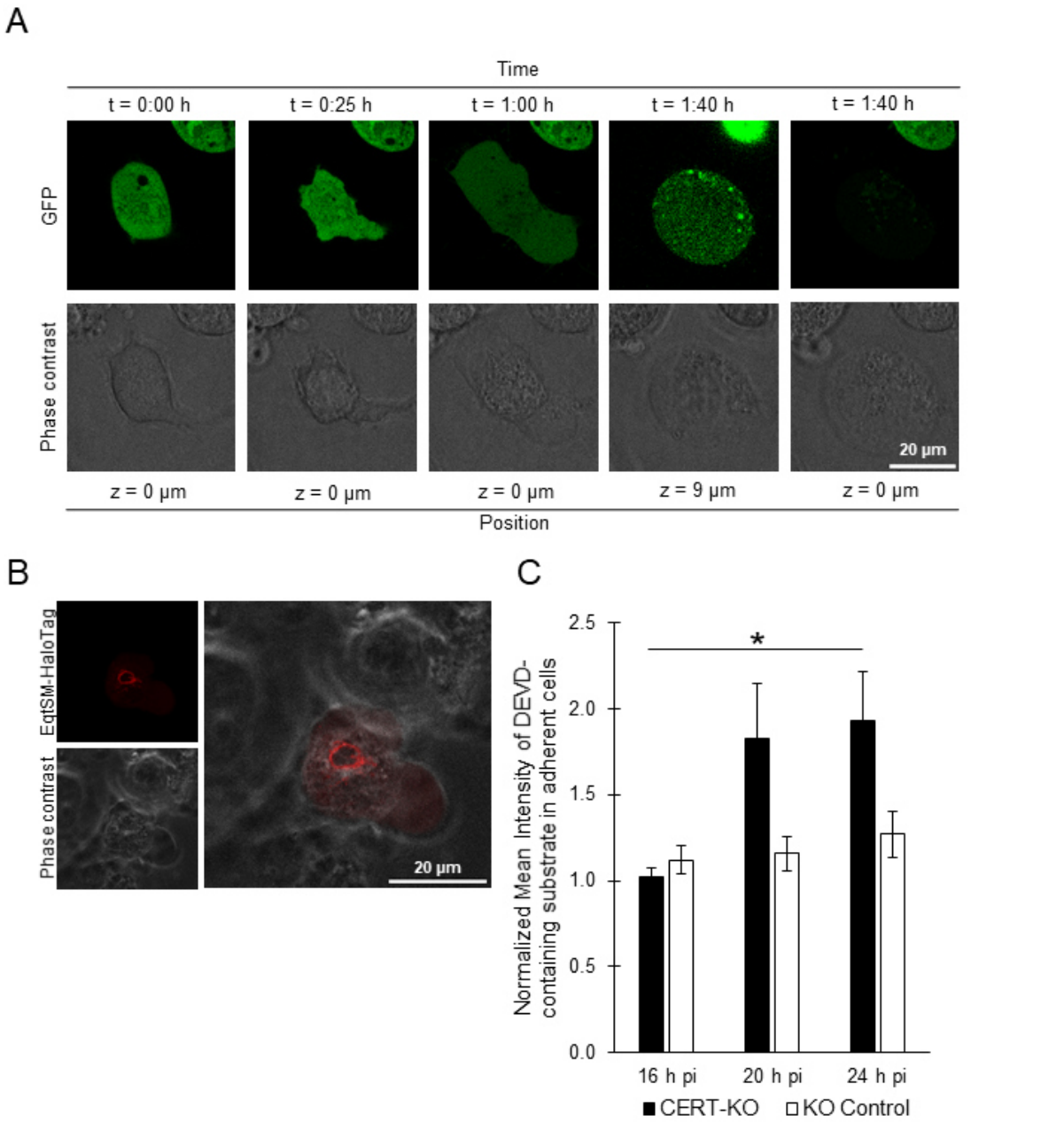

Figure 27. CERT-KO induced early CCS are formed by a sequence of events analogous to mature CCS. (A) During early CCS formation, plasma membrane blebbing occurs and the inclusion membrane destabilizes. HeLa CERT-KO cells transiently expressing eGFP were infected with *C. psittaci* (MOI 2) and monitored starting at 20 h pi using a CLSM equipped with a live-cell chamber. Panels show representative images of a section plane of a CCS forming HeLa CERT-KO cell; n = 3. **(B)** EqtSM is recruited to *C. psittaci* inclusions during early CCS formation. HeLa CERT-KO cells transiently expressing EqtSM-HaloTag were infected with *C. psittaci* (MOI 2). At 20 h pi, cells were labeled with 200 nM Janelia Fluor 585 HaloTag Ligand (Promega) and monitored using a CLSM equipped with a live-cell chamber. Panel shows representative images of an EqtSM-HaloTag recruiting *C. psittaci* inclusion during early CCS formation; n = 3. **(C)** A DEVD cleaving protease is activated during early CCS formation. *C. psittaci*-infected HeLa CERT-KO and KO control cells (MOI 2) were stained with Incucyte Caspase-3/7 Dye for Apoptosis at 16 h pi and monitored using a CLSM equipped with a live-cell chamber for 8 h. Mean fluorescence intensity of infected cells at 16 h pi, 20 h pi, and 24 h pi was normalized to mean fluorescence intensity of uninfected cells at respective time points. Data show mean ± SEM; n = 3; *p < 0.05 (Student's t-test). Modified from Scholz et al., 2024a.

At first, I monitored early CCS formation using HeLa CERT-KO cells transiently expressing eGFP starting at 20 h pi. Before CCS formation, the bacterial inclusion excluded the cytosolic eGFP (Figure 27 A). Then, in all analyzed cells, CCS formation initiates with blebbing of the cellular plasma membrane and influx of eGFP into the inclusion lumen. This was followed by

enlargement of the plasma membrane blebs and subsequent detachment of the entire host cell, which completed the formation of the CCS in the supernatant of the cell culture.

Next, I asked if EqtSM is recruited to the *C. psittaci*-inclusion when early CCS formation starts. To test this, I transiently expressed EqtSM-HaloTag in CERT-KO cells, labeled them with HaloTag Ligand and performed live cell imaging starting at 20 h pi. I observed that CCS forming cells recruit EqtSM to the inclusion when CCS formation begins (Figure 27 B).

In addition, I tested if proteolytic cleavage of a DEVD-containing substrate is increased in adherent CERT-KO cells during early CCS formation. Indeed, I detected a significant increase in fluorescence intensity of a cleaved DEVD-containing substrate compared to uninfected cells from 1.0-fold at 16 h pi to 1.8-fold and 1.9-fold at 20 h pi and 24 h pi, respectively (Figure 27 C). In comparison, in KO control cells the intensity was only slightly increased from 1.1-fold at 16 h pi to 1.2-fold and 1.3-fold at 20 h pi and 24 h pi, respectively.

In sum, this data revealed that CERT-KO induced early CCS are formed by a sequence of events analogous to CCS including plasma membrane blebbing, inclusion membrane destabilization, EqtSM recruitment, and activation of a DEVD cleaving protease. This further supports that the presence and absence of CERT regulates CCS formation.

3.3.4 Similar to mature CCS formation, CERT-KO-induced early CCS formation is calcium-dependent

The formation of mature CCS depends on the extracellular calcium concentration and a peak in the intracellular calcium concentration of the infected cell occurs during CCS formation (see section 3.2.13, section 3.2.14, and section 3.2.15 for more details).

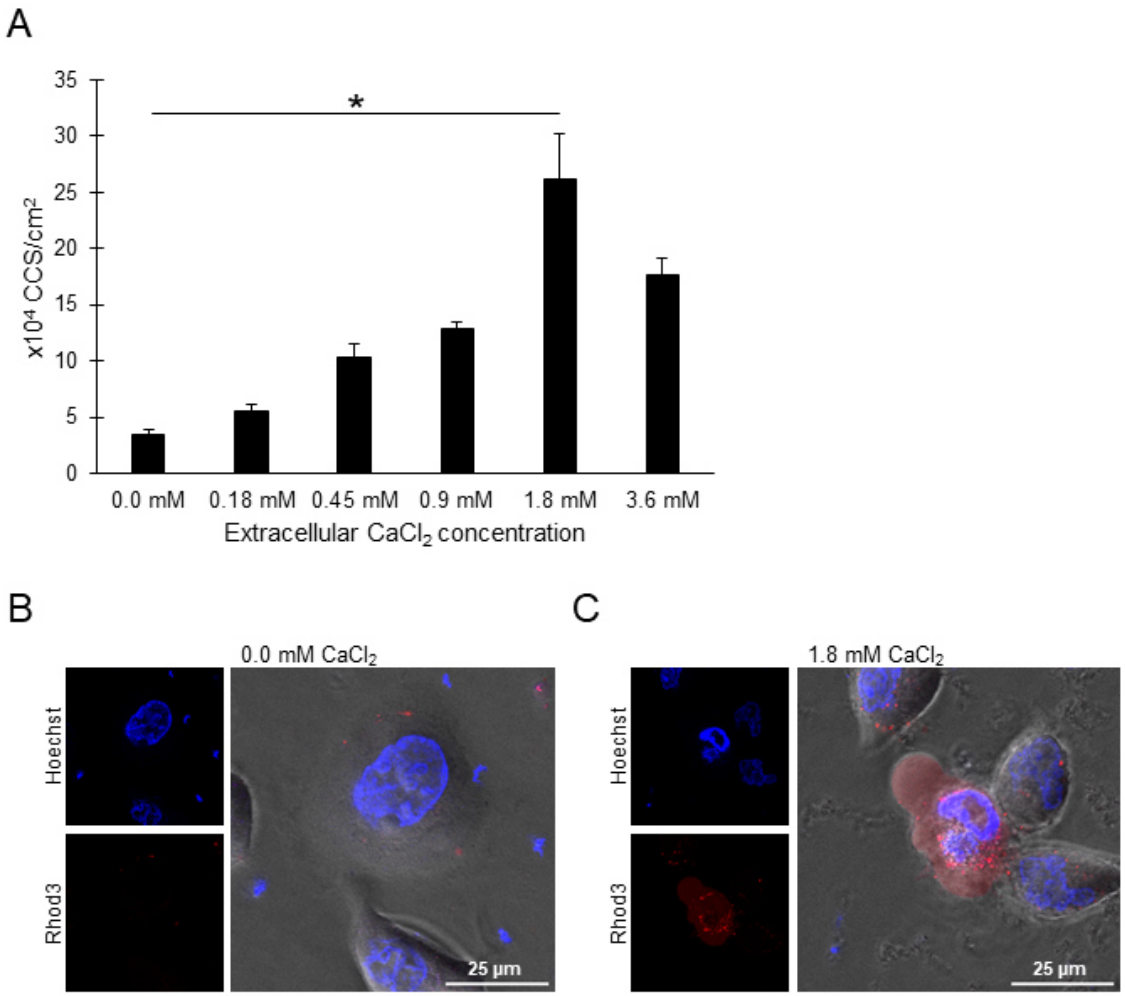

Figure 28. Early CCS formation is calcium-dependent. (A) Early CCS formation depends on the extracellular calcium concentration. HeLa CERT-KO cells were infected with *C. psittaci* (MOI 2). At 20 h pi, culture medium was replaced by serum-free medium supplemented with the indicated concentrations of calcium chloride. CCS in the supernatant were visually quantified at 24 h pi. Data show mean ± SEM; n = 3; *p < 0.05 (Student's t-test). **(B, C)** HeLa CERT-KO cells were infected with *C. psittaci* (MOI 2). At 20 h pi, medium was replaced by serum-free medium supplemented with 0 mM calcium chloride **(B)** or 1.8 mM calcium chloride **(C)**. At 22 h pi, cells were labeled with the calcium sensor Rhod-3 for 1 h. At 24 h pi, DNA was counterstained using Hoechst and images were acquired. Representative images of intact cells (0.0 mM $CaCl_2$) and CCS formation (1.8 mM $CaCl_2$) are shown; n = 2. Modified from Scholz et al., 2024a.

Thus, the role of calcium signaling for early CCS formation was investigated. During mature CCS formation, CCS numbers increased with extracellular calcium concentrations (Figure 22). Similar, during early CCS formation under CERT-KO, I observed a dose-dependent increase in CCS numbers from 3.4 x 10^4 CCS/cm^2 to 26.1 x 10^4 CCS/cm^2 from 0.0 mM to 1.8 mM $CaCl_2$ (Figure 28 A).

Next, I analyzed the intracellular calcium concentration during early CCS formation using the Rhod-3 membrane-permeant cytosolic calcium sensor under conditions containing 0.0 mM and 1.8 mM calcium chloride. At 0.0 mM calcium chloride, I did not detect an increase in cytosolic calcium concentration in *C. psittaci*-infected CERT-KO cells at 24 h pi (Figure 28 B). However, at 1.8 mM calcium chloride, I observed *C. psittaci*-infected CERT-KO cells with blebbing membranes and an increased cytosolic calcium concentration (Figure 28 C).

This data further support that except of the timepoint CERT-KO induced early CCS formation shares key characteristics with mature CCS formation including the dependency on the extracellular calcium concentration and intracellular calcium increase.

3.3.5 CERT-KO induces the formation of RB-containing, non-infectious CCS

At 24 h pi, *C. psittaci* inclusions contain mostly RBs, with only few bacteria starting to redifferentiate to EBs (Figure 8). Thus, I asked if bacteria in early formed CCS are infectious.

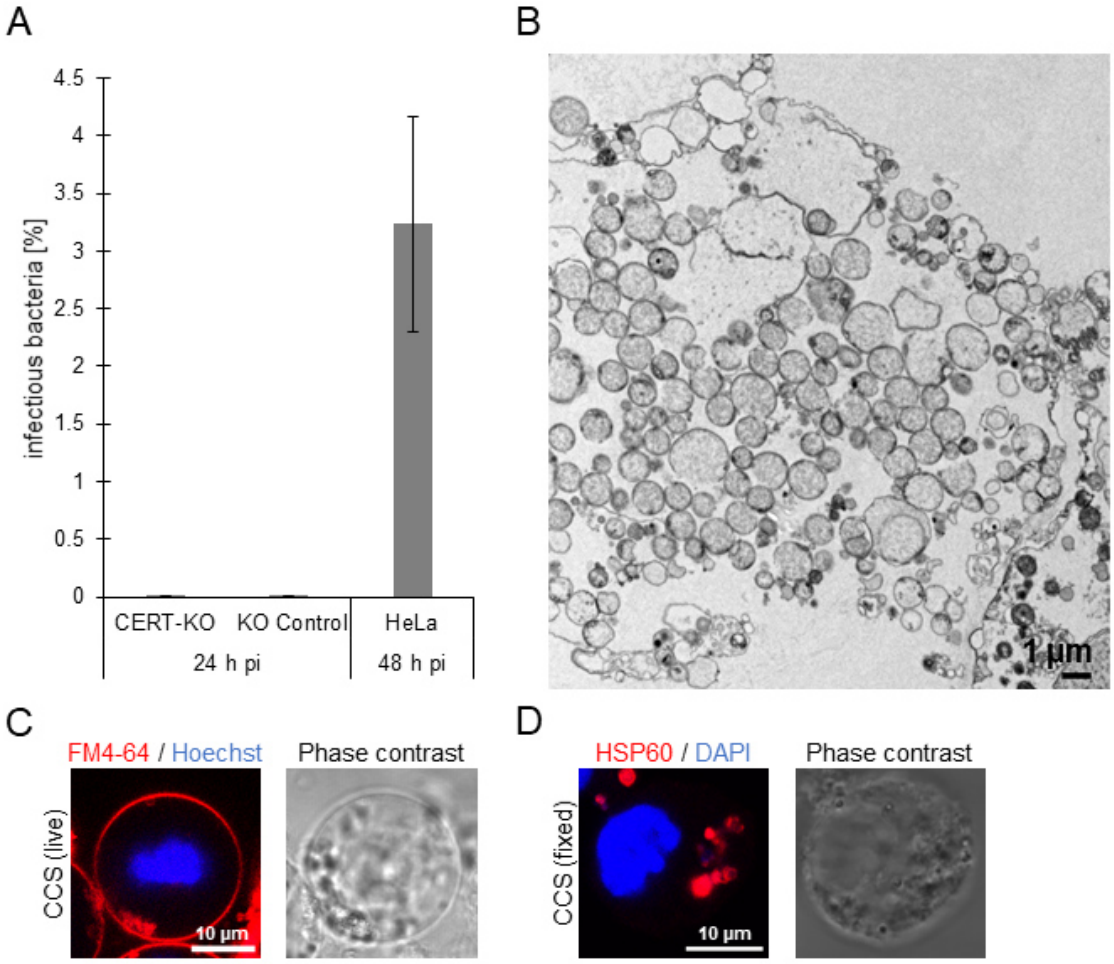

Figure 29. Premature, CERT-KO induced CCS contain mainly non-infectious reticulate bodies. (A) Early CERT-KO induced CCS of *C. psittaci* are not infectious as mature CCS. CCS in the supernatant of *C. psittaci*-infected CERT-KO and KO control cells (MOI 2) were separated from free bacteria by centrifugation (5 min, 300 x *g*, RT) at 24 h pi. Infectious progeny was titrated after glass bead lysis and numbers were normalized to genome copy numbers determined by qPCR. Data show mean ± SEM; n = 3. **(B)** Transmission electron microscopy (TEM) of a thin section through the chemically fixed supernatant of *C. psittaci*-infected HeLa CERT-KO cells (MOI 2, 24 h pi). In the supernatant, numerous *Chlamydia* in RB stage were found; n = 3. *Electron microscopy was performed in the group of M. Laue, RKI, Berlin.* **(C)** Representative fluorescence images of an early live CCS isolated of the supernatant of *C. psittaci*-infected HeLa CERT-KO cells (MOI 2, 24 h pi). The surrounding membrane was visualized using the membrane marker FM 4-64 and DNA was counterstained by Hoechst; n = 3. **(D)** Representative fluorescence images of a PFA-fixed early CCS isolated from *C. psittaci*-infected HeLa CERT-KO cells (MOI 2, 24 h pi). Bacteria inside the CCS were detected using a chlamydial HSP60 (Cy3) antibody and the DNA was counterstained using DAPI; n > 3. Modified from Scholz et al., 2024a.

To test this, I separated CCS from free bacteria present in the supernatant of *C. psittaci*-infected CERT-KO and KO control cells at 24 h pi using differential centrifugation. I then quantified the infectious progeny relative to the bacterial GCN associated with the harvested

CCS. Although more CCS are released in the supernatants from CERT-KO cells than from control cells at 24 h pi, the percentage of the progeny that are infectious are comparable (0.003 ± 0.0016% and 0.006 ± 0.0038%, respectively) (Figure 29 A). These values at 24 h pi are extremely reduced compared to the percentage of infectious progeny in mature CCS released from HeLa cells at 48 h pi (3.2 ± 0.9%).

To assess the presence and morphology of *C. psittaci* released from infected CERT-KO cells, I analyzed the culture supernatants using TEM. Among cellular debris, which is the main component of the supernatant, I found numerous *Chlamydia*, which were, with few exemptions, in RB stage (Figure 29 B). I further analyzed the morphology of early CCS by staining with the membrane dye FM 4-64 and with Hoechst. Fluorescence live cell confocal microscopy revealed that early CCS were surrounded by a membrane and contained concentrated DNA, which are both features of mature CCS (Figure 29 C). Bacteria could be detected in fixed early CCS with antibodies specific for bacterial HSP60. Bacteria were also labeled with the DNA marker DAPI, which also labeled DNA I identified as the host cell nucleus, which is also found within mature CCS (Figure 29 D).

These data show that CCS released early in the absence of CERT rarely contain any infectious EBs although the CCS are morphologically similar to mature CCS. In wildtype infections, CERT recruitment is reduced after RB redifferentiation to EB stage, indicating that stage-controlled changes of the localization of CERT allow release of infectious progeny containing CCS.

3.4 Lipid composition of *C. psittaci* infections

In the past, general investigations of lipids during *C. psittaci* infections were rarely conducted. Thus, in the fourth part of this study I aimed to obtain a comprehensive picture of the lipid profiles during *C. psittaci* infection. To achieve this, I performed an untargeted lipidomics analysis of *C. psittaci*-infected HeLa cells (Figure 30). I focused on two phases of the intracellular development of *C. psittaci* infections: The intracellular RB replication during infection and at the onset of host cell egress at the end of the intracellular development. Thus, I collected samples of *C. psittaci*-infected HeLa cells at 24 h pi and 48 h pi as time points representing middle and late *C. psittaci* infection, respectively, and collected uninfected HeLa cells in parallel as controls. After lipid extraction, I analyzed these samples by LC/MS analysis. Data analysis results in the specific lipidomes of the different conditions. In sum, 224 distinct lipid species were detected and quantified (Supplemental Table S1).

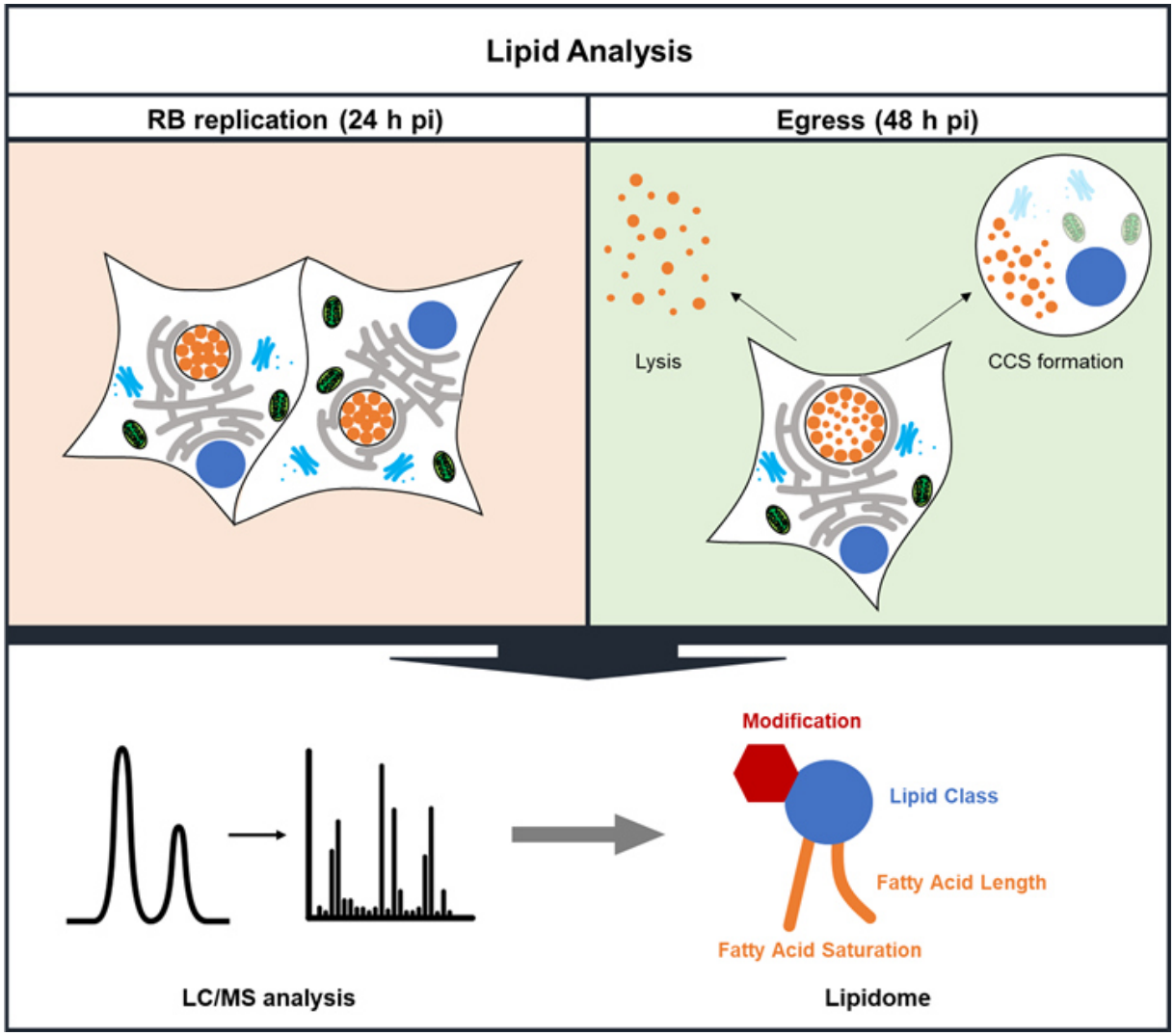

Figure 30. Schematic overview of the study design to characterize the lipidome of *C. psittaci* during RB replication and during egress. Samples of *C. psittaci*-infected HeLa cells during reticulate body (RB) replication and during egress were taken together with uninfected control samples at 24 h pi and 48 h pi, respectively. Lipids were extracted and analyzed by LC-MS/MS analysis. Lipidomes were characterized based on differences regarding lipid the lipid classes, fatty acids and modifications.

3.4.1 Middle and late *C. psittaci* infections have distinct lipidomes

To evaluate if major variation patterns based on the lipid compositions exist between *C. psittaci*-infected and uninfected cells and between both investigated phases of the intracellular development, I performed a principle component analysis (PCA) with the obtained lipid data.

PCA analysis revealed that *C. psittaci* infection during RB replication (24 h pi), *C. psittaci* infection at the onset of egress (48 h pi), and uninfected cells at the respective time points can be distinguished by their lipidome (Figure 31 A). The infected samples clustered at lower PC1 and higher PC2 values compared to the respective uninfected controls, while the 24 h pi samples clustered at lower PC1 and PC2 compared to the 48 h pi samples.

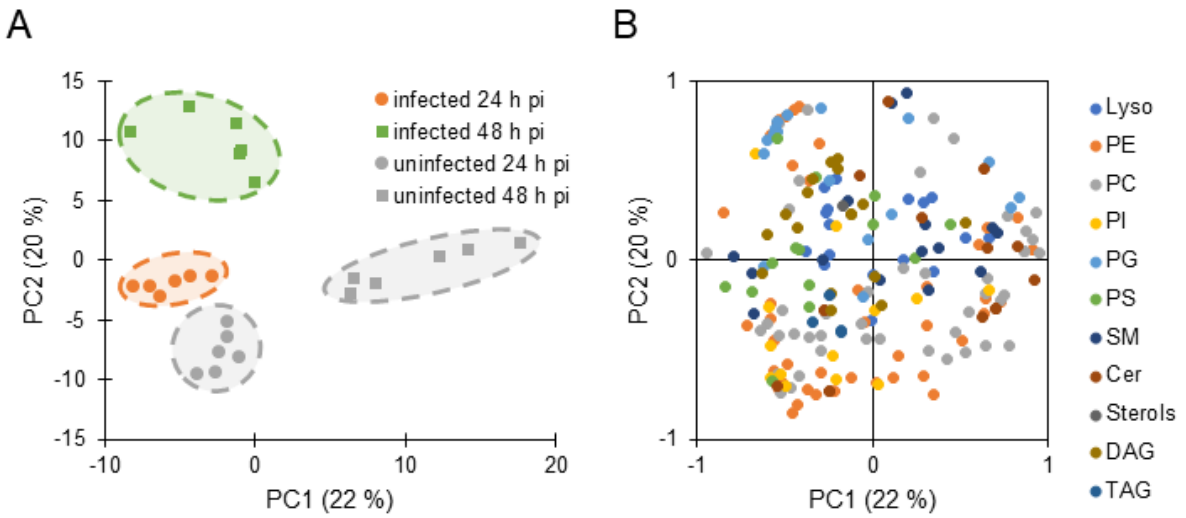

Figure 31. *C. psittaci*-infected HeLa cells during RB replication and during egress harbor a distinct lipidome. **(A)** Score plot and **(B)** loading plot of a principal component analysis of normalized untargeted lipidomic data comparing *C. psittaci*-infected HeLa cells (MOI 2) at 24 h pi, *C. psittaci*-infected HeLa cells (MOI 2) at 48 h pi, and the respective uninfected controls; n = 6. *Lipidomics analysis was performed in the group of L. Bindila, Johannes Gutenberg-Universität, Mainz.*
Abbreviations: **Lyso**: lysophospholipids, **PE**: phosphatidyl ethanolamine, **PC**: phosphatidyl choline, **PI**: phosphatidyl inositol, **PG**: phosphatidyl glycerol, **PS**: phosphatidyl serine, **SM**: sphingomyelin, **Cer**: ceramide, **DAG**: diacylglycerol, **TAG**: triacylglycerol.

PCA loading plot shows that PC1 had positive associations with PC, SM, and ceramides and negative associations with phosphatidyl ethanolamine (PE), phosphatidyl inositol (PI), phosphatidyl glycerol (PG), PS, diacylglycerols (DAG) and triacylglycerols (TAG), while PC2 had positive associations with lysophospholipids (Lyso), PG, and DAG, and negative associations with PE, PC, PI, and TAG (Figure 31 B).

Taken together, analysis of the lipid data shows that different phases of the intracellular development of *C. psittaci* are characterized by a specific lipidome and indicates that these differences could be relevant for successful RB replication and egress.

3.4.2 Specific phospholipid species are increased in *C. psittaci*-infected cells

To characterize the lipidome of *C. psittaci* infection during RB replication, I aimed to identify lipid species that differ significantly between *C. psittaci*-infected HeLa cells and uninfected cells at 24 h pi. Comparative analysis highlighted lipid species that show a significant increase ($p < 0.01$) of at least a one fold during infection (Figure 32 A). I identified 14 species (marked in blue) that were increased during this mid-point of infection. Next, I performed a volcano plot analysis comparing *C. psittaci*-infected HeLa cells at the onset of egress and uninfected cells at 48 h pi (Figure 32 B). I found the species that were increased during RB replication are also high in comparison to uninfected cells at the onset of egress (blue). I furthermore found five additional lipid species (yellow) increased at this late infection time point. Strikingly, in contrast to what has been shown in *C. trachomatis*-infected cells, I see no decrease in any lipid species.

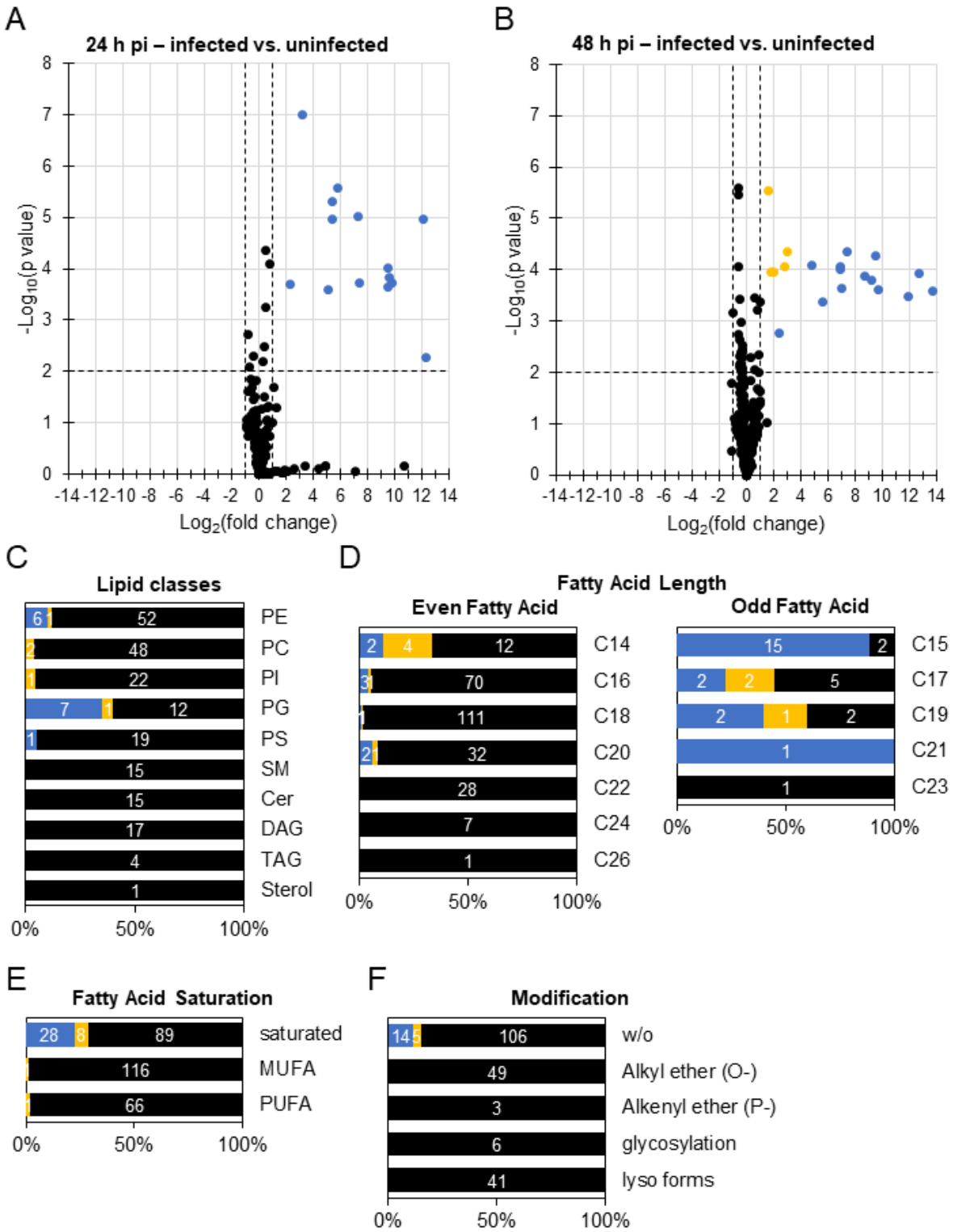

Figure 32. Analysis of the lipid species that differ between *C. psittaci*-infected and uninfected cells at 24 h pi and 48 h pi. (A, B) Volcano plots of Log_2-fold changes calculated from relative lipid abundances between 24 h **(A)** or 48 h **(B)** *C. psittaci*-infected HeLa cells and uninfected cells (n = 6, Student's t-test). Lipid species that are significantly increased during RB replication and at the onset of egress ($p < 0.01$, at least one fold increase) are marked in blue, those which are only increased at the onset of egress are marked in yellow. **(C, D, E, F)** Proportion of upregulated lipid species identified in **(A)** and **(B)** within the subclasses of lipids grouped by their lipid classes **(C)**, their fatty acid length **(D)**, their fatty acid saturation **(E)** and their modification **(F)**. *Lipidomics analysis was performed in the group of L. Bindila, Johannes Gutenberg-Universität, Mainz.*
Abbreviations: **PE**: phosphatidyl ethanolamine, **PC**: phosphatidyl choline, **PI**: phosphatidyl inositol, **PG**: phosphatidyl glycerol, **PS**: phosphatidyl serine, **SM**: sphingomyelin, **Cer**: ceramide, **DAG**: diacylglycerol, **TAG**: triacylglycerol, **MUFA**: Mono unsaturated fatty acids, **PUFA**: Poly unsaturated fatty acids.

Next, I analyzed to which lipid class the increasing lipid species belong. Of the lipid species detected, only phospholipids are increased during *C. psittaci* infection (Figure 32 C). Interestingly, seven of the 20 total detected PG species (35%) were increased during RB replication, and one additional species was increased at the onset of egress.

In addition, I analyzed the length of the fatty acids within the increased lipid species. Fatty acids with length between C14 and C21 were found within the increased lipid species (Figure 32 D). Notably, 61% of the lipid species that include odd chain fatty acids increased during RB replication, and this increases to 70% at the onset of egress. In contrast only 3% or 5% of the lipid species that include even chain fatty acids increased during RB replication or at the onset of egress, respectively.

Furthermore, I analyzed the saturation of the fatty acids within the increased lipid species. All lipid species that are increased at either the middle or late time point of *C. psittaci* infection contain exclusively saturated fatty acids (Figure 32 E). Analysis of the modifications of the increased lipid species revealed that the increased lipid species have no further modification (Figure 32 F).

In sum, these results show that specific lipid species increase during *C. psittaci* infection, and these lipid species are phospholipids that contain saturated odd chain fatty acids, which are likely branched-chain fatty acids. The lipid species that increase prior to egress have similar characteristics to the lipid species that increase during RB replication, suggesting a continuous impact on the lipidome during *C. psittaci* infection.

3.4.3 Direct comparison of the lipidome of *C. psittaci*-infected HeLa cells during RB replication and prior to egress showed an increase of C14-containing phospholipid species late in infection

Next, I aimed to identify lipid species that differ significantly in *C. psittaci*-infected cells between the two analyzed time points. My comparative analysis revealed eight lipid species (red) that were increased at least one fold in infected cells prior to egress in comparison to infected cells during RB replication. Only two lipid species (green) were significantly higher during RB replication than they were at the late infection time point (Figure 33 A).

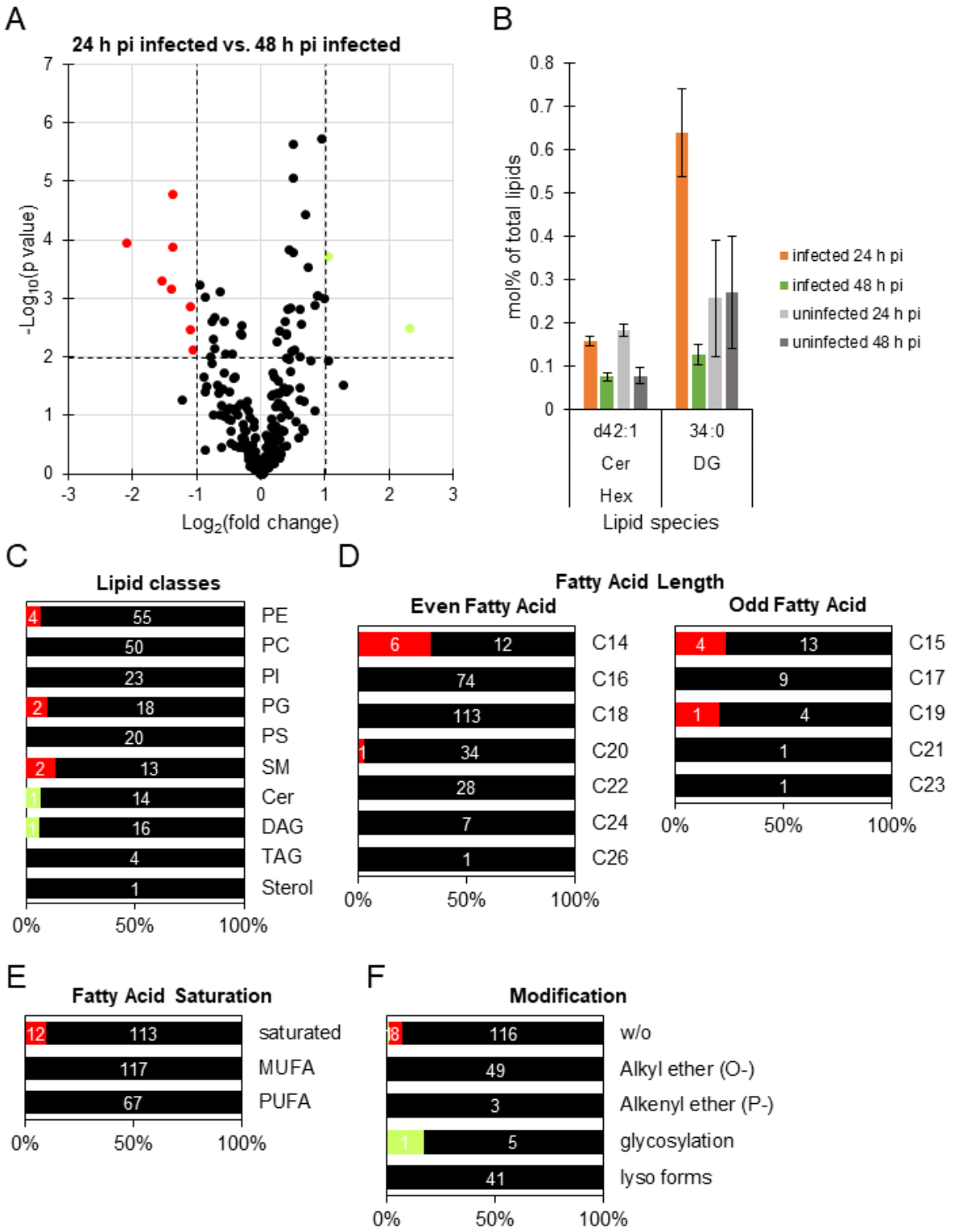

Figure 33. Analysis of the lipid species that differ in *C. psittaci*-infected cells between 24 h pi and 48 h pi. **(A)** Volcano plots of Log_2-fold changes calculated from relative lipid abundances between 24 h and 48 h *C. psittaci*-infected HeLa cells (n = 6, Student's t-test). Lipid species that are significantly increased during infection at 24 h pi or 48 h pi ($p < 0.01$, at least one fold increase) are marked in green and red, respectively. **(B)** Relative abundance of the lipid species that are increased during infection at 24 h pi compared to infection at 48 h pi. Data show mean ± SEM, n = 6. **(C, D, E, F)** Proportion of upregulated lipid species identified in **(A)** within the subclasses of lipids grouped by their lipid classes **(C)**, their fatty acid length **(D)**, their fatty acid saturation **(E)** and their modification **(F)**. *Lipidomics analysis was performed in the group of L. Bindila, Johannes Gutenberg-Universität, Mainz.*
Abbreviations: **PE**: phosphatidyl ethanolamine, **PC**: phosphatidyl choline, **PI**: phosphatidyl inositol, **PG**: phosphatidyl glycerol, **PS**: phosphatidyl serine, **SM**: sphingomyelin, **Cer**: ceramide, **DAG**: diacylglycerol, **TAG**: triacylglycerol, **MUFA**: Mono unsaturated fatty acids, **PUFA**: Poly unsaturated fatty acids.

These two lipid species that are increased during RB replication of *C. psittaci* are a ceramide and a diacylglycerol (Figure 33 B, C). In contrast, the lipid species that are increased prior to egress of *C. psittaci* are PEs, PGs, and SM (Figure 33 C). Because the concentration of these two species in infected cells were not significantly different from uninfected cells at either time point, these were excluded from further analyses (Figure 33 B).

The fatty acids within the increased lipid species at both developmental stages included fatty acids with lengths of C14, C15, C19, and C20 (Figure 33 D). Interestingly, 33% of the lipid species that include C14 fatty acids and 24% of the lipid species that include C15 fatty acids increased prior to egress, while in contrast only 1% of the lipid species with longer fatty acids increased.

Analysis of the saturation of the fatty acids within the lipid species increased during RB replication or increased prior to egress showed that these lipid species contain exclusively saturated fatty acids (Figure 33 E). Moreover, the lipid species increased at both developmental stages have no further modifications (Figure 33 F).

These data highlight that specifically the shorter C14 and C15 fatty acids increase prior to egress of *C. psittaci*.

3.4.4 Phospholipids increased in infection likely originate from both the bacteria and host

In total, 21 lipid species were identified as being significantly increased or decreased by comparing both developmental stages with uninfected cells and to each other (Figure 34 A). Interestingly, all 14 species that were increased during RB replication compared to uninfected cells (blue) were also increased prior to egress compared to uninfected cells (yellow). Six of the species that were increased prior to egress compared to uninfected cells (yellow) were also found to be increased compared to RB replication (red). Four species were identified that were increased during RB replication compared to uninfected cells, prior to egress compared to uninfected cells, and prior to egress compared to RB replication.

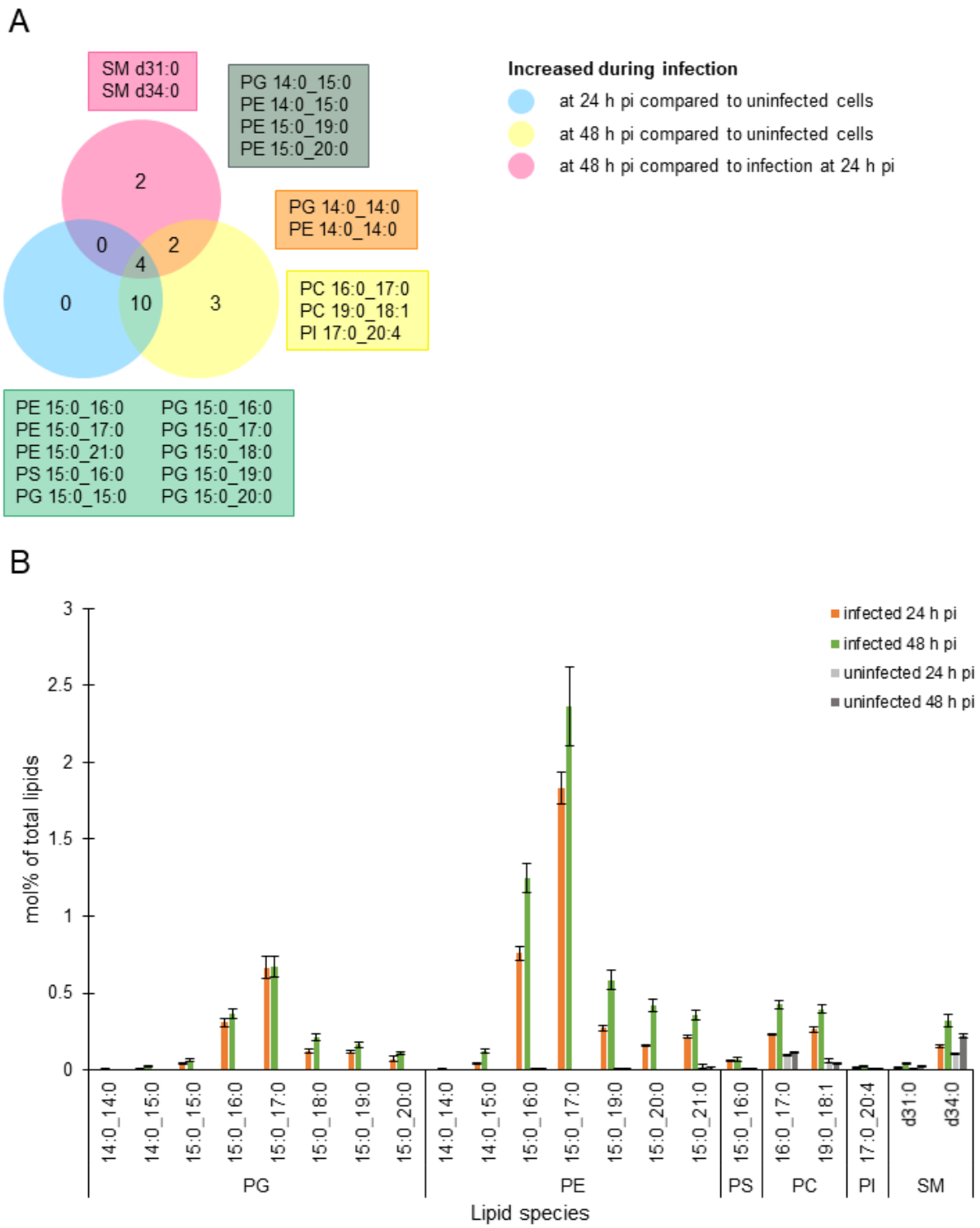

Figure 34. Comparison of lipid species that are significantly increased or decreased during *C. psittaci* infection at 24 h pi or 48 h pi compared to uninfected cells or between both timepoints. (A) Venn diagram showing the lipid species that are increased during infection at 24 h pi compared to uninfected cells, at 48 h pi compared to uninfected cells, and at 48 h pi compared to infection at 24 h pi, in blue, yellow, and red, respectively. **(B)** Relative abundance of the lipid species increased or decreased during *C. psittaci* infection at 24 h pi or 48 h pi compared to uninfected cells or between both timepoints. Data show mean ± SEM; n = 6. *Lipidomics analysis was performed in the group of L. Bindila, Johannes Gutenberg-Universität, Mainz.*
Abbreviations: **PE**: phosphatidyl ethanolamine, **PG**: phosphatidyl glycerol, **PS**: phosphatidyl serine, **SM**: sphingomyelin, **PC**: phosphatidyl choline, **PI**: phosphatidyl inositol, **Cer**: ceramide, **DG**: diacylglycerol, **Hex**: hexosly.

Although many of the lipid species associated with infection were found in relatively low amounts in all samples (less than 1%), I was still able to detect and quantify them. The most

prominent lipids associated with infection were PE 15:0_16:0, PE 15:0_17:0 and PG 15:0_17:0. These are lipids that have also been detected in cells infected with *C. trachomatis* (Yao et al., 2015). Increases in a range of PE and PG species were associated with *C. psittaci* infection, and the fatty acid profiles of these species are similar (Figure 34 B, Supplemental Figure S4 A). This increase in PE and PG species does not appear to be at the expense of other PE or PG species found in the host cells (Supplemental Figure S4 B, C), indicating that the additional PE and PG species are synthesized by the bacteria. Notably, the PI and PC species I see increasing during infection also contain odd-chain fatty acids, which may indicate these fatty acids were synthesized by the bacteria and were attached on host-cell derived PI and PC.

4 Discussion

The release of infectious bacteria from an infected host cell or tissue is crucial for intracellular bacteria to complete their infection cycle and spread within or transmit to a new host. Variations in egress pathways have been associated with specific aspects of pathogen biology, such as transmission, host tropism, and pathogenicity (Flieger et al., 2018; Kerr et al., 2017; Spera et al., 2023; Traven & Naderer, 2014). Therefore, understanding the egress strategies employed by different pathogens is as important as comprehending the adhesion and invasion processes. This understanding provides deeper insights into the biology of a specific pathogen. It is interesting to note that little is known about the biology of the zoonotic bacterial pathogen *C. psittaci* and especially not about its egress mechanisms.

Our knowledge about *C. psittaci*-proteins and their host cellular interaction partners is rare. However, it is known that the lipid transfer protein CERT is recruited to *C. psittaci* inclusions (Koch-Edelmann et al., 2017). *C. psittaci*-infection of CERT-KO cells shows that CERT is crucial for the outcome of infection, which leads me asking if CERT is also of importance for *C. psittaci* egress. CERT was described to take place in the formation of membrane contact sides between the chlamydial inclusion and the ER to facilitate the stabilization of the inclusion (Derré, 2015; Derré et al., 2011; C. A. Elwell et al., 2011; Koch-Edelmann et al., 2017). As the stabilization and destabilization of pathogen-containing vacuoles is crucial for intracellular vacuolar pathogens to facilitate host cell egress, I analyzed the role of CERT for the regulation of the stage-dependent stabilization and destabilization of the inclusion membrane of *C. psittaci* (Hybiske & Stephens, 2008; Kumar & Valdivia, 2009; Petit & Lebreton, 2022). Furthermore, as far as I know, no systemic data about the lipid composition during *C. psittaci* infection is available. This includes on the one hand a lack of knowledge about the lipid composition of *C. psittaci*-infected cells during early- and mid-time infections, but on the other hand an additional lack of knowledge about the lipid composition of *C. psittaci*-infected cells during late infections, which I aimed to close to understand the role of lipids for *C. psittaci* egress.

Here, I characterized for the first time host cell egress of *C. psittaci*. Thereby, I identified a novel, non-lytic egress pathway that I named the formation of *Chlamydia*-containing spheres (CCS). I characterized the mechanism of the formation of CCS and identified the inclusion-stabilizing role of the ceramide transporter CERT as crucial for the time-dependent formation of infectious CCS. In addition, I identified shortened fatty acids in the phospholipids of *C. psittaci*-infected cells as characteristic difference in the lipidome of late infection compared to mid-time infections.

4.1 CCS formation is a unique and novel chlamydial egress mechanism that can be linked with the specific biology of *C. psittaci*

In this study, I demonstrate that *C. psittaci* predominantly uses host cell-derived *Chlamydia*-containing spheres (CCS) as non-lytic egress structures to egress from epithelial cell cultures. CCS are present in the supernatant of infected cell monolayers and are enclosed by a single membrane derived from the host cell plasma membrane. The surrounding membrane retains selective membrane barrier functions and exposes PS on the outer leaflet. In addition to infectious EBs and RBs, CCS also contain host cell DNA and morphologically impaired host cell organelles, including the nucleus. CCS are formed by a sequence of events (Figure 35). First, proteolytic cleavage of a DEVD-containing substrate can be detected inside of the chlamydial inclusions, followed by an increase in the intracellular calcium concentration of the infected cell. Subsequently, blebbing of the plasma membrane begins, the inclusion membrane exposes SM to the cytosol and then destabilizes and the proteolytic cleavage of the DEVD-containing substrate increases rapidly within the whole infected cell. Finally, infected, blebbing cells detach and leave the monolayer resulting in CCS in the supernatant.

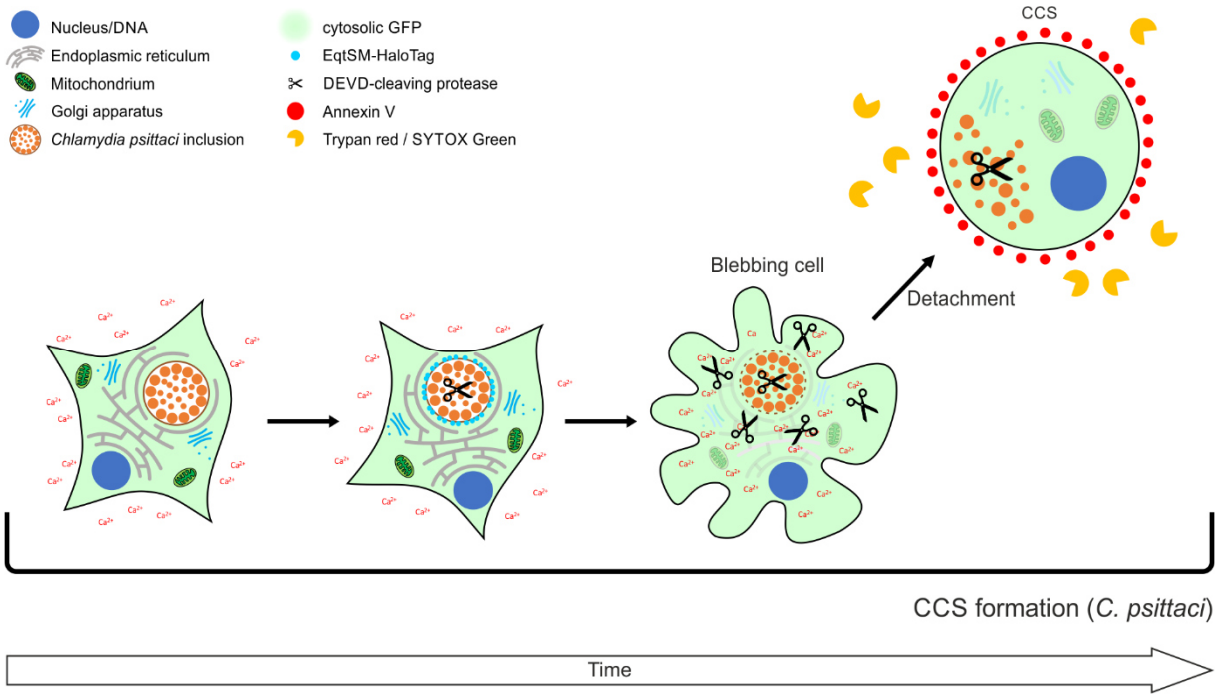

Figure 35. CCS formation of *C. psittaci*. Characteristics of CCS formation are the activation of a DEVD-cleaving protease, rapid calcium influx, the destabilization of the inclusion membrane, plasma membrane blebbing, and the detachment of the whole host cell to form a CCS. Modified from Scholz et al., 2024b and Scholz & Heuer, 2024.

In the following part, this mechanism of CCS formation will be contrasted to previously described chlamydial egress pathways step by step and their roles for the different biology and pathogenicity of *C. trachomatis* and *C. psittaci* will be discussed.

4.1.1 CCS formation differs fundamentally from extrusion formation of *C. trachomatis*

For members of the family *Chlamydiaceae*, egress has mainly been studied in the strict human pathogen *C. trachomatis*. It has been shown that *C. trachomatis* can egress the infected epithelial host cell by lysis of the host cell or by extrusion formation, a non-lytic egress pathway. Although CCS and extrusions are both non-lytic egress pathways, they are distinct in terms of morphology and formation. In contrast to CCS, *C. trachomatis* extrusion formation is characterized as a packaged release process without host cell death (Figure 36) (Hybiske & Stephens, 2007).

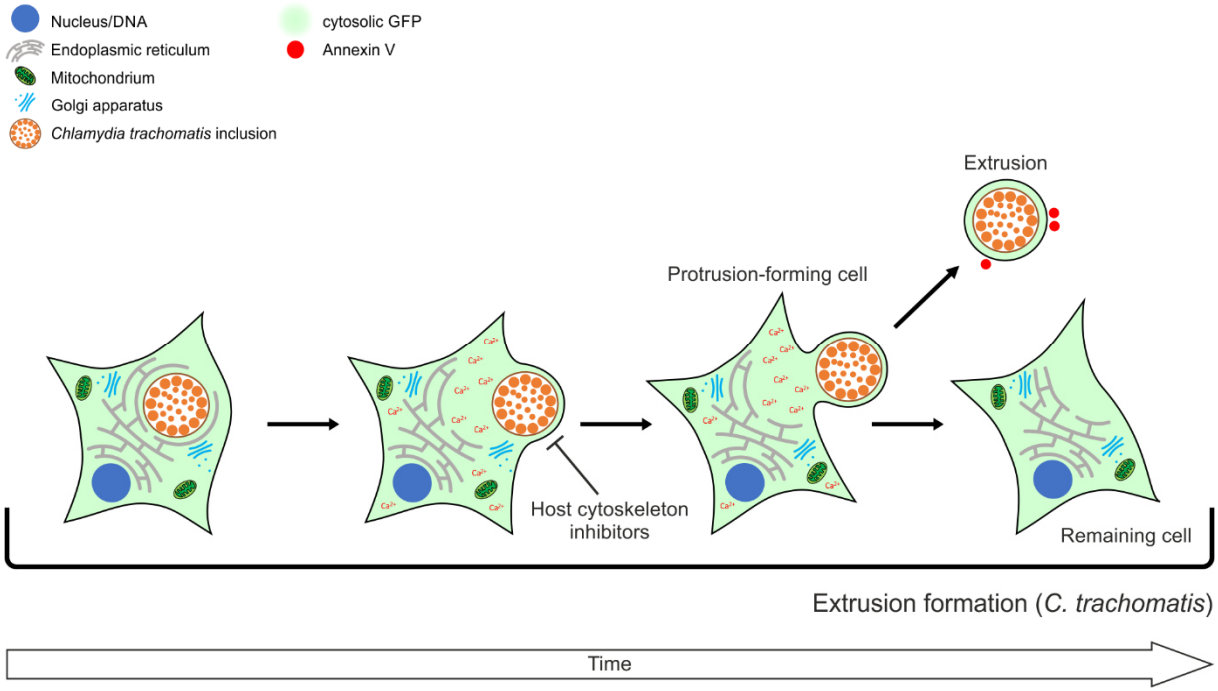

Figure 36. Extrusion formation of *C. trachomatis*. Characteristics of extrusion formation are the dependency on the host cell cytoskeleton, the regulation by the intracellular calcium concentration, which is a prerequisite for the activation of the movement of myosin motor proteins on the actin filaments, and the cytoskeleton-mediated formation of a protrusion, which is finally pinched-off from the surviving host cell to form an extrusion. Modified from Scholz & Heuer, 2024.

During extrusion formation, the intact *C. trachomatis*-filled inclusion is packed into a protrusion in dependence of the host cell cytoskeleton. This protrusion is then pinched off from the surviving host cell by a mechanism depending on the host cell cytoskeleton and RhoA, but not depending on proteases (Hybiske & Stephens, 2007; Lutter et al., 2013; Nguyen et al., 2018). Formed extrusions of *C. trachomatis* are covered by two membrane layers consisting of both the intact inclusion membrane and the plasma membrane of the host cell separated by a thin cytoplasmic layer (Hybiske & Stephens, 2007; Zuck et al., 2017). In addition, only 15.3% of *C. trachomatis* extrusions show extensive surface exposure of PS, while 59.6% of extrusions show a punctate PS pattern and 24.4% of extrusions do not expose PS (Zuck et al., 2017). Furthermore, *C. trachomatis* extrusions are free of host cell nuclei and rarely consist other host

cellular organelles, which is substantial for the survival of the remaining host cell (Hybiske & Stephens, 2007; Zuck et al., 2017).

4.1.2 Common features and differences of lytic egress, CCS formation, and extrusion formation

The mechanisms of the three known chlamydial egress pathways, lytic egress, CCS formation, and extrusion formation, share some characteristics, while they are fundamentally different in terms of other characteristics (Hybiske & Stephens, 2007; Lutter et al., 2013; Nguyen et al., 2018; Zuck et al., 2017).

Comparing the initiation of the three chlamydial egress pathways, lytic egress and CCS formation both start with protease activation and the destabilization of the inclusion membrane (Figure 37). For lytic egress, it was shown that the rupture of the inclusion membrane could be inhibited by cysteine protease inhibitors, but not by serine protease inhibitors (Hybiske & Stephens, 2007). For CCS formation, the proteolytic cleavage of a DEVD-containing fluorescent substrate was observed within the inclusion. After rupture of the inclusion membrane, it was observed within the whole cell. During extrusion formation, the inclusion membrane remains intact, while inhibition of elements of the cytoskeleton as actin nucleation, actin polymerization and myosin II inhibits extrusion formation (Hybiske & Stephens, 2007).

Interestingly, all three chlamydial egress mechanisms depend on calcium signaling (Figure 37). The formation of CCS is inhibited in the absence of calcium in the culture medium and during *C. psittaci* CCS formation, cytosolic calcium concentration increases. In addition, calcium seems to regulate the proteolytic cleavage of a DEVD-containing fluorescent substrate during CCS formation of *C. psittaci*. For *C. trachomatis*, it was initially described that the lytic egress, but not the non-lytic process of extrusion formation, depends on calcium signaling (Hybiske & Stephens, 2007). However, Nguyen et al. (2018) observed a calcium dependency of the formation of extrusions. In addition, they used calcium-free media to test the effect of intracellular calcium chelation using BAPTA-AM. In their experiments, calcium-free conditions themselves do not inhibit extrusion formation, but the use of BAPTA-AM does (Nguyen et al., 2018). This is in contrast to *C. psittaci* CCS formation, where the reduction of the extracellular calcium concentration itself without intracellular calcium chelation reduces CCS formation.

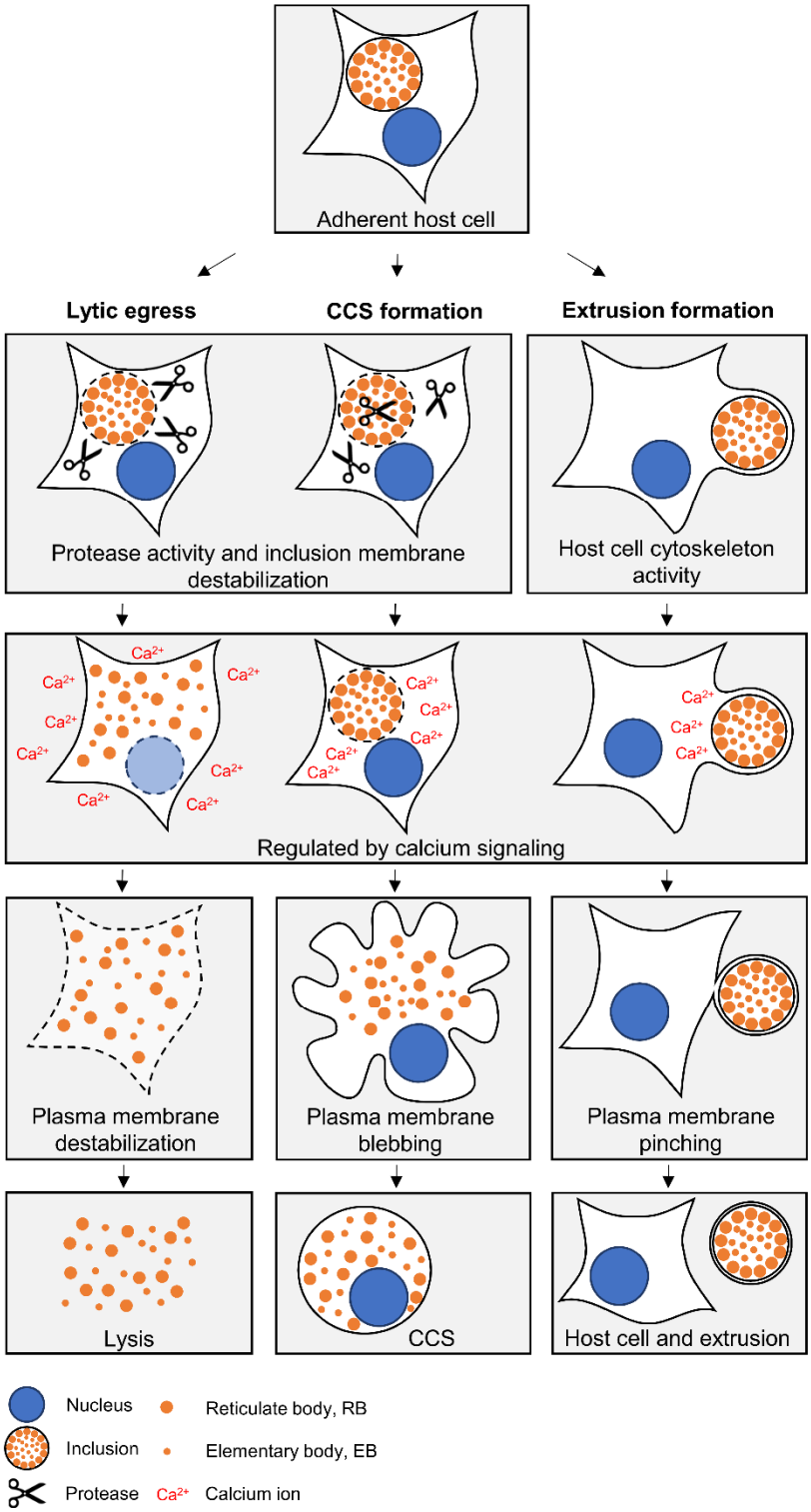

Figure 37. Comparison of the three chlamydial egress pathways: Lytic egress, CCS formation, and extrusion formation. Lytic egress and CCS formation both initiate with the activation of proteases and with the destabilization of the inclusion membrane. In contrast, during extrusion formation, the inclusion membrane remains intact and the inclusion is transported from the nucleus to the plasma membrane, mediated by the host cell cytoskeleton. All three egress pathways are regulated by calcium signaling. During lytic egress, the plasma membrane gets destabilized to release the chlamydia. In contrast, during CCS formation and extrusion formation, the plasma membrane stays intact. However, during CCS formation, the whole host cell detaches after membrane blebbing to form a CCS, while during extrusion formation, the extrusion is pinched-off from the surviving host cell.

The role of the plasma membrane of the host cell is different during the different egress mechanisms (Figure 37). During host cell lysis, the plasma membrane gets permeabilized

within 16 min, and this process is delayed to 62 min in the absence of cellular calcium (Hybiske & Stephens, 2007). During CCS formation, after an increase of the intracellular calcium concentration, plasma membrane blebbing initiates. During the blebbing process, the plasma membrane stays intact and forms finally a CCS. During *C. trachomatis* extrusion formation, a single protrusion is pinched of from the surviving host cell. This step depends on the activity of Rho GTPases to form a contractile ring (Hybiske & Stephens, 2007).

Chlamydial egress is completed with the formation of structurally different egress structures (Figure 37). The CCS formed by *C. psittaci* are covered by a single membrane sheet and filled with bacteria and host cellular organelles, including the nucleus. In comparison, *C. trachomatis* extrusions are covered by two membrane layers consisting of both the intact inclusion membrane and the plasma membrane of the host cell separated by a thin cytoplasmic layer (Hybiske & Stephens, 2007; Zuck et al., 2017). In addition, *C. trachomatis* extrusions are free of host cell nuclei and rarely consist other host cellular organelles, which is substantial for the survival of the remaining host cell (Hybiske & Stephens, 2007; Zuck et al., 2017). In comparison, CCS formation ends with the detachment of the whole host cell and host cell death. After lytic egress, free EBs and RBs are found without coverage by a membrane sheet and consequently, host cell death occurred (Hybiske & Stephens, 2007).

4.1.3 The role of the different chlamydial egress mechanisms for host-pathogen interaction

The different chlamydial egress mechanisms end up in different egress structures and differently influence the host cell and the host cellular monolayer. Thus, it is plausible that these mechanisms have different effects on the host cell defense system, spreading of the bacteria and tissue inflammation.

It has been previously described that *C. trachomatis* extrusions are taken up and survive within dendritic cells or other macrophages (Sherrid & Hybiske, 2017; Zuck et al., 2017). It was analyzed and discussed that the punctured appearance of PS at the outer leaflet of the extrusion membrane leads to extrusions being mistaken for apoptotic cells, which could be the reason for the uptake (Sherrid & Hybiske, 2017; Zuck et al., 2017). Similar strategies were also discussed for *M. marinum* and *L. major* (Davis & Ramakrishnan, 2009; van Zandbergen et al., 2004). As also CCS present PS at the outer leaflet of the CCS membrane, they could be similarly taken up by dendritic cells or other macrophages. Thus, both CCS formation and extrusion formation could subsequently influence the function of those immune cells (Sherrid & Hybiske, 2017). I speculate that both non-lytic egress forms could reduce the activation of the host defense system and tissue inflammation during chlamydial infections compared to lytic egress and suggest a link between egress and pathogenicity of *Chlamydia* spp.

In addition, both CCS formation and extrusion formation delay the release of infectious material and host cell debris. Interestingly, the stability of both structures and hence, the duration of the delay of release is different for the different pathogens and egress mechanisms. In general, CCS formed by *C. psittaci* are more stable than CCS and extrusions formed by *C. trachomatis*. However, individual CCS and extrusions can be stable for several hours up to days, while other lyse within the first hour after formation. I speculate that *in vivo* this could facilitate spreading over different distances within a host cell membranous, protected compartment to different locations or across tissues. As previously discussed for extrusions, this potential spreading within CCS or extrusions could also be supported by hijacking macrophages and by abusing their migration across tissues or to lymph nodes for chlamydial dissemination *in vivo* (Zuck et al., 2017).

While both extrusion and CCS formation leave the bacteria in a host cell membranous, protected compartment, they differ in the way that they leave the cellular monolayer. On the one hand, extrusion formation leaves an intact host cell behind within an intact cellular monolayer. On the other hand, the detachment of the infected host cell during CCS formation also occurs without damaging the surrounding cell monolayer, but the detached cell itself leaves an open space in the monolayer that is closed by the surrounding cells. Thus, if massive CCS formation occurs at the same time in highly infected monolayers, the numerous lesions in monolayer cannot be closed by surrounding cells anymore. Similar, *S. enterica* subspecies *enterica* serotype Dublin infection damages the cellular monolayer in a bovine ileal monolayer model (Kawasaki et al., 2024). Interestingly, in *S. enterica* subspecies *enterica* serotype Dublin infection this causes also activation of the cellular inflammatory immune response (Kawasaki et al., 2024). This suggests that *in vivo* massive CCS formation could also force tissue inflammation processes.

4.1.4 The potential role of the different chlamydial egress mechanisms for chlamydial pathogenicity

C. psittaci performs predominantly CCS formation and in lower frequencies lytic egress, but no extrusion formation. In contrast, *C. trachomatis* is able to perform all three egress pathways. However, *C. trachomatis* performs CCS formation with a lower frequency compared to *C. psittaci*, and *C. trachomatis* CCS are formed only until 55 h pi and are less stable compared to *C. psittaci* CCS. In contrast, *C. trachomatis* extrusion formation becomes more prominent after 65 h pi and shows similar frequencies to host cell lysis at 72 h pi.

While *C. psittaci* is a zoonotic agent infecting a wide range of different host organisms including birds, but also mammals as sheep, cattle, horses, dogs and cats, as well as humans, *C. trachomatis* infects exclusively humans. Interestingly, *C. psittaci* can additionally infect a wide range of tissues, including the lung, heart, liver, kidney, eye, blood, nervous system, and

skin in humans (Dembek et al., 2023; C. Elwell et al., 2016). Thus, the systemic illness caused by *C. psittaci* had a mortality rate about 20% today without treatment and was up to 50% in the past (Dembek et al., 2023; Weston et al., 2023). In contrast, the trachoma, genital tract, and lymphogranuloma venereum biovar of *C. trachomatis* infect mostly the eye, the reproductive system, and the lymph nodes, respectively (C. Elwell et al., 2016; S. M. Murray & McKay, 2021; Sturd & Rucks, 2023). In addition, systemic illness and death caused by *C. trachomatis* is rare (McElligott, 2014; Wang et al., 2016).

As discussed above, it is plausible that the different chlamydial egress pathways influence the pathogenicity of the different chlamydial species. I showed in this study that within my *in vitro* model, CCS formation is more frequent in *C. psittaci* compared to *C. trachomatis*, while extrusion formation was only observed in *C. trachomatis*. The frequency of the different egress pathways *in vivo* and the question if they influence inflammation processes, the transition of local infections to systemic illness, and thus, the pathogenicity of the different chlamydial species should be studied in the future.

4.2 CCS formation differs substantially from known host cell death pathways and egress pathways of other intracellular pathogens

CCS formation results in a form of host cell death, which shares some features of apoptosis, but lacks other features of apoptosis (Mariño & Kroemer, 2013; Rogers et al., 2017; Sukumaran et al., 2021; Y. Zhang et al., 2018). Similar, also egress mechanisms of other intracellular pathogens show similarities, but are not identical with CCS formation (Baer et al., 2007; Burda et al., 2017; Davis & Ramakrishnan, 2009; De Leon-Rodriguez et al., 2018; Schulze-Luehrmann et al., 2024; Shears et al., 2019; van Zandbergen et al., 2004).

Thus, in the following part the mechanism of CCS formation will be compared with host cell death and egress pathways of other intracellular pathogens to present its unique and novel character.

4.2.1 Comparison of CCS formation with host cell death

A role of apoptosis in CCS formation was supported by the observation that the intracellular calcium concentration increases during CCS formation, plasma membrane blebbing and exposure of PS at the CCS membrane surface. However, the following observations are not typical for apoptosis: Active caspase-3 is absent, CCS formation could not be inhibited by different caspase inhibitors including the pan-caspase inhibitor Z-VAD-FMK and nuclear condensation and fragmentation was not detected in CCSs.

In general, host cell death pathways are inhibited by *Chlamydia* spp. during intracellular development (Fan et al., 1998; Sixt, 2022; Waguia Kontchou et al., 2022). However, several studies have demonstrated that the rupture of the *C. trachomatis* inclusion membrane is associated with the cytotoxicity of the infected host cell and the role of distinct cell death pathways during chlamydial infections has been the subject of controversy (Bishop & Derré, 2022; Dimond et al., 2021; Kerr et al., 2017; Sixt et al., 2017; Weber et al., 2017): Interfering with expression of specific *C. trachomatis* Inc-proteins by generating *C. trachomatis* mutants induced premature lysis of the inclusion membrane and cell death by apoptosis, necrosis and aponecrosis (Bishop & Derré, 2022; Dimond et al., 2021; Sixt et al., 2017; Weber et al., 2017). By using a laser ablation strategy to artificially ruptured *C. trachomatis* inclusion membrane, Kerr et al. (2017) showed that after inclusion membrane rupture, the cells underwent necrosis independent of caspases (Kerr et al., 2017). Similar, for *C. trachomatis*, *C. psittaci* and *C. caviae*, it was observed that cellular caspase-3 is not activated during late infections, and it was concluded that *Chlamydia* spp. undergo an atypical form of apoptosis at the end of the developmental cycle (Gibellini et al., 1998; Ojcius et al., 1998; Perfettini et al., 2002).

4.2.2 Comparison of CCS formation with egress pathways of other intracellular pathogens

Compared to other intracellular pathogens, egress mechanisms showing similarities, but are not identical with CCS formation were described.

An example for egress in host cellular membrane covered structures is merosome formation of *Plasmodium* parasites. Here, after rupture of the parasitophorous vacuole membrane, the host cell detaches and subsequently, *Plasmodium* liver stage parasites are released into vesicles budding off from the infected host cell (Burda et al., 2017; Shears et al., 2019). In contrast to CCS formation, no membrane blebbing occurs prior to host cell detachment and the merosomes do not expose PS (Baer et al., 2007).

Other intracellular pathogens as *M. marinum* and *Leishmania spp.* are packed into apoptotic bodies during pathogen induced apoptosis at the end of their developmental cycle (Davis & Ramakrishnan, 2009; van Zandbergen et al., 2004). Macrophages infected with the bacterium *M. marinum* recruit new macrophages, and after apoptotic non-lytic death with the bacteria encased by the intact membrane, they are phagocytosed by new macrophages which thereby get infected (Davis & Ramakrishnan, 2009). Similar, polymorphonuclear neutrophil granulocytes infected with the parasite *Leishmania major* undergo apoptosis and the PS presenting apoptotic bodies are phagocytosed by macrophages, where *L. major* again multiplies (van Zandbergen et al., 2004). In contrast to CCS formation, in both cases the apoptotic process ends with the formation of apoptotic bodies, not with the detachment of the whole host cell.

In addition, the egress of the fungus *C. neoformans* from infected macrophages by phagolysosomal membrane permeabilization is associated with apoptosis (De Leon-Rodriguez et al., 2018). However, *C. neoformans* egresses by lytic exocytosis, not in membrane-bound structures.

Another pathogen which performs an egress pathway that is correlated with apoptosis is *C. burnetii* (Schulze-Luehrmann et al., 2024). In contrast to CCS formation, where the bacteria are being covered by a membrane and egress cannot be blocked by apoptosis inhibitors, *C. burnetii* performs host cell egress without being covered by a host cell membrane and blocking host cell intrinsic apoptosis reduces the amount of spreading bacteria (Schulze-Luehrmann et al., 2024).

Thus, my data is relevant for the general research field focusing on egress of intracellular pathogens as it provides insights into an egress pathway that is novel for the egress of intracellular pathogens.

4.3 The stabilization of the inclusion membrane is critical for regulation of chlamydial egress

Intracellular pathogens apply different strategies to survive within a host cell. In principle, there are two distinct lifestyles which distinguish between the preferred replication niche of the pathogens: Vacuolar pathogens replicate within membrane-bound compartments, while cytosolic pathogens replicate within the cytosol (Kumar & Valdivia, 2009; Petit & Lebreton, 2022). Notably, also pathogens exist that can apply both strategies, as for example *Salmonella* spp. and *Listeria* spp. (Petit & Lebreton, 2022).

Chlamydia spp. belong to the group of intracellular vacuolar pathogens (Banhart et al., 2019; Hybiske & Stephens, 2008). For these intracellular vacuolar pathogens, the stabilization and destabilization of the pathogen-containing vacuole is crucial for their surviving: on the one hand, they need to stabilize the vacuole to facilitate pathogen growth in a protected niche, on the other hand the destabilization of the vacuole plays an important role for numerous host cell egress strategies and thus, for pathogen transmission to other hosts (Hybiske & Stephens, 2008; Kumar & Valdivia, 2009; Petit & Lebreton, 2022).

In the following part, the role of the stabilization and destabilization of the inclusion for the regulation of egress by *Chlamydia* spp. will be discussed.

4.3.1 The role of CERT-stabilized MCS for the stability of the inclusion membrane

The inclusion represents the protective intracellular niche that supports chlamydial growth. Therefore, the lysis of the inclusion membrane must be regulated during the chlamydial cycle of development to avoid premature inclusion membrane lysis, which would activate host cell death pathways and limit the formation of infectious EBs. It is noteworthy that a clear distinction exists between CCS and extrusions. While a defining feature of CCS formation is the destabilization of the inclusion membrane, extrusions are characterized by the preservation of the inclusion and inclusion membrane, as evidenced by the influx of eGFP to the inclusion lumen or the absence of eGFP in the inclusion lumen, respectively.

In this study, I analyzed the role of CERT for the stabilization and destabilization of the inclusion of *C. psittaci*. I showed that CERT recruitment to the inclusion membrane is time-dependent: During RB replication at 24 h pi, CERT is recruited to the inclusion membrane. Here it can stabilize ER-inclusion MCS (Derré, 2015; Derré et al., 2011). In contrast, during CCS formation at 48 h pi, CERT recruitment is reduced and the inclusion loses stability (Figure 38). Premature loss of CERT recruitment that can be induced by using CERT-KO cells, induces the formation of premature, non-infectious RB-containing CCS by a sequence of events analogous to mature CCS formation (Figure 38). I propose that the time-dependent recruitment of CERT stabilizes

the inclusion by ER-inclusion MCS during RB replication and that reduction of CERT at the inclusion after EB maturation allows destabilization of the inclusion by the loss of ER-inclusion MCS prior to CCS formation.

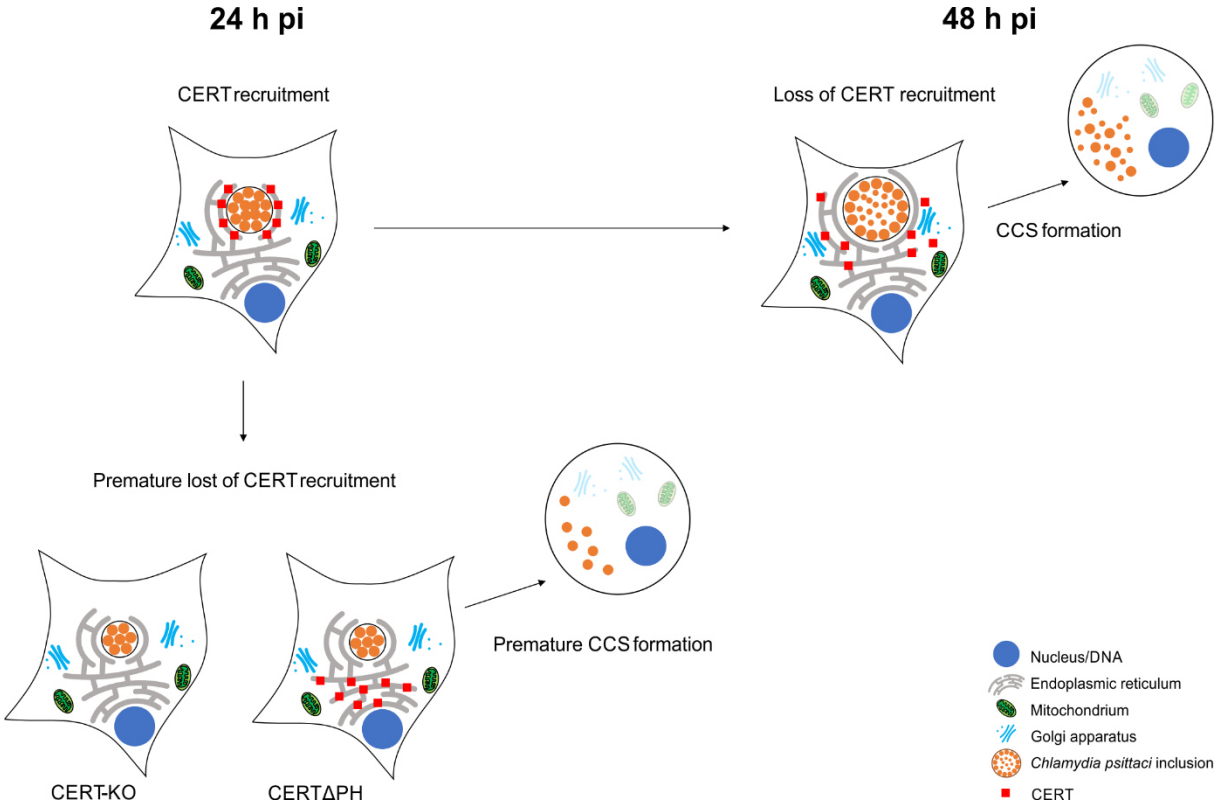

Figure 38. Graphical model of the role of CERT for regulating *C. psittaci* CCS formation. At 24 h pi, the recruitment of CERT to the *C. psittaci* inclusion promotes inclusion stability by CERT-stabilized ER-inclusion membrane contact sites. At 48 h pi, CERT recruitment to the *C. psittaci* inclusion is reduced and the consequential loss of the inclusion stability facilitates CCS formation. Under CERT-KO or CERTΔPH-expressing conditions, where CERT is not present at the inclusion membrane at 24 h pi, this promotes early egress and facilitates the formation of premature, non-infectious CCS. Modified from Scholz et al., 2024a.

The role of the stability of ER-inclusion MCS and egress of *Chlamydia* spp. was previously discussed in terms of the IncS-STIM1 interaction at *C. trachomatis* inclusions (Agaisse & Derré, 2015; Cortina et al., 2022; Cortina & Derré, 2023). Recent studies by Cortina & Derré (2023) demonstrate that the *C. trachomatis* inclusion membrane protein $IncS_{Ct}$ (CTL0402) recruits STIM1 to the *C. trachomatis* inclusion membrane, while the *C. muridarum* analog $IncS_{Cm}$ failed to recruit STIM1 (Cortina et al., 2022; Cortina & Derré, 2023). Furthermore, *C. trachomatis* strains lacking $IncS_{Ct}$ perform higher rates of inclusion lysis at late developmental stages, supporting previous findings using *C. trachomatis* and *C. muridarum* chimeras (Dimond et al., 2021). In addition, Nguyen et al. (2018) showed that depletion of STIM1 reduced extrusion formation in *C. trachomatis*, indicating that the stabilization of the inclusion membrane by STIM1 recruitment supports extrusion formation. Notably, *C. psittaci* does not recruit STIM1 at 24 h pi and 48 h pi (Supplemental Figure S5) and extrusion formation takes not place in *C. psittaci* infections, suggesting that *C. psittaci* ER-inclusion MCS are intrinsically less stable compared to *C. trachomatis* inclusions, which could prevent them from

performing extrusion formation. Following this model, CERT recruitment would be more important for the stabilization of *C. psittaci* ER-inclusion MCS compared to *C. trachomatis* ER-inclusion MCS, which may explain the influence CERT recruitment has in regulating CCS formation in *C. psittaci* in a time-dependent manner. Interestingly, STIM1 is also not recruited to *C. muridarum* inclusions and replacement of *C. trachomatis* IncS by *C. muridarum* IncS blocks STIM1 recruitment to *C. trachomatis* inclusions (Cortina & Derré, 2023). This suggests that also in *C. muridarum* egress could be regulated by the recruitment of CERT.

4.3.2 The role of sphingolipids for the stability of the inclusion membrane

CERT does not only stabilize ER-inclusion MCS in chlamydial infections, but it also plays a crucial role for sphingolipid acquisition of *Chlamydia* spp. (Banhart et al., 2014; Derré et al., 2011; C. A. Elwell et al., 2011; Koch-Edelmann et al., 2017; Kumagai et al., 2018, 2022). In uninfected cells, CERT transports ceramides from the ER to the Golgi apparatus (Banhart et al., 2019; Chung et al., 2021). During this process, the central FFAT motif of CERT interacts with VAPs at the ER membrane, thereby linking CERT to the ER. At the ER, ceramides bind to the C-terminal START domain of CERT, which are then transported to the Golgi apparatus by the N-terminal PH domain of CERT, which interacts with PI4P at the Golgi membrane (Banhart et al., 2019; Chung et al., 2021).

In *C. trachomatis*, *C. muridarum* and *C. psittaci* infections, CERT is recruited to the chlamydial inclusion mediated by the PH domain of CERT, while the FFAT motif of CERT is still linked to the ER and the START domain still binds ceramides, which are then transported to the chlamydial inclusion (Derré et al., 2011; C. A. Elwell et al., 2011; Koch-Edelmann et al., 2017). Thus, chemical inhibition of CERT with the ceramide analogue HPA-12 inhibits ceramide transport to the inclusions and hence, reduces inclusion size and progeny formation (Derré et al., 2011; C. A. Elwell et al., 2011; Koch-Edelmann et al., 2017). Interestingly, CERT-KO does not prevent sphingolipid acquisition to *C. psittaci* inclusions, but HPA-12 treatment does, indicating that a CERT-independent, HPA-12 sensitive ceramide acquisition pathway is used by *C. psittaci* under CERT-KO (Koch-Edelmann et al., 2017). In addition, I showed that expression of a CERT variant lacking the START domain, which is not able to transport ceramides, but localizes at the inclusion membrane, can compensate for the CERT-KO induced premature CCS formation. Again, this supports that premature CCS formation under CERT-KO is based on its mechanistic role in stabilizing ER-inclusion MCS and is not based on its functional role in sphingolipids acquisition during *C. psittaci* infections.

In addition to the characterization of CERT-mediated sphingolipid transport, cytosolic EqtSM, an engineered, non-toxic version of equinatoxin II, was used as a SM reporter to characterize the destabilization of the inclusion membrane during CCS formation (Deng et al., 2016). Similar to pathogen-induced membrane damage and vacuolar escape of *M. marinum* and *S. enterica*,

SM in the inclusion membrane is exposed to the cytosol during CCS formation of *C. psittaci* prior to inclusion membrane destabilization (Niekamp et al., 2022; Scharte et al., 2023). This suggests that a rearrangement of the sphingolipids in the inclusion membrane could trigger its destabilization, thereby indicating that sphingolipids may influence CCS formation.

4.3.3 The role of phospholipids for the stability of the inclusion membrane

Phospholipids are another group of lipids which are acquired by *Chlamydia* spp. from the host cell, however studies using *C. trachomatis* suggest that phospholipids can also be synthesized by the bacteria (Hatch & McClarty, 1998; Scidmore, 2011; Wylie et al., 1997). It is noteworthy that *C. trachomatis* and *C. psittaci* both possess the genes necessary for the synthesis of PS, PE and PG (Seth-Smith et al., 2011; Yao et al., 2015). It is assumed that only the host cells can synthesis PC and PI (Soupene & Kuypers, 2017; Yao et al., 2015). In *C. trachomatis*-infected cells, phospholipids with a branched-chain fatty acid at the sn-2 position were detected (Su et al., 2004; Wylie et al., 1997). It has been proposed that the activation of the host phospholipase cPLA2 during *C. trachomatis* infection hydrolyzes the fatty acid from the sn-2 position of phospholipids and allows import into and modification by *C. trachomatis* (Soupene & Kuypers, 2017; Su et al., 2004; Wylie et al., 1997). The hypothesis that all *C. trachomatis*-associated phospholipids are synthesized by the bacteria has also been proposed by Yao et al. (2015), but incorporation of branched-chain fatty acids, which are a hallmark of bacterial fatty acids, into PC suggests some bacterial modification of host-derived fatty acids (Wylie et al., 1997; Yao et al., 2015).

Here, I showed that during RB replication and during late infections, concentrations of specific phospholipid species, especially PG and PE species and saturated odd-chain fatty acid-containing species, increased in comparison to uninfected cells. At the onset of egress, the amount of specific phospholipids species comprising shorter fatty acids, especially C14, was increased, suggesting that they are a specific characteristic of late infections.

For the PE and PG species I identified as being increased in *C. psittaci*-infected cells, I cannot distinguish whether they originate from the bacteria or host. However, the profile of theses PE and PG species are similar to one another (with PG 15:0_15:0, PG 15:0_20:0, and PE 15:0_21:0 as exemptions), which would be consistent with them arising from a common phosphatidic acid precursor, as it has been suggested for *C. trachomatis* (Yao et al., 2015). Furthermore, I detect odd-chain fatty acids at both the sn-1 and sn-2 positions, and I also do not see a reduction in any PE or PG species caused by infection. These three observations would be consistent with *C. psittaci* synthesis of at least some of the PE and PG species. In contrast to what I see in *C. psittaci*-infected cells, a reduction of specific PE species has been detected in *C. trachomatis*-infected cells and has been attributed to cPLA2 activation (Su et al., 2004; Yao et al., 2015). Whether or not cPLA2 is activated in *C. psittaci*-infected cells has

not yet been evaluated. Notably, I also detect an increase of two PC and one PI species during *C. psittaci* infection. The incorporation of odd-chain fatty acids during infection suggests that these host phospholipids are perhaps modified by *C. psittaci*.

In lipids extracted from *C. psittaci*-infected cultured monkey kidney cells, about 20% branched chain fatty acids were found by quantitative lipid analysis, while in uninfected cells, branched chain fatty acids were only in trace amounts (Makino et al., 1970). The predominantly detected branched-chain fatty acid was anteiso-branched C15, but also iso-branched C16, anteiso-branched C17, iso-branched C18, anteiso-branched C19, and iso-branched C18 were found (Makino et al., 1970). It is important to note however, that Makino et al. (1970) analyzed free fatty acids from hydrolyzed lipid samples and not the intact lipid species. In this study, due to technical reasons I was not able to distinguish between straight, iso-branched or anteiso-branched fatty acids. However, I observed an increase in odd-chain fatty acids in the phospholipid species of infected samples at both time points, and these were mainly C15-species, similar to the branched-chain fatty acids detected by Makino et al. (1970). Analysis of the mobilograms of these species indicated that they are present in different isoforms, which suggests that also *C. psittaci* synthesizes branched-chain fatty acid and incorporates them into bacteria- or host-derived phospholipids.

Interestingly, I observed an increase of short chain (C14 and C15) fatty acid containing phospholipids prior to egress. Even though I do not know about the intracellular localization of these phospholipid species, it is possible that they are located in the inclusion membrane as the presence of the shorter fatty acids correlate in time with other changes of the inclusion membrane: SM exposure and inclusion membrane destabilization. Furthermore, it remains unclear if these changes in the lipid pattern of mid-time infections to late infections are a bacteria- or a host cell driven process process and whether this process is driven by the synthesis of new, shorter fatty acids or by the degradation of longer fatty acids. Notably, I observed a recruitment of Acyl-CoA Dehydrogenase Family Member 11 (ACAD11) to the *C. psittaci* inclusion membrane at 48 h pi, which was not observed at 24 h pi (Supplemental Figure S6), which is a cellular fatty acid dehydrogenase with a specificity for longer fatty acids (M. He et al., 2011). ACAD11 was previously identified as interaction partner of the chlamydial inclusion membrane protein Cps0558 (Gensch, 2022). Thus, I hypothesize that the bacteria secrete Cps0558 into the inclusion membrane during late infections, which recruits ACAD11 to *C. psittaci* inclusions and ACAD11 reduces the fatty acid length of longer fatty acids within the inclusion membrane. As decreased phospholipid tail length is associated with decrease of the hydrophobic thickness of the membrane and increase of the membrane permeability (Frallicciardi et al., 2022), the proposed reduction of fatty acid length within the inclusion membrane may increase the permeability of the inclusion membrane and thus, trigger CCS formation.

4.4 Conclusion

Taken together, this thesis demonstrates that *C. psittaci* predominantly egresses from the host cell by the novel non-lytic mechanism of CCS formation. The process of caspase-independent cleavage of a DEVD-containing substrate, calcium influx, inclusion membrane lysis, plasma membrane blebbing and detachment of the whole infected host cell represents a new egress strategy for intracellular pathogens. In particular, this novel non-lytic egress mechanism is distinct from extrusion formation, the previously described non-lytic egress mechanism of the related but strict human pathogen *C. trachomatis*.

In addition, I showed that the recruitment of CERT stabilizes *C. psittaci* inclusions during RB replication and prevents premature CCS formation. My data suggests that the loss of CERT recruitment in late infections facilitates the destabilization of ER-inclusion MCS and the chlamydial inclusion membrane and consequently promotes CCS formation and bacterial egress. To further understand how the time-dependent recruitment of CERT is regulated, it is crucial to identify the bacterial interaction partner of CERT within the *C. psittaci* inclusion membrane.

Furthermore, lipidomics showed that *C. psittaci*-infected cells harbor a specific lipidome which is characterized by phospholipid species with saturated odd chain fatty acids, probably branched-chain fatty acids. This characteristic lipidome changes at late infection stages prior to egress by the increase in the concentrations of specific phospholipids species comprising shorter fatty acids, suggesting lipid modification either by the bacteria or by the host cell.

Based on these results, I speculate that CCS formation could be linked to the specific biology of the zoonotic pathogen *C. psittaci*. Future studies in more complex cell culture models are needed to shed light on the benefits of specific egress strategies exploited by distinct chlamydial pathogens.

5 References

Abdelrahman, Y., Ouellette, S. P., Belland, R. J., & Cox, J. V. (2016). Polarized Cell Division of *Chlamydia trachomatis*. *PLoS Pathogens*, *12*(8), e1005822. https://doi.org/10.1371/journal.ppat.1005822

Agaisse, H., & Derré, I. (2014). Expression of the effector protein IncD in *Chlamydia trachomatis* mediates recruitment of the lipid transfer protein CERT and the endoplasmic reticulum-resident protein VAPB to the inclusion membrane. *Infection and Immunity*, *82*(5), 2037–2047. https://doi.org/10.1128/IAI.01530-14

Agaisse, H., & Derré, I. (2015). STIM1 is a novel component of ER-*Chlamydia trachomatis* inclusion membrane contact sites. *PLoS ONE*, *10*(4), 1–18. https://doi.org/10.1371/journal.pone.0125671

Aoki, K., Satoi, S., Harada, S., Uchida, S., Iwasa, Y., & Ikenouchi, J. (2020). Coordinated changes in cell membrane and cytoplasm during maturation of apoptotic bleb. *Molecular Biology of the Cell*, *31*(8), 833–844. https://doi.org/10.1091/MBC.E19-12-0691

Aranjuez, G. F., Kim, J., & Jewett, T. J. (2022). The *Chlamydia trachomatis* Early Effector Tarp Outcompetes Fascin in Forming F-Actin Bundles *In Vivo*. *Frontiers in Cellular and Infection Microbiology*, *12*, 811407. https://doi.org/10.3389/fcimb.2022.811407

Bachmann, N. L., Polkinghorne, A., & Timms, P. (2014). *Chlamydia* genomics: providing novel insights into chlamydial biology. *Trends in Microbiology*, *22*(8), 464–472. https://doi.org/10.1016/j.tim.2014.04.013

Baer, K., Klotz, C., Kappe, S. H. I., Schnieder, T., & Frevert, U. (2007). Release of hepatic *Plasmodium yoelii* merozoites into the pulmonary microvasculature. *PLoS Pathogens*, *3*(11), e171. https://doi.org/10.1371/journal.ppat.0030171

Banhart, S., Saied, E. M., Martini, A., Koch, S., Aeberhard, L., Madela, K., Arenz, C., & Heuer, D. (2014). Improved plaque assay identifies a novel anti-*Chlamydia* ceramide derivative with altered intracellular localization. *Antimicrobial Agents and Chemotherapy*, *58*(9), 5537–5546. https://doi.org/10.1128/AAC.03457-14

Banhart, S., Schäfer, E. K., Gensch, J. M., & Heuer, D. (2019). Sphingolipid Metabolism and Transport in *Chlamydia trachomatis* and *Chlamydia psittaci* Infections. *Frontiers in Cell and Developmental Biology*, *7*(October), 1–8. https://doi.org/10.3389/fcell.2019.00223

Bayramova, F., Jacquier, N., & Greub, G. (2018). Insight in the biology of *Chlamydia*-related bacteria. *Microbes and Infection*, *20*(7), 432–440. https://doi.org/10.1016/j.micinf.2017.11.008

Beatty, W. L. (2006). Trafficking from CD63-positive late endocytic multivesicular bodies is essential for intracellular development of *Chlamydia trachomatis*. *Journal of Cell Science*, *119*(Pt 2), 350–359. https://doi.org/10.1242/jcs.02733

Beatty, W. L. (2008). Late endocytic multivesicular bodies intersect the chlamydial inclusion in the absence of CD63. *Infection and Immunity*, *76*(7), 2872–2881. https://doi.org/10.1128/IAI.00129-08

Bébéar, C., & de Barbeyrac, B. (2009). Genital *Chlamydia trachomatis* infections. *Clinical Microbiology and Infection*, *15*(1), 4–10. https://doi.org/10.1111/j.1469-0691.2008.02647.x

Becker, E., & Hegemann, J. H. (2014). All subtypes of the Pmp adhesin family are implicated in chlamydial virulence and show species-specific function. *MicrobiologyOpen*, *3*(4), 544–556. https://doi.org/10.1002/mbo3.186

Bedson, S. P., & Bland, J. O. W. (1932). A Morphological Study of Psittacosis Virus, with the Description of a Developmental Cycle. In *British journal of experimental pathology* (Vol. 13, Issue 5, pp. 461–466).

Bedson, S. P., & Bland, J. O. W. (1934). The Developmental Forms of Psittacosis Virus. In *British Journal of Experimental Pathology* (Vol. 15, Issue 4, pp. 243–247).

Binet, R., & Maurelli, A. T. (2007). Frequency of Development and Associated Physiological Cost of Azithromycin Resistance in *Chlamydia psittaci* 6BC and *C. trachomatis* L2. *Antimicrobial Agents and Chemotherapy*, *51*(12), 4267–4275. https://doi.org/10.1128/aac.00962-07

Bishop, R. C., & Derré, I. (2022). The *Chlamydia trachomatis* Inclusion Membrane Protein CTL0390 Mediates Host Cell Exit via Lysis through STING Activation. *Infection and Immunity*, *90*(6), e0019022. https://doi.org/10.1128/iai.00190-22

Bissig, C., & Gruenberg, J. (2013). Lipid sorting and multivesicular endosome biogenesis. *Cold Spring Harbor Perspectives in Biology*, *5*(10), a016816. https://doi.org/10.1101/cshperspect.a016816

Borel, N., Leonard, C., Slade, J., & Schoborg, R. V. (2016). Chlamydial Antibiotic Resistance and Treatment Failure in Veterinary and Human Medicine. *Current Clinical Microbiology Reports*, *3*(1), 10–18. https://doi.org/10.1007/s40588-016-0028-4

Borel, N., & Sachse, K. (2023). Zoonotic transmission of *Chlamydia* spp.: Known for 140 years, but still underestimated. *Zoonoses: Infections Affecting Humans and Animals*, 793–819. https://doi.org/10.1007/978-3-031-27164-9_53

Borth, N., Litsche, K., Franke, C., Sachse, K., Saluz, H. P., & Hänel, F. (2011). Functional interaction between type III-secreted protein IncA of *Chlamydophila psittaci* and human G3BP1. *PLoS ONE*, *6*(1). https://doi.org/10.1371/journal.pone.0016692

Braun, C., Alcázar-Román, A. R., Laska, A., Mölleken, K., Fleig, U., & Hegemann, J. H. (2019). CPn0572, the *C. pneumoniae* ortholog of TarP, reorganizes the actin cytoskeleton via a newly identified F-actin binding domain and recruitment of vinculin. *PLoS ONE*, *14*(1), e0210403. https://doi.org/10.1371/journal.pone.0210403

Breslow, D. K. (2013). Sphingolipid homeostasis in the endoplasmic reticulum and beyond. *Cold Spring Harbor Perspectives in Biology*, *5*(4), a013326. https://doi.org/10.1101/cshperspect.a013326

Breslow, D. K., & Weissman, J. S. (2010). Membranes in balance: mechanisms of sphingolipid homeostasis. *Molecular Cell*, *40*(2), 267–279. https://doi.org/10.1016/j.molcel.2010.10.005

Burda, P.-C., Caldelari, R., & Heussler, V. (2017). Manipulation of the Host Cell Membrane during *Plasmodium* Liver Stage Egress. *mBio*, *8*, e00139-17. https://doi.org/10.1128/mBio.00139-17

Castro, B. M., Prieto, M., & Silva, L. C. (2014). Ceramide: A simple sphingolipid with unique biophysical properties. *Progress in Lipid Research*, *54*, 53–67. https://doi.org/10.1016/j.plipres.2014.01.004

Chamberlain, N. B., Dimond, Z., & Hackstadt, T. (2022). *Chlamydia trachomatis* suppresses host cell store-operated Ca^{2+} entry and inhibits NFAT/calcineurin signaling. *Scientific Reports*, *12*(1), 1–11. https://doi.org/10.1038/s41598-022-25786-y

Chen, Y., Liu, Y., Sullards, M. C., & Merrill, A. H. (2010). An Introduction to Sphingolipid Metabolism and Analysis by New Technologies. *Neuromolecular Medicine*, *12*, 306–319. https://doi.org/10.1007/s12017-010-8132-8

Childs, T., Simms, I., Alexander, S., Eastick, K., Hughes, G., & Field, N. (2015). Rapid increase in lymphogranuloma venereum in men who have sex with men, United Kingdom, 2003 to September 2015. *Euro Surveillance : Bulletin Europeen Sur Les Maladies Transmissibles = European Communicable Disease Bulletin*, *20*(48), 30076. https://doi.org/10.2807/1560-7917.ES.2015.20.48.30076

Christian, J., Heymann, J., Paschen, S., Vier, J., Schauenburg, L., Rupp, J., Meyer, T.,

Häcker, G., & Heuer, D. (2011). Targeting of a Chlamydial Protease Impedes Intracellular Bacterial Growth. *PLoS Pathogens*, *7*, e1002283. https://doi.org/10.1371/journal.ppat.1002283

Chung, L. H., Liu, D., Liu, X. T., & Qi, Y. (2021). Ceramide Transfer Protein (CERT): An Overlooked Molecular Player in Cancer. *International Journal of Molecular Sciences*, *22*(24). https://doi.org/10.3390/ijms222413184

Clifton, D. R., Fields, K. A., Grieshaber, S. S., Dooley, C. A., Fischer, E. R., Mead, D. J., Carabeo, R. A., & Hackstadt, T. (2004). A chlamydial type III translocated protein is tyrosine-phosphorylated at the site of entry and associated with recruitment of actin. *Proceedings of the National Academy of Sciences of the United States of America*, *101*(27), 10166–10171. https://doi.org/10.1073/pnas.0402829101

Cortina, M. E., Clayton Bishop, R., DeVasure, B. A., Coppens, I., & Derre, I. (2022). The inclusion membrane protein IncS is critical for initiation of the *Chlamydia* intracellular developmental cycle. *PLoS Pathogens*, *18*(9), 1–20. https://doi.org/10.1371/journal.ppat.1010818

Cortina, M. E., & Derré, I. (2023). Homologues of the *Chlamydia trachomatis* and *Chlamydia muridarum* Inclusion Membrane Protein IncS Are Interchangeable for Early Development but Not for Inclusion Stability in the Late Developmental Cycle. *mSphere*, *8*(2). https://doi.org/10.1128/msphere.00003-23

D'Arcy, M. S. (2019). Cell death: a review of the major forms of apoptosis, necrosis and autophagy. *Cell Biology International*, *43*(6), 582–592. https://doi.org/10.1002/cbin.11137

Davis, J. M., & Ramakrishnan, L. (2009). The role of the granuloma in expansion and dissemination of early tuberculous infection. *Cell*, *136*(1), 37–49. https://doi.org/10.1016/j.cell.2008.11.014

De Leon-Rodriguez, C. M., Rossi, D. C. P., Fu, M. S., Dragotakes, Q., Coelho, C., Guerrero Ros, I., Caballero, B., Nolan, S. J., & Casadevall, A. (2018). The Outcome of the *Cryptococcus neoformans*-Macrophage Interaction Depends on Phagolysosomal Membrane Integrity. *Journal of Immunology (Baltimore, Md. : 1950)*, *201*(2), 583–603. https://doi.org/10.4049/jimmunol.1700958

de Vrieze, N. H. N., & de Vries, H. J. C. (2014). Lymphogranuloma venereum among men who have sex with men. An epidemiological and clinical review. *Expert Review of Anti-Infective Therapy*, *12*(6), 697–704. https://doi.org/10.1586/14787210.2014.901169

del Barrio Calvo, C., & Bindila, L. (2024). Integrated cellular 4D-TIMS lipidomics and transcriptomics for characterization of anti-inflammatory and anti-atherosclerotic phenotype of MyD88-KO macrophages. *Frontiers in Cell and Developmental Biology*, *12*(August), 1–19. https://doi.org/10.3389/fcell.2024.1450971

Dembek, Z. F., Mothershead, J. L., Owens, A. N., Chekol, T., & Wu, A. (2023). Psittacosis: An Underappreciated and Often Undiagnosed Disease. *Pathogens*, *12*(9). https://doi.org/10.3390/pathogens12091165

Deng, Y., Rivera-Molina, F. E., Toomre, D. K., & Burd, C. G. (2016). Sphingomyelin is sorted at the trans Golgi network into a distinct class of secretory vesicle. *Proceedings of the National Academy of Sciences of the United States of America*, *113*(24), 6677–6682. https://doi.org/10.1073/pnas.1602875113

Derré, I. (2015). *Chlamydiae* interaction with the endoplasmic reticulum: contact, function and consequences. *Cellular Microbiology*, *17*(7), 959–966. https://doi.org/10.1111/cmi.12455

Derré, I., Swiss, R., & Agaisse, H. (2011). The lipid transfer protein CERT interacts with the *Chlamydia* inclusion protein IncD and participates to ER-*Chlamydia* inclusion membrane contact sites. *PLoS Pathogens*, *7*(6), e1002092.

https://doi.org/10.1371/journal.ppat.1002092

Dimond, Z. E., Suchland, R. J., Baid, S., LaBrie, S. D., Soules, K. R., Stanley, J., Carrell, S., Kwong, F., Wang, Y., Rockey, D. D., Hybiske, K., & Hefty, P. S. (2021). Inter-species lateral gene transfer focused on the *Chlamydia* plasticity zone identifies loci associated with immediate cytotoxicity and inclusion stability. *Molecular Microbiology*, *116*(6), 1433–1448. https://doi.org/10.1111/mmi.14832

Doughri, A. M., Storz, J., & Altera, K. P. (1972). Mode of entry and release of *Chlamydiae* in infections of intestinal epithelial cells. *The Journal of Infectious Diseases*, *126*(6), 652–657. https://doi.org/10.1093/infdis/126.6.652

Elwell, C. A., & Engel, J. N. (2012). Lipid acquisition by intracellular *Chlamydiae*. *Cellular Microbiology*, *14*(7), 1010–1018. https://doi.org/10.1111/j.1462-5822.2012.01794.x

Elwell, C. A., Jiang, S., Kim, J. H., Lee, A., Wittmann, T., Hanada, K., Melancon, P., & Engel, J. N. (2011). *Chlamydia trachomatis* Co-opts GBF1 and CERT to Acquire Host Sphingomyelin for Distinct Roles during Intracellular Development. *PLoS Pathogens*, *7*(9), e1002198. https://doi.org/10.1371/journal.ppat.1002198

Elwell, C., Mirrashidi, K., & Engel, J. (2016). *Chlamydia* cell biology and pathogenesis. *Nature Reviews Microbiology*, *14*(6), 385–400. https://doi.org/10.1038/nrmicro.2016.30

Ende, R. J., Murray, R. L., D'Spain, S. K., Coppens, I., & Derré, I. (2022). Phosphoregulation accommodates Type III secretion and assembly of a tether of ER-*Chlamydia* inclusion membrane contact sites. *eLife*, *11*, e74535. https://doi.org/10.7554/eLife.74535

Everett, K. D. E., Bush, R. M., & Andersen, A. A. (1999). Emended description of the order *Chlamydiales*, proposal of *Parachlamydiaceae* fam. nov. and *Simkaniaceae* fam. nov., each containing one monotypic genus, revised taxonomy of the family *Chlamydiaceae*, including a new genus and five new species, and standards. *International Journal of Systematic and Evolutionary Microbiology*, *49*(2), 415–440. https://doi.org/10.1099/00207713-49-2-415

Fadel, S., & Eley, A. (2007). *Chlamydia trachomatis* OmcB protein is a surface-exposed glycosaminoglycan-dependent adhesin. *Journal of Medical Microbiology*, *56*(Pt 1), 15–22. https://doi.org/10.1099/jmm.0.46801-0

Fan, T., Lu, H., Hu, H., Shi, L., McClarty, G. A., Nance, D. M., Greenberg, A. H., & Zhong, G. (1998). Inhibition of apoptosis in *Chlamydia*-infected cells: blockade of mitochondrial cytochrome c release and caspase activation. *The Journal of Experimental Medicine*, *187*(4), 487–496. https://doi.org/10.1084/jem.187.4.487

Faris, R., Andersen, S. E., McCullough, A., Gourronc, F., Klingelhutz, A. J., & Weber, M. M. (2019). *Chlamydia trachomatis* Serovars Drive Differential Production of Proinflammatory Cytokines and Chemokines Depending on the Type of Cell Infected. *Frontiers in Cellular and Infection Microbiology*, *9*, 399. https://doi.org/10.3389/fcimb.2019.00399

Faris, R., McCullough, A., Andersen, S. E., Moninger, T. O., & Weber, M. M. (2020). The *Chlamydia trachomatis* secreted effector TmeA hijacks the N-WASP-ARP2/3 actin remodeling axis to facilitate cellular invasion. *PLoS Pathogens*, *16*(9), e1008878. https://doi.org/10.1371/journal.ppat.1008878

Favaroni, A., & Hegemann, J. H. (2021). *Chlamydia trachomatis* Polymorphic Membrane Proteins (Pmps) Form Functional Homomeric and Heteromeric Oligomers. *Frontiers in Microbiology*, *12*, 709724. https://doi.org/10.3389/fmicb.2021.709724

Flieger, A., Frischknecht, F., Häcker, G., Hornef, M. W., & Pradel, G. (2018). Pathways of host cell exit by intracellular pathogens. *Microbial Cell*, *5*(12), 525–544. https://doi.org/10.15698/mic2018.12.659

Frallicciardi, J., Melcr, J., Siginou, P., Marrink, S. J., & Poolman, B. (2022). Membrane

thickness, lipid phase and sterol type are determining factors in the permeability of membranes to small solutes. *Nature Communications*, *13*(1), 1605. https://doi.org/10.1038/s41467-022-29272-x

Friedrich, N., Hagedorn, M., Soldati-Favre, D., & Soldati, T. (2012). Prison Break: Pathogens' Strategies To Egress from Host Cells. *Microbiology and Molecular Biology Reviews*, *76*(4), 707–720. https://doi.org/10.1128/mmbr.00024-12

Frischknecht, F., & Pradel, G. (2024). Mechanisms of host cell exit by intracellular pathogens. *Molecular Microbiology*, *121*(3), 325–327. https://doi.org/10.1111/mmi.15239

Galle, J. N., Fechtner, T., Eierhoff, T., Römer, W., & Hegemann, J. H. (2019). A *Chlamydia pneumoniae* adhesin induces phosphatidylserine exposure on host cells. *Nature Communications*, *10*(1), 4644. https://doi.org/10.1038/s41467-019-12419-8

Gambarte Tudela, J., Buonfigli, J., Luján, A., Alonso Bivou, M., Cebrián, I., Capmany, A., & Damiani, M. T. (2019). Rab39a and Rab39b Display Different Intracellular Distribution and Function in Sphingolipids and Phospholipids Transport. *International Journal of Molecular Sciences*, *20*(7). https://doi.org/10.3390/ijms20071688

Gensch, J. M. (2022). Identification and characterisation of *Chlamydia psittaci* Inc proteins and mechanistic elucidation of doxycycline-induced persistence of *Chlamydia trachomatis*. Doctoral Thesis. http://dx.doi.org/10.17169/refubium-36199

Gibellini, D., Panaya, R., & Rumpianesi, F. (1998). Induction of apoptosis by *Chlamydia psittaci* and *Chlamydia trachomatis* infection in tissue culture cells. *Zentralblatt Für Bakteriologie*, *288*(1), 35–43. https://doi.org/10.1016/S0934-8840(98)80095-9

Goellner, S., Schubert, E., Liebler-Tenorio, E., Hotzel, H., Saluz, H. P., & Sachse, K. (2006). Transcriptional response patterns of *Chlamydophila psittaci* in different in vitro models of persistent infection. *Infection and Immunity*, *74*(8), 4801–4808. https://doi.org/10.1128/IAI.01487-05

Gudlur, A., Zeraik, A. E., Hirve, N., Rajanikanth, V., Bobkov, A. A., Ma, G., Zheng, S., Wang, Y., Zhou, Y., Komives, E. A., & Hogan, P. G. (2018). Calcium sensing by the STIM1 ER-luminal domain. *Nature Communications*, *9*(1), 4536. https://doi.org/10.1038/s41467-018-06816-8

Hackstadt, T., Rockey, D. D., Heinzen, R. A., & Scidmore, M. A. (1996). *Chlamydia trachomatis* interrupts an exocytic pathway to acquire endogenously synthesized sphingomyelin in transit from the Golgi apparatus to the plasma membrane. *EMBO Journal*, *15*(5), 964–977. https://doi.org/10.1002/j.1460-2075.1996.tb00433.x

Hackstadt, T., Scidmore, M. A., & Rockey, D. D. (1995). Lipid metabolism in *Chlamydia trachomatis*-infected cells: Directed trafficking of Golgi-derived sphingolipids to the chlamydial inclusion. *Proceedings of the National Academy of Sciences of the United States of America*, *92*(11), 4877–4881. https://doi.org/10.1073/pnas.92.11.4877

Hänsch, S., Spona, D., Murra, G., Köhrer, K., Subtil, A., Furtado, A. R., Lichtenthaler, S. F., Dislich, B., Mölleken, K., & Hegemann, J. H. (2020). *Chlamydia*-induced curvature of the host-cell plasma membrane is required for infection. *Proceedings of the National Academy of Sciences of the United States of America*, *117*(5), 2634–2644. https://doi.org/10.1073/pnas.1911528117

Hatch, G. M., & McClarty, G. (1998). Phospholipid Composition of Purified *Chlamydia trachomatis* Mimics That of the Eucaryotic Host Cell. *Infection and Immunity*, *66*(8), 3727–3735. https://doi.org/10.1128/iai.66.8.3727-3735.1998

Hay, A. (1999). Simulants, Stimulants and Diseases: The Evolution of the United States Biological Warfare Programme, 1945-60. *Medicine, Conflict and Survival*, *15*(3), 198–214. http://www.jstor.org/stable/45351958

He, M., Pei, Z., Mohsen, A.-W., Watkins, P., Murdoch, G., Van Veldhoven, P. P., Ensenauer, R., & Vockley, J. (2011). Identification and characterization of new long chain Acyl-CoA dehydrogenases. *Molecular Genetics and Metabolism*, *102*(4), 418–429. https://doi.org/10.1016/j.ymgme.2010.12.005

He, Z., Wang, C., Wang, J., Zheng, K., Ding, N., Yu, M., Li, W., Tang, Y., Li, Y., Xiao, J., Liang, M., & Wu, Y. (2022). *Chlamydia psittaci* inhibits apoptosis of human neutrophils by activating P2X7 receptor expression. *International Journal of Medical Microbiology*, *312*(8), 151571. https://doi.org/10.1016/j.ijmm.2022.151571

Hegemann, J. H., & Mölleken, K. (2012). Chlamydial Adhesion and Adhesins. In *Intracellular Pathogens I* (pp. 97–125). https://doi.org/10.1128/9781555817329.ch5

Heuer, D., Lipinski, A. R., Machuy, N., Karlas, A., Wehrens, A., Siedler, F., Brinkmann, V., & Meyer, T. F. (2009). *Chlamydia* causes fragmentation of the Golgi compartment to ensure reproduction. *Nature*, *457*(7230), 731–735. https://doi.org/10.1038/nature07578

Heymann, J., Lipinski, A., Bauer, B., Meyer, T., & Heuer, D. (2013). *Chlamydia trachomatis* infection prevents front-rear polarity of migrating HeLa cells. *Cellular Microbiology*, *15*. https://doi.org/10.1111/cmi.12114

Höhler, M., Alcázar-Román, A. R., Schenk, K., Aguirre-Huamani, M. P., Braun, C., Zrieq, R., Mölleken, K., Hegemann, J. H., & Fleig, U. (2024). Direct targeting of host microtubule and actin cytoskeletons by a chlamydial pathogenic effector protein. *Journal of Cell Science*, *137*(17). https://doi.org/10.1242/jcs.263450

Hu, V. H., Holland, M. J., & Burton, M. J. (2013). Trachoma: protective and pathogenic ocular immune responses to *Chlamydia trachomatis*. *PLoS Neglected Tropical Diseases*, *7*(2), e2020. https://doi.org/10.1371/journal.pntd.0002020

Hybiske, K., & Stephens, R. S. (2007). Mechanisms of host cell exit by the intracellular bacterium *Chlamydia*. *Proceedings of the National Academy of Sciences of the United States of America*, *104*(27), 11430–11435. https://doi.org/10.1073/pnas.0703218104

Hybiske, K., & Stephens, R. S. (2008). Exit strategies of intracellular pathogens. *Nature Reviews Microbiology*, *6*(2), 99–110. https://doi.org/10.1038/nrmicro1821

Hybiske, K., & Stephens, R. S. (2015). Cellular Exit Strategies of Intracellular Bacteria. *Microbiology Spectrum*, *3*(6), 3.6.11. https://doi.org/10.1128/microbiolspec.VMBF-0002-2014

Jewett, T. J., Fischer, E. R., Mead, D. J., & Hackstadt, T. (2006). Chlamydial TARP is a bacterial nucleator of actin. *Proceedings of the National Academy of Sciences of the United States of America*, *103*(42), 15599–15604. https://doi.org/10.1073/pnas.0603044103

Jewett, T. J., Miller, N. J., Dooley, C. A., & Hackstadt, T. (2010). The conserved Tarp actin binding domain is important for chlamydial invasion. *PLoS Pathogens*, *6*(7), e1000997. https://doi.org/10.1371/journal.ppat.1000997

Jury, B., Fleming, C., Huston, W. M., & Luu, L. D. W. (2023). Molecular pathogenesis of *Chlamydia trachomatis*. *Frontiers in Cellular and Infection Microbiology*, *13*(October), 1–12. https://doi.org/10.3389/fcimb.2023.1281823

Kawasaki, M., McConnel, C. S., Burbick, C. R., & Ambrosini, Y. M. (2024). Pathogen-epithelium interactions and inflammatory responses in *Salmonella Dublin* infections using ileal monolayer models derived from adult bovine organoids. *Scientific Reports*, *14*(1), 11479. https://doi.org/10.1038/s41598-024-62407-2

Kerr, M. C., Gomez, G. A., Ferguson, C., Tanzer, M. C., Murphy, J. M., Yap, A. S., Parton, R. G., Huston, W. M., & Teasdale, R. D. (2017). Laser-mediated rupture of chlamydial inclusions triggers pathogen egress and host cell necrosis. *Nature Communications*, *8*. https://doi.org/10.1038/ncomms14729

Kitatani, K., Idkowiak-Baldys, J., & Hannun, Y. A. (2008). The sphingolipid salvage pathway in ceramide metabolism and signaling. *Cellular Signalling*, *20*(6), 1010–1018. https://doi.org/10.1016/j.cellsig.2007.12.006

Knittler, M. R., Berndt, A., Böcker, S., Dutow, P., Hänel, F., Heuer, D., Kägebein, D., Klos, A., Koch, S., Liebler-Tenorio, E., Ostermann, C., Reinhold, P., Saluz, H. P., Schöfl, G., Sehnert, P., & Sachse, K. (2014). *Chlamydia psittaci*: New insights into genomic diversity, clinical pathology, host-pathogen interaction and anti-bacterial immunity. *International Journal of Medical Microbiology*, *304*(7), 877–893. https://doi.org/10.1016/j.ijmm.2014.06.010

Knittler, M. R., & Sachse, K. (2015). *Chlamydia psittaci*: Update on an underestimated zoonotic agent. *Pathogens and Disease*, *73*(1), 1–15. https://doi.org/10.1093/femspd/ftu007

Koch-Edelmann, S., Banhart, S., Saied, E. M., Rose, L., Aeberhard, L., Laue, M., Doellinger, J., Arenz, C., & Heuer, D. (2017). The cellular ceramide transport protein CERT promotes *Chlamydia psittaci* infection and controls bacterial sphingolipid uptake. *Cellular Microbiology*, *19*(10), 1–13. https://doi.org/10.1111/cmi.12752

Kocher, F., Applegate, V., Reiners, J., Port, A., Spona, D., Hänsch, S., Mirzaiebadizi, A., Ahmadian, M. R., Smits, S. H. J., Hegemann, J. H., & Mölleken, K. (2024). The *Chlamydia pneumoniae* effector SemD exploits its host's endocytic machinery by structural and functional mimicry. *Nature Communications*, *15*(1), 1–16. https://doi.org/10.1038/s41467-024-51681-3

Kordová, N., Wilt, J. C., & Sadiq, M. (1971). Lysosomes in L cells infected with *Chlamydia psittaci* 6BC strain. *Canadian Journal of Microbiology*, *17*(7), 955–959. https://doi.org/10.1139/m71-152

Kumagai, K., Elwell, C. A., Ando, S., Engel, J. N., & Hanada, K. (2018). Both the N- and C-terminal regions of the Chlamydial inclusion protein D (IncD) are required for interaction with the pleckstrin homology domain of the ceramide transport protein CERT. *Biochemical and Biophysical Research Communications*, *505*(4), 1070–1076. https://doi.org/10.1016/j.bbrc.2018.09.168

Kumagai, K., Sakai, S., Ueno, M., Kataoka, M., Kobayashi, S., & Hanada, K. (2022). Chlamydial Infection-Dependent Synthesis of Sphingomyelin as a Novel Anti-Chlamydial Target of Ceramide Mimetic Compounds. *International Journal of Molecular Sciences*, *23*(23). https://doi.org/10.3390/ijms232314697

Kumar, Y., & Valdivia, R. H. (2009). Leading a sheltered life: intracellular pathogens and maintenance of vacuolar compartments. *Cell Host & Microbe*, *5*(6), 593–601. https://doi.org/10.1016/j.chom.2009.05.014

Laemmli, U. K. (1970). Cleavage of structural proteins during the assembly of the head of bacteriophage T4. *Nature*, *227*(5259), 680–685. https://doi.org/10.1038/227680a0

Lee, J. K., Enciso, G. A., Boassa, D., Chander, C. N., Lou, T. H., Pairawan, S. S., Guo, M. C., Wan, F. Y. M., Ellisman, M. H., Sütterlin, C., & Tan, M. (2018). Replication-dependent size reduction precedes differentiation in *Chlamydia trachomatis*. *Nature Communications*, *9*(1), 45. https://doi.org/10.1038/s41467-017-02432-0

Lee, S.-H., Meng, X. W., Flatten, K. S., Loegering, D. A., & Kaufmann, S. H. (2013). Phosphatidylserine exposure during apoptosis reflects bidirectional trafficking between plasma membrane and cytoplasm. *Cell Death & Differentiation*, *20*(1), 64–76. https://doi.org/10.1038/cdd.2012.93

Leitenberg, M. (2001). Biological weapons in the twentieth century: a review and analysis. *Critical Reviews in Microbiology*, *27*(4), 267–320. https://doi.org/10.1080/20014091096774

Lerner, R., Baker, D., Schwitter, C., Neuhaus, S., Hauptmann, T., Post, J. M., Kramer, S., &

Bindila, L. (2023). Four-dimensional trapped ion mobility spectrometry lipidomics for high throughput clinical profiling of human blood samples. *Nature Communications*, *14*(1). https://doi.org/10.1038/s41467-023-36520-1

Lienard, J., Croxatto, A., Aeby, S., Jaton, K., Posfay-Barbe, K., Gervaix, A., & Greub, G. (2011). Development of a new *Chlamydiales*-specific real-time PCR and its application to respiratory clinical samples. *Journal of Clinical Microbiology*, *49*(7), 2637–2642. https://doi.org/10.1128/JCM.00114-11

Liu, S., Cui, Z., Carr, M. J., Meng, L., Shi, W., & Zhang, Z. (2023). *Chlamydia psittaci* should be a notifiable infectious disease everywhere. *The Lancet Microbe*, *4*(2), e62–e63. https://doi.org/10.1016/S2666-5247(22)00306-8

Luczak, S. E. T., Smits, S. H. J., Decker, C., Nagel-Steger, L., Schmitt, L., & Hegemann, J. H. (2016). The *Chlamydia pneumoniae* Adhesin Pmp21 Forms Oligomers with Adhesive Properties. *The Journal of Biological Chemistry*, *291*(43), 22806–22818. https://doi.org/10.1074/jbc.M116.728915

Lutter, E. I., Barger, A. C., Nair, V., & Hackstadt, T. (2013). *Chlamydia trachomatis* Inclusion Membrane Protein CT228 Recruits Elements of the Myosin Phosphatase Pathway to Regulate Release Mechanisms. *Cell Reports*, *3*(6), 1921–1931. https://doi.org/10.1016/j.celrep.2013.04.027

Makino, S., Jenkin, H. M., Yu, H. M., & Townsend, D. (1970). Lipid composition of *Chlamydia psittaci* grown in monkey kidney cells in defined medium. *Journal of Bacteriology*, *103*(1), 62–70. https://doi.org/10.1128/jb.103.1.62-70.1970

Mariño, G., & Kroemer, G. (2013). Mechanisms of apoptotic phosphatidylserine exposure. *Cell Research*, *23*(11), 1247–1248. https://doi.org/10.1038/cr.2013.115

Matsuo, J., Haga, S., Hashimoto, K., Okubo, T., Ozawa, T., Ozaki, M., & Yamaguchi, H. (2019). Activation of caspase-3 during *Chlamydia trachomatis*-induced apoptosis at a late stage. *Canadian Journal of Microbiology*, *65*(2), 135–143. https://doi.org/10.1139/cjm-2018-0408

Mattson, M. P., & Chan, S. L. (2003). Calcium orchestrates apoptosis. *Nature Cell Biology*, *5*(12), 1041–1043. https://doi.org/10.1038/ncb1203-1041

McElligott, K. A. (2014). Mortality from sexually transmitted diseases in reproductive-aged women: United States, 1999-2010. *American Journal of Public Health*, *104*(8), e101-5. https://doi.org/10.2105/AJPH.2014.302044

Mehlitz, A., & Rudel, T. (2013). Modulation of host signaling and cellular responses by *Chlamydia*. *Cell Communication and Signaling : CCS*, *11*, 90. https://doi.org/10.1186/1478-811X-11-90

Mölleken, K., Becker, E., & Hegemann, J. H. (2013). The *Chlamydia pneumoniae* invasin protein Pmp21 recruits the EGF receptor for host cell entry. *PLoS Pathogens*, *9*(4), e1003325. https://doi.org/10.1371/journal.ppat.1003325

Mölleken, K., & Hegemann, J. H. (2008). The *Chlamydia* outer membrane protein OmcB is required for adhesion and exhibits biovar-specific differences in glycosaminoglycan binding. *Molecular Microbiology*, *67*(2), 403–419. https://doi.org/10.1111/j.1365-2958.2007.06050.x

Moore, E. R., & Ouellette, S. P. (2014). Reconceptualizing the chlamydial inclusion as a pathogen-specified parasitic organelle: An expanded role for Inc proteins. *Frontiers in Cellular and Infection Microbiology*, *4*(OCT), 1–10. https://doi.org/10.3389/fcimb.2014.00157

Moulder, J. W. (1991). Interaction of *Chlamydiae* and host cells in vitro. *Microbiological Reviews*, *55*(1), 143–190. https://doi.org/10.1128/mr.55.1.143-190.1991

Murray, R., & Derré, I. (2018). Making Contact: VAP Targeting by Intracellular Pathogens.

Contact, 1. https://doi.org/10.1177/2515256418775512

Murray, R., Flora, E., Bayne, C., & Derré, I. (2017). IncV, a FFAT motif-containing *Chlamydia* protein, tethers the endoplasmic reticulum to the pathogen-containing vacuole. *Proceedings of the National Academy of Sciences of the United States of America*, *114*(45), 12039–12044. https://doi.org/10.1073/pnas.1709060114

Murray, S. M., & McKay, P. F. (2021). *Chlamydia trachomatis*: Cell biology, immunology and vaccination. *Vaccine*, *39*(22), 2965–2975. https://doi.org/10.1016/j.vaccine.2021.03.043

Nguyen, P. H., Lutter, E. I., & Hackstadt, T. (2018). *Chlamydia trachomatis* inclusion membrane protein MrcA interacts with the inositol 1,4,5-trisphosphate receptor type 3 (ITPR3) to regulate extrusion formation. *PLoS Pathogens*, *14*(3), 1–19. https://doi.org/10.1371/journal.ppat.1006911

Niekamp, P., Scharte, F., Sokoya, T., Vittadello, L., Kim, Y., Deng, Y., Südhoff, E., Hilderink, A., Imlau, M., Clarke, C. J., Hensel, M., Burd, C. G., & Holthuis, J. C. M. (2022). Ca^{2+}-activated sphingomyelin scrambling and turnover mediate ESCRT-independent lysosomal repair. *Nature Communications*, *13*(1). https://doi.org/10.1038/s41467-022-29481-4

Ojcius, D. M., Souque, P., Perfettini, J. L., & Dautry-Varsat, A. (1998). Apoptosis of epithelial cells and macrophages due to infection with the obligate intracellular pathogen *Chlamydia psittaci*. *The Journal of Immunology*, *161*(8), 4220–4226.

Perfettini, J. L., Reed, J. C., Israël, N., Martinou, J. C., Dautry-Varsat, A., & Ojcius, D. M. (2002). Role of Bcl-2 family members in caspase-independent apoptosis during *Chlamydia* infection. *Infection and Immunity*, *70*(1), 55–61. https://doi.org/10.1128/IAI.70.1.55-61.2002

Petit, T. J. P., & Lebreton, A. (2022). Adaptations of intracellular bacteria to vacuolar or cytosolic niches. *Trends in Microbiology*, *30*(8), 736–748. https://doi.org/10.1016/j.tim.2022.01.015

Pinton, P., Giorgi, C., Siviero, R., Zecchini, E., & Rizzuto, R. (2008). Calcium and apoptosis: ER-mitochondria Ca^{2+} transfer in the control of apoptosis. *Oncogene*, *27*(50), 6407–6418. https://doi.org/10.1038/onc.2008.308

Post, J. M., Lerner, R., Schwitter, C., Lutz, B., Lomazzo, E., & Bindila, L. (2022). Lipidomics and Transcriptomics in Neurological Diseases. *Journal of Visualized Experiments*, *2022*(181), 1–24. https://doi.org/10.3791/59423

Prado, L. G., Camara, N. O. S., & Barbosa, A. S. (2023). Cell lipid biology in infections: an overview. *Frontiers in Cellular and Infection Microbiology*, *13*, 1148383. https://doi.org/10.3389/fcimb.2023.1148383

Quinville, B. M., Deschenes, N. M., Ryckman, A. E., & Walia, J. S. (2021). A Comprehensive Review: Sphingolipid Metabolism and Implications of Disruption in Sphingolipid Homeostasis. In *International Journal of Molecular Sciences* (Vol. 22, Issue 11). https://doi.org/10.3390/ijms22115793

Radomski, N., Einenkel, R., Müller, A., & Knittler, M. R. (2016). *Chlamydia*-host cell interaction not only from a bird's eye view: some lessons from *Chlamydia psittaci*. *FEBS Letters*, *590*(21), 3920–3940. https://doi.org/10.1002/1873-3468.12295

Rejman Lipinski, A., Heymann, J., Meissner, C., Karlas, A., Brinkmann, V., Meyer, T. F., & Heuer, D. (2009). Rab6 and Rab11 Regulate *Chlamydia trachomatis* Development and Golgin-84-Dependent Golgi Fragmentation. *PLoS Pathogens*, *5*(10), e1000615. https://doi.org/10.1371/journal.ppat.1000615

Robert Koch-Institut. (2023). Umsetzung der neu eingeführten Meldepflichten nach § 7 Abs. 3 IfSG: Meldung von *Neisseria gonorrhoeae* und *Chlamydia trachomatis* (Serotypen L1-L3). *Epid Bull*, *5*, 10.

https://gpk.de/downloadp/STIKO_2023_Bulletin_KW_05_Rueckgang-von-bakteriellen-Enteritiden-im-Zuge-der-COVID-19-Pandemie.pdf

Rockey, D. D., Fischer, E. R., & Hackstadt, T. (1996). Temporal analysis of the developing *Chlamydia psittaci* inclusion by use of fluorescence and electron microscopy. *Infection and Immunity*, *64*(10), 4269–4278. https://doi.org/10.1128/iai.64.10.4269-4278.1996

Rockey, D. D., Grosenbach, D., Hruby, D. E., Peacock, M. G., Heinzen, R. A., & Hackstadt, T. (1997). *Chlamydia psittaci* IncA is phosphorylated by the host cell and is exposed on the cytoplasmic face of the developing inclusion. *Molecular Microbiology*, *24*(1), 217–228. https://doi.org/10.1046/j.1365-2958.1997.3371700.x

Rockey, D. D., Heinzen, R. A., & Hackstadt, T. (1995). Cloning and characterization of a *Chlamydia psittaci* gene coding for a protein localized in the inclusion membrane of infected cells. *Molecular Microbiology*, *15*(4), 617–626. https://doi.org/10.1111/j.1365-2958.1995.tb02371.x

Rogers, C., Fernandes-Alnemri, T., Mayes, L., Alnemri, D., Cingolani, G., & Alnemri, E. S. (2017). Cleavage of DFNA5 by caspase-3 during apoptosis mediates progression to secondary necrotic/pyroptotic cell death. *Nature Communications*, *8*, 14128. https://doi.org/10.1038/ncomms14128

Romero, M. D., & Carabeo, R. A. (2024). Dynamin-dependent entry of *Chlamydia trachomatis* is sequentially regulated by the effectors TarP and TmeA. *Nature Communications*, *15*(1), 4926. https://doi.org/10.1038/s41467-024-49350-6

Saied, E. M., Banhart, S., Bürkle, S. E., Heuer, D., & Arenz, C. (2015). A series of ceramide analogs modified at the 1-position with potent activity against the intracellular growth of *Chlamydia trachomatis*. *Future Medicinal Chemistry*, *7*(15), 1971–1980. https://doi.org/10.4155/fmc.15.126

Sasset, L., Zhang, Y., Dunn, T. M., & Di Lorenzo, A. (2016). Sphingolipid *de novo* Biosynthesis: A Rheostat of Cardiovascular Homeostasis. *Trends in Endocrinology and Metabolism: TEM*, *27*(11), 807–819. https://doi.org/10.1016/j.tem.2016.07.005

Scharte, F., Franzkoch, R., & Hensel, M. (2023). Flagella-mediated cytosolic motility of *Salmonella enterica* Paratyphi A aids in evasion of xenophagy but does not impact egress from host cells. *Molecular Microbiology*, *April*, 1–18. https://doi.org/10.1111/mmi.15104

Scholz, J., & Heuer, D. (2024). Entschlüsselung eines neuen Austrittswegs von Chlamydien. *BIOspektrum*, *30*(7), 737–740. https://doi.org/10.1007/s12268-024-2334-3

Scholz, J., Holland, G., Laue, M., Banhart, S., & Heuer, D. (2024a). Recruitment of the cellular lipid transport protein CERT to *C. psittaci* inclusions regulates the timing of bacterial egress. *BioRxiv*, 2024.11.26.625409. https://doi.org/10.1101/2024.11.26.625409

Scholz, J., Holland, G., Laue, M., Banhart, S., & Heuer, D. (2024b). *Chlamydia*-containing spheres are a novel and predominant form of egress by the pathogen *Chlamydia psittaci*. *mBio*, *15*(8), e01288-24. https://doi.org/10.1128/mbio.01288-24

Schulze-Luehrmann, J., Liebler-Tenorio, E., Felipe-López, A., & Lührmann, A. (2024). Cell death induction facilitates egress of *Coxiella burnetii* from infected host cells at late stages of infection. *Molecular Microbiology*, *121*(3), 513–528. https://doi.org/10.1111/mmi.15210

Scidmore, M. A. (2011). Recent advances in *Chlamydia* subversion of host cytoskeletal and membrane trafficking pathways. *Microbes and Infection*, *13*(6), 527–535. https://doi.org/10.1016/j.micinf.2011.02.001

Seth-Smith, H. M. B., Harris, S. R., Rance, R., West, A. P., Severin, J. A., Ossewaarde, J. M., Cutcliffe, L. T., Skilton, R. J., Marsh, P., Parkhill, J., Clarke, I. N., & Thomson, N. R.

(2011). Genome Sequence of the Zoonotic Pathogen *Chlamydophila psittaci*. *Journal of Bacteriology*, *193*(5), 1282–1283. https://doi.org/10.1128/jb.01435-10

Shears, M. J., Sekhar Nirujogi, R., Swearingen, K. E., Renuse, S., Mishra, S., Jaipal Reddy, P., Moritz, R. L., Pandey, A., & Sinnis, P. (2019). Proteomic Analysis of *Plasmodium* Merosomes: The Link between Liver and Blood Stages in Malaria. *Journal of Proteome Research*, *18*(9), 3404–3418. https://doi.org/10.1021/acs.jproteome.9b00324

Sherrid, A. M., & Hybiske, K. (2017). *Chlamydia trachomatis* cellular exit alters interactions with host dendritic cells. *Infection and Immunity*, *85*(5), 1–13. https://doi.org/10.1128/IAI.00046-17

Shima, K., Weber, M. M., Schnee, C., Sachse, K., Käding, N., Klinger, M., & Rupp, J. (2020). Development of a Plasmid Shuttle Vector System for Genetic Manipulation of *Chlamydia psittaci*. *mSphere*, *5*(4), 1–12. https://doi.org/10.1128/msphere.00787-20

Singer, R., Baier, M., Wilking, H., & Lachmann, R. (2024). Anstieg von Ornithose-Fallmeldungen in Deutschland. *Epidemiologisches Bulletin*, *10*, 16–18.

Sixt, B. S. (2021). Host cell death during infection with *Chlamydia*: A double-edged sword. *FEMS Microbiology Reviews*, *45*(1), 1–25. https://doi.org/10.1093/femsre/fuaa043

Sixt, B. S. (2022). Keeping the home intact—lessons from *Chlamydia*. *Cell Host & Microbe*, *30*(4), 475–479. https://doi.org/10.1016/j.chom.2022.03.012

Sixt, B. S., Bastidas, R. J., Finethy, R., Baxter, R. M., Carpenter, V. K., Kroemer, G., Coers, J., & Valdivia, R. H. (2017). The *Chlamydia trachomatis* Inclusion Membrane Protein CpoS Counteracts STING-Mediated Cellular Surveillance and Suicide Programs. *Cell Host and Microbe*, *21*(1), 113–121. https://doi.org/10.1016/j.chom.2016.12.002

Sixt, B. S., Núñez-Otero, C., Kepp, O., Valdivia, R. H., & Kroemer, G. (2019). *Chlamydia trachomatis* fails to protect its growth niche against pro-apoptotic insults. *Cell Death and Differentiation*, *26*(8), 1485–1500. https://doi.org/10.1038/s41418-018-0224-2

Soupene, E., & Kuypers, F. A. (2017). Phosphatidylserine decarboxylase CT699, lysophospholipid acyltransferase CT775, and acyl-ACP synthase CT776 provide membrane lipid diversity to *Chlamydia trachomatis*. *Scientific Reports*, *7*(1), 15767. https://doi.org/10.1038/s41598-017-16116-8

Spera, J. M., Guaimas, F., Czibener, C., & Ugalde, J. E. (2023). *Brucella* Egresses from Host Cells Exploiting Multivesicular Bodies. *mBio*, *14*(1). https://doi.org/10.1128/mbio.03338-22

Spona, D., Hanisch, P. T., Hegemann, J. H., & Mölleken, K. (2023). A single chlamydial protein reshapes the plasma membrane and serves as recruiting platform for central endocytic effector proteins. *Communications Biology*, *6*(1), 520. https://doi.org/10.1038/s42003-023-04913-z

Stelzner, K., Winkler, A. C., Liang, C., Boyny, A., Ade, C. P., Dandekar, T., Fraunholz, M. J., & Rudel, T. (2020). Intracellular *Staphylococcus aureus* perturbs the host cell Ca^{2+} homeostasis to promote cell death. *mBio*, *11*(6), 1–24. https://doi.org/10.1128/MBIO.02250-20

Stephens, R. S., Koshiyama, K., Lewis, E., & Kubo, A. (2001). Heparin-binding outer membrane protein of chlamydiae. *Molecular Microbiology*, *40*(3), 691–699. https://doi.org/10.1046/j.1365-2958.2001.02418.x

Stephens, R. S., Myers, G., Eppinger, M., & Bavoil, P. M. (2009). Divergence without difference: Phylogenetics and taxonomy of *Chlamydia* resolved. *FEMS Immunology and Medical Microbiology*, *55*(2), 115–119. https://doi.org/10.1111/j.1574-695X.2008.00516.x

Stiber, J., Hawkins, A., Zhang, Z.-S., Wang, S., Burch, J., Graham, V., Ward, C. C., Seth, M., Finch, E., Malouf, N., Williams, R. S., Eu, J. P., & Rosenberg, P. (2008). STIM1

signalling controls store-operated calcium entry required for development and contractile function in skeletal muscle. *Nature Cell Biology*, *10*(6), 688–697. https://doi.org/10.1038/ncb1731

Sturd, N., & Rucks, E. A. (2023). *Chlamydia trachomatis*. *Trends in Microbiology*, *31*(5), 535–536. https://doi.org/10.1016/j.tim.2022.11.002

Su, H., McClarty, G., Dong, F., Hatch, G. M., Pan, Z. K., & Zhong, G. (2004). Activation of Raf/MEK/ERK/cPLA2 Signaling Pathway Is Essential for Chlamydial Acquisition of Host Glycerophospholipids. *Journal of Biological Chemistry*, *279*(10), 9409–9416. https://doi.org/10.1074/jbc.M312008200

Subtil, A. (2011). Rerouting of Host Lipids by Bacteria: Are You CERTain You Need a Vesicle? *PLoS Pathogens*, *7*(9), e1002208. https://doi.org/10.1371/journal.ppat.1002208

Sukumaran, P., Da Conceicao, V. N., Sun, Y., Ahamad, N., Saraiva, L. R., Selvaraj, S., & Singh, B. B. (2021). Calcium signaling regulates autophagy and apoptosis. *Cells*, *10*(8), 1–20. https://doi.org/10.3390/cells10082125

Todd, W. J., & Storz, J. (1975). Ultrastructural cytochemical evidence for the activation of lysosomes in the cytocidal effect of *Chlamydia psittaci*. *Infection and Immunity*, *12*(3), 638–646. https://doi.org/10.1128/iai.12.3.638-646.1975

Traven, A., & Naderer, T. (2014). Microbial egress: a hitchhiker's guide to freedom. *PLoS Pathogens*, *10*(7), e1004201. https://doi.org/10.1371/journal.ppat.1004201

van Zandbergen, G., Klinger, M., Mueller, A., Dannenberg, S., Gebert, A., Solbach, W., & Laskay, T. (2004). Cutting edge: neutrophil granulocyte serves as a vector for *Leishmania* entry into macrophages. *Journal of Immunology (Baltimore, Md.: 1950)*, *173*(11), 6521–6525. https://doi.org/10.4049/jimmunol.173.11.6521

Vanrompay, D., Nguyen, T. L. A., Cutler, S. J., & Butaye, P. (2018). Antimicrobial Resistance in *Chlamydiales*, *Rickettsia*, *Coxiella*, and Other Intracellular Pathogens. *Microbiology Spectrum*, *6*(2). https://doi.org/10.1128/microbiolspec.arba-0003-2017

Waguia Kontchou, C., Gentle, I. E., Weber, A., Schoeniger, A., Edlich, F., & Häcker, G. (2022). *Chlamydia trachomatis* inhibits apoptosis in infected cells by targeting the pro-apoptotic proteins Bax and Bak. *Cell Death and Differentiation*, *29*(10), 2046–2059. https://doi.org/10.1038/s41418-022-00995-0

Wan, W., Li, D., Li, D., & Jiao, J. (2023). Advances in genetic manipulation of *Chlamydia trachomatis*. *Frontiers in Immunology*, *14*, 1209879. https://doi.org/10.3389/fimmu.2023.1209879

Wang, H., Naghavi, M., Allen, C., Barber, R. M., Bhutta, Z. A., Carter, A., Casey, D. C., Charlson, F. J., Chen, A. Z., Coates, M. M., Coggeshall, M., Dandona, L., Dicker, D. J., Erskine, H. E., Ferrari, A. J., Fitzmaurice, C., Foreman, K., Forouzanfar, M. H., Fraser, M. S., … Murray, C. J. L. (2016). Global, regional, and national life expectancy, all-cause mortality, and cause-specific mortality for 249 causes of death, 1980–2015: a systematic analysis for the Global Burden of Disease Study 2015. *The Lancet*, *388*(10053), 1459–1544. https://doi.org/10.1016/S0140-6736(16)31012-1

Weber, M. M., Lam, J. L., Dooley, C. A., Noriea, N. F., Hansen, B. T., Hoyt, F. H., Carmody, A. B., Sturdevant, G. L., & Hackstadt, T. (2017). Absence of Specific *Chlamydia trachomatis* Inclusion Membrane Proteins Triggers Premature Inclusion Membrane Lysis and Host Cell Death. *Cell Reports*, *19*(7), 1406–1417. https://doi.org/10.1016/j.celrep.2017.04.058

Weston, K. M., Polkinghorne, A., & Branley, J. M. (2023). Psittacosis contagion in 1930: an old story in a new era of zoonotic disease. *Microbes and Infection*, *25*(4), 105076. https://doi.org/10.1016/j.micinf.2022.105076

World Health Organization. (2016). *WHO Guidelines for the Treatment of Chlamydia trachomatis.* www.who.int/reproductivehealth/publications/rtis/chlamydia-treatment-guidelines/en/

World Health Organization. (2023). *Chlamydia*. Fact Sheets. https://www.who.int/news-room/fact-sheets/detail/chlamydia

World Health Organization. (2024). *Psittacosis – European region*. Disease Outbreak News (DONs). https://www.who.int/emergencies/%0Adisease-outbreak-news/item/2024-DON509

Wylie, J. L., Hatch, G. M., & McClarty, G. (1997). Host cell phospholipids are trafficked to and then modified by *Chlamydia trachomatis*. *Journal of Bacteriology*, *179*(23), 7233–7242. https://doi.org/10.1128/jb.179.23.7233-7242.1997

Yamaji, T., & Hanada, K. (2015). Sphingolipid metabolism and interorganellar transport: localization of sphingolipid enzymes and lipid transfer proteins. *Traffic (Copenhagen, Denmark)*, *16*(2), 101–122. https://doi.org/10.1111/tra.12239

Yao, J., Cherian, P. T., Frank, M. W., & Rock, C. O. (2015). *Chlamydia trachomatis* relies on autonomous phospholipid synthesis for membrane biogenesis. *Journal of Biological Chemistry*, *290*(31), 18874–18888. https://doi.org/10.1074/jbc.M115.657148

Yuan, Y., Lyng, K., Zhang, Y. X., Rockey, D. D., & Morrison, R. P. (1992). Monoclonal antibodies define genus-specific, species-specific, and cross-reactive epitopes of the chlamydial 60-kilodalton heat shock protein (hsp60): specific immunodetection and purification of chlamydial hsp60. *Infection and Immunity*, *60*(6), 2288–2296. https://doi.org/10.1128/iai.60.6.2288-2296.1992

Zhang, Y., Chen, X., Gueydan, C., & Han, J. (2018). Plasma membrane changes during programmed cell deaths. *Cell Research*, *28*(1), 9–21. https://doi.org/10.1038/cr.2017.133

Zhang, Z., Zhou, H., Cao, H., Ji, J., Zhang, R., Li, W., Guo, H., Chen, L., Ma, C., Cui, M., Wang, J., Chen, H., Ding, G., Yan, C., Dong, L., Holmes, E. C., Meng, L., Hou, P., & Shi, W. (2022). Human-to-human transmission of *Chlamydia psittaci* in China, 2020: an epidemiological and aetiological investigation. *The Lancet Microbe*, *3*(7), e512–e520. https://doi.org/10.1016/S2666-5247(22)00064-7

Zuck, M., Ellis, T., Venida, A., & Hybiske, K. (2017). Extrusions are phagocytosed and promote *Chlamydia* survival within macrophages. *Cellular Microbiology*, *19*(4), 1–12. https://doi.org/10.1111/cmi.12683

Zuck, M., Sherrid, A., Suchland, R., Ellis, T., & Hybiske, K. (2016). Conservation of extrusion as an exit mechanism for *Chlamydia*. *Pathogens and Disease*, *74*(7), 1–4. https://doi.org/10.1093/femspd/ftw093

6 Appendix

6.1 Supplementary Figures

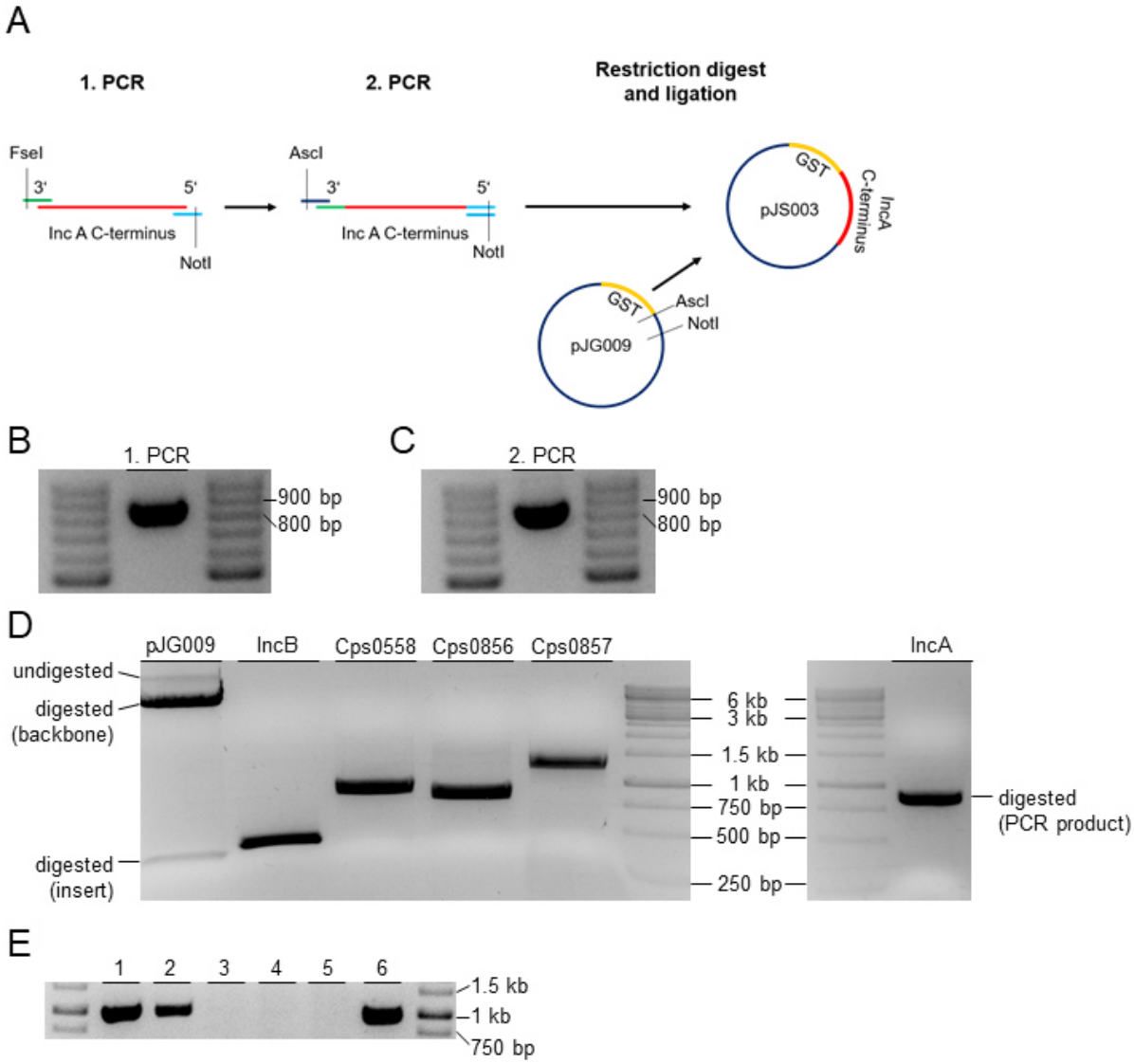

Supplemental Figure S1. Cloning of an IncA-GST expression vector. (A) Cloning strategy to generate an expression vector expressing the C-terminal cytoplasmic domain of *C. psittaci*-IncA fused to GST. With a first overlap PCR, a FseI (green) and a NotI (light blue) restriction site were attached on the 3' and 5' end of the coding sequence of the IncA C-terminal domain (red), respectively. With a second overlap PCR, an AscI (dark blue) restriction site was attached on the 3' end. Restriction enzyme digest of the PCR product and a GST expression vector (pJG009) and ligation of both to form a GST-IncA C-terminus expression vector (pJS003) were performed. **(B)** Agarose gel electrophorese of the PCR product of the first PCR. **(C)** Agarose gel electrophorese of the PCR product of the second PCR. **(D)** Restriction digest of pJG009 and the second PCR product with AscI and NotI. **(E)** PCR analysis of six transformants with pJS003. Sanger sequencing of plasmids of transformants 1, 2, and 6 revealed them containing the correct plasmid pJS003. *Cloning of the Cps0558-GST expression vector was performed following an analogical cloning strategy.*

A

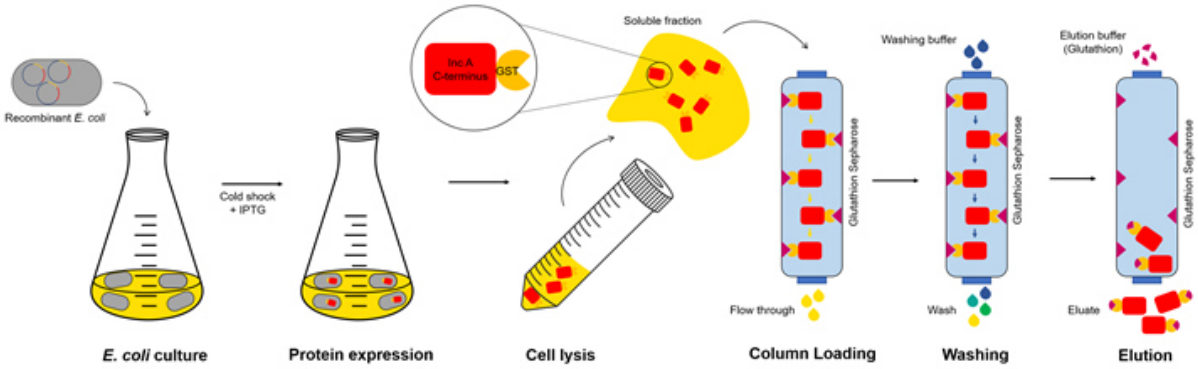

B

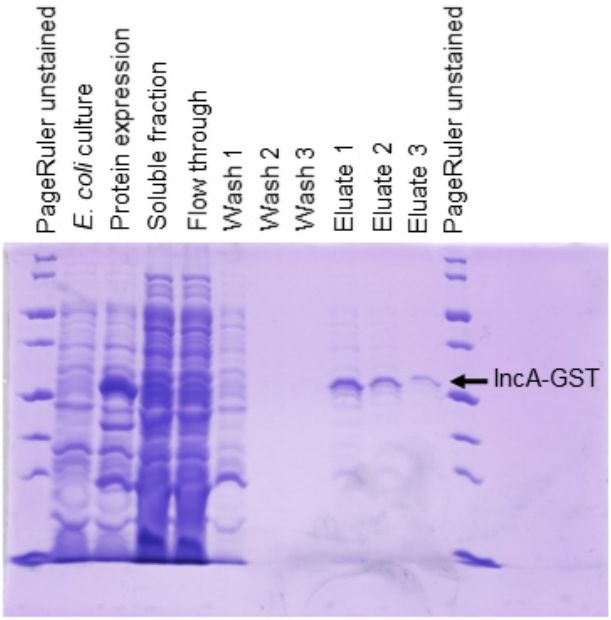

Supplemental Figure S2. Expression and purification of IncA-GST. (A) Schematic of the expression and purification procedure to obtain the purified C-terminal IncA-GST fusion protein. *E. coli* transformed with pJS003 were cultivated in liquid culture. Expression of the C-terminal IncA-GST fusion protein was induced by cold shock and addition of IPTG. After cultivation overnight, cells were lysed and a glutathione sepharose column was loaded with the soluble fraction. After column washing, the protein of interest was eluted using glutathione containing elution buffer. **(B)** Representative Coomassie stained SDS-PAGE gel showing the purification of the C-terminal cytosolic domain of IncA fused to GST. *Expression and purification of Cps0558-GST was performed following an analogical expression and purification procedure.*

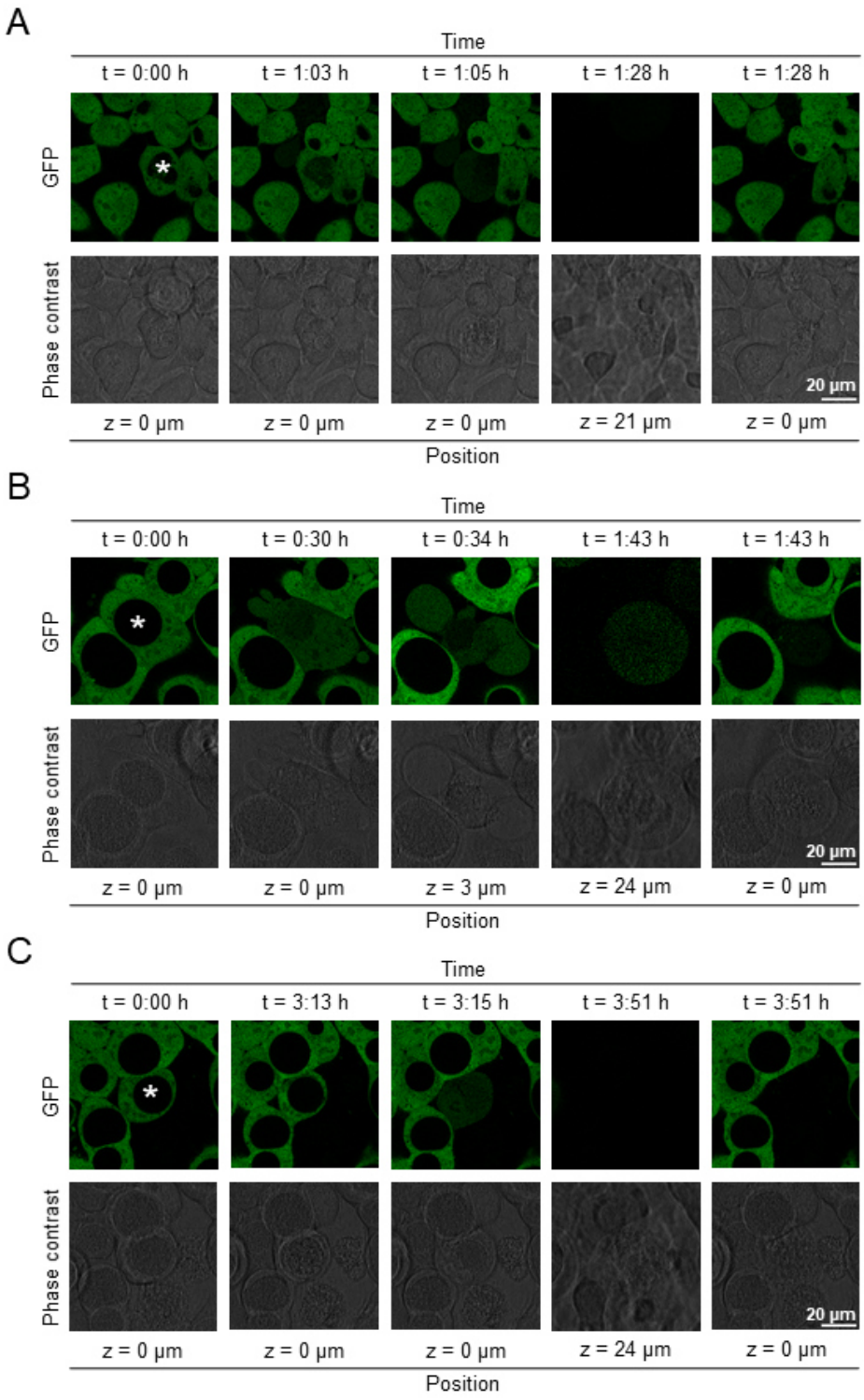

Supplemental Figure S3. Time course of *C. psittaci* host cell lysis (A), *C. trachomatis* L2 CCS formation (B) and *C. trachomatis* L2 host cell lysis (C). *C. psittaci*-infected **(A)** or *C. trachomatis* L2-infected **(B, C)** HeLa cells (MOI 2) stably expressing GFP were monitored from 42 h pi to 74.5 h pi using a CLSM equipped with a live-cell chamber. Panels show representative images of **(A)** a section plane of a *C. psittaci*-infected HeLa cell that undergoes host cell lysis, **(B)** a section plane of a *C. trachomatis* L2-infected CCS forming HeLa cell, or **(C)** a section plane of a *C. trachomatis* L2-infected HeLa cell that undergoes host cell lysis; n = 2. Asterisk indicates chlamydial inclusion. Modified from Scholz et al., 2024.

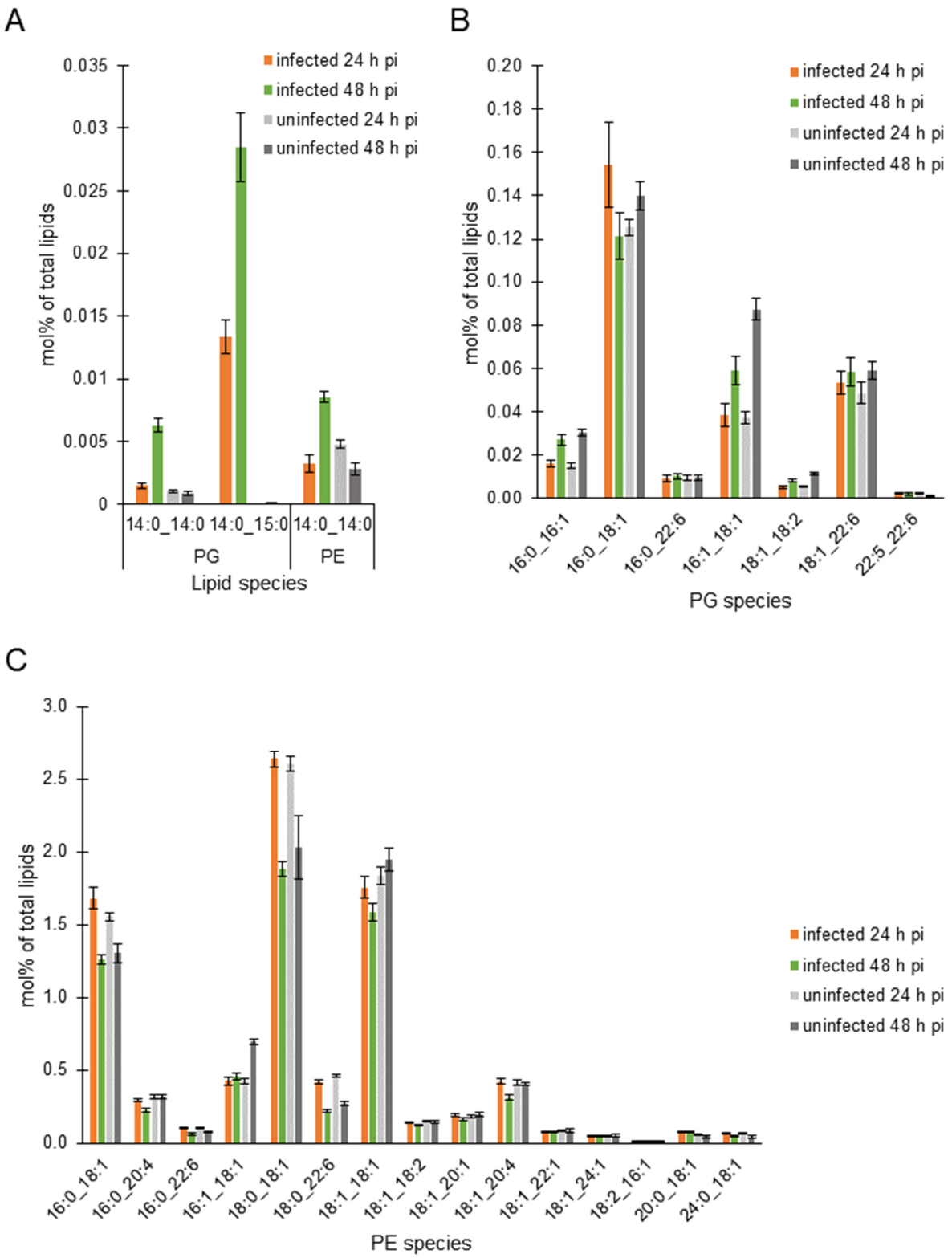

Supplemental Figure S4. Relative abundance of lipid species. (A) Magnification of the low abundant increasing lipid species shown in **Figure 34 B**. Data show mean ± SEM, n = 6. **(B, C)** Relative abundance of the phosphatidyl glycerol **(B)** and ethanolamine **(C)** species in HeLa cells during *C. psittaci* infection at 24 h pi or 48 h pi compared to uninfected cells that are not significantly changed during infection. Data show mean ± SEM; n = 6. *Lipidomics analysis was performed in the group of L. Bindila, Johannes Gutenberg-Universität, Mainz.*

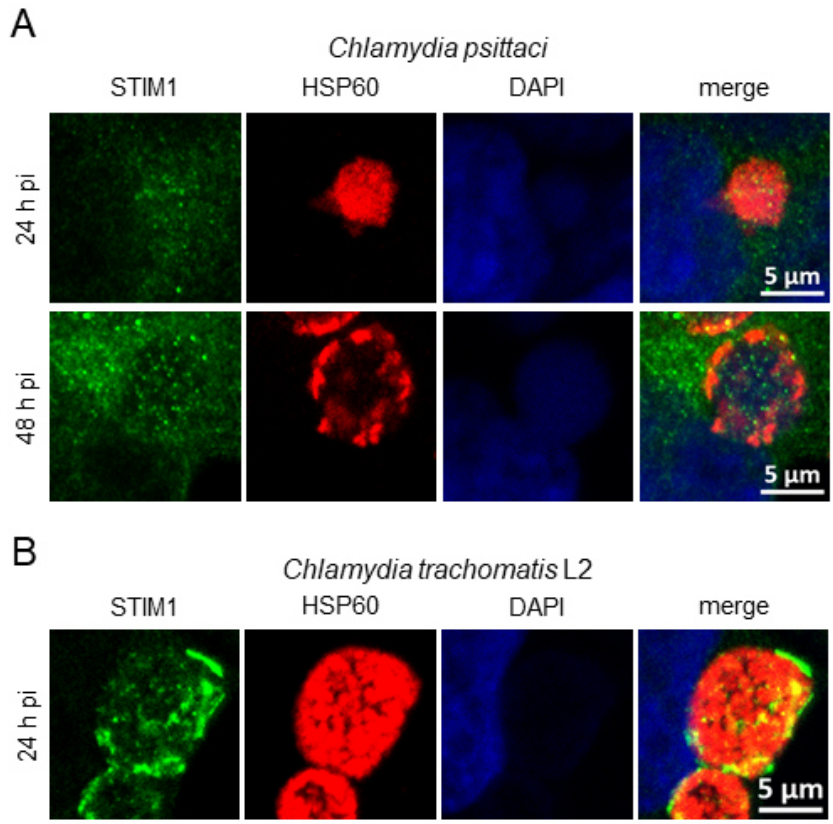

Supplemental Figure S5. In contrast to *C. trachomatis* L2, *C. psittaci* does not recruit STIM1 to the chlamydial inclusion. (A) Representative immunofluorescence images of *C. psittaci*-infected HeLa cells (MOI 2) at 24 h pi and 48 h pi. PFA-fixed cells were stained for *C. psittaci* and endogenous STIM1 using a mouse-anti-HSP60 (Cy3) and a rabbit-anti-STIM1 (AF488) antibody, respectively. DNA was counterstained using DAPI. n = 3. **(B)** Representative immunofluorescence images of *C. trachomatis* L2-infected HeLa cells (MOI 2) at 24 h pi. PFA-fixed cells were stained for *C. trachomatis* L2 and endogenous STIM1 using a mouse-anti-HSP60 (Cy3) and a rabbit-anti-STIM1 (AF488) antibody, respectively. DNA was counterstained using DAPI. n = 3. Modified from Scholz et al., 2024a.

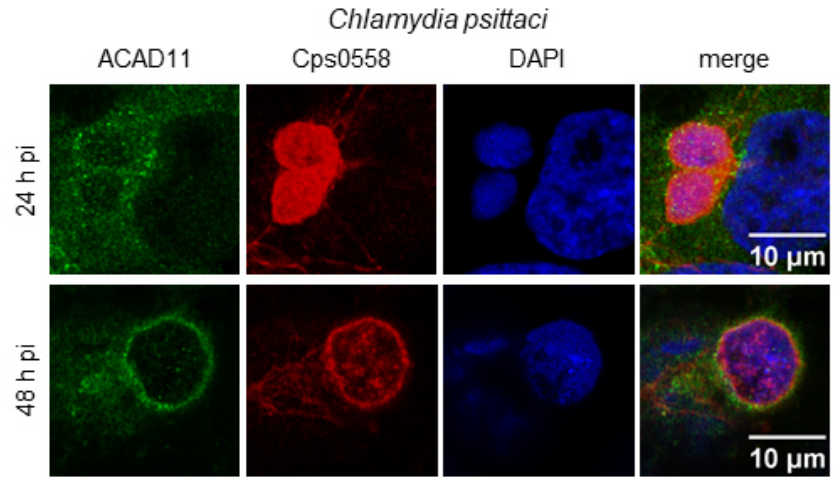

Supplemental Figure S6. ACAD11 is recruited to the *C. psittaci* inclusion at 48 h pi, but not at 24 h pi. Representative fluorescence images of *C. psittaci*-infected HeLa cells (MOI 2) at 24 h pi and 48 h pi. PFA-fixed cells were stained for Cps0558 and ACAD11 using a rabbit-anti-Cps0558 (Cy3) and a mouse-anti-ACAD11 (AF488) antibody, respectively. DNA was counterstained using DAPI. Scale bar, 10 µm; n = 2.

6.2 Supplementary Tables

Supplemental Table S1. **List of identified lipid species.**
Abbreviations: **PE**: phosphatidyl ethanolamine, **PC**: phosphatidyl choline, **PI**: phosphatidyl inositol, **PG**: phosphatidyl glycerol, **PS**: phosphatidyl serine, **SM**: sphingomyelin, **Cer**: ceramide, **DAG**: diacylglycerol, **TAG**: triacylglycerol, **O**: alkyl ether, **P**: alkenyl ether, **Hex**: hesosyl, **Lyso**: lysophospholipids.

Lipid species			Ø concentration (mol% of total lipids)			
Class	Fatty Acid	Modification	24 h pi		48 h pi	
			infected	uninfected	infected	uninfected
PE	14:0_14:0	-	0.0033	0.0048	0.0085	0.0028
PE	14:0_15:0	-	0.0421	0.0008	0.1220	0.0010
PE	15:0_16:0	-	0.7584	0.0047	1.2521	0.0075
PE	15:0_17:0	-	1.8330	0.0004	2.3653	0.0028
PE	15:0_19:0	-	0.2751	0.0064	0.5851	0.0044
PE	15:0_20:0	-	0.1591	0.0038	0.4198	0.0036
PE	15:0_21:0	-	0.2164	0.0237	0.3570	0.0126
PE	16:0_18:1	-	1.6804	1.5528	1.2587	1.3056
PE	16:0_20:4	-	0.2921	0.3120	0.2258	0.3121
PE	16:0_22:6	-	0.1022	0.0995	0.0613	0.0750
PE	16:1_18:1	-	0.4228	0.4263	0.4543	0.6924
PE	18:0_18:1	-	2.6352	2.6026	1.8804	2.0301
PE	18:0_22:6	-	0.4197	0.4606	0.2186	0.2679
PE	18:1_18:1	-	1.7550	1.8350	1.5850	1.9447
PE	18:1_18:2	-	0.1401	0.1490	0.1221	0.1431
PE	18:1_20:1	-	0.1866	0.1775	0.1600	0.1985
PE	18:1_20:4	-	0.4213	0.4088	0.3089	0.4007
PE	18:1_22:1	-	0.0819	0.0882	0.0776	0.0844
PE	18:1_24:1	-	0.0476	0.0479	0.0459	0.0500
PE	18:2_16:1	-	0.0106	0.0128	0.0108	0.0156
PE	20:0_18:1	-	0.0789	0.0614	0.0802	0.0428
PE	24:0_18:1	-	0.0673	0.0650	0.0510	0.0401
PE	32:2	O	0.1424	0.1540	0.1877	0.2538
PE	16:1_18:1	O	0.9777	1.0077	0.9828	1.1059
PE	16:1_20:4	O	0.9818	1.0682	0.8317	0.9160
PE	16:1_22:6	O	0.5571	0.5614	0.4224	0.4851
PE	17:1_20:4	O	0.0526	0.0524	0.0485	0.0416
PE	17:1_22:6	O	0.0272	0.0258	0.0328	0.0236
PE	18:1_16:0	O	0.0354	0.0431	0.0232	0.0211
PE	18:1_20:5	O	1.2773	1.3897	0.8372	0.8759
PE	18:1_22:4	O	0.0442	0.0447	0.0335	0.0303
PE	18:1_22:5	O	0.4485	0.4810	0.3166	0.3585
PE	18:2_18:1	O	0.4634	0.4777	0.5108	0.6130

Lipid species			Ø concentration (mol% of total lipids)			
Class	Fatty Acid	Modification	24 h pi		48 h pi	
			infected	uninfected	infected	uninfected
PE	18:2_20:4	O	0.7330	0.8543	0.6129	0.7208
PE	18:2_20:5	O	0.0841	0.0871	0.0798	0.1067
PE	18:2_22:6	O	0.1714	0.1775	0.1415	0.1790
PE	34:3	O	0.0794	0.0811	0.0886	0.1051
PE	36:4	O	0.1228	0.1335	0.1146	0.1572
PE	38:4	O	0.1673	0.1655	0.1204	0.1433
PE	39:6	O	0.0338	0.0314	0.0424	0.0282
PE	18:0_18:1	P	0.6192	0.6315	0.5664	0.4987
PE	18:0_20:4	P	0.6752	0.6907	0.5027	0.5767
PE	16:0	Lyso	0.0220	0.0200	0.0226	0.0183
PE	16:1	Lyso	0.0742	0.1190	0.0878	0.1622
PE	17:1	Lyso	0.0115	0.0190	0.0112	0.0193
PE	18:0	Lyso	0.0615	0.0667	0.0582	0.0575
PE	18:1	Lyso	0.4623	0.7205	0.4317	0.6502
PE	18:2	Lyso	0.0358	0.0597	0.0334	0.0584
PE	18:3	Lyso	0.0045	0.0064	0.0047	0.0057
PE	20:1	Lyso	0.0036	0.0041	0.0030	0.0036
PE	20:3	Lyso	0.0668	0.1241	0.0517	0.0908
PE	20:4	Lyso	0.4843	0.8079	0.3894	0.5703
PE	20:5	Lyso	0.1213	0.2241	0.0893	0.1605
PE	22:2	Lyso	0.0046	0.0085	0.0050	0.0106
PE	22:5	Lyso	0.2451	0.4568	0.1867	0.3304
PE	22:6	Lyso	0.3400	0.5565	0.2379	0.4053
PE	24:0	Lyso	0.0051	0.0047	0.0051	0.0049
PE	18:1	Lyso, O	0.0229	0.0221	0.0225	0.0246
PE	20:1	Lyso, O	0.0273	0.0288	0.0171	0.0222
PC	14:0_14:0	-	0.3327	0.3492	0.3515	0.3946
PC	14:0_15:0	-	0.0545	0.0692	0.0493	0.0758
PC	14:0_16:0	-	1.6031	1.6451	1.4905	1.5856
PC	16:0_16:0	-	1.8188	1.7739	1.6241	1.5268
PC	16:0_16:1	-	4.0465	4.3274	4.1175	4.8354
PC	16:0_17:0	-	0.2306	0.0941	0.4264	0.1183
PC	16:0_18:0	-	0.4955	0.4473	0.4745	0.2406
PC	16:0_18:1	-	10.4497	10.6539	9.8509	9.9116
PC	16:0_22:6	-	0.0899	0.1020	0.0714	0.0401
PC	16:1_16:1	-	0.5335	0.4152	0.9055	0.8551
PC	16:1_18:1	-	3.0238	3.4040	3.0657	4.5186

Lipid species			Ø concentration (mol% of total lipids)			
Class	Fatty Acid	Modification	24 h pi		48 h pi	
			infected	uninfected	infected	uninfected
PC	17:1_18:1	-	0.4711	0.4718	0.4284	0.5179
PC	18:0_18:1	-	2.1303	2.0491	2.3138	1.8974
PC	18:0_22:6	-	0.0418	0.0526	0.0263	0.0156
PC	18:1_18:1	-	6.8103	7.0426	6.9613	7.6402
PC	18:1_18:2	-	0.4808	0.5082	0.4018	0.5079
PC	18:1_19:1	-	0.1889	0.1917	0.1756	0.1798
PC	18:1_20:1	-	0.7186	0.7245	0.7776	0.9419
PC	18:1_20:2	-	0.1444	0.1206	0.1631	0.0949
PC	18:1_20:4	-	0.3068	0.3296	0.1549	0.1678
PC	18:1_22:1	-	0.0604	0.0592	0.0747	0.0718
PC	19:0_18:1	-	0.2636	0.0572	0.3973	0.0489
PC	14:0_14:0	O	0.0347	0.0361	0.0294	0.0420
PC	14:0_16:1	O	0.0312	0.0360	0.0322	0.0414
PC	16:0_14:0	O	1.0317	1.1743	0.9092	1.3772
PC	16:0_15:0	O	0.1228	0.1298	0.1432	0.1638
PC	16:0_16:0	O	2.3455	2.5594	2.0766	2.6427
PC	16:0_16:1	O	1.6488	1.8614	1.9085	2.8401
PC	16:0_17:0	O	0.1304	0.1180	0.2025	0.1746
PC	16:0_20:5	O	0.0832	0.0605	0.0345	0.0405
PC	16:0_22:6	O	0.0625	0.0708	0.0533	0.0422
PC	16:1_14:0	O	0.5389	0.5494	0.4361	0.3693
PC	16:1_16:0	O	0.5998	0.3391	0.3766	0.5530
PC	16:1_20:5	O	0.2763	0.2769	0.1546	0.1766
PC	16:1_22:6	O	0.0324	0.0615	0.0374	0.0441
PC	18:0_16:0	O	1.5800	1.6360	1.1146	1.2139
PC	18:0_18:1	O	1.2166	1.2988	1.1752	1.3871
PC	18:1_18:1	O	0.5343	0.3690	0.3405	0.4677
PC	18:0_20:4	O	0.1303	0.1423	0.0855	0.0821
PC	18:1_16:0	O	4.5480	4.8594	4.8475	5.7711
PC	18:1_16:1	O	0.3872	0.4631	0.5151	0.8048
PC	18:1_18:1	O	1.3699	1.3984	1.7162	2.3363
PC	18:1_22:6	O	4.5480	4.8594	4.8475	5.7711
PC	20:0_16:0	O	0.0703	0.0671	0.0551	0.0559
PC	18:0_20:4	P	0.1623	0.1633	0.1050	0.1100
PC	14:0	Lyso	0.0423	0.0664	0.0370	0.0575
PC	16:0	Lyso	0.0639	0.0796	0.0720	0.0734
PC	16:1	Lyso	0.0688	0.0822	0.0662	0.1087

Lipid species			Ø concentration (mol% of total lipids)			
Class	Fatty Acid	Modification	24 h pi		48 h pi	
			infected	uninfected	infected	uninfected
PC	18:1	Lyso	0.4018	0.4112	0.3073	0.4257
PC	16:0	Lyso, O	0.0318	0.0440	0.0394	0.0459
PI	16:0_16:1	-	0.0356	0.0569	0.0366	0.0332
PI	16:0_18:1	-	0.2613	0.3079	0.2655	0.1993
PI	16:0_20:4	-	0.0932	0.1197	0.0754	0.0639
PI	16:1_18:1	-	0.1627	0.2275	0.1367	0.1726
PI	16:1_18:2	-	0.0017	0.0023	0.0020	0.0023
PI	17:0_20:4	-	0.0177	0.0125	0.0261	0.0063
PI	18:0_18:1	-	0.4355	0.5711	0.3902	0.2984
PI	18:0_20:2	-	0.0776	0.0951	0.1135	0.0803
PI	18:0_20:3	-	0.1140	0.1503	0.0846	0.0819
PI	18:0_20:4	-	0.5887	0.7649	0.4349	0.3564
PI	18:1_18:1	-	0.8659	1.0270	0.9019	0.9513
PI	18:1_18:2	-	0.0563	0.0756	0.0678	0.0985
PI	18:1_20:5	-	0.0089	0.0116	0.0073	0.0077
PI	16:0	Lyso	0.0119	0.0122	0.0136	0.0135
PI	16:1	Lyso	0.0084	0.0051	0.0075	0.0058
PI	18:0	Lyso	0.1100	0.1126	0.1127	0.1196
PI	18:1	Lyso	0.0883	0.0804	0.0759	0.1036
PI	18:2	Lyso	0.0068	0.0032	0.0067	0.0080
PI	20:2	Lyso	0.0078	0.0073	0.0087	0.0135
PI	20:3	Lyso	0.0067	0.0062	0.0061	0.0049
PI	20:4	Lyso	0.0305	0.0317	0.0201	0.0262
PI	22:4	Lyso	0.0058	0.0048	0.0076	0.0051
PI	22:6	Lyso	0.0048	0.0055	0.0076	0.0065
PG	14:0_14:0	-	0.0015	0.0011	0.0063	0.0009
PG	14:0_15:0	-	0.0134	0.0000	0.0285	0.0001
PG	14:0_16:0	-	0.0024	0.0018	0.0033	0.0028
PG	14:0_22:6	-	0.0027	0.0021	0.0031	0.0024
PG	15:0_15:0	-	0.0418	0.0002	0.0629	0.0000
PG	15:0_16:0	-	0.3089	0.0004	0.3650	0.0005
PG	15:0_17:0	-	0.6670	0.0009	0.6747	0.0011
PG	15:0_18:0	-	0.1247	0.0002	0.2158	0.0000
PG	15:0_19:0	-	0.1182	0.0035	0.1662	0.0034
PG	15:0_20:0	-	0.0732	0.0000	0.1122	0.0000
PG	16:0_16:1	-	0.0161	0.0153	0.0272	0.0305
PG	16:0_18:1	-	0.1543	0.1253	0.1213	0.1400

Lipid species			Ø concentration (mol% of total lipids)			
Class	Fatty Acid	Modification	24 h pi		48 h pi	
			infected	uninfected	infected	uninfected
PG	16:0_22:6	-	0.0092	0.0096	0.0103	0.0099
PG	16:1_18:1	-	0.0385	0.0373	0.0591	0.0873
PG	18:1_18:2	-	0.0055	0.0054	0.0083	0.0115
PG	18:1_22:6	-	0.0536	0.0486	0.0587	0.0590
PG	22:5_22:6	-	0.0026	0.0023	0.0022	0.0014
PG	16:0	Lyso	0.0027	0.0019	0.0029	0.0015
PG	18:0	Lyso	0.0022	0.0017	0.0031	0.0016
PG	18:1	Lyso	0.0037	0.0040	0.0046	0.0058
PS	15:0_16:0	-	0.0572	0.0116	0.0688	0.0125
PS	16:0_16:1	-	0.0627	0.0649	0.0557	0.0526
PS	16:0_18:1	-	0.4667	0.4164	0.4218	0.3276
PS	16:0_18:2	-	0.0630	0.0639	0.0753	0.0911
PS	18:0_18:1	-	1.1271	1.3031	1.0738	0.5937
PS	18:0_20:4	-	0.0282	0.0287	0.0254	0.0141
PS	18:0_22:5	-	0.0470	0.0641	0.0227	0.0167
PS	18:1_18:1	-	0.2557	0.2762	0.3121	0.2950
PS	18:1_22:1	-	0.1234	0.1059	0.1292	0.0746
PS	18:1_24:1	-	0.0277	0.0260	0.0293	0.0205
PS	16:0_16:1	O	0.0102	0.0113	0.0186	0.0142
PS	16:0_18:1	O	0.0703	0.0471	0.1083	0.0402
PS	18:0_18:1	O	0.0755	0.0906	0.0755	0.0629
PS	18:1_18:1	O	0.0130	0.0163	0.0159	0.0182
PS	16:0	Lyso	0.0077	0.0073	0.0067	0.0057
PS	16:1	Lyso	0.0111	0.0073	0.0111	0.0116
PS	18:0	Lyso	0.6700	0.3312	0.5472	0.3526
PS	18:1	Lyso	0.0823	0.0635	0.0612	0.0719
PS	19:1	Lyso	0.0088	0.0053	0.0059	0.0037
PS	22:6	Lyso	0.0084	0.0058	0.0072	0.0057
SM	d31:0	-	0.0156	0.0095	0.0403	0.0263
SM	d32:1	-	0.2101	0.2071	0.2252	0.2804
SM	d32:2	-	0.0101	0.0119	0.0134	0.0181
SM	d33:1	-	0.0742	0.0776	0.0806	0.0835
SM	d34:0	-	0.1552	0.1086	0.3232	0.2233
SM	d34:1	-	1.5393	1.4934	1.4941	1.7048
SM	d34:2	-	0.1621	0.1832	0.1731	0.2161
SM	d39:1	-	0.0097	0.0125	0.0123	0.0084
SM	d40:1	-	0.2692	0.2452	0.2397	0.1806

Lipid species			Ø concentration (mol% of total lipids)			
Class	Fatty Acid	Modification	24 h pi		48 h pi	
			infected	uninfected	infected	uninfected
SM	d40:2	-	0.0625	0.0585	0.0605	0.0683
SM	d41:1	-	0.0676	0.0609	0.0538	0.0473
SM	d42:1	-	0.5654	0.4577	0.4923	0.3591
SM	d42:2	-	0.9611	0.8706	0.8268	0.9403
SM	d42:3	-	0.1487	0.1610	0.1393	0.1735
SM	d44:2	-	0.0380	0.0280	0.0355	0.0349
Cer	d18:1/16:0	-	0.0305	0.0370	0.0523	0.0538
Cer	d18:1_22:0	-	0.0133	0.0145	0.0243	0.0171
Cer	d18:1/23:0	-	0.0051	0.0072	0.0120	0.0126
Cer	d18:1_24:0	-	0.0630	0.0775	0.0619	0.0611
Cer	d18:1_24:1	-	0.1086	0.1218	0.1320	0.1831
Cer	d18:1/26:0	-	0.0630	0.0775	0.0619	0.0611
Cer	d18:2/16:0	-	0.0046	0.0063	0.0062	0.0083
Cer	d18:2/24:1	-	0.0253	0.0433	0.0355	0.0684
Cer	d34:0	-	0.0122	0.0083	0.0236	0.0139
Cer	d34:1	Hex	0.0462	0.0513	0.0377	0.0569
Cer	d42:1	Hex	0.1595	0.1850	0.0772	0.0789
Cer	d42:0	Hex	0.0043	0.0045	0.0038	0.0054
Cer	d42:2	Hex	0.1381	0.1336	0.0758	0.0997
Cer	d42:0	Hex	0.0043	0.0045	0.0038	0.0054
Cer	d42:2	Hex	0.1381	0.1336	0.0758	0.0997
Cholesterol			4.4309	4.9473	5.4115	4.4433
DAG	32:0	-	0.6186	0.4222	0.3616	0.4116
DAG	32:1	-	0.4929	0.7642	0.7743	0.5925
DAG	34:0	-	0.6417	0.2582	0.1283	0.2714
DAG	34:1	-	1.0272	1.3992	1.8642	1.1074
DAG	34:2	-	0.1116	0.1817	0.1881	0.1350
DAG	35:1	-	0.0261	0.0254	0.0318	0.0424
DAG	35:2	-	0.0494	0.0632	0.0738	0.0409
DAG	36:1	-	0.3561	0.3966	0.5133	0.3333
DAG	36:2	-	0.7886	1.0966	1.4790	0.7898
DAG	36:3	-	0.0656	0.0743	0.0750	0.0505
DAG	37:2	-	0.0258	0.0293	0.0356	0.0221
DAG	38:3	-	0.0285	0.0359	0.0396	0.0199
DAG	40:4	-	0.0222	0.0261	0.0264	0.0152
DAG	40:5	-	0.0380	0.0375	0.0341	0.0230
DAG	42:2	-	0.0124	0.0189	0.0199	0.0151

Lipid species			Ø concentration (mol% of total lipids)			
Class	Fatty Acid	Modification	24 h pi		48 h pi	
			infected	uninfected	infected	uninfected
DAG	30:0	O	0.0971	0.1149	0.0904	0.0918
DAG	34:0	O	0.3698	0.2929	0.2073	0.3095
TAG	24:0	-	0.0194	0.0190	0.0133	0.0139
TAG	26:0	-	0.0556	0.0620	0.0485	0.0486
TAG	38:0	-	0.0159	0.0283	0.0128	0.0133
TAG	40:0	-	0.0384	0.0622	0.0362	0.0371

6.3 List of abbreviations

ABB	Annexin Binding Buffer
ACAD11	Acyl-CoA Dehydrogenase Family Member 11
APS	Ammonium Persulfate
BHT	Butyl hydroxy toluene
BSA	Bovine Serum Albumin Fraction V
CCS	*Chlamydia*-containing spheres
Cer	Ceramides
CERT	Ceramide transport protein
CLSM	Confocal Laser scanning microscopy
CoA	Coenzyme A
DAG	Diacylglycerols
DAPI	4′,6-Diamidino-2-Phenylindole
DDSA	Dodecenyl succinic anhydride
DEVD	Peptide sequence Aspartate-Glutamate-Valine-Aspartate
DMEM	Dulbeccos Modified Eagle Medium
DMP-30	2,4,6-Tris(dimethylaminomethyl)phenol
DMSO	Dimethyl sulfoxide
DNA	Deoxyribonucleic acid
EBs	Elementary bodies
EDTA	Ethylenediaminetetraacetic acid
eGFP	enhanced GFP
EK	Elementarkörperchen
ELISA	Enzyme linked immunosorbent assay
EqtSM	Non-toxic variant of equinatoxin II
EqtSM-HaloTag	Halo-tagged variant of EqtSM
ER	Endoplasmic reticulum
FBS	Fetal bovine serum
FFAT	Two phenylalanines (FF) in an acidic tract
GCN	Genome copy number
GFP	Green fluorescent protein
GST	Glutathione *S*-transferase
h pi	Hours post infection
HEPES	4-(2-hydroxyethyl)-1-piperazineethanesulfonic acid
HIV	Human immunodeficiency virus
HPLC	High-performance liquid chromatography
IBs	Intermediate bodies
IFU	Infection forming units
Inc-protein	Inclusion membrane protein
IPTG	Isopropyl β-D-1-thiogalactopyranoside
IQR	Interquartile range
ISTDs	Deuterated internal standards
KO	Knock out
LB	Lysogeny broth
LC	Liquid chromatography
LLE	Liquid-liquid extraction
MCS	Membrane contact sides
MNA	Methylnadic anhydride

MOI	Multiplicity of infection
MS/MS	Tandem mass spectrometry
MTBE	Methyl tert-butyl ether
MUFAs	Monounsaturated fatty acids
MVBs	Multivesicular bodies
N-WASP	Neural Wiskott-Aldrich syndrome protein
O ether	Alkyl ether
OD600	Optical density at 600 nm
P ether	Alkenyl ether
PBS	Phosphate-Buffered Saline
PC	Phosphatidyl choline
PCA	Principle component analysis
PCR	Polymerase chain reaction
PE	Phosphatidyl ethanolamine
PFA	Paraformaldehyde
PG	Phosphatidyl glycerol
PH domain	Pleckstrin homology domain
PI	Phosphatidyl inositol
PI4P	Phosphatidyl inositol-4-phosphate
PMP	Phagolysosomal membrane permeabilization
PS	Phosphatidyl serine
PUFAs	Polyunsaturated fatty acids
PVDF	Polyvinylidene difluoride
qPCR	Quantitative Real-Time PCR
RBs	Reticulate bodies
rDNA	Ribosomal DNA
RK	Retikularkörperchen
RP	Reversed-phase
rpm	Rounds per minute
RPMI	Roswell Park Memorial Institute
RT	Room temperature
SDS	Sodium Dodecyl Sulfate
SDS-PAGE	Sodium Dodecyl Sulfate – PolyAcrylamid Gel Electrophoresis
SEM	Standard error of the mean
SM	Sphingomyelin
SOB	Super optimal broth
SPT	Serine palmitoyl transferase
START domain	Steroidogenic acute regulatory protein-related lipid-transfer domain
STIM1	Stromal Interaction Molecule 1
TAG	Triacylglycerols
TarP	Translocated actin recruiting protein
TEM	Transmission electron microscopy
TEMED	Tetramethyl-ethylenediamine
TIMS-qToF	Trapped Ion Mobility Spectrometry-quadrupole Time-of-Flight
TmeA	Translocated membrane effector A
UHPLC	Ultra-HPLC
VAP proteins	Vesicle-associated membrane protein-associated proteins
WHO	World Health Organization

6.4 List of Figures

Figure 1. The developmental cycle of *Chlamydia* spp. 5
Figure 2. Different concepts to categorize lytic and non-lytic egress strategies of different intracellular pathogens. 8
Figure 3. Structure of sphingolipids. 11
Figure 4: *De novo* synthesis of sphingolipids. 12
Figure 5. Functional domains of the ceramide transport protein CERT. 14
Figure 6. Schematic of ER-inclusion MCS of *C. trachomatis* 16
Figure 7. Time course of replication and progeny formation of *C. psittaci* during the infection of HeLa cells. 43
Figure 8. Time course of *C. psittaci* differentiation stages during the time course of infection of HeLa cells. 45
Figure 9. HSP60- and IncA-immunofluorescent staining is characteristic for the different phases of intracellular development of *C. psittaci*. 47
Figure 10. CCS formation represents the predominate *C. psittaci* egress pathway and is characterized by membrane blebbing and destabilization of the inclusion membrane. 50
Figure 11. Extrusion formation of *C. trachomatis* is characterized by a stabilized inclusion membrane, surviving of the host cell and dependency on the host cell cytoskeleton. 52
Figure 12. CCS are distinct from infected adherent cells, apoptotic cells and extrusions on an ultrastructural level. 54
Figure 13. CCS are formed in *C. psittaci*-infected A549 cells. 56
Figure 14. CCS formation is the predominant egress pathway of *C. psittaci* and is also present, but less frequent for *C. trachomatis*. 58
Figure 15. Distribution of egress pathways of *C. trachomatis* L2. 60
Figure 16. During CCS formation, sphingolipids in the *C. psittaci* inclusion membrane are reorganized, followed by its destabilization and CCS formation. 61
Figure 17. CCS show a similar AnnexinV staining pattern compared to apoptotic cells. 63
Figure 18. In contrast to apoptotic cells, CCS retain their membrane integrity. 64
Figure 19. In CCS, the nucleus and the mitochondria are not condensed in contrast to apoptotic cells 65
Figure 20. CCS formation is independent of caspase-3 activation, while a DEVD-containing substrate is proteolytically cleaved during CCS formation. 67
Figure 21. The caspase-3 inhibitor Z-DEVD-FMK blocks neither CCS formation nor the proteolytic cleavage of the DEVD-containing substrate. 69
Figure 22. Variations in the extracellular calcium concentration affect CCS formation. 71
Figure 23. Intracellular calcium increase in late infections and proteolytic DEVD-cleavage are depending on extracellular calcium 73
Figure 24. The cytosolic calcium concentration and the DEVD-cleaving activity increase before CCS formation. 75
Figure 25. In late infections, CERT recruitment to *C. psittaci* inclusions is reduced and CERT-KO induce early egress of *C. psittaci* by CCS formation at 24 h pi 78
Figure 26. In contrast to full CERT and CERT variants lacking the START- or FFAT-domain, a CERT variant lacking the PH domain is not recruited to *C. psittaci* inclusions and cannot prevent premature CCS formation. 80
Figure 27. CERT-KO induced early CCS are formed by an analogous sequence of events as mature CCS. 82
Figure 28. Early CCS formation is calcium-dependent 84
Figure 29. Premature, CERT-KO induced CCS contain mainly non-infectious reticulate bodies. 85
Figure 30. Schematic overview of the study design to characterize the lipidome of *C. psittaci* during RB replication and during egress. 87

Figure 31. *C. psittaci*-infected HeLa cells during RB replication and during egress harbor a distinct lipidome. 88
Figure 32. Analysis of the lipid species that differ between *C. psittaci*-infected and uninfected cells at 24 h pi and 48 h pi. 90
Figure 33. Analysis of the lipid species that differ in *C. psittaci*-infected cells between 24 h pi and 48 h pi. 92
Figure 34. Comparison of lipid species that are significantly increased or decreased during *C. psittaci* infection at 24 h pi or 48 h pi compared to uninfected cells or between both timepoints. 94
Figure 35. CCS formation of *C. psittaci* 97
Figure 36. Extrusion formation of *C. trachomatis*. 98
Figure 37. Comparison of the three chlamydial egress pathways: Lytic egress, CCS formation, and extrusion formation. 100
Figure 38. Graphical model of the role of CERT for regulating *C. psittaci* CCS formation. ..107

6.5 List of Tables

Table 1: Overview of *Chlamydia*-species 1
Table 2. Eukaryotic Cell Lines 18
Table 3. Bacteria 18
Table 4. Primer used for Cloning 18
Table 5. Primer used for qPCR 19
Table 6. Sequencing primer 19
Table 7. Plasmids 19
Table 8. Cell culture media 20
Table 9. Media for *E. coli* cultivation 21
Table 10. Buffers and Solutions 21
Table 11. Primary Antibodies 22
Table 12. Secondary Antibodies 23
Table 13. Chemicals 23
Table 14. Kits and Enzymes 25
Table 15. Consumables 26
Table 16. Equipment 28
Table 17. Software 28
Table 18. Standard reaction mixture for PCR 37
Table 19. Standard cycling protocol for PCR 37
Table 20. Standard reaction mixture for Colony PCR 38
Table 21. Standard cycling protocol for Colony PCR 38

Publications

Articles

In vitro maturation of *Toxoplasma gondii* bradyzoites in human myotubes and their metabolomic characterization

Céline Christiansen, Deborah Maus, Ellen Hoppenz, Mateo Murillo-León, Tobias Hoffmann, Jana Scholz, Florian Melerowicz, Tobias Steinfeldt, Frank Seeber, Martin Blume

Nature Communications 13, 2022, https://doi.org/10.1038/s41467-022-28730-w

Chlamydia*-containing spheres are a novel and predominant form of egress by the pathogen *Chlamydia psittaci

Jana Scholz, Gudrun Holland, Michael Laue, Sebastian Banhart, Dagmar Heuer

mBio 15, 2024, https://doi.org/10.1128/mbio.01288-24

Entschlüsselung eines neuen Austrittswegs von Chlamydien

Jana Scholz and Dagmar Heuer

BIOspektrum 30, 2024, https://doi.org/10.1007/s12268-024-2334-3

Recruitment of the cellular lipid transport protein CERT to *C. psittaci* inclusions regulates the timing of bacterial egress

Jana Scholz, Gudrun Holland, Michael Laue, Sebastian Banhart, Dagmar Heuer

Scientific Reports, submitted, preprint available at https://doi.org/10.1101/2024.11.26.625409

Lipidome of middle and late *Chlamydia psittaci* infections in HeLa cells

Jana Scholz, Julia Maria Post, Alyssa Ingmundson, Laura Bindila, Dagmar Heuer

Molecular Microbiology, in preparation

Egress of *Chlamydia* spp.

Jana Scholz, Alyssa Ingmundson, Dagmar Heuer

Molecular Microbiology, in preparation

Split-Inc protein-based interactomics reveals host cellular interactions of Cps0558, a novel *Chlamydia psittaci* inclusion protein.

Jean-Marc Gensch, Jana Scholz, Laura Rose, Jörg Döllinger, Sebastian Banhart, Dagmar Heuer

Pathogens and Disease, in preparation

Talks

7th Joint Microbiology & Infection Conference of the German Society for Hygiene and Microbiology (DGHM) and the Association of General and Applied Microbiology (VAAM)
02.-05-06-2024, Würzburg
"*Chlamydia-containing spheres are the predominant egress structure of the zoonotic pathogen Chlamydia psittaci*"

20th German Chlamydia Workshop
21.-23.02.2024, Ascona
"*Chlamydia-containing spheres are the predominant egress structure of the zoonotic pathogen Chlamydia psittaci*"

75th Annual Meeting of the German Society of Hygiene and Microbiology (DGHM)
18.-20.09.2023, Lübeck
"*The zoonotic pathogen Chlamydia psittaci egresses from the host cell via formation of Chlamydia-containing spheres, a novel non-lytic egress pathway*"

Annual Conference of the Association of General and Applied Microbiology (VAAM)
10-13.09.2023, Göttingen
"*The zoonotic pathogen Chlamydia psittaci exits the host cell via formation of Chlamydia-containing spheres, a novel non-lytic egress pathway*"

EXIT Symposium
29.03.-01.04.2023, Brühl
"*The non-lytic exit pathway of Chlamydia psittaci*"

19th German Chlamydia Workshop
02.-03.03.2023, Düsseldorf
"*The non-lytic egress of Chlamydia psittaci*"

74th Annual Meeting of the German Society of Hygiene and Microbiology (DGHM)
05.-07.09.2022, Berlin
"*Deciphering the role of sphingolipids in bacterial egress*"

Status workshop SPP2225 "Exit strategies of intracellular pathogens"
05.-06.05.2022, Aachen
"*Deciphering the role of sphingolipids in bacterial egress*"

Virtual project meeting SPP2225 "Exit strategies of intracellular pathogens"
30.09.-01.10.2021, online
"*Deciphering the role of sphingolipids in bacterial egress*"

Curriculum Vitae

Aus datenschutzrechtlichen Gründen in der Online-Version nicht enthalten.